INSTABILITY OF COMPOSITE BEAMS IN HOGGING BENDING

By

Shiming Chen

Submitted for the degree of Doctor of Philosophy

to the Higher Degrees Committee

University of Warwick

Department of Engineering

University of Warwick, Coventry, U. K.

July 1992

Contents

Acknowledgements

I would like to express my sincere thanks to my supervisor, Prof. R. P. Johnson for his continuous support and constructive criticism throughout the course of my research.

I am indebted to the University of Warwick, the ORS award organization, the Chinese Education Commission for their financial support which made this research possible.

I would also like to thank Mr. C. Banks and his team for their devoted support in the laboratory.

Finally, but not least, I am very grateful to my family and particularly my wife, Liping. Without their support, this thesis would not have been completed.

Shiming Chen

Declaration

I hereby declare that the work described in this thesis is the result of my own investigations except where reference is made to the work of others.

It has not been submitted for a degree at any other University.

Shiming Chen

Synopsis

This work is concerned with local buckling and lateral distortional buckling, two aspects of instability that govern the design of composite beams in hogging regions.

Local buckling in hogging regions of a continuous composite beam was modelled by moment curvature characteristics of a cantilever, modified by two curvature ratios, K_1 and K_2. Test based expressions for K_1 and K_2, in terms of a combined slenderness λ_c were developed, and subsequently used in numerical analyses of 50 two-span composite beams to assess moment redistribution allowed for Class 2 beams by draft Eurocode 4. The analyses include effects of non-linear material properties, residual stresses and local buckling. The parametrical studies include adverse values, in relation to practice, of relative length of adjacent spans, span-to-depth ratio, and ratio of hogging to sagging moment of resistances. It is concluded that the redistribution of elastic bending moments allowed by the draft Eurocode 4 is safe and economical.

Distortional lateral buckling of composite beams with both continuous and discrete U-frame actions was studied experimentally. Distortional lateral buckling was found in the tests of two composite beams with inverted U-frame actions. Web distortion was effectively reduced by vertical web stiffeners, which form a part of discrete U-frames together with the slab and the connection of U-frame. The work provides background to assess lateral buckling strength for composite beams with both continuous and discrete U-frame actions. A further theoretical approach on the topic of discrete inverted U-frame action was presented.

Strength and stiffness of discrete U-frame connections were also studied. The strength of a discrete U-frame connection was found to be influenced by both the shear failure of concrete, and the yielding of steel top flange in the connection. A simple rule to assure strength of U-frame connections is proposed by checking these two failures separately. The prediction of shear failure of a U-frame connection is based on a truss model, and the prediction of failure in the steel top flange is based on a rigid plastic mechanism. A semi-empirical formula for flexibility of a U-frame connection was derived. They were all checked against test results. Interactive U-frame force and U-frame stiffness were also studied. A tentative design method for discrete U-frame composite beams was proposed.

List of Notation

- A —- area of cross-section
- B —- distance between steel members of U-frame beams / breadth
- b —- breadth; width
- C —- stiffness of lateral restraints
- C_4—- factor regarding moment gradient
- c —- stiffness of lateral restraints per unit length, breadth of out flanges
- d —- depth of cross-section
- E —- modulus of elasticity for structural steel
- E_c —- modulus of elasticity for concrete (short term)
- F —- lateral restraint force
- f_{cu} —- strength of concrete (cubic)
- f_r —- flexibility of U-frame connection
- f_y —- yield stress for structural steel
- G —- shear modulus for structural steel
- g —- dead load
- h —- height of steel member
- h_d —- height of stud
- I —- second moment of area
- I_{afz}—- second moment of area of bottom flange
- I_{st} —- St Venant torsion constant for steel section
- K_1, K_2, K_3 —- curvature ratios

- k_θ — transverse stiffness for U-frame, per unit length
- k —- transverse stiffness regarding parts of U-frame, per unit length
- L —- length of a span
- l, l_e —- length; effective length
- M — bending moment
- N —- axial force
- P —- point load
- q —- imposed load
- R —- rotation capacity
- t —- thickness
- u —- buckling parameter in BS5950; coefficient regarding single and multi bays of U-frames
- w —- distributed load
- x —- coordinate along the longitudinal axis of a beam; torsional index
- y —- coordinate normal to the plane of the steel web
- z —- coordinate in the vertical direction
- α —- slope; fraction of web depth in compression
- β —- slenderness ratio
- δ —- lateral flexibility for U-frame; deflection
- Δ —- lateral displacement
- ϵ —- strain; factor of material strength
- η —- factor regarding distributed compression
- γ —- factor of material

- λ —- load factor; slenderness ratio
- λ_c —- combined slenderness ratio
- ϕ —- curvature; angle
- θ —- rotation
- μ —- fraction of M_p by which support moment drops in numerical analysis
- σ —- stress

Other symbols are defined in the text where they appear.

Subscripts

- a —- steel; label A
- b —- buckling; bracing; label B
- c —- concrete; composite; compression
- cr —- crack; elastic critical
- d —- distortional; design
- e —- elastic; effective
- f —- flange; failure
- i —- inelastic
- ini —- initial value
- L —- lateral
- LT —- lateral torsional
- max —- maximum value
- p, ps —- plastic(hogging); plastic(sagging)

- pe —- hypothetic elastical
- r, rt —- reinforcement
- y —- yield
- s —- steel; stiffener
- st —- regarding stud
- t —- top; transverse
- u —- uncracked, ultimate state, U-frame
- w —- web, warping
- z —- minor axis

Chapter 1

General Introduction

In recent years, composite beams have been found to be an economic form of construction. It is a result of continuous innovations in the design of composite construction that a rapid growth of using composite construction has taken place in the last ten years, and on the other hand, it also stimulates further research and development.

The composite beams considered here are made up of steel I-sections, welded stud shear connectors, and insitu concrete slabs, with or without metal decking. In practice, composite beams are usually designed as simply-supported, but at longer spans, continuous beams can provide a more economic design. Plate girders are used for the longer spans in bridge structures, while in a building structure, the minimum economic span can be reduced to below 20 m by the use of rolled universal beams.

This research project forms part of a long-term study into the strength and behaviour of continuous composite beams in the hogging moment region near an intermediate support, at the ultimate state. The design of composite beams in this region is governed by effects of local and distortional lateral buckling. Lateral buckling of the bottom flange can be eliminated by either cross bracing to the bottom flange or by the partial lateral restraint provided by a pair of webs and the slab, which form an inverted U-frame. When a beam is restrained from lateral buckling, part of the web and the bottom flange in compression near the support are prone to local buckling. It has been found from the previous research and practice that for the majority of rolled sections, it is not necessary to introduce additional restraint when a composite beam is designed up to a limit on the moment capacity, i.e. the plastic moment capacity, in the hogging moment region. This is especial in building structures, when beams with compact cross sections are designed related to the plastic moment resistance. However, at the longer spans in bridge structures, the beams usually have slender cross sections, and distortional lateral buckling may govern the ultimate strength of the beams.

The work reported in this thesis consists mainly of two parts relevant to the

ultimate strength of continuous composite beams affected by instability in the hogging moment region: (i)a parametric study to investigate the amount of moment redistribution for beams with Class 2 cross-sections related to local buckling; (ii) an experimental study to investigate distortional lateral buckling of Class 3/4 (slender) composite beams with inverted U-frame action. The scopes of the research therefore apply to the continuous composite beam design in building structures, and to the design of composite bridges in the hogging moment region.

A lot of experimental and theoretical research has been done on local buckling and its effect on moment redistribution in continuous composite beams. This piece of work focuses on moment redistribution related to inelastic local buckling in continuous composite beams with Class 2 cross-sections. The objective of the work was to check the margin of safety of a quasi-elastic design method adopted in the recently drafted EC4 [1] for buildings, which allows 30% moment redistribution from the hogging internal support to the sagging region based on elastic global analysis. The computer program used for the non-linear numerical analysis was developed by the present author. It includes the effects of non-linear material properties, residual stresses and local buckling.

For continuous composite beams, the steel bottom flange in the hogging moment regions may be vulnerable to distortional lateral buckling. This instability impairs the ultimate load carrying capacity of the beam, and so sometimes bracings are required in order to achieve an economic design. However, it is widely believed that the provision of lateral bracing is inconvenient, costly and unnecessary, especially for those beams with rather compact cross-sections (Class 1 or 2), such as hot-rolled universal beam sections. It is logical to assume that, depending on the flexural stiffness of the web, the lateral restraint from the concrete slab should be able to transfer to the compression bottom flange, so that the design of bridge structures(or buildings) with parallel main composite girders with inverted U-frame action can be simplified by eliminating the bracing in hogging bending regions. Instead of bracing, in U-frame beams, continuous restraint is provided to the compression flange by the slab and the web for unstiffened plate girders, and discrete restraint is provided to the compression flange by the intermediate vertical stiffeners which act as discrete inverted U-frames together with a part of the slab. Unfortunately,

there is not sufficient experimental evidence to substantiate this view, especially for those beams used in composite bridges, which usually have much more slender cross-sections, with vertical stiffeners which are usually provided for vertical shear, but also increase the flexural stiffness of the web.

The objective of this part of the work was therefore to investigate experimentally the distortional lateral buckling of composite beams with inverted U-frame action. Firstly, distortional lateral buckling of a continuous composite beam with continuous inverted U-frame action is assessed at the ultimate state, and then secondly, the distortional lateral buckling of a continuous composite beam with discrete inverted U-frame action is studied, and finally, the strength and the stiffness of discrete inverted U-frames are evaluated based on a series of tests on isolated U-frame configurations.

No general method of assessing the distortional lateral buckling of composite beams with inverted U-frame action is yet available. The only relevant design method regarding U-frame action is the one given in the Bridge Code(BS5400) [2] for steel beams, so that the test results have been compared with this relevant design method. The experimental work also provides background for the theoretical approach on the topic of distortional lateral buckling of composite beams with discrete inverted U-frame action, upon which, a new design method is proposed.

There are ten chapters in this thesis. Chapter 1 gives a general introduction of the research. An attempt is made to describe the aim and topic of the research. Then each subsequent chapter is outlined.

In Chapter 2, comprehensive literature reviews, on local buckling and moment redistribution for composite beams, and on distortional lateral buckling of composite beams are given. The relevant investigation of U-frame action is also summarized.

In Chapters 3 and 4, local buckling and moment redistribution in continuous composite beams are studied. Numerical analysis is carried out on continuous composite beams with Class 2 cross sections.

Investigation of distortional lateral buckling of composite beams with both continuous U-frame and discrete U-frame action is described in Chapters 5, 6, and 7. Chapter 5 gives specimen design and test preparations. Chapter 6 presents the test results and in Chapter 7, analysis and assessment of the test results are given.

Investigation of U-frame action is described in Chapter 8. Both strength and stiffness of U-frames are studied. The U-frame action in the global beam tests is also assessed.

A theoretical approach to investigate distortional lateral buckling of composite beams with U-frame action is described in Chapter 9. The interactive U-frame force and stiffness are also studied. A tentative design method for discrete U-frame composite beams is proposed.

In Chapter 10, conclusions and design recommendations for composite beams with discrete U-frame action are summarized.

Chapter 2

Literature Review

2.1 Introduction

The ultimate strength of continuous composite beams has been a main concern in limit state design for many years. Many problems have been tackled previously including the effect of local buckling, ultimate moment of resistance, ultimate shear capacity, partial shear connection, redistribution of moments, cracking, and more recently distortional lateral buckling of the bottom flange. In hogging moment regions, buckling is an important structural problem.

There are two main areas of research in this project: local buckling and moment redistribution, and distortional lateral buckling of beams with U-frame action, and so this chapter is divided into two parts, one devoted to each piece of work.

The first part gives a review of research on local buckling in composite beams and its effect on redistribution of moments. The background for the present research is given, following a discussion of the current design philosophy for Class 2 continuous composite beams in accordance with draft Eurocode 4 [1].

The second part of this chapter is concerned with the investigation of distortional lateral buckling of composite beams, and of U-frame action. The review of the research on distortional lateral buckling in composite beams will begin with the studies which have led to the present design methods. In addition, the present design method for restraint of distortional lateral buckling by U-frame action is outlined and commented on.

2.2 Local buckling and moment redistribution

2.2.1 Local buckling and cross-section classification

Local buckling refers to conditions under which the compression flange or portion of the web in compression, buckles in a local region. Local buckling of thin-walled steel sections has been researched extensively over the past forty years because of its

prominent influence on the strength of beams and columns. There is a comprehensive basic literature [3, 4, 5].

The behaviour of local buckling is very similar in a steel beam and in a composite beam; however, for composite beams, the steel top flange is attached to the concrete slab, so that only part of the web and the bottom flange in the hogging moment region adjacent to an internal support of a continuous support, are prone to local buckling.

Local buckling is generally considered in design codes by limiting the width-to-thickness ratios of the flange and web. Stowell [6] derived an expression for the compressive strain at the onset of buckling of a flange, which is assumed to be free to rotate along the line of the web. Lay and Galambos [7] and Southward [8] extended this analysis to include the effect of the web. It has been identified that local buckling is affected by the width-to-thickness ratios of the flange and web, the moment gradient over the buckling wave length, lateral buckling slenderness and also the strain-hardening properties, especially when yield occurs in the steel member.

The use of cross-section classification(or compactness) to deal with the influence of local buckling on cross-section resistance is well established. As the resistances of cross-sections and their ability to deform are closely related to the slenderness of the web and flange in compression, codes of practice in many countries give limitations on these slendernesses for the purpose of assessing the bending resistance as well as choosing the most appropriate method of structural analysis.

In early 1970's, the introduction of limit state design philosophy into codes of practice for design of structures began to take place in Europe and North America, which encouraged the development of plastic design, especially in buildings. In U.K., classification of cross-sections in steel structures first appeared in BS5400: part 3 [2]. Cross-sections are defined as either compact or non-compact, according to several slenderness provisions.

The more recent codes of practice [1, 9, 10] have taken one step further than BS5400 in classification of cross-sections, by dividing them into four classes, depending on the level of susceptibility to local buckling.

Eurocode 4 is the most relevant to the present work. The four classes of cross-

section are defined by the limiting width-thickness ratios for compression flanges and webs given in Tables 4.1 (flange) and 4.2 (web) of draft Eurocode 4 [1]. In Eurocode 4, the plastic neutral axis is used for webs in Class 1 or 2, and the elastic neutral axis is used for webs in Class 3 or 4. This leads a small discontinuity, in that a web just on the Class 3 side of the Class 2/3 boundary may have a depth in compression (according to the elastic theory) less than the depth in compression of a Class 2 web by the plastic theory. Implications of this classification system for the design of composite beams in buildings have been discussed by Johnson [11] and Brett et al [12, 13].

An effective web in Class 2 is introduced for uncased Class 3,assuming that the depth of web that resists compression is limited to 20 $t_w\epsilon$ adjacent to the compression flange, and 20 $t_w\epsilon$ adjacent to the new plastic neutral axis, as shown in Fig.2.1 for hogging bending. t_w is the thickness of web and ϵ is a steel strength factor, defined by:

$$\epsilon = \sqrt{\frac{235}{f_y}} \tag{2.1}$$

where f_y is yield stress of the steel in N/mm^2 units.

The relation between the classification and rotation capacity is shown diagrammatically in Fig.2.2 and interpreted as follows, in accordance with Eurocode 4 [1]:

- *Class 1 (plastic) The cross-sections can develop a plastic hinge with sufficient rotation capacity to allow full redistribution of bending in the structure.*

- *Class 2 (compact) The cross-sections can develop the plastic moment capacity of the sections though local buckling and/or crushing concrete limit rotation at constant bending moment.*

- *Class 3 (semi-compact) The cross-sections can not develop the plastic moment, owing to the limit of yield stress in the extreme compression fibres because of local buckling.*

- *Class 4 (slender) The cross-sections are liable to local buckling of the structural steel by compressive stress less than the yield stress.*

For Class 1 and 2 cross sections, rotation capacity is defined as the ability of a

beam to deform and to rotate at critical cross sections while maintaining the plastic moment M_p, and it is subject to the limits due to the local buckling of steel sections in a hogging region and the crushing of concrete in a sagging region.

The rotation capacity requirements in the design of continuous composite beams have been discussed by Kemp [14], in relation to their classification for local buckling. He found that for Class 2 cross-sections, the maximum redistribution of moments of 30% from an internal support to the mid-span by an elastic uncracked analysis corresponds to a required rotation capacity of 1.6. This is consistent with the values of 2.2 and 2.0, the minimum available rotation capacities for specimens U2 and U3 in Fan's tests [15].

As there are no appropriate design guidelines which account for interaction between the local buckling of the compression flange and web, the classification is based on width-to-thickness ratio limitation for the flange and the web independently.

Kato [16] introduced an interaction formula between the width-to-thickness ratios of flanges and web in accordance with the rotation capacity requirements. Polyzois [17] developed the expressions for evaluating buckling coefficients for the compression flange and the web, accounting for the interaction between the web and the flange, using finite element analysis. However, both lack general test evidence.

2.2.2 Moment redistribution in continuous composite beams

Most of the early research work was related to the application of plastic design to composite beams. To enable a plastic design, it is assumed that there is sufficient rotation capacity in developing a collapse mechanism. However, this is subject to the limitation of rotation capacity due to the local buckling of steel sections in a hogging region and the crushing of concrete in a sagging region.

Barnard et al [18] studied the ultimate behaviour in the sagging region, and verified the validity of using simple plastic theory for the design of simply supported beams. Barnard [19] also presented a method for estimating the curvature of a cross-section in sagging bending. It was then found [20] that the amount of rotation at maximum moment can vary extensively depending on the cross-section dimensions and span length.

Van Dalen [21] tested seventeen composite double cantilevers in hogging bending

to simulate the hogging moment region of a continuous beam. The account of the work includes many detailed conclusions and design recommendations [22]. The evidence of severe local buckling in composite beams was also noted.

The moment-rotation characteristic as affected by local buckling in the hogging region was studied by Climenhaga [23] both theoretically and experimentally. In his tests, the hogging region of a continuous beam was modelled as a double cantilever, and it was then found that local buckling only occurs close to an internal support. Four types of cross-section, in relation to local buckling behaviour, were identified.

Further research was carried out by Hamada and Longworth [24] to study the buckling of composite beams in hogging bending. They concluded that ultimate moment capacity of composite beams is affected by local flange buckling, and the bending resistance decreases significantly with increase in the flange width-thickness ratio.

Hope-Gill [25] used the results on moment-rotation or moment-curvature characteristic from Barnard [18] and Climenhaga [23] for sagging and hogging regions respectively, to conduct a computer study to determine the conditions under which continuous composite beams will reach the plastic design loads. The work was further complemented by tests on three-span continuous composite beams [26]. By comparison with the moment rotation curves M-θ for a cantilever beam of similar cross-section, it was then found that the hogging regions are stronger in a continuous beam, even though the strain-hardening characteristics of the steels are similar. Hope-Gill [27] subsequently extended the work on redistribution of moment to cover composite beams of slender cross-sections which cannot be designed plastically.

In relation to the moment curvature characteristics in sagging bending, Ansourian [28] proposed a limiting value of 1.4 for the ductility factor χ, defined as the ratio of the limiting neutral axis depth to the conventional neutral axis depth at ultimate strength, based on continuous beam tests, to allow moment shedding from hogging to sagging regions in continuous composite beams.

Bradford presented a finite strip method [29] of analysis for the inelastic local buckling of composite beams in hogging bending, which included non-linear material behaviour and residual stresses.

Meanwhile, in North American, research [30, 31, 32] has been focused on ex-

perimental tests and design studies aimed at extending the ALFD (Alternate Load Factor Design) concepts to non-compact steel plate-girder sections. The procedures in ALFD methods permit direct consideration of inelastic load redistribution in the determination of strength under the maximum load, and thus they rely on the development of plastic rotations at interior supports. Compact beams proportioned for plastic design are able to sustain such rotations at the full plastic moment M_p, while non-compact beams are designed based either on a mechanism analysis with an "effective plastic moment" less than M_p, or on the use of realistic lower-bound moment rotation curves directly in the analysis.

More recently, Johnson and Fan [33] carried out a computer study using realistic material properties and moment-rotation characteristic curves based on Climenhaga's test data [34] to check the redistribution limit for Class 3 cross-sections in draft Eurocode 4 [1]. It was then found up to 20% redistribution of elastic moment based on cracked stiffness (EI_{cr}) is satisfactory.

2.2.3 Design of Class 2 continuous composite beams

When a composite beam is loaded, a redistribution of moments occurs in relation to the distribution of moments expected from elastic analysis. This fact is used in the method of design specified in various codes [2, 9, 1], in composite beam design at the ultimate state.

If a continuous composite beam is designed plastically, the ultimate strength of a uniform continuous composite beam is dependent on how much of the support moment can be redistributed to the mid-span before collapse rather than on the attainment of maximum moment of resistance at the support.

To achieve better economy in the design of composite beams, draft Eurocode 4 has proposed a quasi-elastic method allowing a certain amount of redistribution of support moment to midspan in addition to the conventional elastic analysis at the ultimate limit state. This method is based on the assumption that pre-buckling plasticity and post-buckling rotation capacity in the hogging region can be relied on to shed at least that certain amount of bending moment before collapse occurs.

When uncracked flexural stiffnesses (EI_u) are used in the global analysis, draft EC4: Part 1 [1] allows up to 30% redistribution for Class 2 beams at the ultimate

limit state as does BS5950: Part 3 [9].

Apparently, the method, which allows substantial moment redistribution, could be thought to be too liberal.

2.3 Distortional lateral buckling of composite beams and U-frame action

2.3.1 Distortional lateral buckling of composite beams

When the tension flange of an I beam is restrained against lateral displacement and twist, distortional lateral buckling may occur, which could be considered as an interaction between web distortion and lateral overall buckling.

It is a common form of top flange restraint when floor beams are connected to a longitudinal plate girder so as to restrain the top flange in the lateral direction. The most significant instance can be found in composite beam design when shear studs are used to connect a concrete slab to the top flange of a girder. These structures are susceptible to lateral buckling only in a distortional mode in hogging regions because the steel top flange is laterally and torsionally restrained, while the bottom flange is restrained partially from lateral displacement by the web, but the level of restraint is dependent largely on the flexural stiffness of the web.

The distortional buckling failure mode was studied as early as 1944 by Goodier and Barton [35], who treated the web as a series of thin vertical beams each with an equivalent modulus of E/(1 - μ), where E is Young's modulus and μ is Poission's ratio. The study led to the important conclusion that web deformation could be represented by a cubic polynomial function.

Suzuki and Okumura [36] and Kollbrunner and Hadjin [37] have used the folded plate approach while others have employed more powerful finite element/strip techniques, based on either all plate elements or a combination of beam (flanges) and plate (web) elements for distortional buckling analysis. Among the prominent attempts is work by Hancock (1978) [38], who presented a finite strip technique capable of handling the interaction between local and lateral buckling in I-beams under various flange restraint conditions. A limit of this method, however is that only uniform

bending moment can be considered, because stresses in longitudinal strips must be kept constant.

Bradford and Trahair [39] studied inelastic buckling problems by using the finite element method under various conditions of loading, end support and restraint, and further extended to distortional bucking, but they could not include the effect of initial geometrical imperfections.

More research using the finite strip method has been carried out in Australia to study web distortional overall buckling in I-beams systematically. The general results indicated that for I-beams with compact cross-sections, the effects of web distortion are small, so that their buckling loads are close to the values calculated by the classical rigid web method.

Most of the earlier research could not tackle geometrical and material non-linearity, and only a few people have studied distortional lateral buckling in the inelastic range. Bradford [40] investigated inelastic distortional buckling of determinate hot-rolled I-beams by a finite element method. Dowling at el [41] used a non-linear finite element program to study the overall stability of plate girders. Both geometrical and material non-linearities were included in the analysis, however, the work was limited to plate girders.

Although elastic analysis of distortional lateral buckling for I-beams has been progressing well, very little research has been done to investigate distortional lateral buckling of continuous composite beams especially in the inelastic range. Recognizing the two main features of the buckling; top flange restraint and cross-sectional distortion, Johnson and Bradford [42] used the finite element method to conduct a parametric study of elastic buckling of unstiffened, fixed ended composite beams. In absence of direct test evidence, they assumed that the destabilising effects of residual stresses, geometrical imperfections, and yielding of steel (for compact cross sections), were the same for distortional buckling under moment gradient as those for non-distortional buckling.

The resulting elastic critical stresses were found to depend principally on d/t_w, as in the expression

$$\sigma_{cr}/f_y = 600(d/t_w)^{-1.4} \tag{2.2}$$

where d and t_w are clear depth and thickness of the web as shown in Fig.2.3.

This expression gave a safe estimate of the elastic critical stress σ_{cr} for distortional lateral buckling. However, the result gave a design hogging resistance much higher than that given by the Bridge Code [2], raising the possibility that local buckling, which was not modelled in the analysis, could make the results unsafe.

A further 11 beams were analysed by the same workers [43], using the same approach, and were compared with the results for critical local buckling moments given by an inelastic finite strip analysis. It was found that inelastic local buckling always preceded lateral buckling in composite beams with a non-compact compression flange, whereas lateral buckling appeared to be the critical failure mode if the compression flange were compact. To cover both possibilities of buckling, a design method was proposed in which, the design hogging resistance at the face of an internal support was determined from either a local buckling slenderness ratio β_L or a lateral buckling slenderness ratio β_d, whichever was higher, being the beam slenderness β used in the design method (BS5400: Part 3 [2]), with β_d based on equation 2.1 or expressed as;

$$\beta_d = 3.08(d/t_w)^{0.7} \tag{2.3}$$

and

$$\beta_L = 3.5(\beta_f \beta_w)^{0.5} \tag{2.4}$$

where β_f and β_w are slenderness of the bottom flange and the web, defined in the Bridge Code [2].

Because local and lateral buckling were not modelled in the same analysis, the method may exclude an adverse interaction.

Weston and Nethercot [44] modelled both local and lateral buckling in the same numerical analysis, using a large deflexion elasto-plastic finite element program developed by Crisfied [45], which was capable of modelling initial imperfections.

In the finite element analysis, the top and bottom flanges of a mono-symmetrical I-beam were treated as stiffeners, which attached to the adjacent web plate elements. The top flange was fully prevented from lateral displacement, and twist along the member was restrained by a degree appropriate to the slab stiffness, but at the fixed-ended support, the boundary condition permitted the bottom flange to rotate about

Table 2.1: Ranges of slenderness ratios used in parametric studies

Authors	Web d/t_w	$b_{f(bot)}/t_{f(bot)}$	L/$b_{f(bot)}$
Bradford and Johnson [42] [43]	39-107	5-15	48-90
Weston and Nethercot [44]	39-117	2-13	55-330

a vertical axis. That is the same condition as adopted by Johnson and Bradford [42, 43]. A parametric study was carried out and 19 beams with spans ranging from 23 m to 33 m were analysed. They found that buckling failure was always concentrated in the region adjacent to the support, and concluded that the dominant mode of failure in compact or near compact bridge girders is likely to be inelastic local buckling adjacent to internal supports.

In contrast to the finding by Johnson and Bradford [43], the results indicated that the slenderness of the bottom flange is also an important parameter to determine the critical load for distortional lateral buckling. A new design method was proposed, which was intended for use with the existing lateral buckling rules in the present Bridge Code(BS5400: Part 3 [2]). The slenderness parameter for lateral buckling is calculated as a function of the geometrical parameters as follows:

$$\beta = 1.28(L/r_z)^{0.5}(d/t_w)^{0.33} - 29 \tag{2.5}$$

where L is the distance between two fully lateral restraints(span of a beam), and r_z is the radius of gyration of the bottom flange.

The ranges of the three relevant slendernesses are given in Table 2.1, in which the notation is as given in Fig.2.3.

Both methods are based on parametric studies with uniformly distributed loading, and the length of the hogging moment region ranges from 0.21 L for a fixed-end beam to 0.24 L for multi-span continuous beams so that the moment gradients were steep. A comparison of the two methods is given in Fig.2.4, in which the slenderness β is plotted against the ratio $L/b_{f(bot)}$, where $b_{f(bot)}$ is the width of the bottom flange. The range of d/t_w is from 39 to 117 in the parametric studies, so that only the curves corresponding to d/t_w of 40 and 100 are given. When $L/b_{f(bot)}$ ranges from 50 to 100, the values of β given by equations 2.3 and 2.5 are very close, and when $L/b_{f(bot)}$ is

beyond 100, the curves based on eq.2.3 are lower than those based on eq.2.5. This is because that eq.2.3 is based on the numerical study, with the range of $L/b_{f(bot)}$ from 48 to 90. A wider range of $L/b_{f(bot)}$ is covered by eq.2.5. Only three specimens with the ratio of $L/b_{f(bot)}$ from 50 to 100 were found dominated by local bucking failure in the numerical study [44], and the others were found failing in lateral buckling, especially those with $L/b_{f(bot)}$ beyond 100.

However the two methods suffer the same drawbacks, neglecting the effect of variation of moment gradients other than the case of fixed-ended beams, and the effect of the flexibility of the slab or the $b_{f(bot)}/t_{f(bot)}$ ratio of the bottom flange.

Svensson [46] analysed the problem using a different approach. He examined the stability of an elastically supported column subjected to a varying axial force along its length and then modelled the free flange of a composite girder as such a member. The partial lateral restraint of the web to the free flange is introduced by the foundation modulus expressed in terms of web stiffness and slab stiffness. The variation of axial force was represented as a quadratic function in the governing equation of the buckling problem. The quadratic coefficients are chosen to relate closely to the pattern of moments in the beams. However, the effect of local buckling is excluded and the elastic critical buckling stress is also underestimated by assuming the boundary conditions at the two ends of the column as pin-ended. William and Jemah [47] have used finite strip programs to tackle the problem as an assemblage of flat plates, and further extended the scope of Svensson's work to cover all possible contributions of beam end conditions. To achieve a better agreement between the predictions from the plate theory and the equivalent column concept, they suggested adding 15% of the web area to the flange area when the bottom flange is modelled as an elastically supported column.

Goltermann and Svensson [48] presented a refinement of the column on elastic foundation method, which includes the effect of rotational restraint at the top flange. The Saint Venant torsional effect was also introduced into the problem this time, which was previously ignored by Svensson.

For design purposes, the limiting compressive stress σ_{li} at the bottom flange was suggested (in accordance with the approach adopted in Eurocode 3 [10]) as being:

$$\frac{\sigma_{li}}{f_y} = \frac{1}{\sqrt{1+\bar{\lambda}^4}} \tag{2.6}$$

with $\bar{\lambda}$ is defined as:

$$\bar{\lambda} = \sqrt{\frac{f_y}{\sigma_{cr}}} \tag{2.7}$$

where σ_{cr} is the elastic buckling stress of the bottom flange and f_y is the yield stress of the steel.

The comparison in [44] with the results from [46] suggests that susceptibility to local buckling may not have much influence on lateral buckling, which is consistent with the finding that when test data on lateral buckling of steel members were being used as a basis for the design curve in the Bridge Code, the performance of members of slender section (i.e. Class 3) was not found to be inferior to that of compact members (i.e. Class 1 and 2). This assumption is made in two recently-developed design procedures, namely SCI method [49] and EC4 method [1], for lateral buckling of composite beams described as follows.

The method proposed by the Steel Construction Institute (SCI method) is basically for the design of composite beams with haunched steelwork, but also applied to the unhaunched beams. To be consistent with current design practice for lateral-torsional buckling of steel beams in BS5950: Part 1 [50], the effective slenderness λ_{LT} is used, which is defined in the code by:

$$\lambda_{LT} = nuv_t\lambda \tag{2.8}$$

and

$$\lambda = L_n/r_z \tag{2.9}$$

where

- u is a buckling parameter (= 0.9 for universal beams).
- v_t is a slenderness factor, which includes effects of Saint Venant torsion, cross section shape, and etc.,
- n is the slenderness correction factor for the shape of the bending moment diagram,

- L_n is the calculated critical length, and r_z is the minor-axis radius of gyration of the steel section.

It is derived for a composite beam with an undistorted I section rotating through angle θ about the same point, subject to uniform hogging moment, by using the usual energy method. In the analysis, the top flange was assumed to be fully restrained both laterally and torsionally. The web distortion is introduced by adding the energy of bending of the web to the total strain energy of the system. It includes St Venant torsion, lateral bending, and axial shortening of the bottom flange, but not the effects of restrained warping, and the transverse flexibility of the concrete slab. The compression force in bottom flange is also assumed as M_{cr}/D throughout the beam length, where M_{cr} is the elastic critical moment and D is the overall depth of the steel section, as shown in Fig.2.3.

The slenderness factor v_t is expressed as:

$$v_t = \frac{1}{[1 + (\lambda/x)^2/40 + (L/D)^3 I_w L_n/16 I_y]^{0.5}} \tag{2.10}$$

and the critical buckling length L_{cr} is found as:

$$L_{cr} = 3.74(I_z)^{0.25}(D/t)^{0.75} \tag{2.11}$$

where

- I_w is the second moment of area of the web per unit length, $t^3/12$,
- I_z is the second moment of area of the steel beam about its minor axis,
- x is the torsional index of the steel section,
- D is the overall depth of the steel section.

The critical buckling length L_{cr} is found as:

$$L_{cr} = 3.74(I_z)^{0.25}(D/t)^{0.75} \tag{2.12}$$

However, the calculated critical length L_n is chosen either as L_{cr} or L_1, the distance from the support to the next lateral restraint to the bottom flange, whichever is less.

Like the SCI method, the EC4 method is also an approximate energy based method to give the elastic critical moment. It originated in work conducted in the University of Bochum [51, 52]. The method is more versatile and its applicability is wider: it takes account of the transverse flexibility of the concrete slab, and includes provisions for steel I-sections that are asymmetric or partially encased in concrete. No assumption is made for the longitudinal compression force in the bottom flange, and the moment M_{cr} on the composite section is replaced by equivalent internal forces and moments determined by the elastic theory, considering the composite interaction.

The elastic critical moment is given by

$$M_{cr} = \frac{C_4 k_c}{L} \sqrt{(GI_{at} + k_\theta (\frac{L}{\pi})^2) EI_{afz}} \tag{2.13}$$

where

- L is the distance between points at which the bottom flange of the beam is restrained,
- I_{afz} is the minor-axis second moment of area of the bottom flange,
- k_c is a property of the cross-section, different for symmetric and asymmetric sections,
- C_4 is a property of the distribution of bending moment, based on the finite-element analysis,
- k_θ is the transverse stiffness of a U-frame.

The EC4 method takes account of U-frame action provided by the slab/deck via the webs. For a slab/deck multi-beam system, the stiffness k_θ is expressed in terms of the web stiffness and the slab stiffness, regarding the potential benefit of U-frame action in stabilizing the unstiffened and unbraced beams.

Then it is assumed in the EC4 method that the relationship between true ultimate strength and elastical critical load will be the same for the distortional buckling of composite beams as it is for the traditional form of the lateral buckling for I-section steel beams. To be consistent with Eurocode 3 [10] in dealing with lateral-torsional

buckling of steel beams, the buckling resistance moment is determined by using the EC3 [10] design curves, regarding the compactness of the cross-sections.

Unfortunately, all the design methods mentioned so far or used in practice are only applicable for composite beams, built up of unstiffed steel beams, which are only provided with vertical stiffeners and lateral bracings at the supports. For composite beams with vertical stiffeners along the beam length, lateral and torsional restraints from the slab to the compression flange are greatly enhanced, due to discrete inverted U-frame action. Further comments are given in the later sections regarding this U-frame action.

Experimental work on distortional lateral buckling of continuous composite beams is very limited, possibly because of its cost. Three twin I-section steel beams coupled by connecting beams and pre-cast reinforced concrete slabs were tested by Nakamura and Wakabayashi [53]. However, in the tests, the pre-cast slab units were discontinuous longitudinally along the beams, and therefore the reinforced concrete slab did not contribute any additional strength to the composite cross-section apart from restraining the top flange laterally and torsionally. The test specimens were essentially inverted U-frames. Although the slab was quite flexible, the lateral displacement and twist of the top flange of the specimens was very small. The maximum strength was 8% higher than the plastic moment of resistance for the bare steel beam under linear moment gradient, but when the bottom flange was subject to uniform compression under uniform hogging bending moment, the maximum strength was about 7% lower than the plastic moment. It was concluded that the bracing effect by the reinforced concrete slabs was sufficient large so that the maximum moment resistance of the beam could be beyond the full-plastic moment of a steel section under moment gradient. However, the specimens are for only one web slenderness ($d/t = 200/6$), and the composite action (in bending) due to friction at the bolts used to fix the slab is also not taken into account.

An experimental investigation to the distortional lateral buckling of continuous composite beams was conducted by Johnson and Fan [54]. The relevant test models are three double cantilevers namely U1, U2 and U3 to simulate the hogging regions of continuous composite beams. Specimen U1 is a composite T-beam, on which tests in elastic range had been carried out, so that torsional restraint to its bottom

flange from the already cracked slab would be less stiff than continuous U-frame action. Specimens U2 and U3 are two double cantilevers, with twin beams coupled by the concrete slab, forming inverted U-frame sections. All the cross-sections were near the boundary between Class 2 and Class 3 to draft EC4 [1]. The ultimate strength of each of the four beams in specimens U2 and U3 was found to be governed by a complex interaction between local and distortional lateral buckling, strongly influenced by initial imperfections.

The tests provide spot checks on, and confirm, the predictions of various design methods, at the interface between class 2 and class 3 cross sections. Compared with the other design methods, the EC4 method is the most versatile, while the method based on the Bridge Code [2] is much too conservative.

The tests further suggested the finding by Weston and Nethercot [44] that in compact or near compact composite beams, the dominant mode of failure be more likely to be inelastic local buckling adjacent to internal supports.

Two full scale tests on composite bridge girders were carried out in Bochum University [55]. The specimens represented a multi-beam composite bridge deck, with rolled universal beams of class 3 cross sections to draft EC4 [1]. The specimens were supported at the midspan and loaded at the ends of cantilever extensions to simulate the hogging moment region of continuous beams. In both tests, the ultimate load was determined by local buckling of the web above the midspan support. Though the cross sections are Class 3 to draft EC4, a typical Class 2 behaviour was observed in the beam tests, and the plastic moments (hogging) were reached. These results claim that the classification system of EC4 is conservative especially for Class 3 cross sections, and further confirm that local buckling is more likely to be the dominant mode of failure for composite beams even with Class 3 rolled cross sections.

2.3.2 Bracing for composite beams

In practice, a main beam is often braced to ensure that the member reaches its full cross-sectional plastic moment capacity M_p. In terms of structural members, bracing consists of additional members that are attached to main beams, to restrain the lateral movement.

The research of bracing systems for steel I-section beams has been well documented [56]. Taylor and Ojalvo [57] studied torsionally braced beams using numerical integration for three different loading cases. They found that with continuous torsional restraint, the critical load on a beam increases with the stiffness of the torsional restraint, while with a point torsional restraint, the critical load is limited by the two half-wave solution of lateral buckling. Nethercot [58] analysed laterally or torsionally restrained beams by the finite element method for three loading cases at three load levels. Mutton and Trahair [59] dealt in an approximate manner with laterally and torsionally braced beams for both uniform moment and concentrated load at midspan. The minimum value of restraint stiffness required to cause a column or a beam to buckle in its second mode was obtained.

Bracing strength was evaluated by Medland [60] for columns with variable numbers of bays and braces. It was found that bracing strength requirements varied linearly with initial deflexion magnitude. Wakaybashi and Nakamura [53] tested a series of unbraced beams and beams braced by purlins or sub-beams under different moment gradients. The tests conducted by Wang-chung and Kitipornchai [61] confirmed that a lateral brace placed at the shear center was effective as torsional bracing. Wang and Nethercot [62] investigated the interrelationship between bracing stiffness, bracing force and ultimate load of the braced members by using the finite element method. The numerical results confirmed the linear relationship between strength requirement and the magnitude of initial deflexion in the main members.

However, it is always assumed that the bracing is equally spaced, and less attention has been paid for continuous composite beams, where cross bracing at the sections close to the internal supports, but not elsewhere, might effectively improve lateral stability of the beams.

More recently, Stanway et al [63] studied the behaviour of an initially imperfect column with an intermediate elastic restraint at any position, using critical buckling and non-linear elasto-plastic finite element analysis. They found that restraint forces and required restraint stiffness vary greatly according to span ratio. A tentative design method was proposed [64] for the restraint requirements and the column strength. Further research will be needed before it could be applied to multi-restrained columns. The methodology used might be helpful to study a

braced beam problem, in which the member subjects to bending other than axial compression, however the weakness of the method is still that only uniform axial compressive load is considered.

2.3.3 U-frame action in stabilizing composite beams

The use of 'U' frames in plate girders as a means of stabilizing laterally the compression flanges of the main girders originates from 'half-through' type railway bridges. U-frame action was first introduced in a revision of the old Bridge Code (BS153) [65] in 1956, mainly for the design of 'half-through' type bridges.

The new Bridge Code (BS5400)[2] followed the similar U-frame approach adopted in BS153. The stiffness of U-frames comprising the cross members and the vertical stiffened webs in the main girders is identical to that in the old Bridge Code, but it takes account of the connections between the main and cross girders. However, regarding the strength of the U-frame, BS5400 adopts an expression of lateral U-frame force based on a laterally restrained Euler strut with initial bow, while in BS153, this transverse U-frame force is taken a value equal to 1.25% of the force in the flange.

Design for lateral torsional buckling of U-frame beams in BS5400 Part 3 is by determining the effective length for the partially restrained flanges (eg. restrained by U-frames). In deriving the expression for the effective length l_e, it is assumed that the compression flange is subject to a uniform axial force, with partial lateral U-frame restraints uniformly distributed along the axial length. Apparently, the Bridge Code assumes that the effective length obtained from buckling analysis of the bottom flange, is also valid for the whole beam. The method is known to be very conservative. The departure between reality and the code results is largely affected by the way that the effective length is calculated. A comprehensive discussion is given by Johnson [66].

Besides, it is important to note that Fig.10 in BS5400: Part3 [2], was derived for plain steel beams only, unrestrained against lateral torsional buckling. It is not suitable for composite beams with U-frame action, because the top flange is laterally restrained by the stiff concrete slab, and the overall buckling occurs in a web distortional mode provided that there are no failures in the U-frame connection.

The design value for the strength of all U-frames within the span L is assumed to be the same, according to clause 9.12.2.2 of BS5400. This is rather conservative, because the lateral restraint force is only reached where the lateral deflection is maximum. For simply supported 'half-through' type bridge girders, the maximum lateral deflection occurs at the mid length of l_e, and the lateral force decreases for U-frames away from this position. Beams with discrete U-frame action were studied by Chwalla in 1959 [67]. He developed a matrix method, taking account of the moment distribution over the whole span in calculating the limiting buckling load of the compression flange. In his study, the U-frames along the entire span were replaced by springs, which provided an equivalent lateral restraint to the flange. To assess the error made by assuming the lateral restraint force constant over the beam length, Van de Pitte [68] applied Chwalla's method to a simply supported 'half-through'-type bridge girder under uniformly distributed load and found that the lateral force dropped by 50% at a distance of 0.16 L away from midspan, where $M/M_{max} = 0.88$.

However, in continuous composite beams, the axial compression force decreases very rapidly away from the internal support region due to a high moment gradient, and inverted U-frames, as a variant U-frame form, comprise the decking slab, the either stiffened, or unstiffened web, and the connection between the slab and the steel top flange. Therefore, the assumptions adopted in BS5400 are no longer valid for continuous composite beams with U-frame action.

Coupled behaviour of overall and local buckling of welded U-shaped beams subject to uniform bending was studied by Fukumoto and Kubo [69]. In the experimental studies,diaphragms were provided at six cross sections equally spaced along the beam length in the UD series of specimens to prevent an excessive drop in bending strength due to cross-sectional distortion. Another three specimens known as the UK series were tested to investigate the effect of a knee brace, placed at the midspan of the beams. It was then found that the overall buckling strength was primarily affected by ratio of the span length to the spacing of the webs. Overall buckling may arise with a low buckling stress in the elastic range in a long span beam. The web distortions were greatly decreased for the stiffened beams by diaphragms, and therefore, for beams with rather close vertical web stiffeners, the influence of distortion

of the cross sections on the overall buckling may be negligible.

The effect of web stiffeners on buckling strength was also studied by Albert and Dawe [70], using a finite element technique. Only those beams with lateral and rotational top restraint are relevant to the composite beams. They found that typically, the behaviour of short unstiffened girders is governed by vertical web buckling (local buckling), while that of long girders is controlled by lateral flange buckling, and distortional buckling prevails in the intermediate range. Actually, the addition of web stiffeners significantly increases the buckling strength of short spans by limiting the extent of web buckling.

The design of composite beams with inverted U-frame action could be simplified by eliminating bracings in hogging bending regions. U-frame action is used as a means of stabilizing laterally the compression flanges of the main girders. Continuous U-frame restraint is provided to the compression flange by the slab and the web for unstiffened plate girders. Discrete restraint is provided to the compression flange by intermediate vertical stiffeners which act as a part of discrete inverted U-frames. However, for discrete U-frames, concentrated moments act on the shear connections above the stiffeners, so that reliance needs to be placed upon the rigidity and the strength of the slab to top flange connections via the shear studs.

The typical arrangement of inverted U-frames is shown in Fig.2.5.

Johnson and Fan [54] investigated inverted U-frame action in hogging regions of composite beams. Two inverted U-frame double cantilevers known as specimen U2 and U3, were tested , as mentioned in the previous section. It was demonstrated in these tests that continuous U-frame type restraint by the slab and the web is sufficient to allow the plastic moment to be achieved for specimens U2 and U3, which are on the borderline of the compact/non-compact (or Class 2/Class 3) cross section classification to draft EC4 [1]. It was also found that failure moments of specimens U2 and U3 exceeded the predictions of the BS5400 method, for a Class 2 cross section, by well over 200%, and the EC4 method [1], by 23-33%.

Discrete inverted U-frame action exists in composite beams with intermittent vertical web stiffeners in the hogging bending region near the internal supports. The design method in BS5400: Part 3 for discrete U-frame action gives values for the transverse flexibility of a number of standard structural steel connections which

are used in the calculation of the effective buckling length and the lateral deflection of the bottom flange. To obtain similar values for steel-concrete joints, Johnson and Molenstra [71] studied the effectiveness of discrete U-frame action in a composite configuration. Tests were carried out to scale 1:1 on six flange-slab connections with different stud configurations.

All test specimens failed either in shear or by pulling out of the studs, and a truss analogy model was used to predict the shear failures. The transverse elastic flexibilities of the joints, which are much higher than the values suggested in the Bridge Code (BS5400: Part 3), represent only the behaviour of the similar joints in a complete structure. However all specimens were in one size of steel flange and a fixed flange length(600 mm), so that a general design method cannot be deduced from these results along. Besides, it is more likely that the failure of the joints will be influenced by the steel flange if the steel top flange is weak in torsional rigidity.

Jeffers studied [72] U-frame restraint against instability of steel beams in bridges. The difficulties in design practice relating the provisions of U-frame action in BS5400: Part 3 were identified. The limited use of U-frame restraint by designers and contractors more likely reflects the uncertainty of knowledge and proper guidance in design practice. Attention has been drawn to the recent research work relating to U-frame action, by Travers Morgan [73]. However, the work is only related to steel U-frames, and the basic problems of strength and stiffness which comprise U-frame action for composite beams have not been tackled, and it is still assumed that U-frame force is constant in the compression flange of the beams, so that no substantial progress has been made regarding discrete inverted U-frame action. Besides, it is vague for one to interpret the U-frame restraint forces based on either effective intermediate discrete lateral restraints, or rigid lateral restraints.

2.3.4 Design to distortional lateral buckling of beams with discrete U-frame action

The only design method relevant to distortional lateral buckling of composite beams with discrete U-frame action is BS5400. For composite beams with intermediate vertical web stiffeners, the 'discrete U-frame' model of clause 9.6.5 of BS5400 is appropriate. Intermittent restraint is provided to the compression flange by attachment

of vertical stiffeners connected to the main girder (Fig.2.5). The sections where the intermittent restraints occur are considered as discrete and stiff U-frames at spacing L_u.

The design formulae for stiffness and strength of U-frames and inverted U-frames in accordance with BS5400: Part 3 are as follows:

- **Stiffness of U-frames and the effective length:** In order to calculate the effective length, l_e, of the compression flange, the flange is treated as a strut with continuous elastic support from U-frames and with the ends restrained in position by somewhat stiffer end frames. The intermediate restraint to the compression flange is provided by U-frames in accordance with clause 9.12.2(strength requirement), the effective length l_e should be taken as:

$$l_e = 2.5k_3(EI_cL_u\delta)^{0.25} \tag{2.14}$$

where

  - k_3 is a coefficient related to the support condition, and may conservatively be taken as 1.0, but a lower value is also suggested when the compression flange is restrained against rotation in plan at the supports,
  - E is Young's modulus of the steel section,
  - I_c is the second moment of area of the compression flange about its centroidal axis parallel to the web of the beam at the point of maximum bending moment,
  - L_u is the distance between U-frames,
  - δ is the lateral deflection per unit horizontal force at the level of the centroid of the compression flange per U-frame. In the cases of symmetrical U-frames, where cross members and verticals are each of constant moment of inertia throughout their own length, it is expressed by

$$\delta = \frac{d_1^3}{3EI_1} + \frac{uBd_2^2}{EI_2} + f_r d_2^2 \tag{2.15}$$

where

- I_1 is the second moment of area of the effective section of the vertical about its axis of bending,
- I_2 is the second moment of area of the cross member of the U-frame about an axis perpendicular to the plane of the U-frame,
- u is 0.5 for an outer beam, or 0.33 for an inner beam,
- f_r is the flexibility of the joint between the cross member and the verticals of the U-frame.

- **The strength of U-frames:** According to clause 9.12.2.2 of BS5400:part 3, each U-frame has to be designed to carry a transverse force F_u per U-frame, in addition to transverse force due to wind load. The design value of F_u for the strength of all U-frames within l_e is given by:

$$F_u = [\frac{l_e}{667\delta}][\frac{1}{\sigma_{cr}/\sigma_{fc} - 1}] \tag{2.16}$$

and

$$F_u \leq \frac{EI_c}{16.7L_u^2}[\frac{1}{\sigma_{cr}/\sigma_{fc} - 1}] \tag{2.17}$$

- σ_{cr} is non distortional elastic critical stress of the bottom flange,
- σ_{fc} is the maximum compressive stress in the bottom flange.

However, the assumptions adopted in deriving eq.2.16 and eq.2.17 are no longer valid for continuous composite beams with intermediate vertical stiffeners acting as inverted U-frames. In continuous composite beams with U-frame action, the factor $1/(\sigma_{cr}/\sigma_{fc}-1)$defined in the equations reaches its peak value at the internal support section but decreases very rapidly away from the support due to the high moment gradient. The value of this factor is also conservative as only distortional buckling can occur in these types of beams, and the Bridge Code does not provide expressions for elastic critical distortional buckling stresses nor does it provide data from lateral distortional buckling tests.

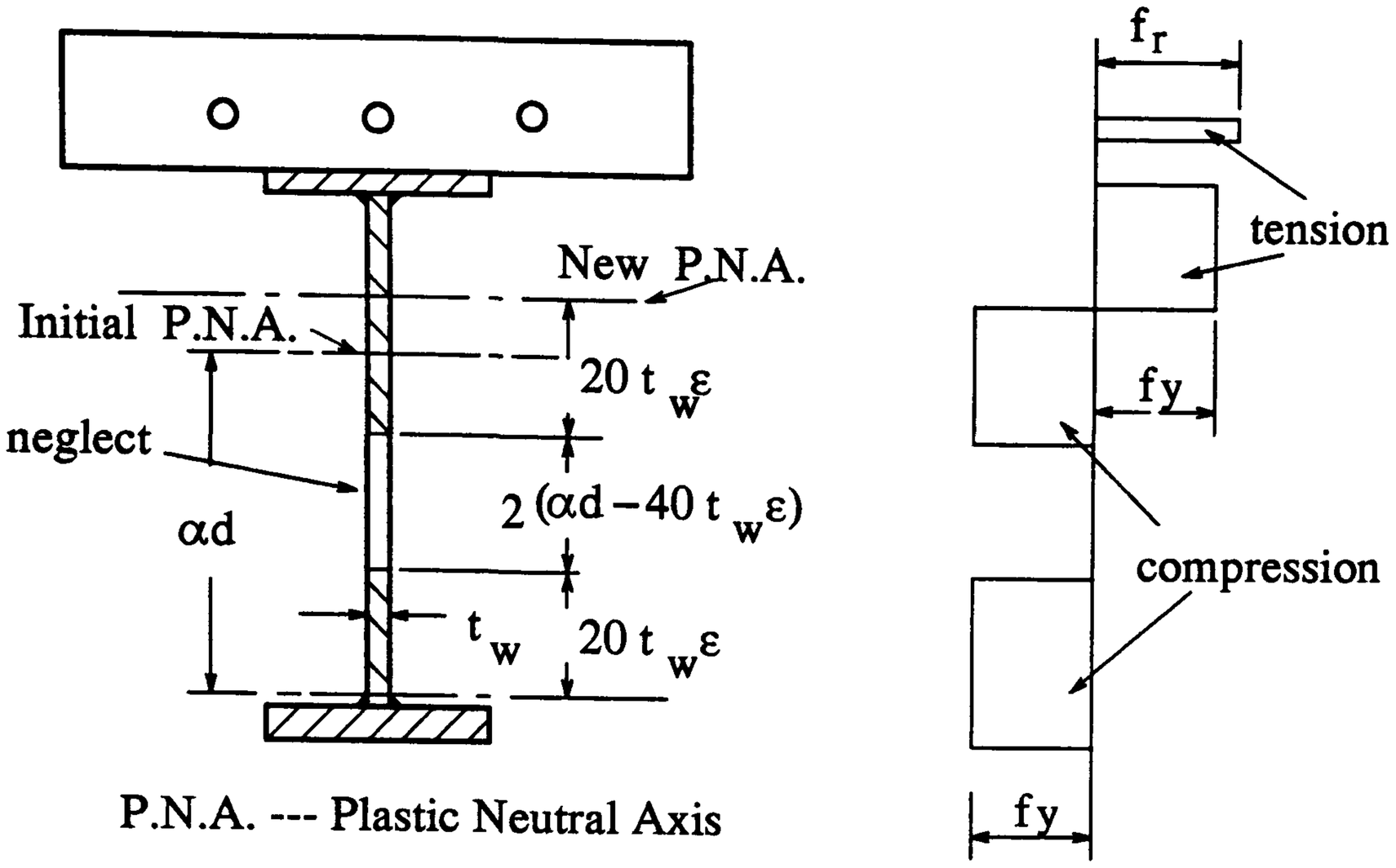

Figure 2.1: Use of an effective web in Class 2 for a Class 3 web in hogging bending

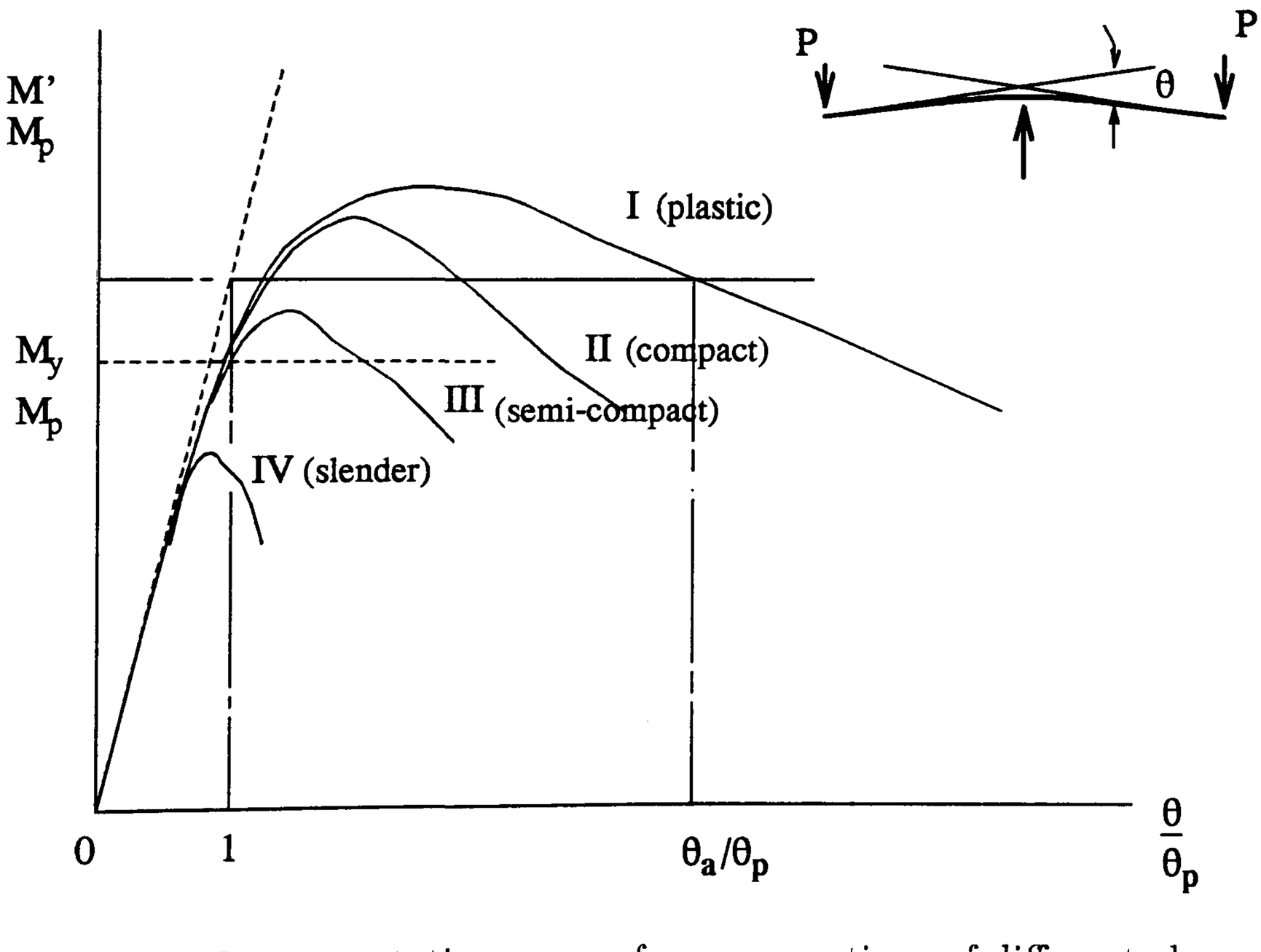

Figure 2.2: Moment-rotation curves for cross-sections of different classes

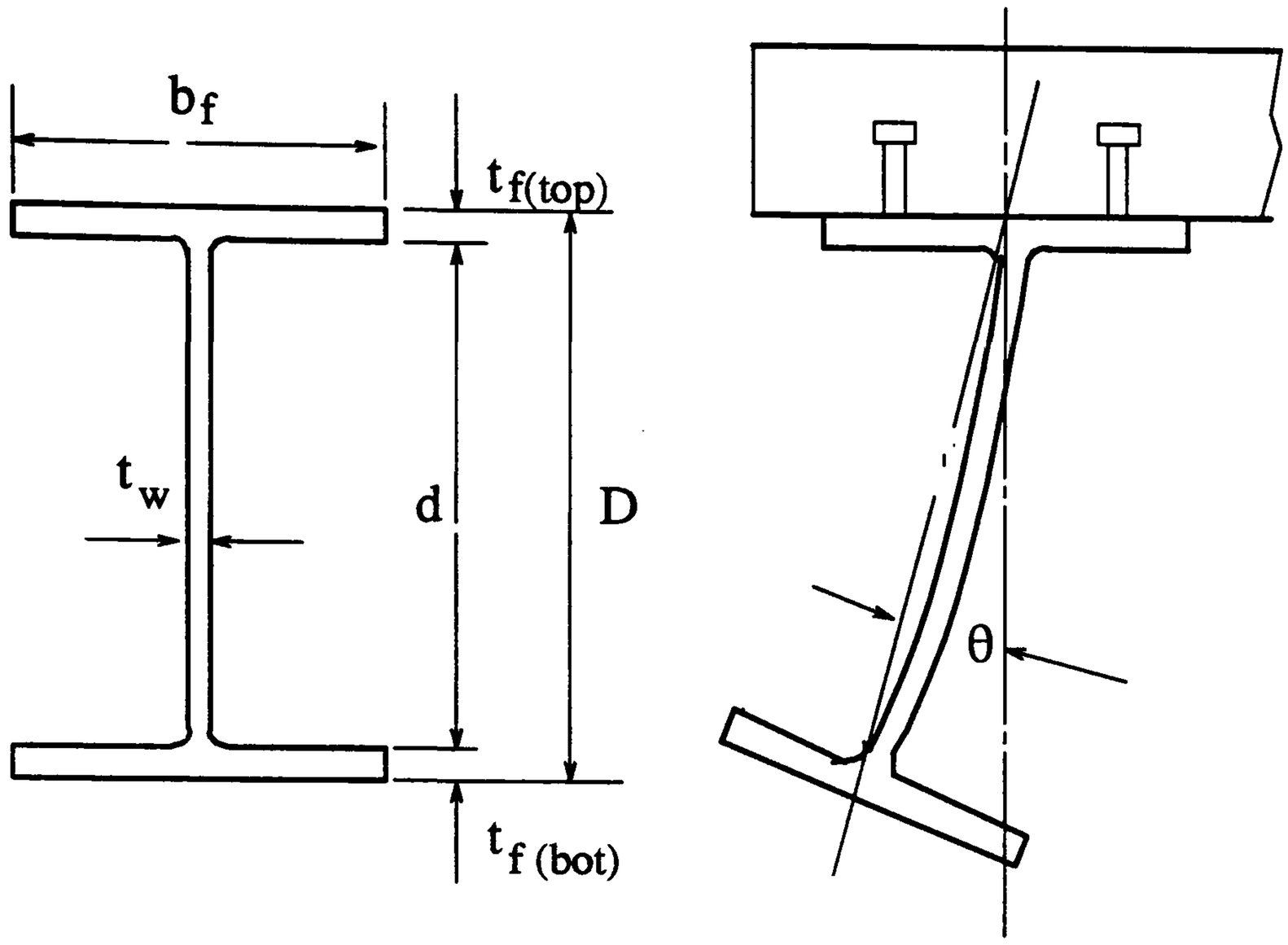

Figure 2.3: Notation and lateral buckling mode

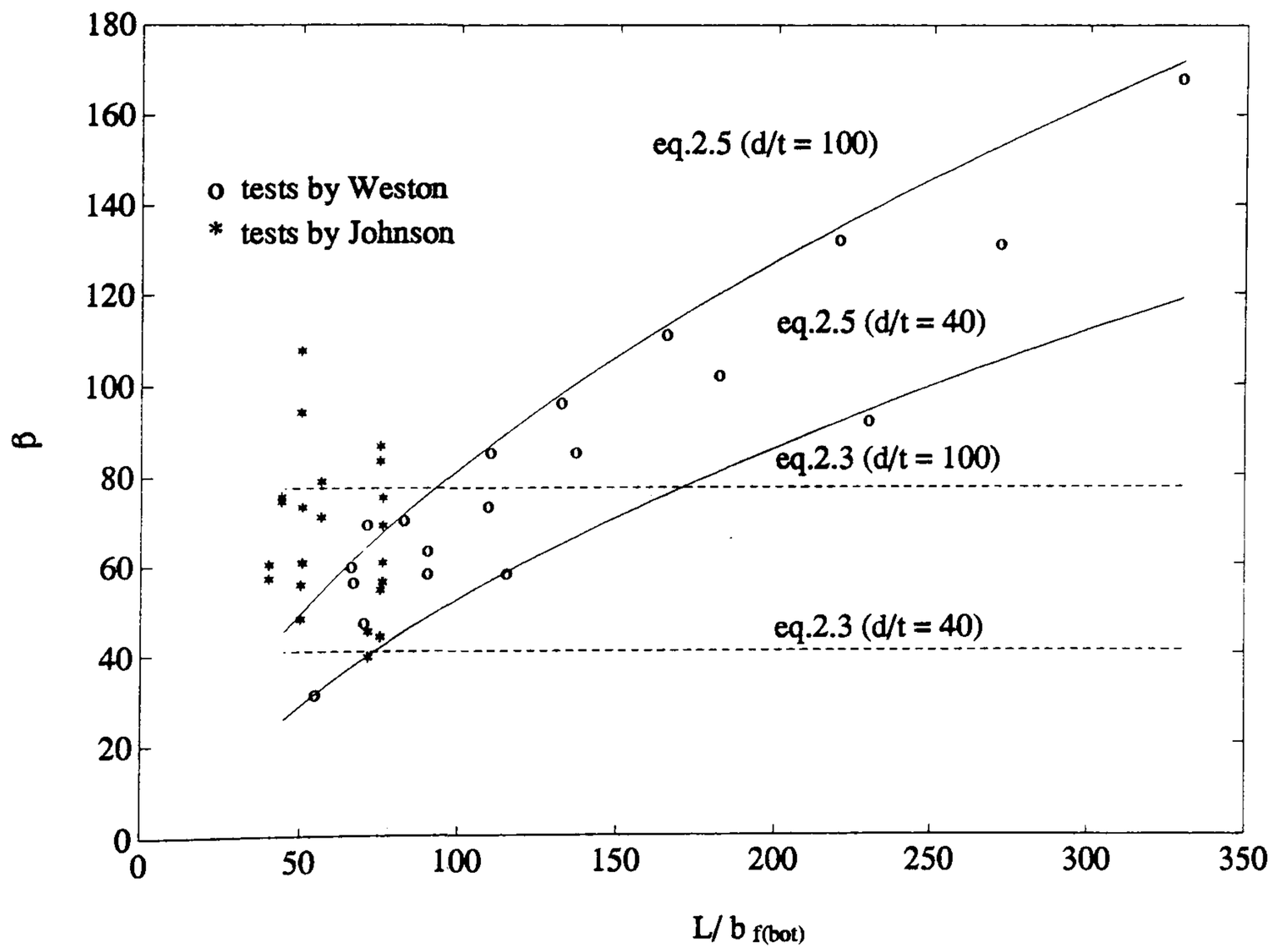

Figure 2.4: Comparison of the two design methods

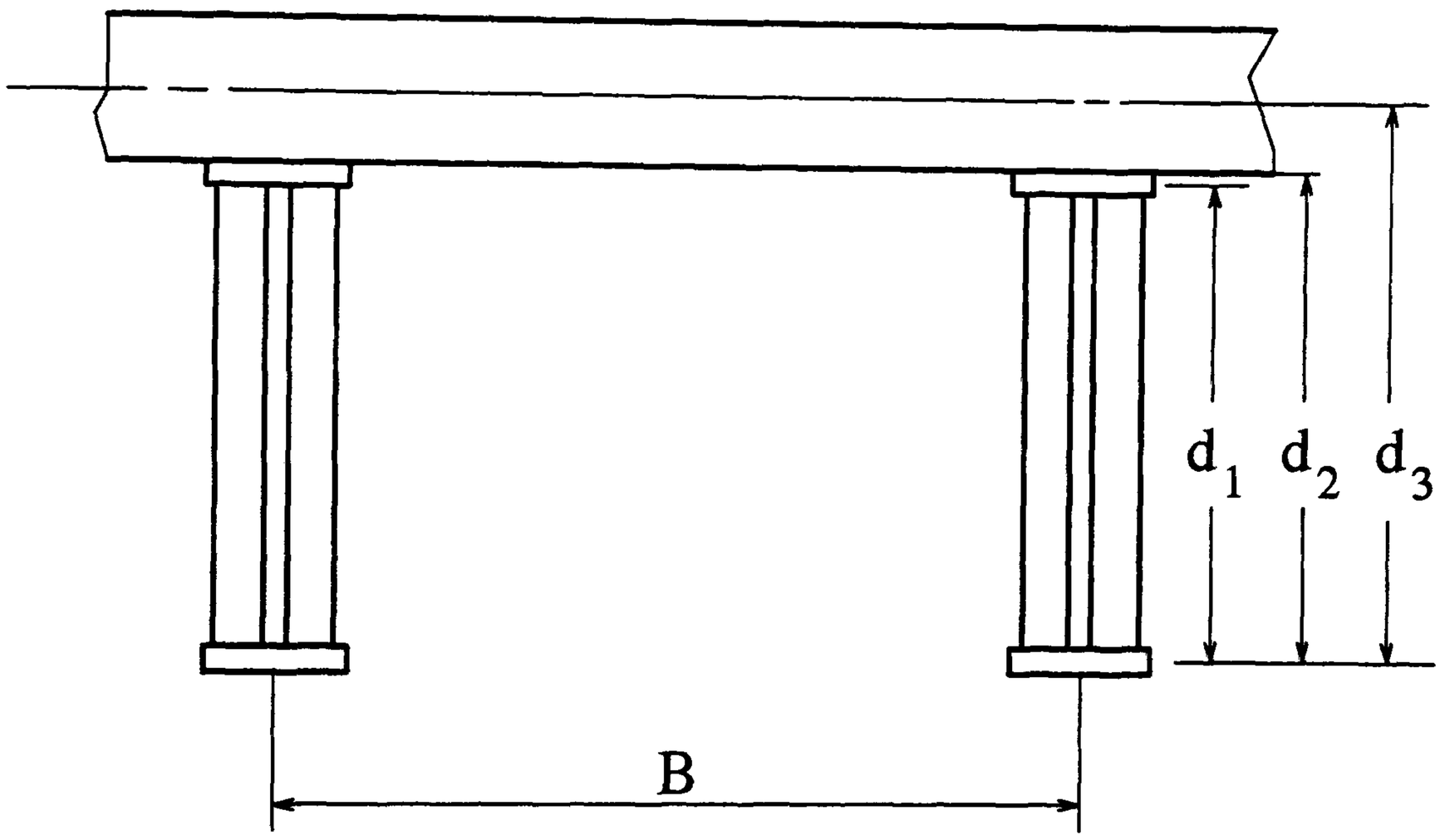

Figure 2.5: A composite inverted U-frame cross section

Chapter 3

Inelastic local buckling tests and computer simulations

3.1 Introduction

When a continuous composite beam is loaded, a redistribution of moment occurs in relation to the moment distribution expected from elastic analysis. The amount of moment redistribution is closely related to the rotation capacity of the beam in both hogging and sagging regions. When lateral-torsional buckling is not a controlling factor, the ultimate carrying capacity of the beam is influenced by initiation of local buckling at critical cross-sections in the hogging regions near the internal supports.

To assess the amount of moment redistribution in Class 2 composite beams, a non-linear computer program SCC has been developed to simulate the behaviour of hogging regions of a continuous composite beam before and after local buckling. Realistic material properties and inelastic moment-curvature ($M - \Phi$) curves are used and test data from steel and composite cantilevers with local buckling, are introduced to modify the $M - \Phi$ curves for hogging bending.

It is assumed that complete shear connection is provided and the bottom flange of the beams is free of lateral-torsional buckling.

The objective was to evaluate the rotation capacity related to hogging regions of Class 2 composite beams based on relevant reported test results [34, 74, 75]. As a result, the hogging region of a continuous beam is modelled by moment-curvature characteristic at the critical section, modified by curvature ratio parameters K_1, K_2 and K_3, which are determined and subsequently applied in the non-linear analysis of a continuous composite beam, as explained in the next chapter.

3.2 Local buckling and rotation capacity

3.2.1 Moment rotation characteristic

Depending on the level of stress when local buckling occurs, cross-sections of composite beams are identified as four classes. In design, local buckling is allowed for by limiting the width-to-thickness ratios of the flange and web [1, 9].

For a beam with Class 2 cross section(or Class 2 beam) local buckling occurs when the bending moment is beyond plasticity at the critical cross-section. Fig.3.1 illustrates a typical moment/rotation curve for a Class 2 beam. The amount of plastic rotation allowed for Class 2 beams is defined as rotation capacity, R as

$$R = \theta_a/\theta_p - 1 \tag{3.1}$$

where θ_a is the range of plastic rotation before the moment falls below the plastic resistance M_p, owing to local buckling and θ_p is the hypothetical elastic rotation at the fully plastic moment that would be achieved.

Obviously, rotation capacity R varies with the expected plastic moment of resistance. The subsequently reported rotation capacity R is related to the hogging plastic moment of resistance M_p, which is calculated using rectangular stress blocks [1], with all γ factors = 1, as shown in Fig.3.2

The moment-rotation relationship of the critical section in hogging regions of a composite beam can be either obtained from tests or by integration of the moment-curvature functions for hogging bending.

3.2.2 Modelling of local buckling

Fig.3.3 shows a composite cantilever of length L_c subject to a point load P at the free tip. Tests on composite cantilevers give curves of end slope θ_t due to the increasing point load P. Specimens are usually double cantilevers, with vertical stiffeners at the support ($x = 0$). Local buckling usually occurs at a location close to the support, with a buckling half-wavelength of about $h/2$, where h is the overall depth of the steel section.

It is assumed that in the following model, all of the inelastic rotation due to

buckling occurs at the section $x = h/4$. It is also at this section that the limiting bending resistance, M_p, is assumed to be reached.

For a Class 2 section, local buckling does not occur at a hogging bending moment below M_p. It has been found [54] that elastic analysis based on the "cracked reinforced" section (stiffness EI_{cr}) gives an accurate prediction of the end slope of a cantilever at the yield moment, M_y (residual stress excluded). Therefore, the total end rotation θ_t of a cantilever is written as

$$\theta_t = \theta_i + PL_c^2/2EI_{cr} \tag{3.2}$$

where the first term θ_i is the inelastic rotation due to the yielding and buckling and the second item is the elastic end rotation.

The inelastic rotation θ_i is assumed to result from an inelastic curvature Φ_i due to yielding and buckling, constant over a length $h/2$ adjacent to the support. By integration of the curvatures along the beam length, the total end rotation is by

$$\theta_t = \int_0^{L_c} \Phi(x)dx \tag{3.3}$$

and

$$\theta_i = \Phi_i h/2 \tag{3.4}$$

Determination of the hogging moment curvature relationship of a composite section is similar to that described in [33], using a bi-linear stress-strain curve for reinforcement, a trilinear curve for structural steel with strain hardening (at modulus $E/33$) commencing at a strain of $8\epsilon_y$, where ϵ_y is the yield strain, and limited by the stress in the steel reaching 1.3 f_y as shown in Fig.3.4.

Fig.3.5 shows the moment-curvature curve at the critical section of a Class 2 beam. The effect of inelastic local buckling is included in the moment-curvature characteristic by two curvature ratios K_1 and K_2 as follows.

Let the computed moment-curvature be OAB (Fig.3.5), where

$$\Phi_{pe} = \frac{M_p}{EI_{cr}} \tag{3.5}$$

Because of yielding and buckling, the portion AB is replaced by ACD, defined by K_1 and K_2, which are multiples of Φ_{pe}, to be determined. The plastic ductility

of a cross-section before and after local buckling is quantified by the ratios K_1 and K_2. The value of K_3 is Φ_i/Φ_{pe} when $\mathrm{P}(L_c - h/4) = M_p$, and is calculated from the computed moment-curvature curve, where Φ_i is the inelastic curvature given in eq.(3.4).

Tests on composite beams usually give moment-rotation curves, or the rotation capacity R, to quantify their plastic ductility. In the moment-curvature curve of the buckling model (Fig.3.5), the ratio K_1 is defined by

$$K_1 = \Phi_i/\Phi_{pe} \tag{3.6}$$

and it can be calculated from the rotation capacity R as follows.

For a cantilever subject to a point load at the free tip(Fig.3.3), the maximum elastic curvature Φ_{pe} is related to the elastic slope θ_{pe} at the tip by

$$\Phi_{pe} = 2\theta_{pe}/L_c \tag{3.7}$$

where θ_{pe} is the hypothetical elastic slope at the full plastic moment M_p, the ratio of θ_i/Φ_i is given in equation 3.4. Therefore K_1 is related to R by

$$K_1 = (L_c/h)R \tag{3.8}$$

This formula is used in the subsequent work to calculate K_1 from R, which can be found in the relevant reported test results.

3.2.3 Choices of cantilever tests

The test data required are curves (P-θ_t) for composite cantilevers as shown in Fig.3.3. Tests usually continue until local buckling has caused the maximum bending moment at the supports to fall below $0.8M_p$. The cross sections of the specimens are compact, so that the stress level in the critical sections are beyond yielding when the beams fail. The only results found so far are composite double cantilevers HB40 and HB41, tested by Climenhaga and Johnson [34]. They found that since buckling occurred only near the edge of the member remote from the concrete slab, the effect of the slab reinforcement could be simulated by attaching a steel plate to the top flange of a rolled I-section. Four of their tests of this type, SB2,3,8 and 9 are relevant here.

For each of the specimens, two slopes were reported [23]. They correspond to two individual cantilevers each side of the support. In the tests, local buckling was found to occur in one side only near the support of the double cantilevers, whenever moment rotation curves are reported for both ends in a double cantilever test, the greater of the two is used. Table 3.1 gives the relevant parameters of these beams.

The notation for the cross sections is illustrated in Fig.3.6. The slabs were 105 mm in depth. In Table 3.1, A_{r1} and A_{r2} are the area of top and bottom reinforcement at positions 25 mm and 80 mm from the top of the slab. f_{fy} is the measured yield stress for the steel flange which is slightly lower than the mean value of the strengths of the web and flange, adopted in [34]

Local buckling was also found in tests on 43 simply-supported steel beams under centre load reported by Kuhlmann [75], Lukey [74] and Kemp [76]. These steel beams can be considered as inverted double cantilevers with A_r=0, and α=0.5. The relevant parameters of these test specimens are summarized in Tables 3.2, 3.3 and 3.4.

For a simply supported beam, the cross-section with the maximum lateral displacement is subjected to the maximum bending moment, whereas in a cantilever, the cross-section with the maximum lateral displacement(i.e. at the tip) is subjected to the minimum bending moment. However, when lateral buckling of the bottom flange is excluded, the effect on the rotation capacity by this difference is minimized.

In the tests by Kuhlmann [75] and Lukey [74], lateral displacements and twist out of the vertical plane of the beams were prevented at midspan and at the supports.

3.2.4 Classification and combined slenderness λ_c

Rotation capacity R here is relevant to local buckling, and so depends on the slendernesses of the steel web and compression(bottom) flange. The limitations of slenderness for flange and web are prescribed independently of each other in specifications of various codes [9, 1]. Obviously, flange is restrained by web and, vice versa, the web is restrained by flanges, and therefore an independent slenderness is not reasonable in assessment of the rotation capacity. However, theoretical and experimental backgrounds for their interaction are not necessarily clear.

In Eurocodes 3 and 4 [77, 1], the web slenderness relevant to a Class 2 section,

λ_w, is defined as

$$\lambda_w = \alpha d/w\epsilon \tag{3.9}$$

where

- αd is the depth of web in compression(Fig.3.6).
- w is the thickness of web.
- $\epsilon = \sqrt{235/f_y}$ is the material correction factor.
- f_y is the yield strength of the steel in N/mm^2 units.

For Class 2 webs, the slenderness limits given in the Eurocodes [77, 1] reduce as α increases as

$$for \quad \alpha = 0.5, \quad 36 \leq \alpha d/w\epsilon \leq 41.2$$

and

$$for \quad \alpha = 1.0, \quad 33 \leq \alpha d/w\epsilon \leq 38$$

On the other hand, slenderness of welded flanges differs from that of rolled flanges in the Eurocodes. For welded flanges, the slenderness λ_f is by

$$\lambda_f = c/t\epsilon \tag{3.10}$$

and for rolled flanges, the Eurocodes use

$$\lambda_f = b_f/t\epsilon \tag{3.11}$$

- c is the flange outstand for welded cross-sections (Fig.3.6).
- b_f is the breadth of the flanges.
- t is the thickness of the flanges

In the subsequent work (for simplicity), the outstand c is assumed to be $0.45b_f$. so that the expression $c/t\epsilon$ (equation 3.10) can be used for all flanges.

For Class 2 flanges, the slenderness limits given in the Eurocodes are

$$9 \leq c/t\epsilon \leq 10$$

Fig.3.7 shows the flange and web slendernesses of the relevant cross-sections of the 49 beams used in determination of K_1. The boundaries of Classes of cross sections are also shown.

In a study of local buckling in steel beams [75], Kuhlmann found that the rotation capacity, R depends mainly on the slenderness of the compression flange, but also on two other variables; the moment gradient and the slenderness of the web.

For a given member, R decreases as the beam length L_c increases. This effect has little influence on K_1, because of the factor L_c in equation 3.8.

The influence from the web, was also studied. The relevant parameter was taken [75] as a stiffness based on the web acting as a torsional restraint for the flange. Almost all of the 43 webs for steel beams used to determine K_1 were in Class 1 (plastic) according to the classification of draft Eurocodes 3 and 4, so that the webs restrained local buckling of the flanges. However, in composite beams, the Class of a section is usually governed by the web, not the flange, and the conventional web slenderness, λ_w $(\alpha d/w\epsilon)$ is more relevant, so is used hereafter.

To find expressions for K_1 and K_2, as functions of slendernesses of both the compression flange and the steel web, a combined slenderness λ_c is defined, which is the geometric mean of the web and flange slendernesses, weighted according to the relative areas of the web (A_w) and the compression (A_f):

$$\lambda_c = [(\frac{\alpha d}{w\epsilon}\frac{3A_w}{A})(\frac{c}{t\epsilon}\frac{3A_f}{A})]^{1/2} \tag{3.12}$$

where A ie the area of the steel cross section.

3.3 Simulation of inelastic local buckling of composite cantilevers

3.3.1 Computer simulation of inelastic local buckling for cantilevers

For continuous composite beams, local buckling normally occurs at the hogging regions near the internal supports with a half-wavelength of about h/2 (h is the overall depth of the steel section). As most test data are related to the moment rotation curves of composite cantilevers, a computer program SCC was developed to simulate the local buckling characteristic of Class 2 composite cantilevers.

The realistic moment-curvature relationships of composite cross-sections are calculated based on the following assumptions:

1. Plane sections remain plane.

2. No slip occurs at the steel-concrete interface.

3. Materials obey the simplified constitutive stress-strain curves given in Fig.3.4.

4. In hogging bending, concrete is assumed to be fully cracked and tension stiffening is ignored.

The procedures for determining the hogging moment-curvature relationship are similar to those described in [15]. An initial curvature Φ is assumed, then the strains ϵ throughout the cross-section can be calculated with a trial position for the neutral axis. The longitudinal stress σ_s at any position in the steel section and the longitudinal stress σ_r in the reinforcement can be obtained from the material stress- strain curves corresponding to strain distribution. The neutral axis position is iterated until axial equilibrium is reached (for pure bending). Then the moment is calculated by integration of stress over the cross section. By increment of curvature Φ, a full set of hogging moment-curvature curves is obtained.

The moment-curvature curve is modified with K_1 and K_2, including the effect of local buckling, as shown in Fig.3.5. The curve is divided into three pieces corresponding to three stages, described as follows;

1. Pre-plastic stage: the inelastic moment-curvature curve OAB (Fig.3.5) for the cracked section in the cantilever and the values of M_p and Φ_{pe} are found as explained in the previous sections. End rotations are found by intergration of these curvatures for end loads P up to a limit given by

$$P_p = M_p/(L_c - h/4) \tag{3.13}$$

When the load reaches P_p, the curvatures along length OF of the cantilever (Fig.3.3) correspond to those along curve GF in Fig.3.5, because the maximum bending moment at the support exceeds M_p (as it always does in tests on Class 2 sections).

2. Plastic buckling stage: this is assumed to occur at constant P_p(piece AC in Fig.3.5), and causes an additional inelastic rotation, concentrated at point $x = h/4$, given by

$$\theta_{i2} = (K_1 - K_3)\Phi_{pe}h/2 \tag{3.14}$$

3. Post-buckling stage: the load is assumed to fall from P_p to a value μP_p, where $0.8 \leq \mu \leq 1.0$. This has two effects. One is elastic rotation recovery along the whole of length L_c, causing a change in end rotation given by

$$\theta_{e3} = -(1 - \mu)P_p L_c^2/EI_{cr} \tag{3.15}$$

The other is the inelastic curvature along the length OF (Fig.3.3), causing an additional inelastic rotation

$$\theta_{i3} = 5(1 - \mu)(K_2 - K_1 + 0.2)\Phi_{pe}h/2 \tag{3.16}$$

Curvature line CD in Fig.3.5 corresponds to this post-buckling stage. The effect of elastic rotation recovery corresponds to the curvature line CH. When the load P drops to 0.8 P_p, the value of θ_{i3} corresponds to curvature DH (Fig.3.5) along length h/2, where P_p is the value of the load when the maximum moment at the support equals to M_p.

3.3.2 Determination of K_1 and K_2

Determination of K_1 is based on test data of 49 steel and composite cantilevers. Table 3.1 gives the relevant parameters of the six composite double cantilevers [23]. The relevant parameters of the other 43 steel simply-supported beams [75, 74, 76] are given in Tables 3.2, 3.3 and 3.4.

For specimens reported in [75], [74] and [76], K_1 is calculated from the reported rotation capacity R, using equation 3.8. For specimens reported in [34], K_1 is calculated by trial and error to trace the reported moment rotation curves, following the three stages as described in the previous section.

Fig.3.8 illustrates computed and observed moment-rotation curves for the cantilevers tested by Climenhaga [23]. The solid lines are for the computer simulation, and the dashed lines are from the test results. There are two reported moment rotation curves for both ends in a double cantilever test, but only the one with a greater rotation has has been used.

The calculated values of λ_c are plotted against K_1 in Fig.3.9 to enable an expression for K_1 to be deduced. The mean line found by a regression of K_1 on the combined slenderness λ_c is also shown and the characteristic (5% fractile) line (the lower solid line) is

$$K_1 = 134 - 7.29\lambda_c \tag{3.17}$$

The value of K_2 is also based on tests. Trial and error calculation has been carried out, based on the test specimens where a sufficient length of the falling branch of $M - \theta$ curves has been reported. Relevant results are from double cantilever tests reported by Climenhaga [23]. Computed moment rotation curves are compared with the moment rotation curves from the tests (Fig.3.8). It was concluded that K_2 could safely be taken as $3.1K_1$, or

$$K_2 = 415 - 22.5\lambda_c \tag{3.18}$$

These two expressions for K_1 and K_2 are used in the subsequent analysis of the two span continuous composite beams.

3.3.3 Scope and validation of the computer program:SCC

A computer program (SCC) was written to simulate moment rotation behaviour of a composite cantilever with Class 2 (or 1) cross section.

Elasto-plastic moment curvature curves are calculated, following realistic stress-strain relationships. The effect of residual stresses is included.

The input includes dimensions of the cross section, the beam length, the yield stresses of the steel and reinforcement, and the relevant parameter of residual stress.

K_1 and K_2 are required to be input to give the modified moment rotation curves, affected by local buckling.

The output is a full length of moment rotation curve of the cantilever.

All input and output are in N, mm, radian units.

3.4 Summary

The moment rotation behaviour of hogging regions of a continuous composite beam is modelled by a composite cantilever, using the realistic inelastic moment-curvature $(M - \Phi)$ curves.

The moment-curvature characteristic at the critical section is modified by curvature ratio parameters K_1, K_2 and K_3, based on the test data from steel and composite cantilevers, with local buckling.

A combined slenderness λ_c is defined, leading to expressions for K_1 and K_2. Trial and error computer simulations are used to trace the reported full length of the moment rotation curves.

The characteristic values of K_1 and K_2 based on regressions of test results are found in terms of the combined slenderness λ_c, and are subsequently used in the parametrical studies of the Class 2 continuous composite beams.

Table 3.1: Details of composite cantilevers

specimen	b_f mm	t_f mm	h_w mm	t_w mm	A_{r1} N/mm^2	A_{r2} N/mm^2	f_{fy} N/mm^2	L mm
SB2	134.9	8.2	184.9	6.1	486	486	315	1880
SB3	134.2	9.5	184.9	6.1	552	552	293	1880
SB8	134.9	8.2	184.9	6.1	486	486	315	1270
SB9	134.2	9.5	184.9	6.1	552	552	293	1270
HB40	134.2	9.5	184.9	6.1	784	428	293	1270
HB41	101.5	6.7	241.2	5.9	495	63	323	1270

Table 3.2: Details of specimens

specimen	b_f mm	t_f mm	h_w mm	t_w mm	f_{fy} N/mm^2	f_{wy} N/mm^2	L mm	R
A-1	203.5	10.8	228.9	7.7	285	309	1740	11.8
A-2	170.0	10.8	228.9	7.7	285	309	1473	13.6
B-1	102.6	5.3	189.6	4.5	373	396	777	2.9
B-2	73.9	5.3	189.6	4.5	373	396	518	10.4
B-3	86.1	5.3	189.6	4.5	373	396	627	6.7
B-4	94.0	5.3	189.6	4.5	373	396	699	3.4
B-5	96.8	5.3	189.6	4.5	373	396	724	3.2
C-1	101.9	5.3	239.9	4.6	373	352	686	4.2
C-2	73.7	5.3	239.9	4.6	373	352	480	13.7
C-3	85.9	5.3	239.9	4.6	373	352	584	8.0
C-4	93.5	5.3	239.9	4.6	373	352	648	4.2
C-5	89.9	5.3	239.9	4.6	373	352	620	6.5

Table 3.3: Details of specimens

specimen	f mm	t_f mm	h_w mm	t_w mm	f_{fy} N/mm^2	f_{wy} N/mm^2	L mm	R
9A2	146	9.03	236	6.35	340	358	1830	1.7
2F4	145	10.57	231	6.82	285	329	1830	5.4
4S5	149	8.56	235	6.78	340	358	915	11.1
6S6	140	10.77	231	6.76	288	329	915	14.9
5S7	149	8.44	234	6.78	294	300	915	14.8
8W9	154	9.83	140	7.44	313	300	1830	8.6
3F12	106	7.05	288	5.85	332	388	1830	2.1

Table 3.4: Details of specimens

specimen	b_f mm	t_f mm	h_w mm	t_w mm	f_{fy} N/mm^2	f_{wy} N/mm^2	L mm	R
1	141	8	278	5	236	217	1702	8.0
2	150	8	278	5	236	217	1852	7.0
3	160	8.5	277	5.5	449	217	2000	1.0
4	160	8	261	6	287	260	1270	12.7
5	160	8	258	5	287	252	1318	8.6
6	160	8	259	4	287	252	1358	4.6
7	160	8	280	5	287	252	898	13.5
8	160	8	280	5	287	252	1098	11.5
9	160	8	279	5	287	252	1299	7.8
10	170	8	279	5	236	217	1401	5.5
11	182	8	278	5.5	236	217	1501	8.9
12	190	8	278	5.5	236	217	1700	7.6
13	141	10.2	239.6	5.5	333	709	1500	5.1
14	150	10	239	5.5	333	709	1600	3.8
15	160	10.4	237.2	5.5	333	709	1754	3.6
16	160	10.2	148.6	5.5	333	709	1152	10.5
17	160	10	200	5.5	333	709	1102	9.5
18	161	10	279	5.5	333	349	1050	6.6
19	160	10	278	6	333	349	1000	12.0
20	160	10	279	6	333	349	1201	8.7
21	160	10	279	6	333	349	1402	7.2
22	170	10	279	6	333	349	1203	10.0
23	183	10.3	278.4	6	333	349	1250	6.7
24	190	10.2	278.6	6	333	349	1350	5.2

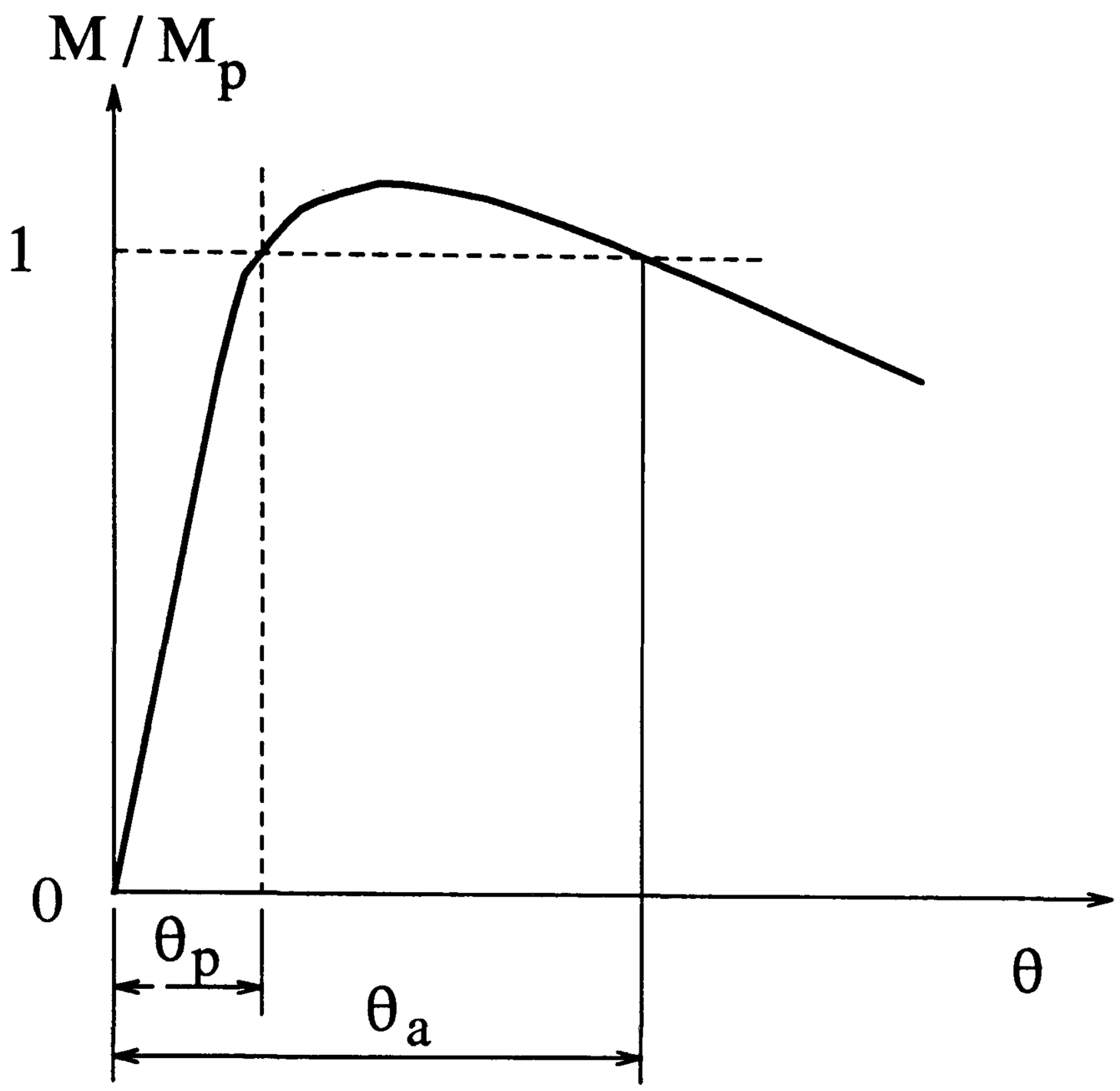

Figure 3.1: Moment rotation curve of a Class 2 beam

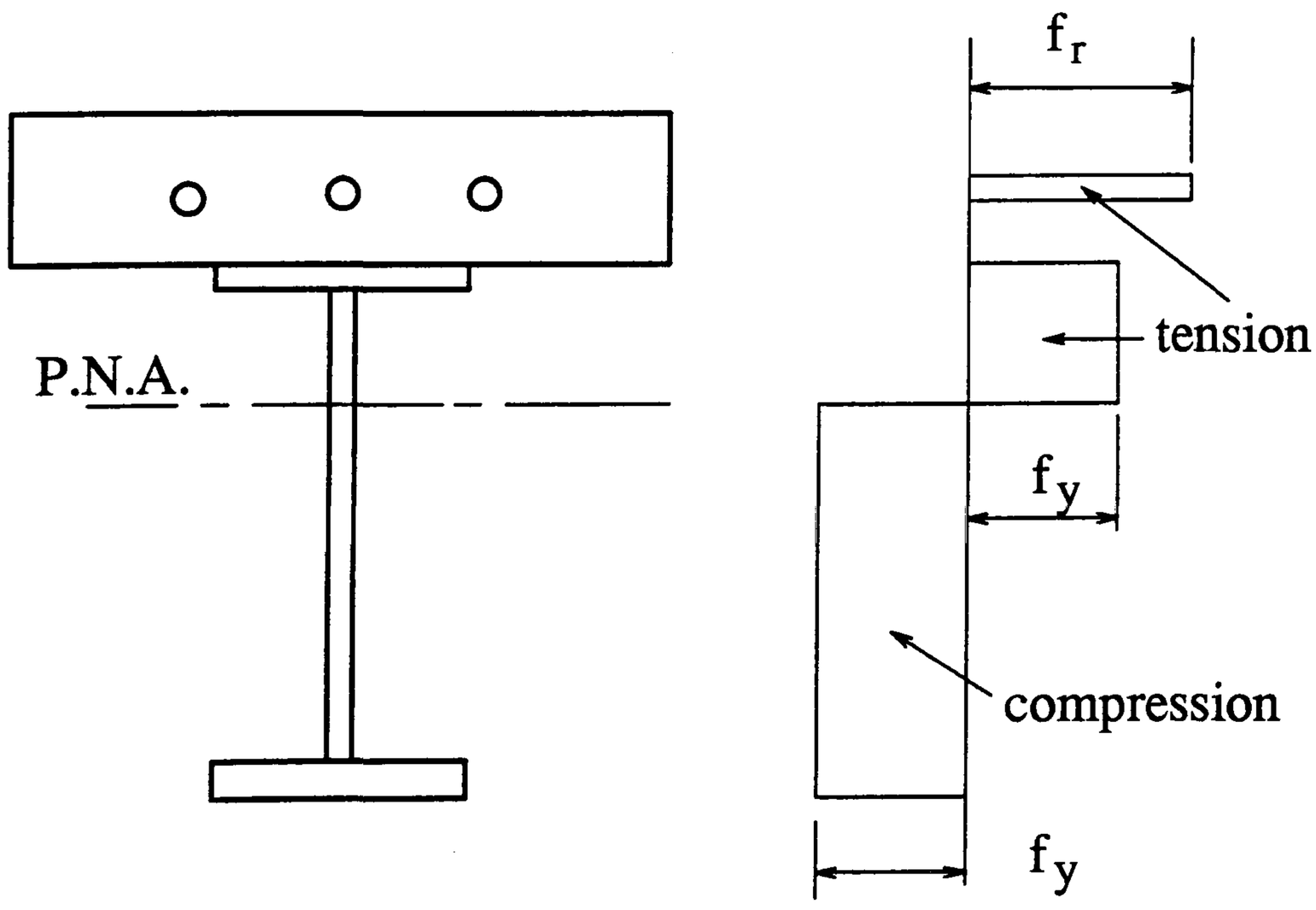

Figure 3.2: Rectangular stress blocks: hogging plastic moment of resistance

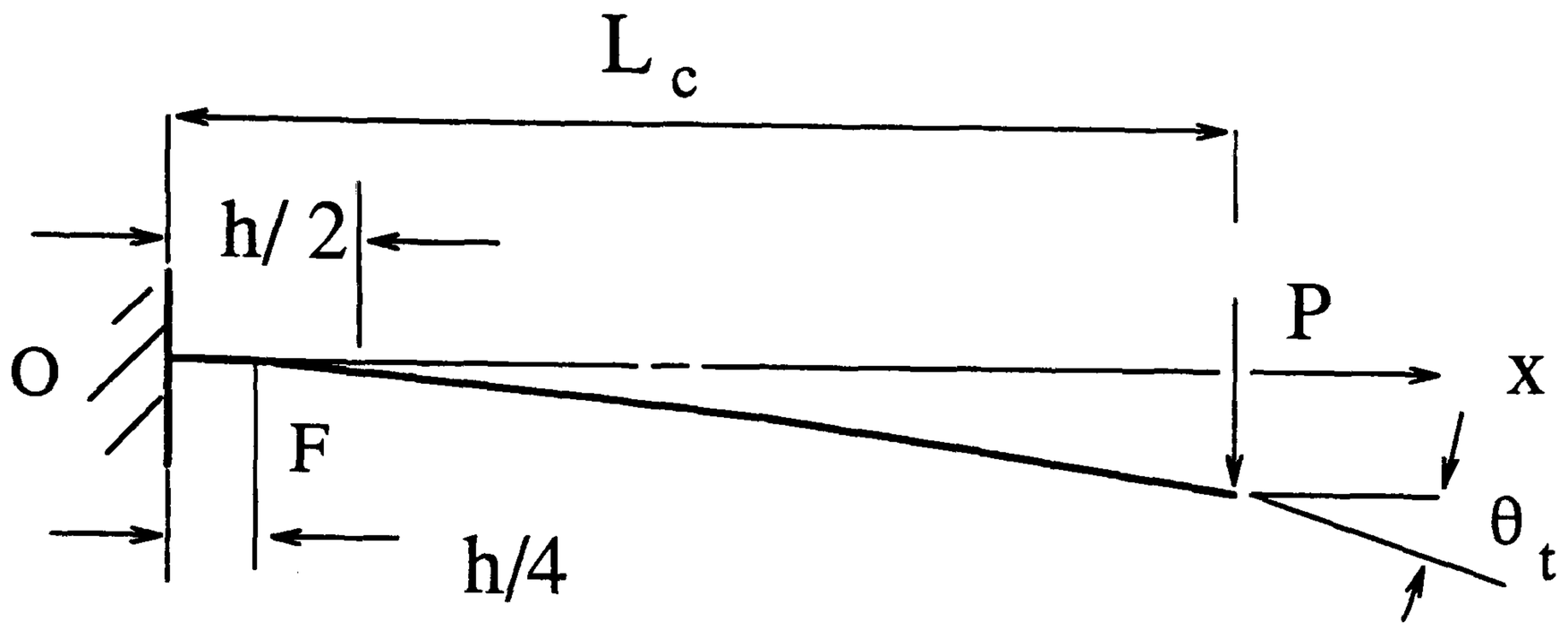

Figure 3.3: Composite cantilever with local buckling at x = h/4

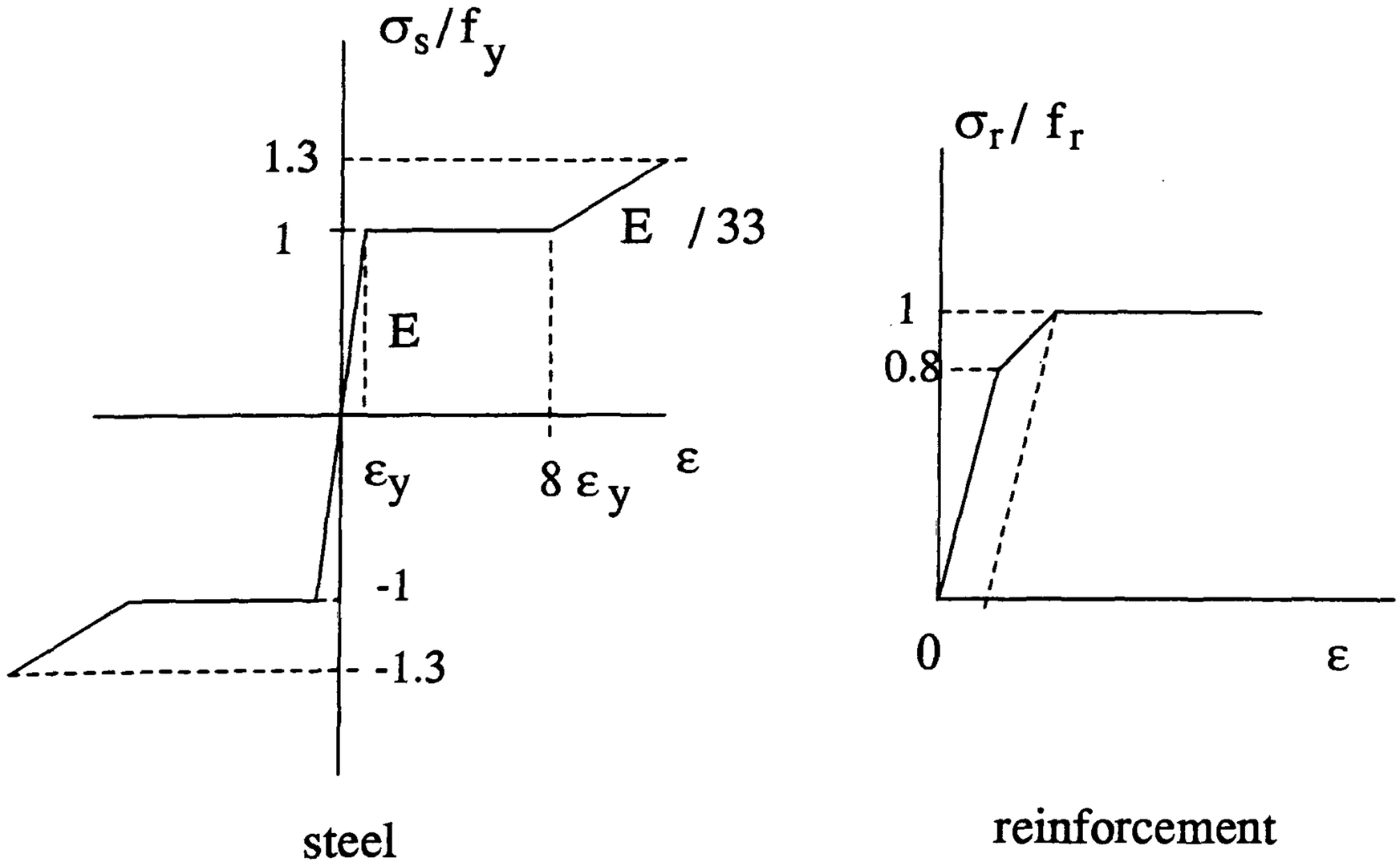

Figure 3.4: Stress-strain relationship of steel and reinforcement

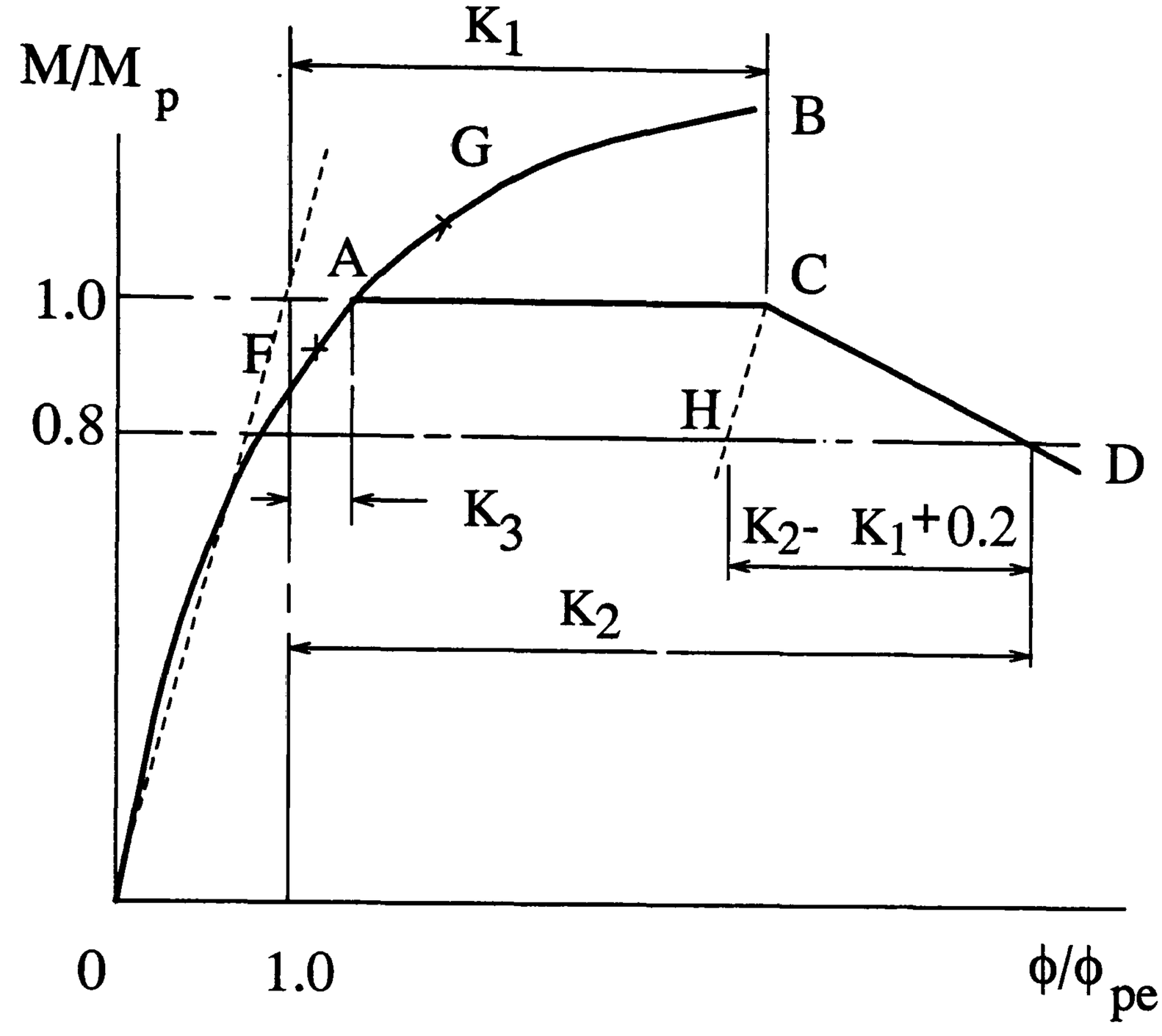

Figure 3.5: Moment curvature curve of inelastic buckling

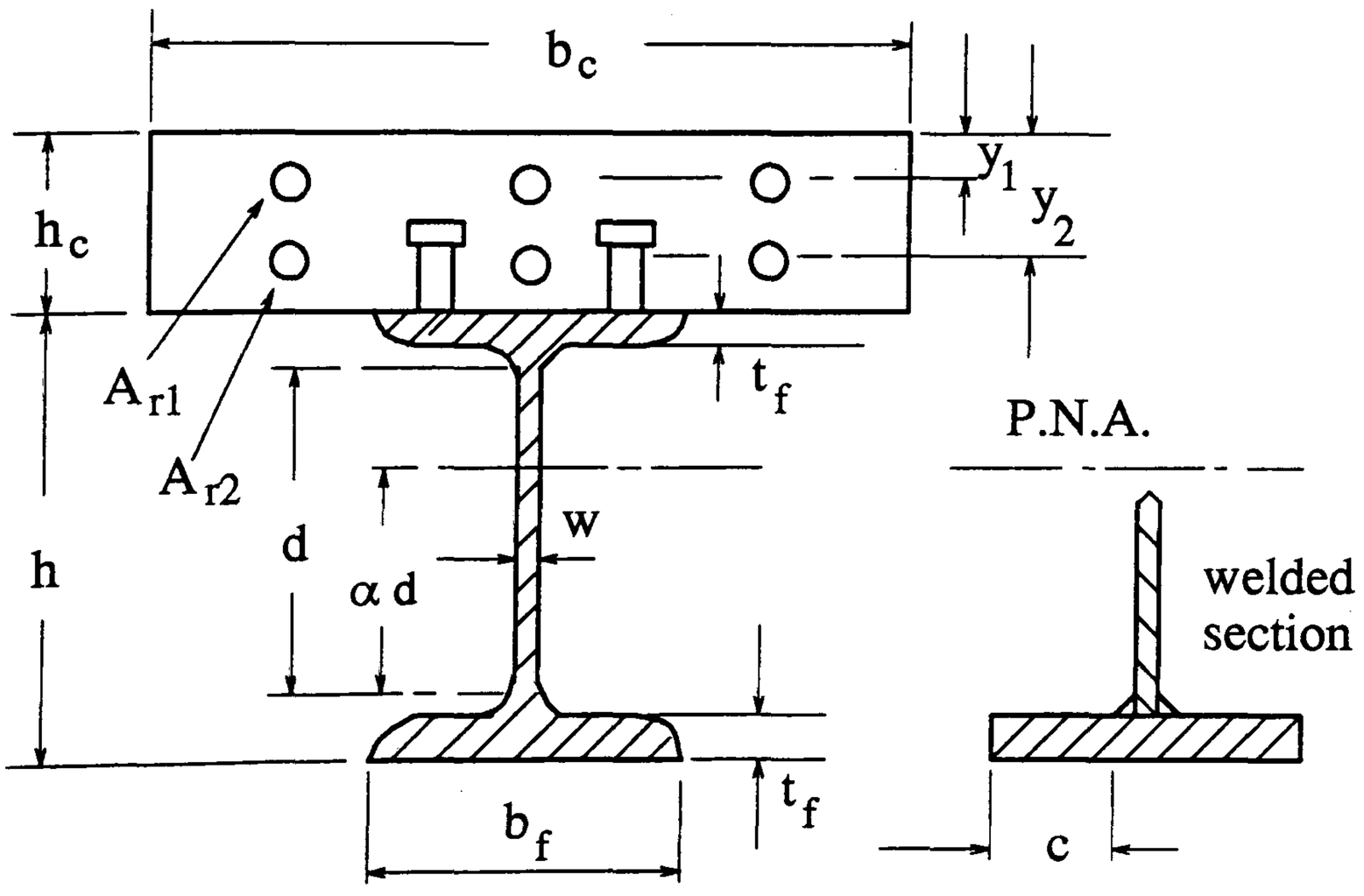

Figure 3.6: Notation of cross-sections

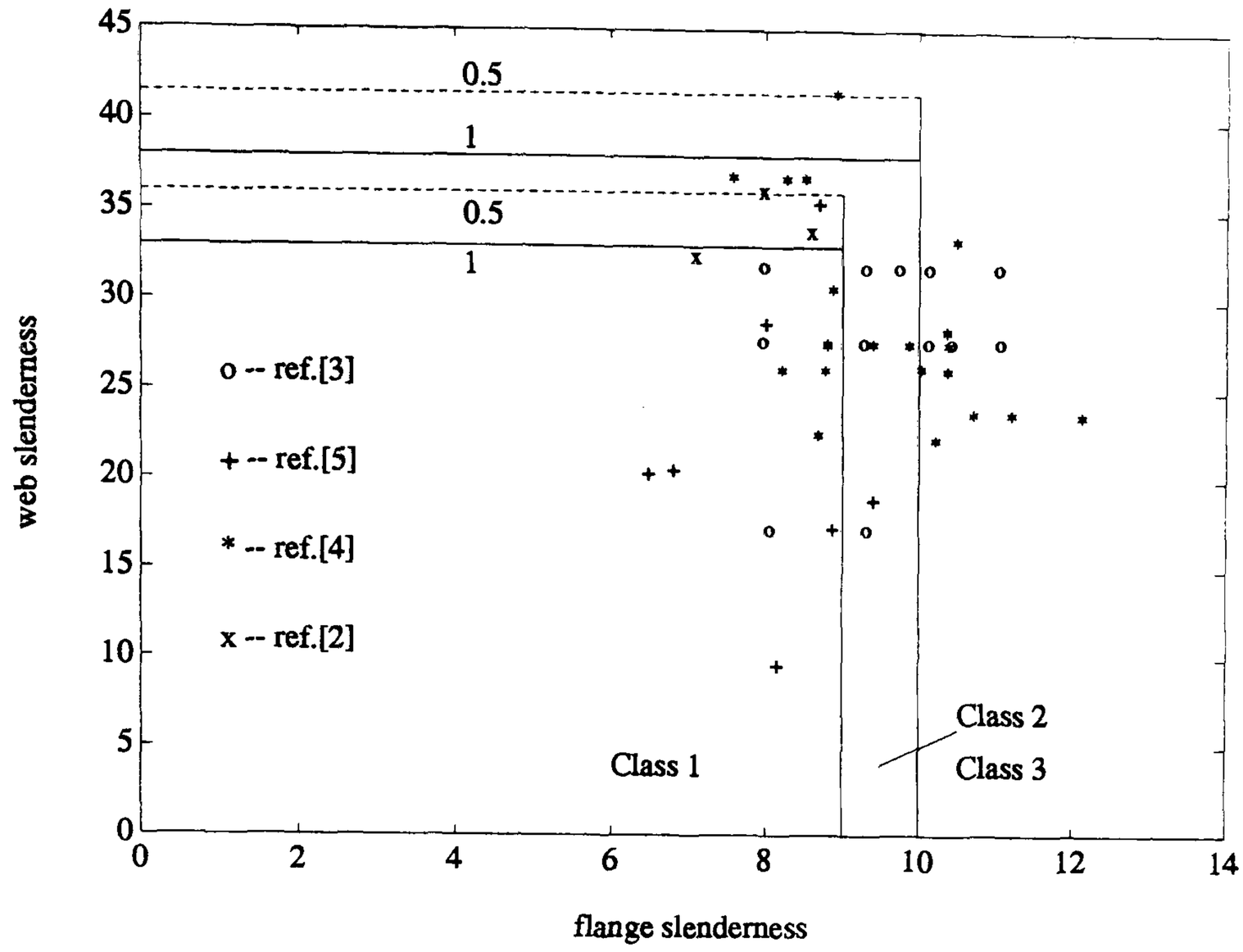

Figure 3.7: Classification to draft Eurocode 4 of sections tested

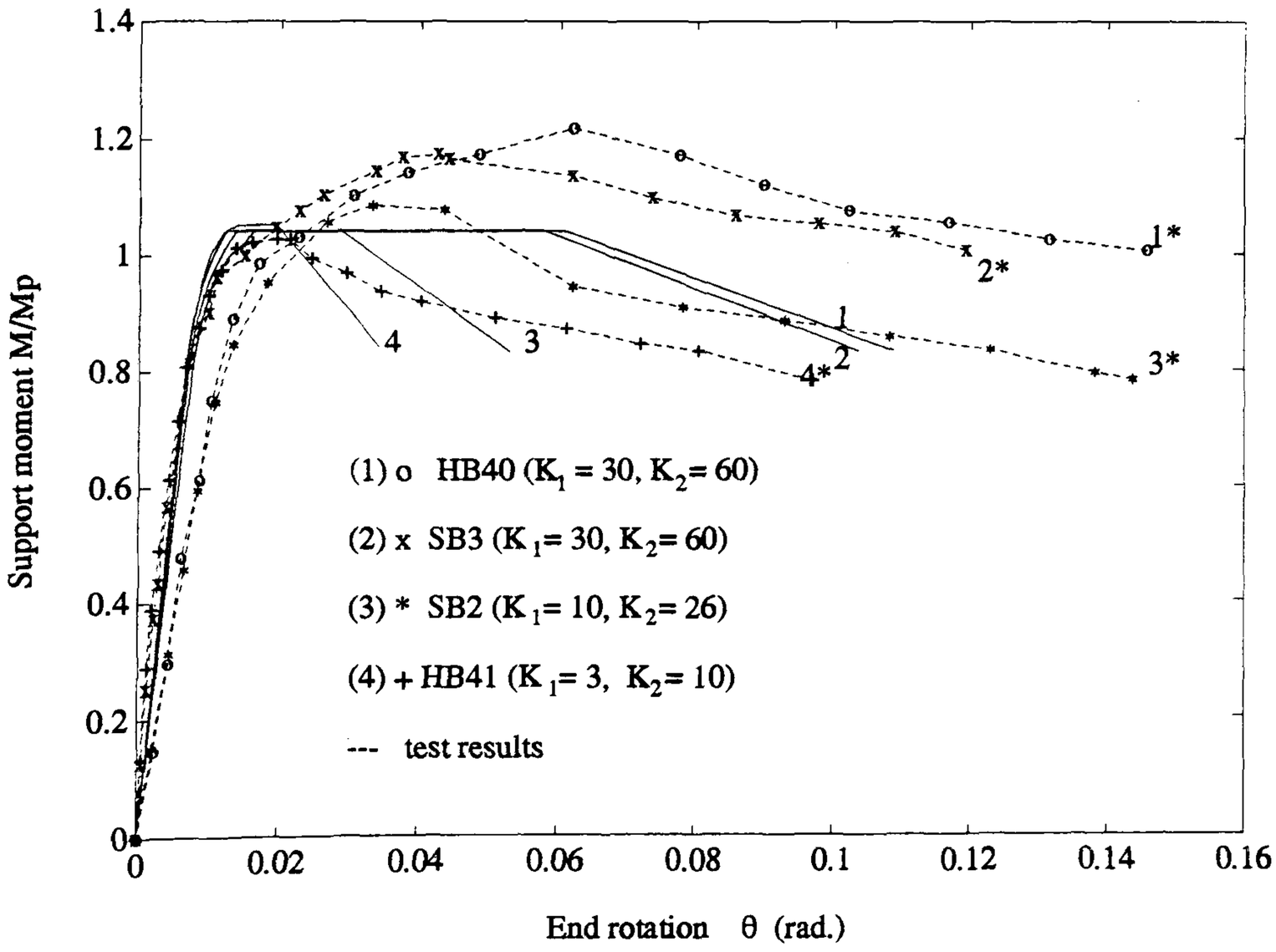

Figure 3.8: Computed and observed moment-rotation curves for cantilevers

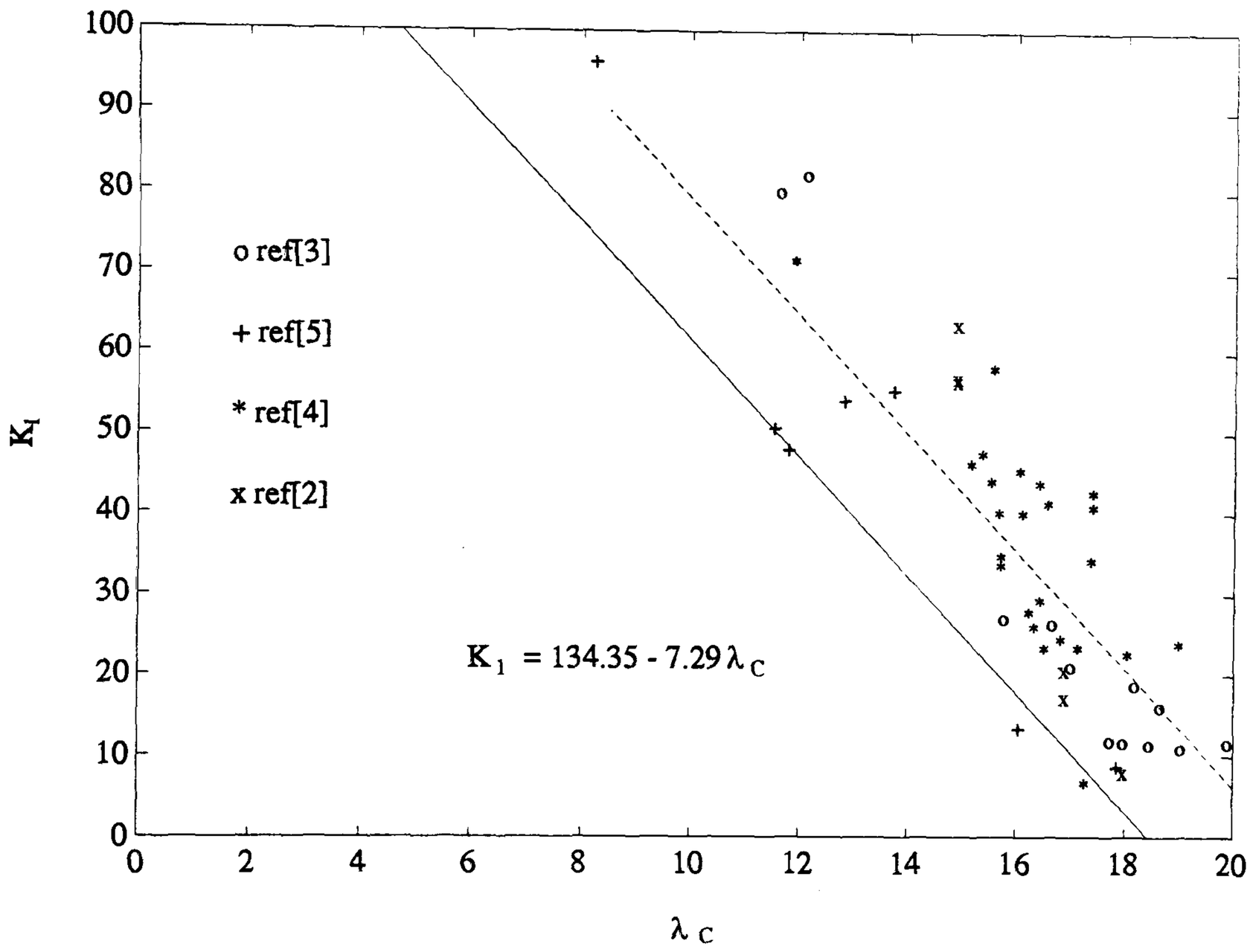

Figure 3.9: Characteristic value for K_1, in terms of slenderness λ_c

Chapter 4

Moment redistribution in Class 2 continuous composite beams

4.1 Introduction

For continuous composite beams of uniform cross section, economic design can be achieved where a quasi-elastic analysis is used, which is based on an elastic global analysis, with redistribution of moments from internal supports to midspan regions. When lateral buckling of the bottom flange of the beams is prevented, the amount of redistribution that can be allowed is limited by local buckling at critical cross-sections.

In chapter 3, local buckling of the hogging regions of a continuous composite beam is modelled by moment curvature characteristics of a cantilever, modified by K_1 and K_2, and test based expressions for K_1 and K_2, in terms of a combined slenderness λ_c.

Draft EC4: Part 1 [1] allows up to 30% redistribution for Class 2 beams at the ultimate limit state, when uncracked flexural stiffnesses (EI_u) are assumed throughout the beam length in the quasi-elastic analysis, and so does BS5950: Part 3 [9]. Besides, EC4 also allows 10% moment redistributed from midspan regions to internal supports for Class 2 beams, which can be useful when one of the adjacent spans carries minimum loading.

In this chapter, a numerical analysis is carried out to assess the moment redistribution that occurs in Class 2 composite beams in comparison with the limit proposed by draft Eurocode 4. The analysis includes effects of non-linear material properties, residual stresses and local buckling, but excludes the effects of initial imperfections, shrinkage and slip, as well as lateral buckling of the bottom flange, so that the scope of the research is limited to the beams with full shear connections and free of lateral buckling. Slip will increases rotation capacity R, and so will it be benefit to the moment redistribution, but it will also decrease the full plastic

moment resistance. Therefore, the results are capable of being used for the beams with partial shear connections, when the full plastic moment M_p is replaced by a partial plastic moment M_p^i. The effect of partial shear connections on the ultimate moment strength is studied by Molenstra [78] and it is beyond the scope of the present research.

A non-linear computer program MRTSCB was developed to simulate the behavior of two-span continuous composite beams. The program was written by the present author, based on program BAULS (described in the Ph.D thesis by C.K.R. Fan [15] and [33]). The treatments of compatibility and equilibrium criteria are the same as those in program BAULS. Program BAULS is for analysis of Class 3 continuous composite beams, and local buckling occurs when the maximum hogging moment reaches to the yielding moment, so that there are two stages in the whole analysis: pre-buckling elastic and post buckling. However, for Class 2 beams, local buckling does not occur below the plastic moment at critical sections. The pre-buckling plasticity makes the numerical simulation procedures more complex than those for Class 3 beams.

The realistic moment curvature curves are used, with local buckling introduced by K_1 and K_2, as described in Fig.3.5. Most of the work has been described in the paper by Johnson and Chen [79]. Instructions for using program MRTSCB (moment redistribution in two-span composite beams) are enclosed in Appendix A.

4.2 Simulation of two-span continuous composite beams

4.2.1 Mathematical model and method of analysis

For a two-span continuous beam subject to a uniformly distributed loading as shown in Fig.4.1, the bending moment at the internal support is indeterminate. The computer simulation divided into three stages: pre-plastic, pre-buckling plastic and post-buckling. These stages correspond to the stages described for cantilevers. The iterative technique is used based on the moment-curvature characteristic, equilibrium and compatibility relevant to the above three stages as follows.

Pre-plastic stage

Assume the geometry of the beam and the design load w_{d1} , w_{d2} on span L_1 and L_2 are known. At the pre-plastic stage, the hogging moments along the beam except in the internal support region are smaller than M_p. An initial load factor λ (lower than the expected λ_p is guessed, where λ_p is load factor at which the hogging plastic moment is first reached at location E shown in Fig.4.1), then all the loads λw_{d1} and λw_{d2} on the beam are known. The moment at the internal support M_B is guessed(less than M_p), so that the bending moment distribution along the beam is determined.

The curvature distribution in the hogging regions of the beam can be calculated in accordance with the moment-curvature curve shown as the portion OAB in Fig.3.5. The procedures to determine the sagging moment-curvature characteristics are the same as those for the hogging regions, except that reinforcement in the slab is ignored and compression in the slab is included. The full set of sagging moment-curvature curve is obtained, finding the neutral axis position of the cross section by iteration as in [15].

The slope at any sections of the beam can be calculated by integration of the curvature along the beam length. The compatible solution is obtained by satisfying condition of the slope continuity at the internal support. Let α_1 and α_2 be the two slopes at each side of the internal support (Fig.4.2), then the compatibility equation at the internal support is

$$\alpha_1 = \alpha_2 \tag{4.1}$$

where α_1 and α_2 are derived as follows [15]

$$\alpha_1 = [\int_0^{L_{o1}} \Phi'(L_1 - x)dx - \int_{L_{o1}}^{L_1} \Phi(L_1 - x)dx]/L_1 \tag{4.2}$$

$$\alpha_2 = [\int_{L_{o2}}^{L_2} \Phi(L_2 - x)dx - \int_0^{L_{o2}} \Phi'(L_2 - x)dx]/L_2 \tag{4.3}$$

Referring to Fig.4.2, where

- L_1 and L_2 are the two span lengths (Fig.4.1).

- L_{o1} and L_{o2} are the length of hoggings in spans L_1 and L_2 respectively.

- $\Phi^{'}$ and Φ are hogging and sagging curvatures respectively.

At the support section, presence of vertical stiffeners (Fig.4.1) not only stops web crippling due to bearing action but also prevent local buckling at that position. Local buckling usually occurs at the side with the less steep moment gradient near the internal support, so that the moment at location E, distance h/4 from the support (Fig.4.1) is checked. If the moment at E is smaller than M_p, the multiple λ is then modified, and the whole procedure repeats until a compatible solution ($\alpha_1 = \alpha_2$) is found. The iteration continues till the moment at E reaches to M_p, at which the load factor is the plastic load factor λ_p.

Pre-buckling plastic stage of the model

Fig4.3 illustrates the loading and unloading of the cross section owing to the moment redistribution in a continuous beam. It is assumed that a plastic hinge, resulting from plastic deformation and local buckling, occurs at point E (Fig.4.3). If λ ($\lambda > \lambda_p$) is increased by $\Delta\lambda$, then in the hogging regions, the cross-sections subject to increasing loading will follow the moment-curvature path 1 (Fig.4.3), the plastic rotation at E follows path 2, and the unloading cross-sections follow a series of parallel paths 3, while the hogging moment at E remains constant at M_p. The moment diagram is then fully defined. At this stage, except for the presence of the plastic hinge at E on the right side(with less steeper moment gradient), everything is the same as that in the left side.

The compatibility condition at the support is similar to equation 4.1. However because of presence of the plastic hinge at E, a plastic rotation θ_i is induced. So that at this stage, the two slopes at each side of the support, α_1 and α_2 (Fig.4.2) are derived by

$$\alpha_1 = [\int_{L_{o1}}^{L_1} \Phi(L_1 - x)dx - \int_0^{L_{o1}} \Phi^{'}(L_1 - x)dx]/L_1 \tag{4.4}$$

and

$$\alpha_2 = [\int_0^{L_{o1}} \Phi'(L_2 - x)dx - \int_{L_{o2}}^{L_2} \Phi(L_2 - x)dx + \theta_i(L_2 - 0.5h)]/L_2 \qquad (4.5)$$

where

- θ_i is the concertrated plastic rotation at E.
- h is the overall depth of the steel beam.
- all other parameters are the same as those in the previous stage.

The equations 4.4, 4.5 are similar to the equations 4.2 and 4.3 for the pre-plastic stage except that a concentrated plastic rotation is introduced at location E in equation 4.5. The concentrated plastic rotation is assumed at the buckling side, which corresponds to θ_i in equation 4.5. Initially, let θ_i be one tenth of the maximum plastic rotation θ_a, which is limited by local buckling, where

$$\theta_a = (K_1 - K_3)\Phi_{pe}h/2 \qquad (4.6)$$

where K_1, K_3, and Φ_{pe} are described in the previous chapter (Fig.3.5).

If the compatibility condition (equation 4.1) is not satisfied, θ_i is increased by $\Delta\theta$, until the compatible solution is found ($\alpha_1 = \alpha_2$). Then λ ($\lambda > \lambda_p$) gains another $\Delta\lambda$, while the moment at E remains M_p, and the whole process repeats until the concentrated plastic rotation θ_i at E is equal to θ_a. This is the end of the stage. The current value of λ is output as λ_b.

Post buckling stage of the model

In this stage, load still increases, but the moment at the point E(shown in Fig.4.3) drops to μM_p (where μ is guessed value between 1.0 and 0.8). Let the moment at E drop to $(1 - \mu)M_p$. At $M_E = \mu M_p$, the concentrated rotation is increased by $\Delta\theta_i$ $= 5(1 - \mu)$ $(K_2 + 0.2 - K_1)\Phi_{pe}h/2$ (θ_{i3}in equation 3.16). By fixing $M_E = \mu M_p$ at location E, for any $\lambda = \lambda_b + \Delta\lambda$, the bending moment diagram is determined. All curvatures are found as in stage 2. Iteration on λ continues until the incompatibility of rotation vanishes. Then a solution for λ ($\lambda > \lambda_b$) is found. Next the moment at point E is decreased by a further amount ΔM, so that $M_E = \mu M_p$, where μ is

an updated value lower than the previous value. The new plastic rotation $\Delta\theta_i$ is obtained, and the whole process repeats.

The iteration stops at the failure load factor, λ_f, when any of the following first occurs:

— μ falls to 0.8

— a midspan region reaches the end of its $M - \Phi$ curve or

— the iteration for new load increment fails to converge.

K_3 is calculated for each cross section from moment curvature curves. If $K_1 \leq K_3$, at the critical section, the curve OFGB in Fig.3.5 passes to the right of point C. There is then no value λ_p corresponding to the intersection of the curve with line CD.

4.2.2 Design ultimate loads by Eurocode 4

The design ultimate loads w_{d1} and w_{d2} for a two-span beam as shown in Fig.4.1 are calculated in accordance with clause 4.5.3.4 (Table 4.3) in draft Eurocode 4 [1]. These are loads then used as references in the numerical analysis. The loads applied are represented by $w_1 = \lambda w_{d1}$ and $w_2 = \lambda w_{d2}$, where λ is a load factor. The "uncracked" flexural stiffness EI_u is assumed to be uniform throughout the beam, in calculation of the design load.

Let the characteristic uniform loads for both spans be g(dead load) and q (imposed load) per unit length. Typically, the partial coefficients γ_f are taken as 1.35 (γ_g) and 1.5 (γ_q) for dead and imposed loads respectively in accordance with draft Eurocode 4. Usually, the ratio of q/g varies between 1.0 and 3.0. In the case of propped construction, the ratio is chosen (usually, $w_2 = w_1$). The load is then scaled so that the elastic global analysis of the beam gives a bending moment $M_p/0.7$ at the internal support (B in Fig.4.1). Redistribution of this moment, as allowed by Eurocode 4, leaves a moment M_p at B, which the beam can just resist. Therefore, the design ultimate load w_d is

$$w_d = \frac{8}{0.7} \frac{M_p}{L_1^3 + L_2^3} (L_1 + L_2) \tag{4.7}$$

where M_p is the hogging bending moment resistance of the beam.

This design ultimate load w_d is used in the subsequent parametric studies. An

elastic analysis is done with $w_2 = w_d$ on span L_2 (representing 1.35 g + 1.5 q) and $w_1 = w_d$ on span L_1 (representing a minimum load 1.35g), giving moment M_B at B. If this exceeds M_p, it can be redistributed. If it is less than M_p, it is increased either to M_p or by 10 %, whichever is less, to represent the redistribution from midspan to the internal support allowed for Class 2 beams by Eurocode 4:Part 1, and corresponding reductions are made to the sagging moments in the spans. This is to check the strength of the sagging regions when the hogging bending resistance at the internal support governs the calculation of the ultimate design load w_d.

4.2.3 Material properties and details of beams analysed

The cross-sections used in the numerical analysis are divided into two groups. Group 1 is based on the specimens tested by Climenhaga [34], among which, only two of these sections (HB40,HB41) are unchanged, with the yield stresses of the steel based on the measured yield strength of the steel flange. For the four SB specimens, the yield strength of the steel beams were taken as 335 N/mm^2. The steel cover-plates to the top flanges were replaced by equal areas A_{r1} and A_{r2} (Fig.3.6) of reinforcement with the yield strength $f_y = 460 N/mm^2$, so chosen that the original position of the plastic neutral axis was maintained. For group 2, steel sections are based on the sections in the tests by Kulmann [75], Lukey [74] and Kemp [76]. Values for A_{r1} and A_{r2} were chosen such that the cross sections in the hogging regions are in Class 2. The yield strengths of steel were all taken as 335 N/mm^2, and of reinforcement as 460 N/mm^2.

Dimensions of the twelve cross sections used in the parametric study of two-span continuous composite beams are given in Table 4.1, with notation as in Fig.3.6. The yield strengths, slendernesses of web and flange of the cross sections are given in Table 4.2. The combined slenderness λ_c, and the curvature ratios K_1, K_2 are also listed in Table 4.2. The web and flange slendernesses are plotted in Fig.4.4, which shows that all the cross sections are in or near to Class 2 and extend over the available range of slenderness.

The parabolic-rectangular curve used for concrete is shown in Fig.4.5. The maximum stress and the maximum strain are 0.67 f_{ck} and 0.0035 respectively. The cylinder strengths f_{ck} of the concrete are all taken as 31.5 N/mm^2 in the numerical

analysis. The assumed residual stress distribution in the rolled sections are also shown in Fig.4.5. For each composite section studied, a bi-linear stress-strain curve is used for reinforcement and a tri-linear curve for structural steel. They are all illustrated in Fig.3.4.

4.2.4 Numerical results

Three groups of calculations were carried out. The first group is for beams with equal spans of 10 m. The ratios of span to overall depth $(h + h_c)$ for these beams range from 23.1 to 32.8. The second group of calculations is for beams with unequal span: $L_2 = 1.25\ L_1$. The ratios of the longer span to overall depth are from 23.1 to 40.5. The third group of calculations is for beams with unequal span: $L_2 = 1.6\ L_1$. The ratios of the longer span to overall depth are from 23.9 to 52.5. It is unlikely in design practice that uniform cross sections are used along the length of these beams, so that this group of calculations is only used in analysis of influence from the span ratio.

K_1 and K_2 used in the numerical analysis are given in Table 4.2. The values of M_p and M_p/M_{ps} are given in Table 4.3. The design ultimate loads to Eurocode 4 w and the computed results for both equal and unequal span beams are given in Tables 4.3 and 4.4 and 4.5 respectively. Propped construction was assumed.

4.2.5 Analysis and discussions of results

Load factors λ_p,λ_b, and λ_f

The load factors, λ_b and λ_f are the multiples of the design load w_d when the beams buckle and fail. All the computed values of both λ_b and λ_f exceed 1.0, except that in three situations for cross-sections SB2 and HB41, when the ratio of lengths of spans is 1.6 $(L_2/L_1 = 1.6)$, the multiples (λ_b, and λ_f) are slightly lower than 1.0. However, the mean values of the load factors, even for span ratio of 1.6 $(L_2/L_1 = 1.6)$, are greater than 1.0. In practice, a beam with that span ratio $(L_2/L_1 = 1.6)$ will not be designed having uniform cross-sections everywhere along its length, so that the design method of draft Eurocode 4 is safe for these beams.

For most beams, the load factor λ_b is not influenced by K_2 (except $K_1 \leq K_3$,

therefore the values of λ_b at onset of local buckling also show that the method is not over-conservative.

Fig.4.6 gives a comparison with the results of rigid-plastic global analysis (not allowed in Eurocode 4 for Class 2 beams). λ_f corresponding to the ultimate state of the beams in the non-linear analysis is plotted against the ratios of hogging and sagging moment resistances (M_p/M_{ps}). The relevant ratio w_p/w_d is also plotted, where w_p is the rigid plastic collapse load for the longer span, and w_d is the design load (draft Eurocode 4). The results (w_p/w_d) from the rigid-plastic analysis are greater than the results (λ_f) from the non-linear analysis. This confirms the restriction for Class 2 cross-sections in Eurocode 4.

The influences on the numerical results of several parameters are discussed in the following sections.

Convergency of load factors λ_p,λ_b, and λ_f

In the numerical analysis, increment of the multiples (λ) was taken as 0.001, and a good convergency in the numerical results of λ_p, λ_b, and λ_f has been obtained. The results are not affected by further refinement of the increment.

Effect of ratio of lengths of spans, L_2/L_1

When span ratio (L_2/L_1) increases, λ_b and λ_f decrease in all cases.

The mean values for λ_b are: 1.232 ($L_2/L_1 = 1$); 1.138 ($L_2/L_1 = 1.25$); and 1.058 ($L_2/L_1 = 1.6$). The mean values for λ_f are: 1.295($L_2/L_1 = 1$); 1.166 ($L_2/L_1 = 1.25$); and 1.080 ($L_2/L_1 = 1.6$). Although the lowest values of λ_b and λ_f are found slightly lower than 1.0 (λ_f =0.975 in HB41 when $L_2/L_1 = 1.6$), these results are acceptable, because it is unlikely that for span ratio as high as 1.6, the same cross section would be used in both spans.

Effect of span/depth ratio, $L/(h + h_c)$

For a beam of given cross-section, increasing the spans slightly reduces λ_b and λ_f. The values of λ_p, λ_b and λ_f in tables 4.3, 4.4, 4.5 show that beams of longer spans and with higher span ratio L_2/L_1 tend to decrease slightly. Therefore, in the parametric study, the span/depth ratio of the beams was chosen well above the range used in

practice.

In building structures, practical span/depth ratio ranges from 12 to 25, so that this slight decline of λ_b and λ_f is negligible as compared with the much greater influence on λ_b of the proportions of the composite section.

Effect of factors K_1 and K_2

Since the greater K_1, hence R (rotation capacity) a beam has, the greater moment redistribution there will occur, so that it is expected that λ_b increases with K_1. However, there is only slight evidence of this for the beams of equal span. Table 4.3 shows that all those beams with $\lambda_b \leq 1.15$ have $K_1 \leq 5$, except for section k20 ($K_1 = 3.3 < K_3$, $\lambda_b = 1.245$).

But for unequal spans, there is no clear evidence; for instance:

- beam k20 with $K_1 = 3.3$, $\lambda_b = 1.16$
- beam HB40, with $K_1 = 26$, $\lambda_b = 1.11$

There is also no clear evidence that λ_f increases with K_2. The reason is probably that the effect from K_2 is hidden by influence on the ultimate beam strength of sagging regions. As there are few values of either λ_b or λ_f less than 1.10, failure of Class 2 beam is more influenced by stable inelasticity than it is by buckling.

Effect of ratio of bending resistances, M_p/M_{ps}

For a continuous composite beam with uniform cross section, the hogging bending resistance M_p increases with the effective area of reinforcement at internal supports; and the sagging bending resistance M_{ps} increases with the effective breadth of the slab at midspan.

In Eurocode 4 [1], effective breadths for sagging regions are taken as $0.25 \times 0.8L$, where L is span length. In the numerical analyses, the effective breadth used for sagging is generally less than $0.2L$. Since breadth of slab b_c (Table 4.1) influences only the calculations of the sagging bending resistance, it gives ratios M_p/M_{ps} in the upper part of practical range.

The effective breadth at an internal support does not influence the calculation of M_p, and is typically about 0.65 times that at midspan. The values of reinforcement

ratio ($(A_{r1}+A_{r2})$ /0.65 $b_c h_c$) used in the parametric study ranged from 0.21%(section k23) to 1.77% (section HB40). These are high compared with the practical range in buildings, where slab reinforcement is usually less than 0.5%. This also contributed to the high ratios M_p/M_{ps} (all > 0.5) of the specimens in the parametric study, whereas values of M_p/M_{ps} are usually below 0.4 in practice.

When M_p/M_{ps} increases, it is expected that lowest value of λ_b and λ_f can be found when design of a beam is governed by its bending strength at midspan, M_{ps}, as well as by M_p at the internal support. However, this did not occur in any of the analyses.

In practice, it also cannot occur in two-span beams with uniform section, distributed loads. Let load factors be $\gamma_g = 1.35$ for dead load and $\gamma_q = 1.5$ for imposed load. The strength of the beam governed by both M_p and M_{ps} occurs only when the ratio q/g of imposed to dead load per unit length is exceptionally high.

To check this, the minimum load ($0.25w_1$) was applied to the shorter span of a two-span continuous beam, which corresponds to $q = 2.7g$, and an elastic analysis was carried out. In the analysis, elastic moments at internal supports were increased by up to 10%, as allowed in Eurocode 4 for Class 2 beams. It was found that the design of two-span continuous beams be governed by both hogging and sagging bending strengths occurs when

$$|\frac{M_{ps}}{M_p}| = 0.5[1 - \frac{0.7}{8\nu^2}\frac{(1+\nu^3)}{(1+\nu)} - \frac{2\nu^2}{0.7}\frac{(1+\nu)}{(1+\nu^3)}] \tag{4.8}$$

where ν is span ratio L_2/L_1.

For beams with span ratio $L_2 = 1.25L_1$, M_p/M_{ps} can reach the high value of 0.81 before the bending strength is made of full use at midspan (in design to draft Eurocode 4). For equal spans, the ratio is even higher (1.0).

Therefore, the only potentially unsafe situation is when the effective breadth of a concrete flange at midspan is much less than it is at internal supports (for beams with distributed loads). This will lead values of M_p/M_{ps} high enough for failure of midspan regions to be possible.

To study this, further analyses were carried out, using two cross sections with high (SB3) and low (HB41) values of K_1 and K_2. The span ratio L_2/L_1 is 1.25(L_2 = 12.5 m and L_1 = 10 m). The values of b_c were reduced, hence increasing the

ratios M_p/M_{ps} of the beams. In Fig.4.7, λ_f and λ_b are plotted against b_c. The ratios of M_p/M_{ps} for each value of b_c are also given in the figure. The results show that the rate of reduction of M_p/M_{ps} with b_c is low. The limiting ratio 0.81 is not reached, even with very narrow concrete flanges (600 mm for HB41 and 750 mm for SB3), which corresponds to effective breadths at mid span 0.06 L(HB41) and 0.075 L (SB3) ($< 0.2\ L$, the value given in Eurocode 4).

In the numerical analyses, the mode of failure changed from "hogging moment drops to $0.8M_p$" to "maximum concrete strain at midspan reaches 0.0035", at b_c = 800 mm for SB3, and b_c = 700 mm for HB41. Therefore, for these beams, with uniform distributed loads, the ultimate state strength governed by both hogging and sagging bending resistances (M_p and M_{ps}) occurs when the ratio M_p/M_{ps} is about 0.685 (SB3, $K_1 = 26$) and 0.665 (HB41, $K_1 = 3$).

Values of λ_f drop below 1.0 for HB41 when b_c = 650 mm, which is a highly improbable flange width at the centre of a 10 m span. The beam failed in the sagging mid span. In practice, the effective breadths are at least three times that at mid span ($0.25 \times 0.8\ L$), so that the beam is governed by the hogging bending resistance M_p, and λ_f is above 1.0.

In the numerical studies, the beams were all assumed having uniform cross sections along their length. However, the results are limited to the restriction in draft Eurocode 4 to beams of "uniform depth within each span" (Clause 4.5.3. (2)-(a)).

This restriction can be relaxed in the following conditions; when

- In hogging region, slenderness of the cross-section of the longer span is higher than slenderness of the cross-section of the shorter span so that local buckling still occurs on longer span side(less moment gradient, in uniform distributed loads), or
- Slenderness of the smaller cross section is in Class 2, or
- The smaller of the two hogging bending resistance M_p governs design of the beam.

4.3 Comments on the design method of draft EC4

Design using elastic analysis for continuous beams is related to the bending moment redistribution, which takes account of the effects of cracking of concrete, inelastic behaviour of materials and local buckling of structural steel. When "uncracked" flexural stiffnesses (EI_u) are used throughout the length of a beam, draft EC4 allows up to 30% moment redistribution from internal supports to midspan for Class 2 beams. In design, the required cross-sections are then chosen such that the maximum moments (after moment redistribution) do not exceed the plastic bending resistance at hogging regions, when applied loads w_1 and w_2 are known.

This provision has been shown to be safe for two-span continuous composite beams with Class 2 cross-sections. For continuous beams with uniform cross sections other than two-span, one might expect more onerous loading arrangements, so that a stronger section would be chosen, leading to the provision of more surplus strength than that in two-span beams.

Alternatively, EC4 allows up to 10% moment redistribution by increasing the maximum hogging moments for "uncracked" elastic analysis. This provision is useful when one of a pair of adjacent spans carries its minimum loading and also been checked by an elastic analysis, with loading w_2 on span L_2 (longer span) and loading $0.25w_1$ (representing a minimum load) on span L_1. As the first provision is only for design of hogging bending, the second provision is relevant to the strength required at the sagging regions. For equal span beams (10 m/10 m), the maximum sagging moment is then $0.97M_p$ and for unequal span beams(8 m/10 m), the maximum sagging moment is 1.26 M_p. For composite beams with uniform cross sections the ratio M_{ps}/M_p is greater than 1.5, so that it is checked to be safe.

As it is likely that, with uniform cross-sections, hogging cross sections can be designed in accordance with the first provision, then sagging regions are checked in accordance with the second provision.

Generally, the second provision is conservative and it is very likely that full plasticity is not attained in midspan for practical ranges of composite beams.

4.4 Conclusions

Design of continuous composite beams in hogging bending is governed by local buckling and lateral distortional bucking in the bottom flanges near internal supports. When the beams are free of lateral instability, economic design can be made by redistributing certain amount of moment either from internal supports to mid span or vise versa. The research is a continuous part of the work to check the margin of safety of the quasi-elastic design method in Eurocode 4, that allows moment redistribution expected from elastic global analysis. The scope of the research is limited to continuous composite beams in which the steel beams are of Class 2 uniform cross sections in accordance with draft Eurocode 4:Part 1 [1]. Full shear connection is provided, and the design ultimate loads are assumed to be uniformly distributed.

Rotation capacity of beams affected by local buckling is studied. Moment-rotation curves for hogging moment regions are deduced from moment-curvature curves. Due to the localised buckling feature, at the critical sections (buckling), the moment-curvature curves are defined by ratios K_1, K_2 and K_3. Hogging region of a continuous beam is modeled as a cantilever. Characteristic values of K_1 are obtained, as a function of a combined slenderness ratio λ_c, based on reported test data on 49 beams from four laboratories. Computed moment-rotation curves for cantilevers are compared with test data from 4 composite cantilevers. Trial and error calculations lead to approximate values for K_2, which is also related the combined slenderness ratio λ_c. Ratios K_3 are calculated from moment-curvature curves, allowing for residual stresses.

These K_1 and and K_2 have been used in numerical analyses of 50 two-span beams, leading to load factors λ_b, at which buckling commences, and λ_f, at which "failure" occurs. The value $\lambda = 1$ corresponds to design load to draft Eurocode 4.

The mean λ_f was 1.18. The lowest value was 0.975, for section HB41, with a high span ratio ($L_2/L_1 = 1.6$). However, it is unlikely in a beam with that high span ratio ($L_2/L_1 = 1.6$), when uniform section will be used in practice. For other span ratios ($L_2/L_1 = 1$ and 1.25), the lowest λ_f 1.03.

The mean λ_b was 1.14. The lowest λ_b for span ratio ($L_2/L_1 = 1$, 1.25) is 1.00.

The computed values of the ultimate loads that correspond to λ_f, are slightly lower than the collapse loads calculated by the rigid-plastic global analysis. That

would be expected for Class 2 beams, because design based on the rigid-plastic global analysis makes use of the full bending resistance of both hogging and sagging regions of a span. It is shown that in design of Class 2 beams to draft Eurocode 4, this does not occur, even when concrete flanges at midspan are exceptionally narrow.

The analyses also include adverse values, in relation to practice, of relative length of adjacent spans, span-to-depth ratio, and ratio of hogging to sagging moment of resistance.

In conclusion, the redistribution of elastic bending moments allowed by draft Eurocode 4 has been found to be safe and economical, and to reflect the real behaviour of two-span beams. For beams continuous over more than two spans, the method is believed to be slightly more conservative. These results are consistent with those from a study of Class 3 beams [33].

Table 4.1: Properties of cross-sections

Section	b_c mm	h_c mm	b_f mm	t mm	w mm	d_f mm	A_{r1} mm^2	y_1 mm	A_{r2} mm^2	y_2 mm
SB2	1000	105	134.9	8.2	6.1	184.9	486	25	486	80
SB3	1000	105	134.2	9.5	6.1	184.9	552	25	552	80
HB40	1000	105	134.2	9.5	6.1	184.9	784	25	428	80
HB41	1000	105	101.5	6.7	5.9	241.2	495	25	63	80
SB4	1000	120	103.5	7.3	6.0	298.5	250	30	250	90
SB10	1000	120	103.5	7.3	6.0	298.5	150	30	150	90
a1	2000	120	203.5	10.8	7.7	228.9	600	30	600	90
a2	2000	120	176.0	10.8	7.7	228.9	600	30	600	90
b3	600	105	86.1	5.3	4.5	189.6	125	25	125	80
k17	1500	120	160.0	10.0	5.5	200.0	350	30	350	90
k20	1500	120	160.0	10.0	6.0	279.0	200	30	200	90
k23	1500	120	183.0	10.3	6.0	278.4	125	30	125	90

Table 4.2: Yield strength and slenderness for composite sections

Beam	f_y N/mm^2	f_r N/mm^2	$\alpha d/w\epsilon$	$c/t\epsilon$	λ_c	K_1	K_2
SB2	315	460	33.8	8.6	17.1	10.0	30.0
SB3	293	460	32.4	7.1	14.89	26.0	81.0
HB40	293	397	32.4	7.1	14.89	26.0	81.0
HB41	323	435	36.0	8.0	17.97	3.0	11.0
SB4	335	460	37.9	7.6	17.95	3.5	11.1
SB10	335	460	34.0	7.6	16.99	10.5	32.7
a1	335	460	33.2	10.1	17.54	6.5	20.4
a2	335	460	33.2	8.7	16.77	12.0	37.7
b3	335	460	33.6	8.7	18.13	2.2	7.1
k17	335	460	39.5	8.9	17.37	7.7	24.2
k20	335	460	35.8	8.9	17.98	3.3	10.5
k23	335	460	32.2	10.0	17.53	6.6	20.6

Table 4.3: Beams with two equal spans of 10.0 m

Beam	M_p kNm	M_p/M_{ps}	w_d kN/m	$L/(h+h_c)$	λ_p	λ_b	λ_f
SB2	123.5	0.65	14.18	32.7	1.055	1.167	1.194
SB3	137.9	0.67	15.76	32.4	1.010	1.240	1.335
HB40	140.1	0.68	16.01	32.4	0.980	1.212	1.267
HB41	125.7	0.64	14.37	27.9		1.045	1.127
SB4	155.8	0.59	17.81	23.1		1.125	1.245
SB10	140.8	0.53	16.09	23.1	1.370	1.462	1.537
a1	282.8	0.61	32.32	27.0	1.160	1.230	1.253
a2	258.9	0.61	29.59	27.0	1.165	1.290	1.346
b3	58.1	0.53	6.64	29.4		1.115	1.160
k17	171.9	0.56	19.64	30.8	1.195	1.292	1.335
k20	230.2	0.57	26.31	23.9		1.245	1.296
k23	246.0	0.55	28.11	23.9	1.335	1.362	1.404
Mean					1.158	1.232	1.295

Table 4.4: Beams with unequal spans: $L_2 = 1.25\ L_1$

Section	L_1 m	L_2 m	w_d kN/m	λ_p	λ_b	λ_f	$L/(h+h_c)$
SB2	8	10	16.88	1.020	1.077	1.098	26.2, 32.7
	10	12.5	11.39	1.005	1.060	1.068	32.7, 40.9
SB3	8	10	18.76	0.980	1.140	1.189	25.9, 32.4
	10	12.5	12.01	0.970	1.110	1.173	32.4, 40.5
HB40	8	10	19.06	0.955	1.112	1.161	25.9, 32.4
	10	12.5	12.20	0.950	1.085	1.154	32.4, 40.5
HB41	8	10	17.10		1.020	1.046	22.2, 27.8
	10	12.5	10.95		1.005	1.028	27.8, 34.8
SB4	8	10	21.20		1.125	1.245	18.5, 23.1
	10	12.5	13.57		1.065	1.101	23.1, 28.9
SB10	8	10	19.15	1.270	1.327	1.358	18.5, 23.1
	10	12.5	12.26	1.250	1.302	1.339	23.1, 28.9
a1	8	10	38.47	1.095	1.130	1.146	21.6, 27.0
	10	12.5	12.26	1.250	1.302	1.339	23.1, 28.9
a2	8	10	38.47	1.095	1.130	1.146	21.6, 27.0
	10	12.5	22.5	1.090	1.155	1.187	27.0, 33.8
b3	8	10	7.91		1.110	1.143	26.2, 32.8
	10	12.5	5.06		1.095	1.127	32.8, 41.0
k17	8	10	23.39	1.145	1.197	1.232	23.5, 29.4
	10	12.5	14.97	1.120	1.172	1.198	29.4, 36.8
k20	8	10	31.33		1.160	1.182	19.1 23.9
	10	12.5	20.05		1.100	1.134	23.9, 29.9
k23	8	10	33.47	1.220	1.240	1.271	19.1, 23.9
	10	12.5	21.42	1.205	1.220	1.238	23.9, 29.9
Mean				1.091	1.138	1.166	

Table 4.5: Beams with unequal spans: $L_2 = 1.6\ L_1$

Section	L_1 m	L_2 m	w_d kN/m	λ_p	λ_b	λ_f	$L/(h+h_c)$
SB2	6.25	10	18.52	0.965	1.017	1.034	20.4, 32.7
	10	16	7.23	0.945	0.987	0.993	32.4, 52.3
SB3	6.25	10	20.59	0.930	1.067	1.086	20.3, 32.4
	10	16	8.04	0.920	1.015	1.050	32.4,51.8
HB40	6.25	10	20.91	0.915	1.042	1.068	20.3, 32.4
	10	16	8.17	0.890	1.002	1.047	32.4, 51.8
HB41	6.25	10	18.77		0.970	0.988	17.4, 27.8
	10	16	7.33		0.954	0.975	27.8, 50.0
a1	6.25	10	42.21	1.035	1.062	1.070	16.9, 27.0
	10	16	16.49	1.005	1.030	1.030	27.0, 43.2
a2	6.25	10	38.65	1.035	1.100	1.105	16.9, 27.0
	10	16	15.10	1.015	1.060	1.079	27.0, 43.2
b3	6.25	10	8.67		1.085	1.105	20.5, 32.8
	10	16	3.39		1.070	1.087	32.8, 52.5
k17	6.25	10	25.66	1.080	1.125	1.149	18.4, 29.4
	10	16	10.02	1.060	1.087	1.093	29.4, 47.0
k20	6.25	10	34.37		1.070	1.093	14.9, 23.9
	10	16	13.43		1.045	1.053	23.9, 38.2
k23	6.25	10	36.72	1.150	1.157	1.177	14.9, 23.9
	10	16	14.34	1.105	1.110	1.133	23.9, 38.2
Mean				1.016	1.058	1.080	

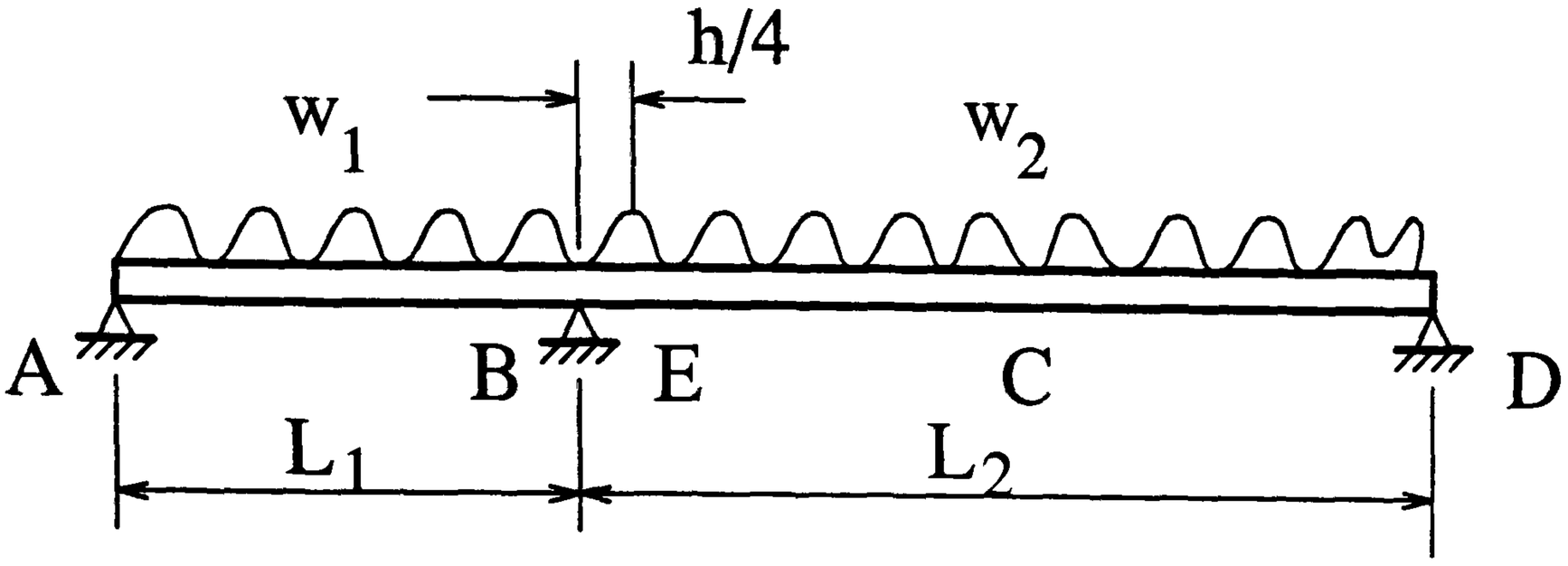

Figure 4.1: Loading on a two span continuous beam

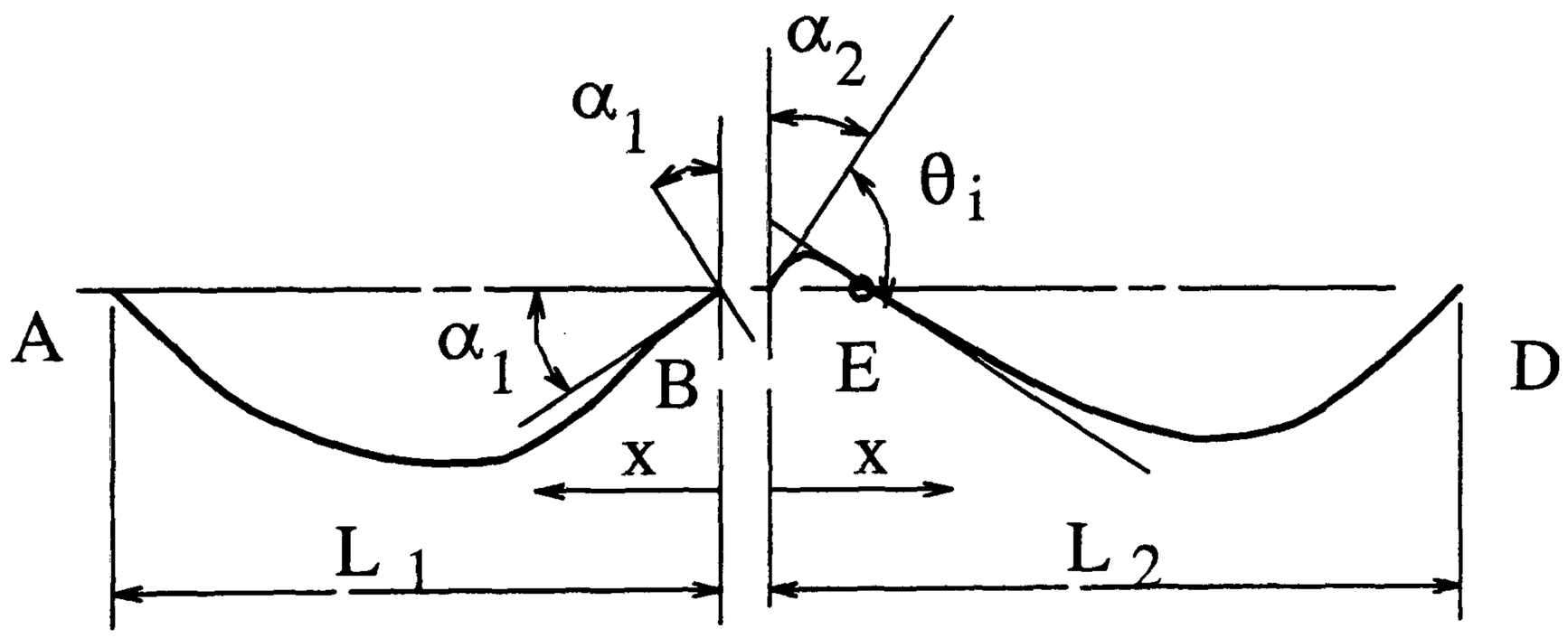

Figure 4.2: Deflection shape of a two span continuous beam

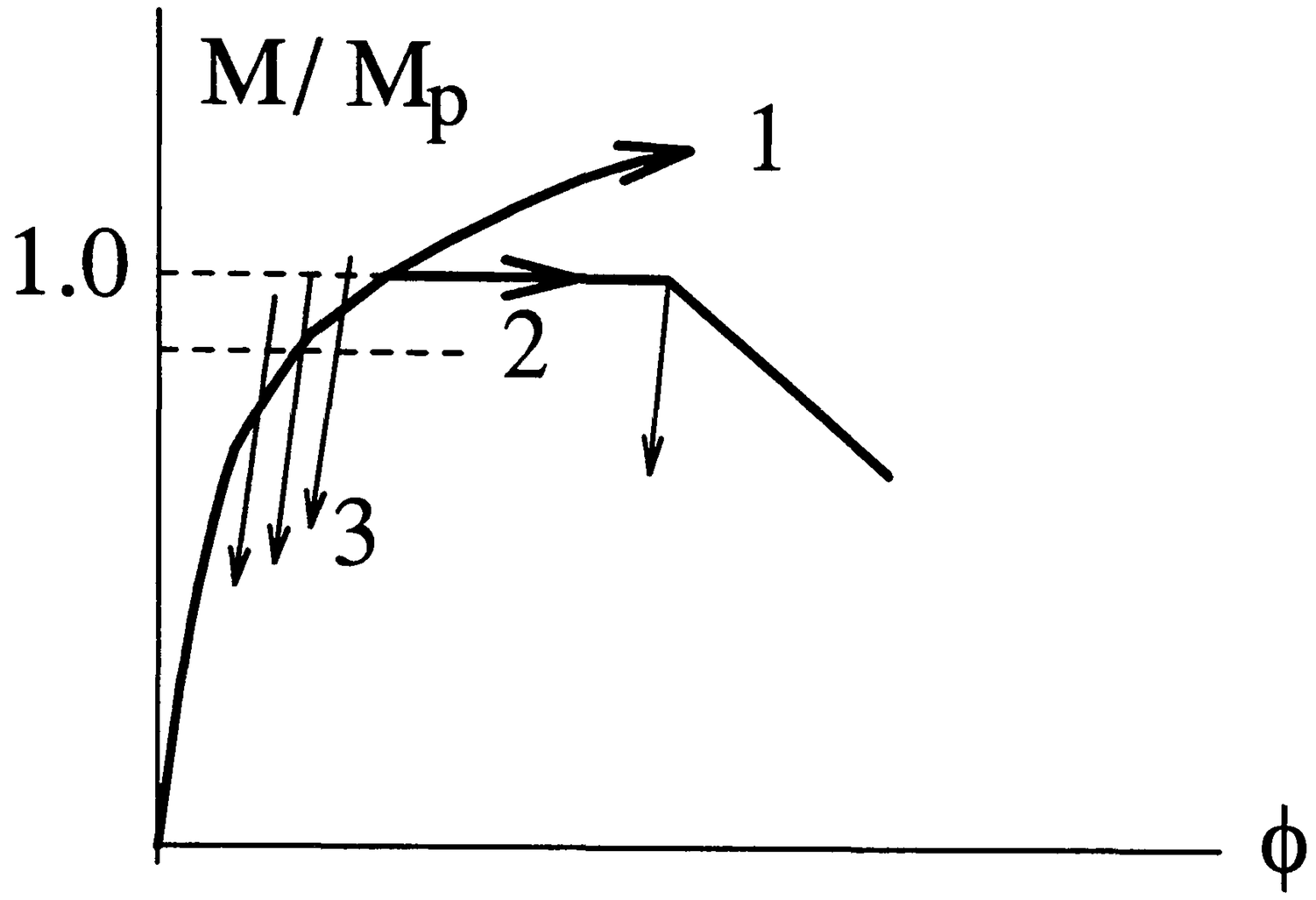

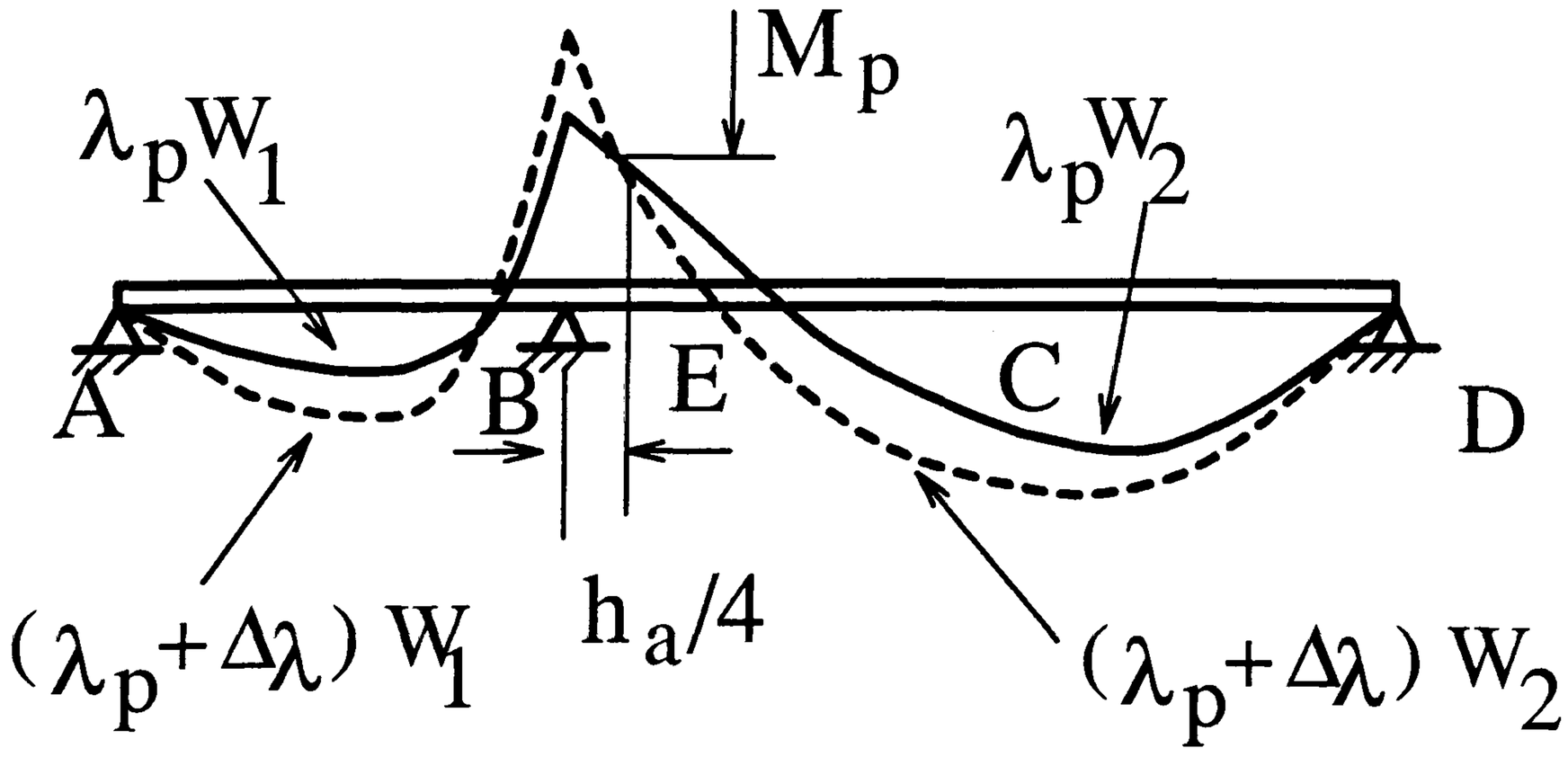

Figure 4.3: Loading and unloading of cross sections along the beam

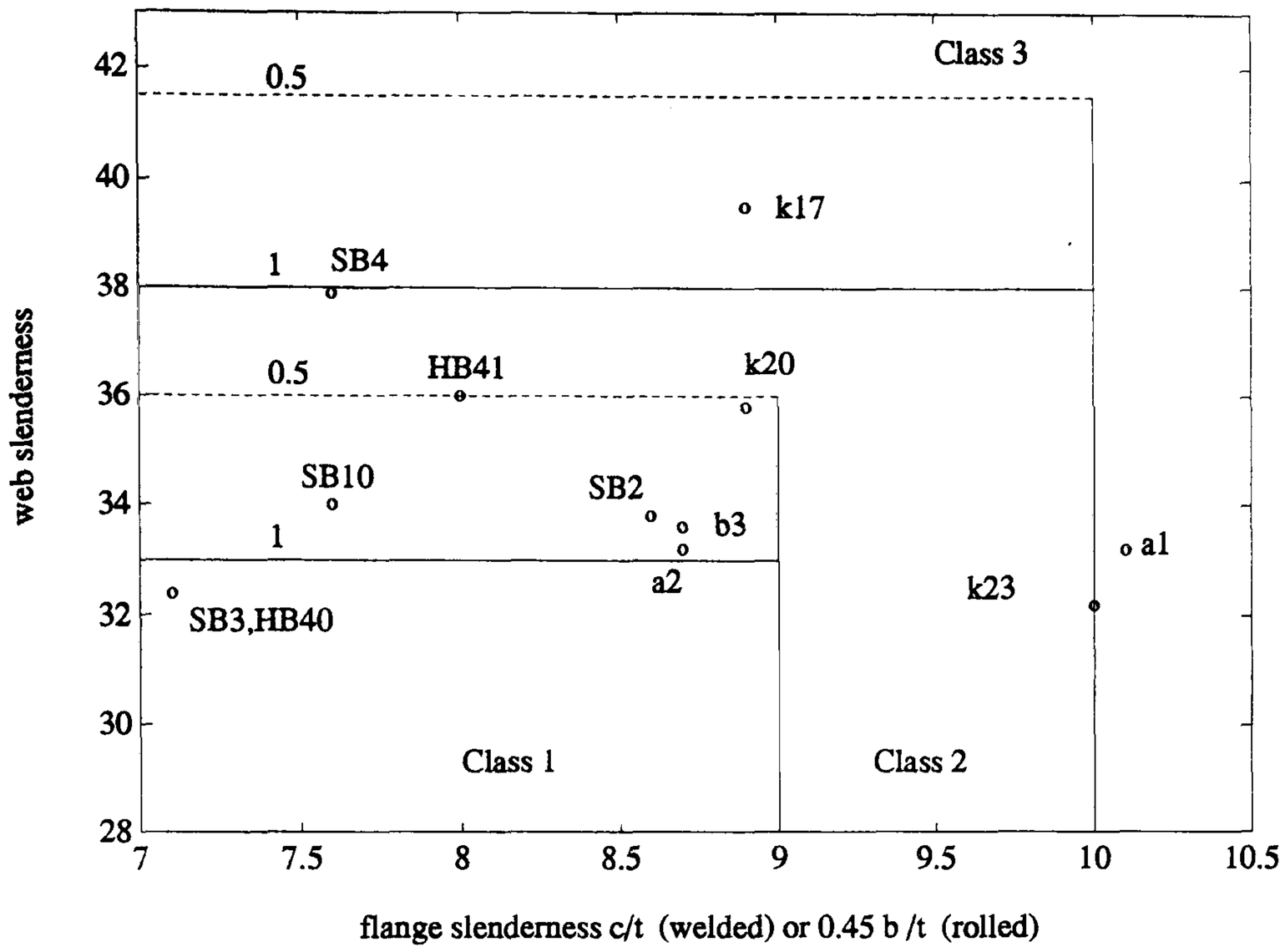

Figure 4.4: Slenderness of sections used in parametric study

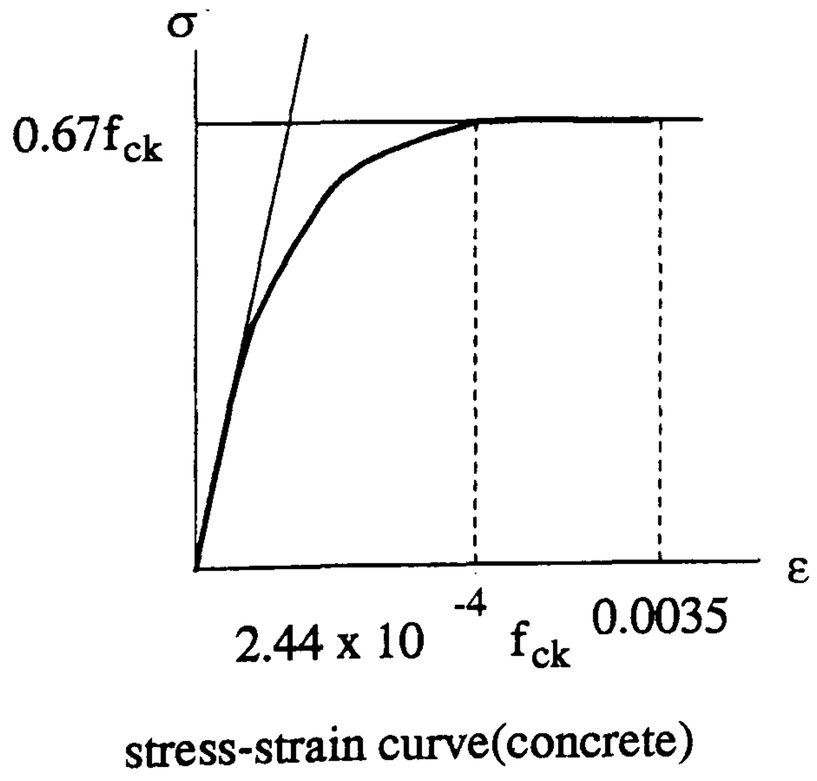

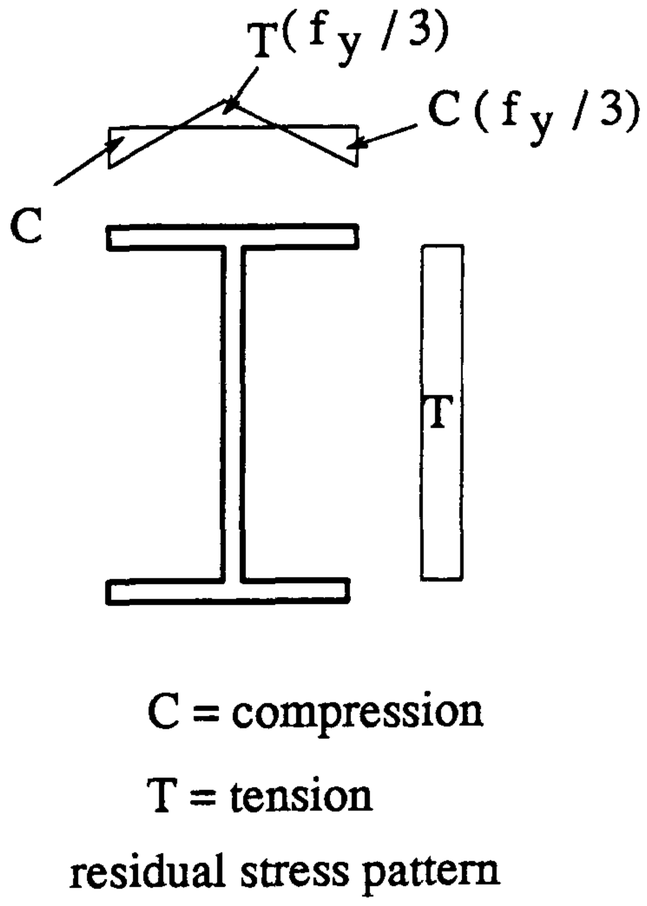

Figure 4.5: Stress-strain curves and residual stress

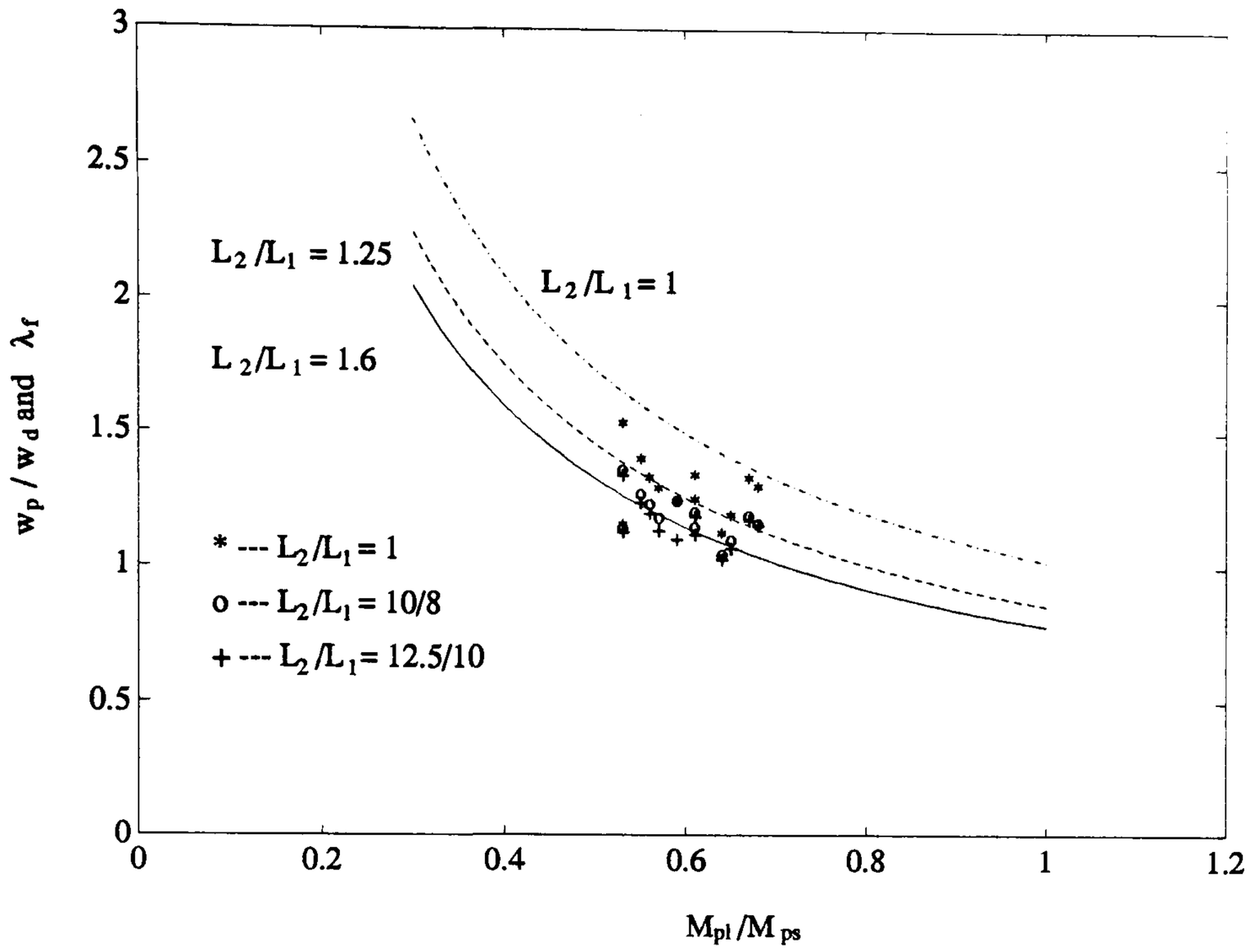

Figure 4.6: Comparison to the rigid-plastic global analysis

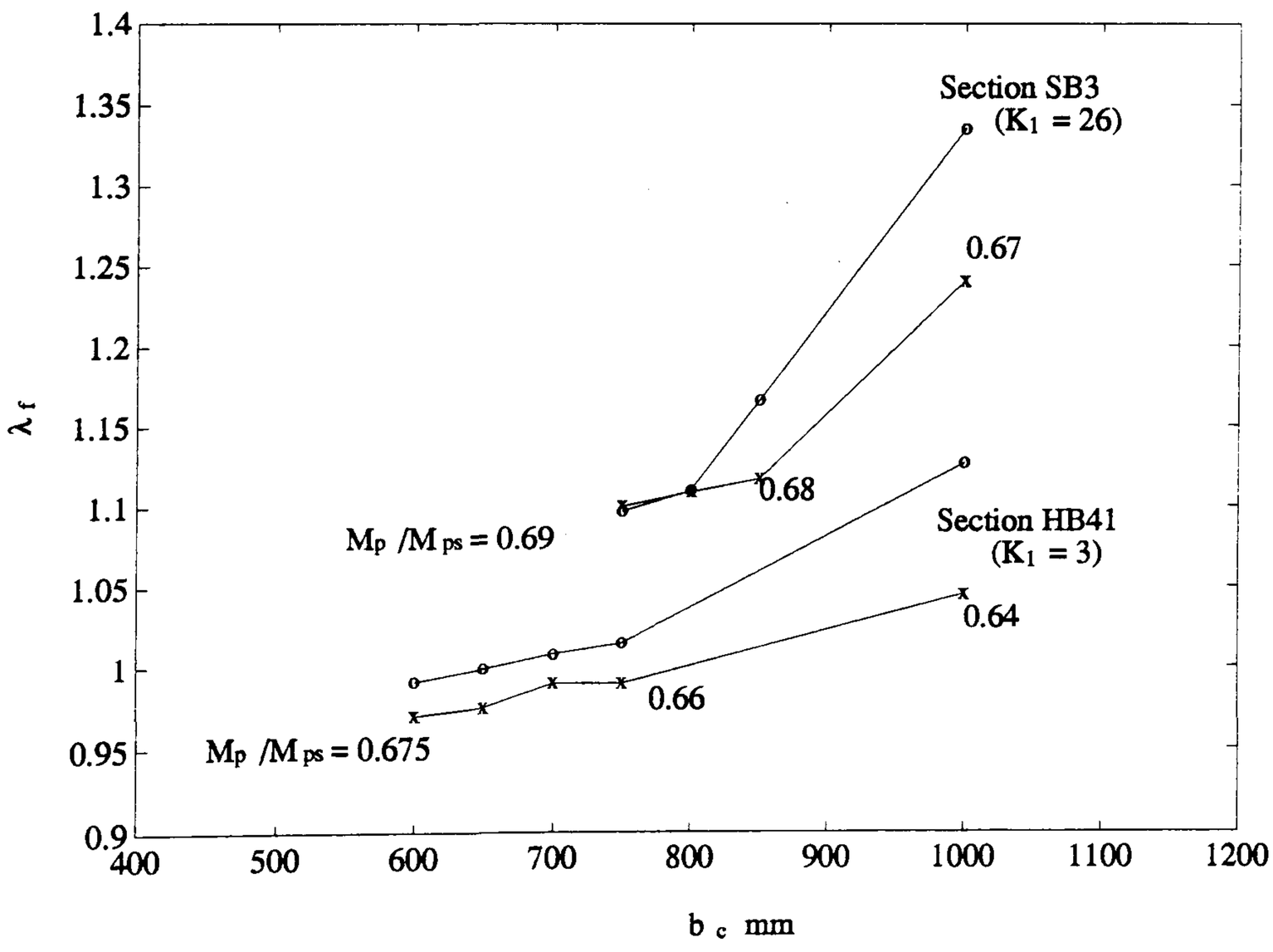

Figure 4.7: Influence of breadth of concrete flange on λ_b and λ_f

Chapter 5

Tests on Inverted U-frame Action in Composite Beams

5.1 Introduction

The Bridge code (BS5400:Part3) [2] provides design methods for both continuous and discrete U-frame action in steel beams in the UK, but the methods are very conservative because they are based on the strut buckling theory. Besides, in design practice for composite construction, the method for discrete U-frames is irrelevant, because of uncertainty of the strength and stiffness of the U-frame connection and the validation of smearing the discrete U-frames over the beam span when the BEF theory (beam on elastic foundation) is used.

Draft Eurocode 4:Part 1 [1] (referred to here as EC4) provides a design method for distortional lateral buckling. Its predictions have been compared[33] with the results of tests on two pairs of double-cantilever beams restrained by inverted-U frame action(U2 and U3). It was found that for Class 2 cross sections, the maximum hogging moments reached in the tests exceeded the values predicted by the BS5400 method by over 200%, and by 23% to 33% by the EC4 method. No further experimental evidence has been found for beams with slender sections(class 3 and class 4) and beams with stiffened webs.

Tests are now reported on two inverted U-frame composite girders, U4 and U5. The objectives of the tests were to study the U-frame action in enhancing the overall resistance of a beam against distortional lateral buckling, and to provide experimental data for the development of a rational design approach.

5.2 Test specimens

5.2.1 Choice of specimen

Two inverted U-frame composite girders, U4 and U5, were tested. Both specimens were designed as double cantilevers to simulate the hogging region between two contraflexure points near an internal support of a continuous beam.

The member length and choice of cross sections of the specimens were based on the design of a typical bridge structure, assuming a span-depth ratio of 24. Considering a bridge with continuous spans of 30 m, the length of the hogging moment region near the internal supports can be up to 10 m. This was the basis for choosing the cantilever length of 5 m(half scale), to allow for the worst arrangement of imposed loading likely to happen. The cross section of interest was one with a web slenderness just outside the existing limit for class 3 (EC4). This was achieved by using slab reinforcement and an appropriate section for the plate girders.

Figs.5.1 and 5.2 illustrate the geometries and dimensions of specimens U4 and U5. The two specimens have identical cross sections. Each consists of two parallel plate girders. Specimen U4 was designed to simulate beams with continuous U-frame action. There were no web stiffeners except at the support section. Specimen U5 was designed with vertical web stiffeners along the beam length to simulate a discrete U-frame composite girder. Double and single sided stiffeners were used in the different parts of the specimen to compare their behaviour.

Two layers of high strength reinforcement bars were used in both longitudinal and transverse directions.(T10 bars at 150 mm each way). The reinforcement ratio for hogging bending is 1% , which is common in bridge design.

The slab is 110 mm in depth and 2000 mm in width.

5.2.2 Specimen U4

Specimen U4 consists of two plate girders, labelled U4A,U4B. The plate girders were constructed by welding grade 50D steel plates.

For each of U4A and U4B, double sided vertical bearing stiffeners were provided at the support section. The bearing stiffeners were 10 mm in thickness. Fig.5.3 shows light internal cross bracings used in the specimen. The light horizontal and

diagonal internal bracings were provided at the support section, to prevent lateral movement and tilting of each beam, but not to restrain rotation in plan, about a vertical axis.

At two cross sections, 1.2 m and 1.6 m away from the support each side, lateral cross bracings were provided during the second part of the test only. They are identical to the central diagonal bracing, but without the horizontal member. All the connections between the girders and the bracings were fastened by using M16 bolts, with a torque of 25 kNm, to ensure a moment transmission.

The stud arrangements for specimen U4 are shown in Fig.5.4. All shear studs have 13 mm shanks. The nominal height after welding is 65 mm. Two rows of studs were welded to the top flange for each beam, with a transverse spacing 85 mm symmetric to the centre line of the top flange and a longitudinal spacing of 200 mm. Full shear connection is achieved in accordance with BS5400:Part 5 [80].

5.2.3 Specimen U5

Similar to U4, specimen U5 also consists of two plate girders, namely U5A and U5B. Their cross sections are identical to those of U4A, and U4B.

Two types of stiffeners were used. On one half length of each beam, the stiffeners were designed as double sided at a spacing of 1200 mm, and on the other half, stiffeners were single sided. Fig.5.5 shows the details of the two types of stiffeners. These stiffeners were designed as having the same values of the second moment of area about the principal axis parallel to the web (Fig5.5) over a width up to 16 times the web thickness on each side of the centreline of its connection, in accordance with Clause 9.6.5 of BS5400:Part 3 [2].

Fig.5.6 illustrates the details of the stud arrangements for specimen U5. Provision of the shear connection was similar to U4 by using TRW Nelson shear studs 65 mm high and 13 mm in diameter. Transverse spacing was 85 mm and longitudinal spacings were different for different parts of the specimen as shown in Fig.5.6.

Similar to specimen U4, double sided bearing stiffeners were used at the support section. The light horizontal and diagonal internal bracings were also provided at the support section, connected by M16 HSFG bolts.

The web panels near the central section were strengthened by 25×25 ×5 angles

for the second part of the test, to prevent the local web buckling, as shown in Fig.5.7.

5.2.4 Construction of test specimens

Specimen U4

The construction of the plate girders for U4 was carried out by the Ward Structures LTD in North Yorkshire. In fabrication of the girders, full length of double sided welding of web to flanges was made by automatic welding machine. The fillet weld size was 5 mm. The stiffeners at the central section were then manually welded, with the fillet weld size of 4 mm.

Stud welding was done by using the Nelson series 6000(TR2400) dual gun system in the structural laboratory of Warwick University. Performance tests were carried out before welding to ensure reliability and workmanship in accordance with TRW Nelson's recommendation.

Propped construction was used. The twin plate girders were propped by four temporary cross frames. Timber shutterings was used for the concrete slab.

Ready mix concrete grade C30, with slump of 60 mm, was used to cast slab U4. Twelve 150×150 cubes were taken and they were tested in pairs at intervals. The concrete slab was cast with top flanges of the steel beam horizontal in the transverse direction. All temporary works were dismanted 7 days after casting.

Specimen U5

Similar to U4, fabrication of the girders for U5 was carried out, by the same fabricator. Single sided welding and double sided welding of web to flanges were used in different parts of the specimen. Fig.5.8 illustrates the welding details. The fillet weld size was 5 mm between the web and the flanges. The stiffeners were then manually welded along the beam length, with the fillet weld size of 4 mm.

Stud welding was similar to that for U4.

Ready mix concrete grade C35 was used, with slump of 60 mm. Casting was similar to that for U4, with the plate girders propped, and timber shuttering for the concrete slab. Twelve 150×150 cubes were taken. The temporary works were dismanted one week after casting.

5.2.5 Testing rigs

Testing rigs were exactly the same for both specimens U4 and U5. Two portal reaction frames built up from standard structural "Meccano" were erected at each end of the specimens. The loading arrangement is shown in Fig.5.9. The central supports were held stationary and loads were applied to the specimen through hydraulic jacks at the four corners.

Two semi-cylindrical roller bearings of 50 mm in diameter (Fig.5.10) were used at the central support section underneath each of the twin beams. At four corners of the beams, the end bearing system, which was an assembly of a roller slider on top of a spherical ball joint seating(Fig.5.11), provided complete freedom in rotations and longitudinal movement.

Preliminary analyses of the deflections showed that jack travel of 250 mm would be needed.

5.3 Instrumentation

5.3.1 Specimen U4

Two 25-tonne and two 50-tonne load cells were used to measure the loads applied at the four corners.

Strain gauges were bonded onto the girders before casting. 28 No. TML electrical resistance strain gauges with gauge length 10 mm were bonded each on U4A and U4B. Near the support region, post-yield gauges were used(YL-10 TML). On the bottom flanges, the strain gauges were installed in pairs in such a way that mean compression strains as well as the bending strains (as a result of possible lateral buckling at high loads) could be picked up. The strain gauge positions on U4B are shown in Fig.5.12.

The in-plane and transverse rotations were measured by using a portable inclinometer at the positions shown in Fig.5.13.

Four LVDTs were used to measure vertical movements at the four loading positions, underneath the bottom flanges. Another four LVDTs were used to detect the longitudinal slips between the steel beams and the slab at the four ends of the

beams. Lateral movements of the bottom flanges and the slab were measured by two theodolites, by offset with reference to an initial datum line. The offset was obtained by reading a steel ruler, rocked like a levelling staff, to obtain the minimum reading.

5.3.2 Specimen U5

The load cells used were similar to those for the U4 test. The four LVDTs used in detection of the deflections were 100 mm in travel, and the LVDTs for measurement of the longitudinal slips were 25 mm in travel.

It was found that measurement of the lateral movements of the bottom flanges by the theodolites was not accurate enough to evaluate the U-frame action, so a lateral measurement device was designed to pick up the relative displacement between the bottom flanges. A LVDT transducer was installed onto a wood bar, one end of which was sited on a ball, allowing the bar to rotate in the transverse plane, the other end was on a rolling tube, allowing relative lateral movement when there is a lateral movement. The arrangement of the device is illustrated in Fig.5.14. Transverse rotation of the bottom flange would induce an error in the measurement of the relative displacement. This is analysed in Appendix.B.

The strain gauges bonded onto the bottom flanges were similar to those for U4, installed in pairs, to pick up the bending strains. The strain gauges bonded onto the webs were installed in a way to pick up the transverse bending of the web. Fig.5.15 illustrates the monitoring positions of strain gauges for beam U5B.

Besides the strain gauges bonded onto the girders, ten strain gauges were bonded onto the studs above the stiffeners closest to the central section in U5B. Fig.5.16 shows the positions of these strain gauges on the studs. The strain gauges were bonded in such a way to give a transverse bending between the stud pairs, and the anti-damage layers were also provided to protect the strain gauges as shown in Fig.5.16.

The inclinometer positions for U5 specimen are shown in Fig.5.17.

Fig.5.18 shows the lateral displacement measurement arrangements. The absolute lateral movements of the bottom flanges and the slab were measured by two theodolites, which defined vertical datum planes along both sides of the specimen.

Four dial gauges used near the central support of U5A, to give more accurate measurements. Eight lateral measurement devices were mounted underneath the twin girders spacing at 300 mm near the central support. The absolute lateral displacement of the bottom flange in U5B was calculated by the difference of the readings from dial gauges and the LVDTs on the wood bars.

5.3.3 Calibration of instruments

The load cells were calibrated before and after each test, using 3MN Denison testing machine. Test results were calculated using average values from the two sets of calibration data.

The LVDTs were also calibrated by measuring the adding up of slip gauges, before and after the tests. Mean values of the readings were taken in linear regressions of the calibration graphs.

All electric digital data were collected using a Schlumberger Orion 3531D data logger, controlled by a micro computer via RS232 interface. The accuracy and repeatability were checked by using LVDTs at different values of movement calibrated by a set of standard measuring gauges.

The repeatability of the lateral measurement device was also checked before and after the tests, by fitting the standard measurement gauges, with repeatability less than 0.05 mm.

5.4 Auxiliary tests

5.4.1 Properties of materials

Grade 50D steel was used to construct the plate girders for both specimens, U4 and U5. Coupon samples were cut from the plates in the same batch provided by the fabricator. The test specimens were tested in a 25-tonne Dartec tensile machine in accordance with BS18 [81]. Two specimens were tested for each of the top flange, bottom flange and web of U4A, U4B, U5A and U5B. In elastic region, strain was measured by means of a Sandner extensometer extensometer of gauge length 25 mm and sensitivity 2.5%. All data were logged to a micro-computer and material

properties were calculated automatically.

High-yield reinforcing bars were sampled randomly and four bars were taken. Tensile tests were performed on the samples using a 10-tonne Monsanto Extensometer machine and the material properties were taken as the average from four tests.

Concrete cubes were tested using a 3MN Denison machine in accordance with BS1881 part 116 [82]. Tests were carried out at regular intervals after casting of the slab.

Table 5.1 gives the strengths of the steel, the reinforcement bars and the strength of the concrete. The strength of concrete, f_{cu} in Table 5.1 is a mean value of that from a pair of cubes tested on the days when the beam tests were completed for specimens U4 and U5 respectively.

5.4.2 Dimensions and imperfections

Fig.5.19 illustrates notations for the cross sections. Measurements of thickness of the flanges were taken at regular intervals using a micrometer, eight locations, uniformly spaced. The thickness of the webs was also measured at the two ends of each beam, four positions over depth, by the micrometer. The width and depth of the cross-sections were measured using a vernier caliper at half metre intervals along beam length. The mean values of the dimensions are given in Table 5.2.

Cross section areas of the reinfocement, A_{r1} and A_{r2}, were calculated by using the nominal diameter (T10 bar spacing at 150 mm) provided by fabricators.

The initial lateral imperfections of the bottom flange relative to the top flange were measured before tests. A "theoretical straight flange edge" was located by offsetting uniformly by a distance equal to half of the average width of the top flange from the centre line, which was marked joining the ends where the web and the top flange intersect. Lateral imperfections were referred to this straight edge.

Figs.5.20 and 5.21 show the initial lateral imperfections of the specimens U4 and U5.

5.4.3 Tests on welded stud shear connections

Tensile tests were carried out on studs to find out the strength of the studs. Two studs were welded to a steel plate of 8 mm thickness, as shown in Fig.5.22. Two

such specimens were tested. The maximum loading gave the strength of the studs. One specimen failed at a tensile force of 66 kN and the other failed at the value of 70 kN, so that the mean value of the strength is 68 kN (or $544 N/mm^2$).

5.5 Test procedures

5.5.1 Specimen U4

Two tests were carried out on specimen U4 and the tests lasted for 4 days. Test 1 was done when the beams had no cross bracings except at the central supports. It was stopped when distortional lateral buckling occurred. Test 2 was carried out with cross bracings at one section each side of the central supports.

There were 27 load stages. Stage 0 to stage 16 was for test 1, and stage 18 to 27 was for test 2. Stage 17 was a transient stage when beams were unloaded from the maximum loading in test 1 to the starting position of test 2.

Test 1 started at stage 0 with the beams propped at six points and therefore the deflections and rotations of beams by self-weight were measured. The subsequent readings of transverse rotations and lateral displacements of bottom flanges were additional to the values at stage 1 (self-weight only).

At an early stage of the test, two small load cycles were carried out to check the workability of the test arrangement. The initial transverse crack appeared at a very small loading: less than 5 kN on the slab.

Readings of strain gauges and LVDTs were taken at every stage, while the readings of the inclinometers and the theodolite were taken at selected stages.

To prevent transverse bending introduced by unequal loading on each beam, the deflections at each end were controlled to be almost equal at each stage, and this was achieved by comparing differences of the deflections on each end of beams U4A and U4B.

Test 2 started at load stage 18 when the four jack forces were zero.

The cross bracings adjacent the central section each side were installed before the start of the test 2. M16 bolts were used at the connections of the bracings and the girders, with a fastening torque of 25 kNm.

5.5.2 Specimen U5

The test on U5 started when the beams were propped at six positions (stage 0). The deflections and the longitudinal rotations of the beams at their ends caused by self-weight then were measured at stage 1 when the beams were propped on the two central supports with four jacks free of force. The subsequent readings of transverse rotation and lateral movement of the bottom flanges were based on this stage, while other readings were based on stage 0.

In order to prevent the transverse bending introduced by unequal loading of U5A and U5B, the deflections at each end have to be kept almost equal at each stage. On both sides of the central section, the difference between the deflections of the ends of the two beams was controlled within 0.2 mm, and for each beam, the difference between the deflections of its two ends was within 2 mm.

In the first part of the test, the beams were loaded up to stage 12, at which the support moments were 362 kNm in U5A($1.00M_{ya}$) and 358.7 kNm in U5B($1.02M_{yb}$), when local web buckling was observed near the supports. Then the beams were unloaded and the web panels near the support section were strengthened by adding angles (25×25×5) in the way shown in Fig.5.7.

The second part of the test started at stage 20. The creep effect of the beams is eliminated by subtracting the readings at stage 19 from stage 20 (where stage 19 is the final stage of the first part of the test, when beams were unloaded with four jacks free of force and the beams were propped at the two supports at the central section). Continuous test readings have been achieved.

The tests lasted for four days.

Table 5.1: Material strengths of steel and concrete

specimen	f_{ty} N/mm^2	f_{by} N/mm^2	f_{wy} N/mm^2	f_r N/mm^2	f_{cu} N/mm^2
U4A	386.5	362.0	418.0	459.0	38.6
U4B	402.5	360.0	412.5	459.0	
U5A	383.0	360.5	390.0	459.0	36.5
U5B	369.0	360.0	393.0	459.0	

Table 5.2: Dimensions of cross-sections

specimen	b_{ft} mm	t_{ft} mm	b_{fb} mm	t_{fb} mm	h_w mm	t_w mm	A_{r1} mm^2	A_{r2} mm^2
U4A	124.34	8.08	125.45	10.12	498.83	5.95	524	524
U4B	123.74	8.06	123.86	10.03	498.17	5.99	524	524
U5A	125.50	8.00	125.90	9.90	500.00	6.10	524	524
U5B	121.50	8.00	121.30	9.90	498.50	6.10	524	524

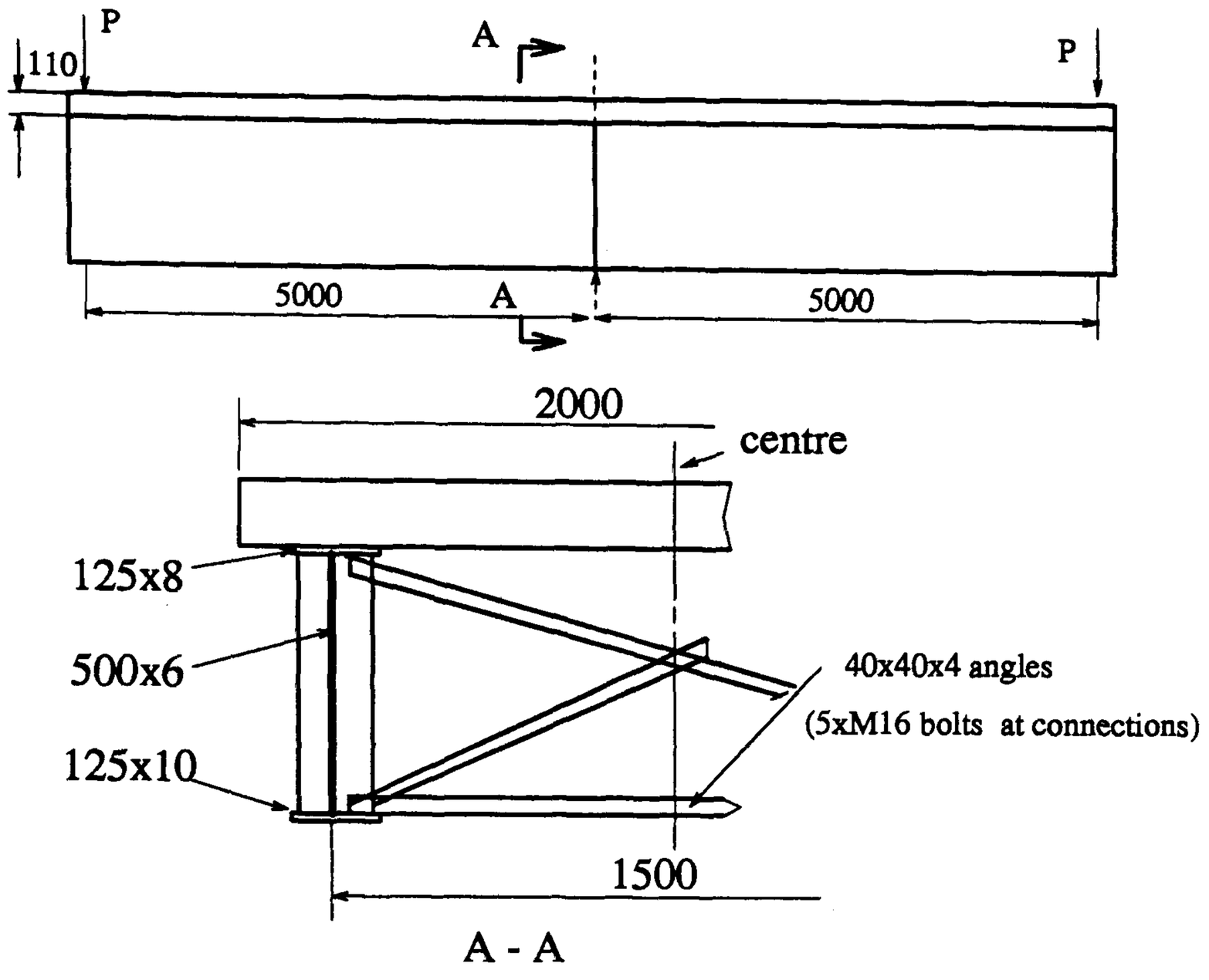

Figure 5.1: Geometry of specimen U4

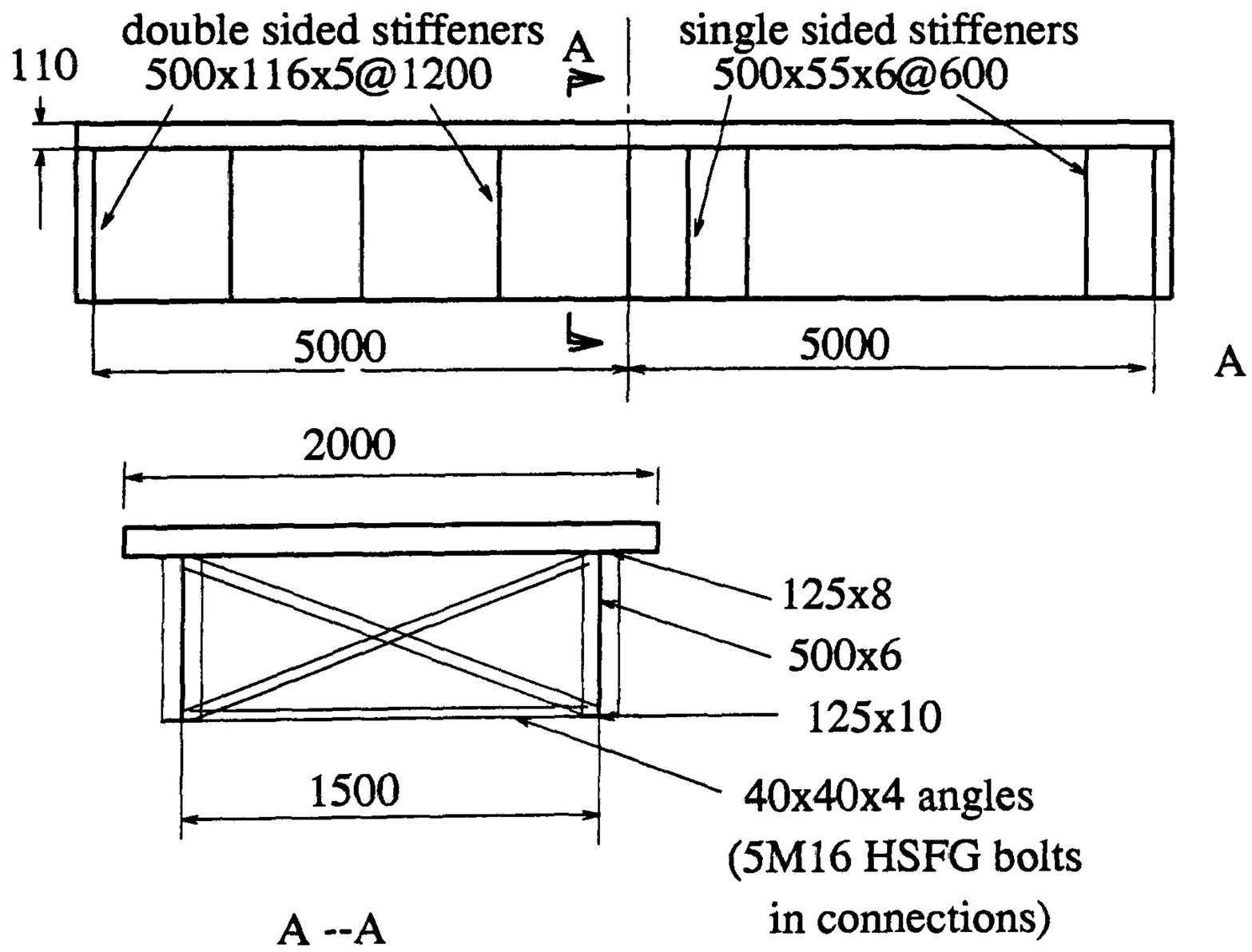

Figure 5.2: Geometry of specimen U5

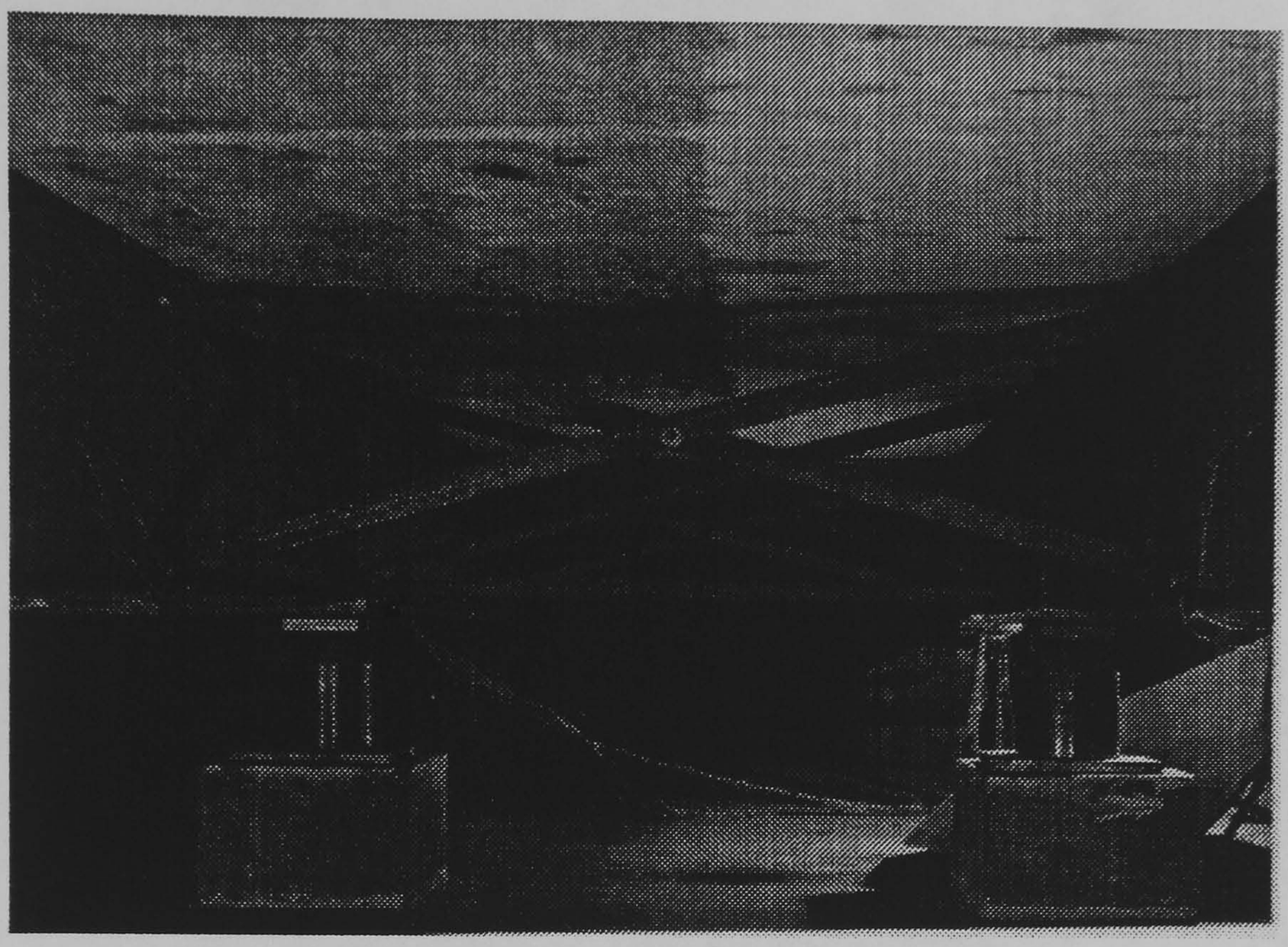

Figure 5.3: Internal cross bracings

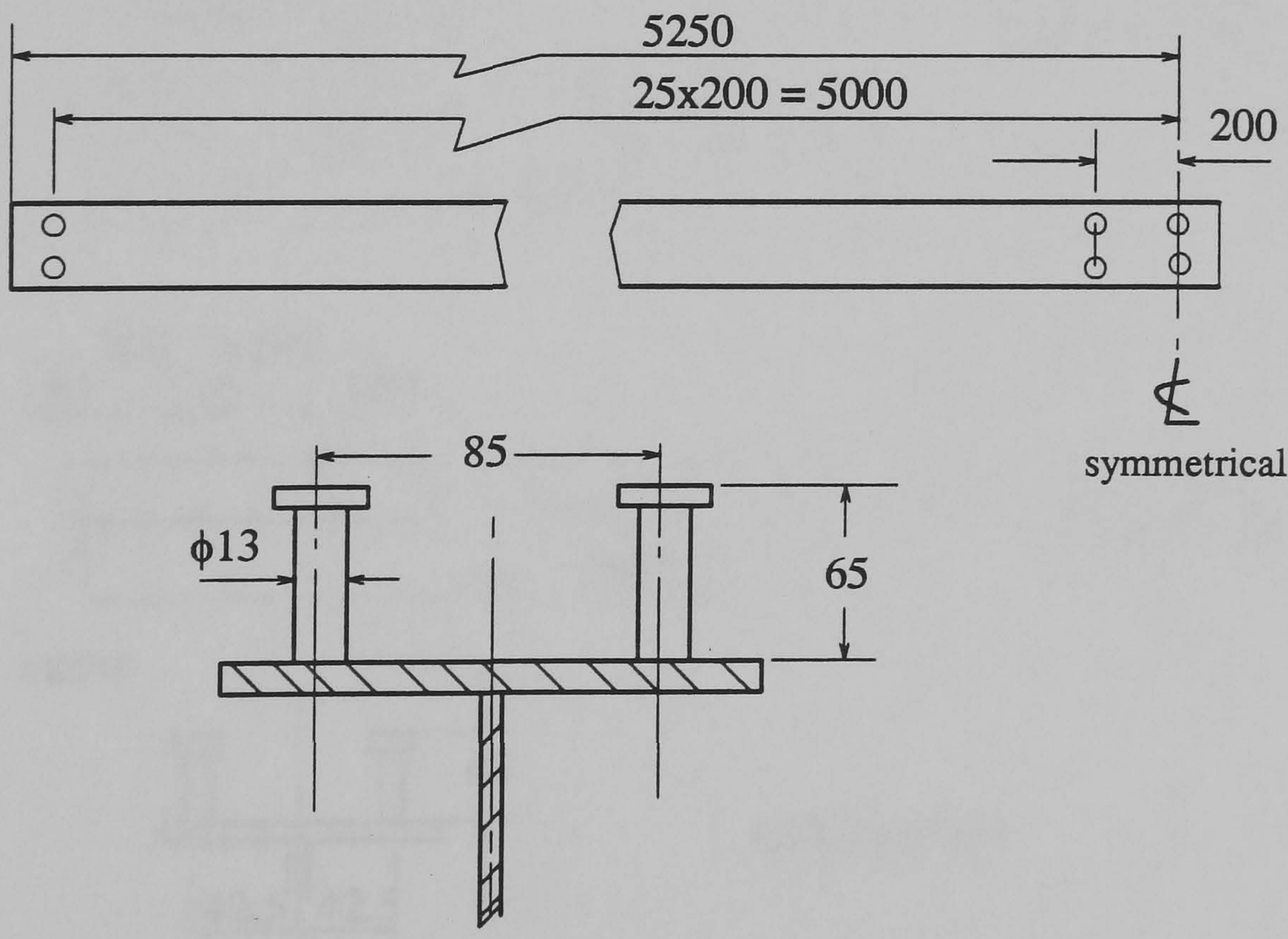

Figure 5.4: Stud arrangements of specimen U4

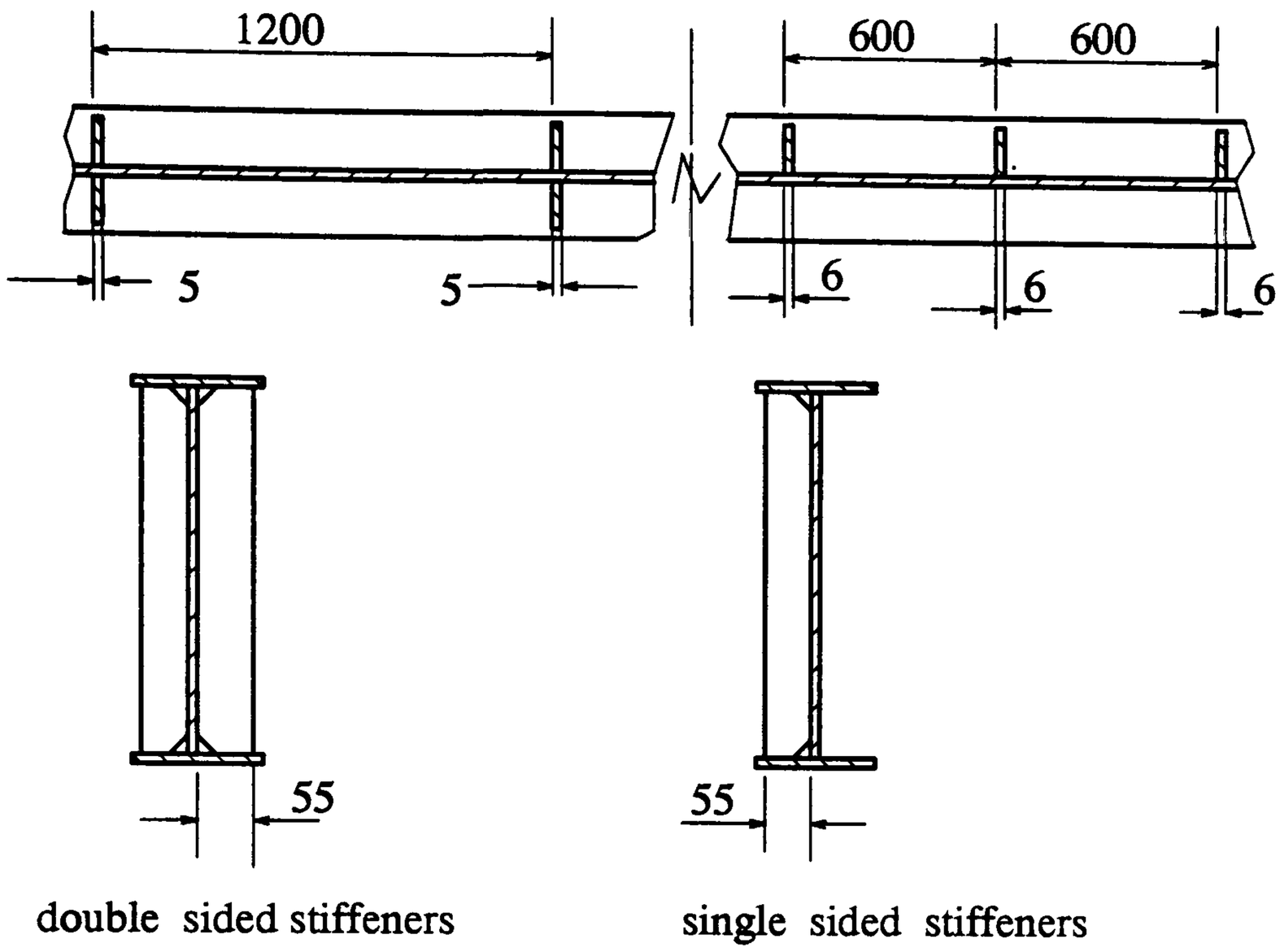

Figure 5.5: Stiffener deatils (specimen U5)

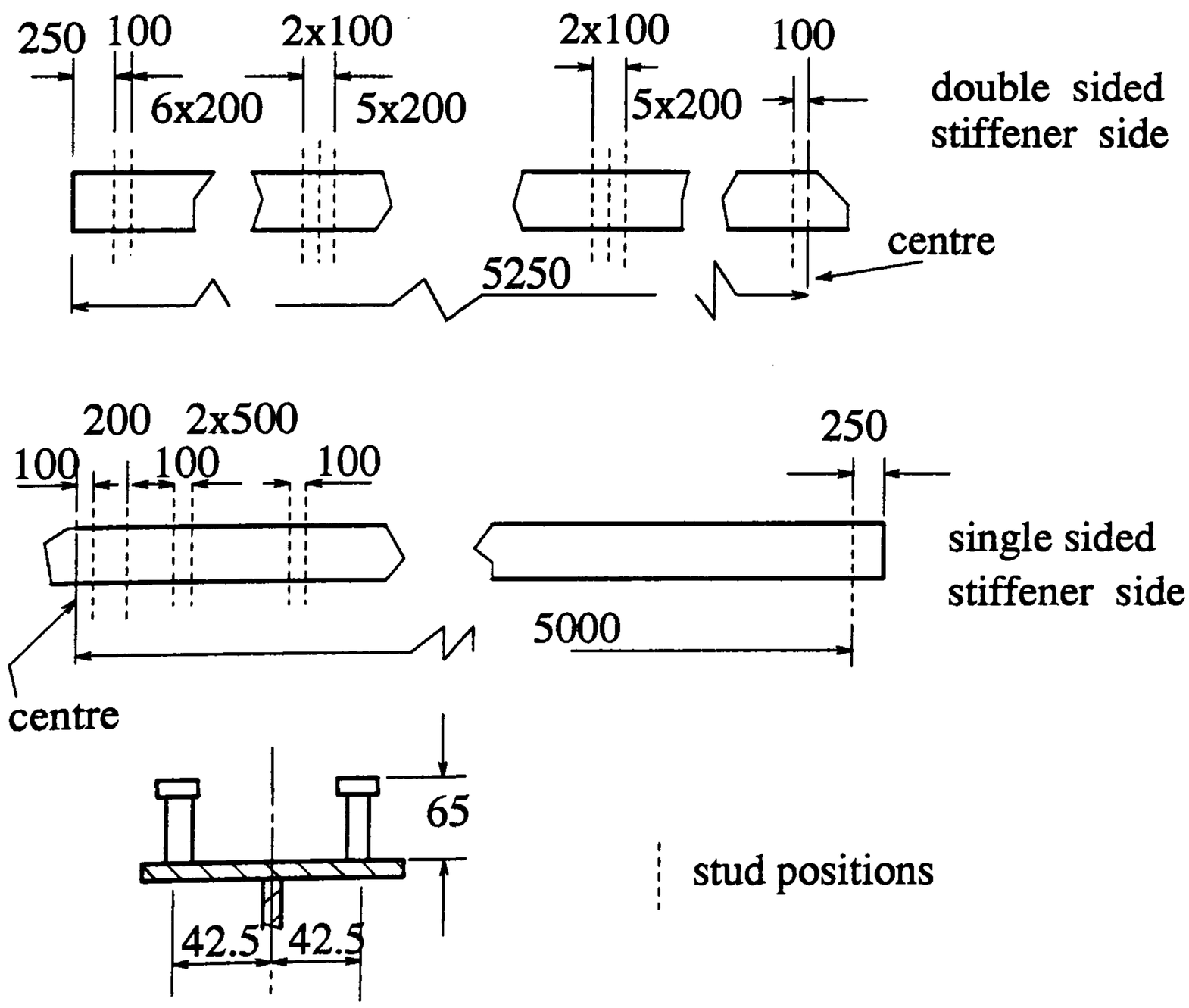

Figure 5.6: Stud arrangements of specimen U5

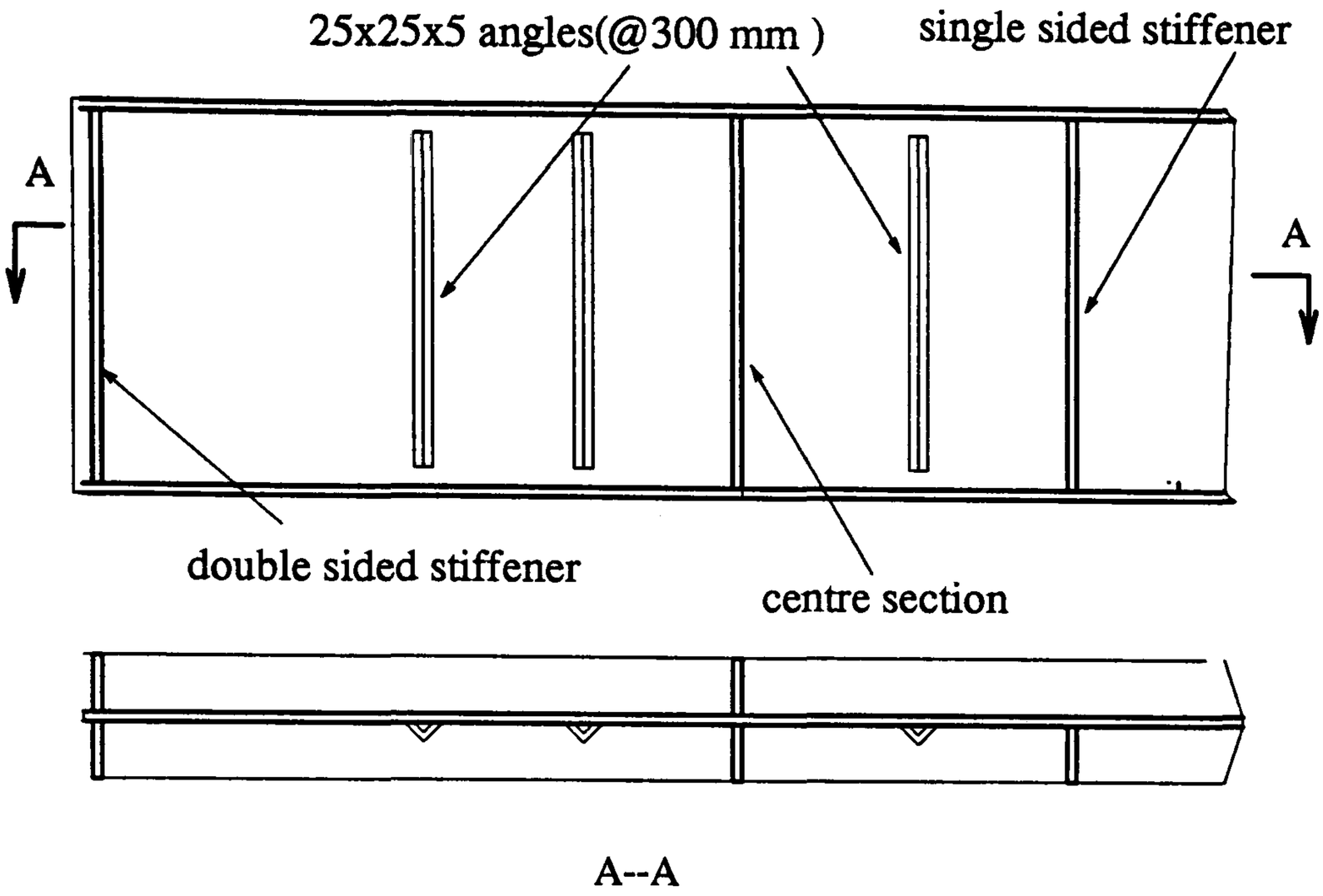

Figure 5.7: The strengthened web panels (U5)

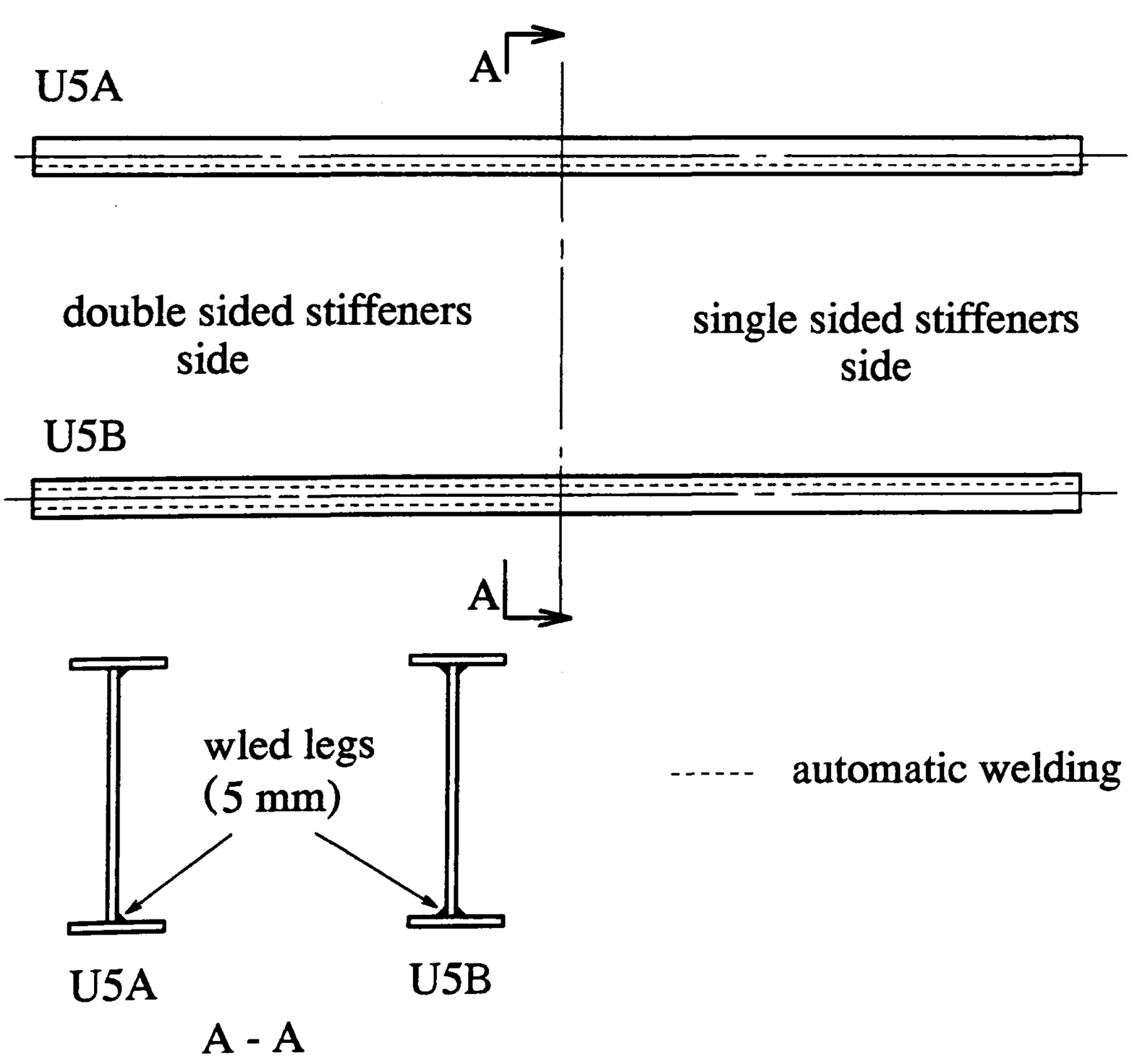

Figure 5.8: Welding details of specimen U5

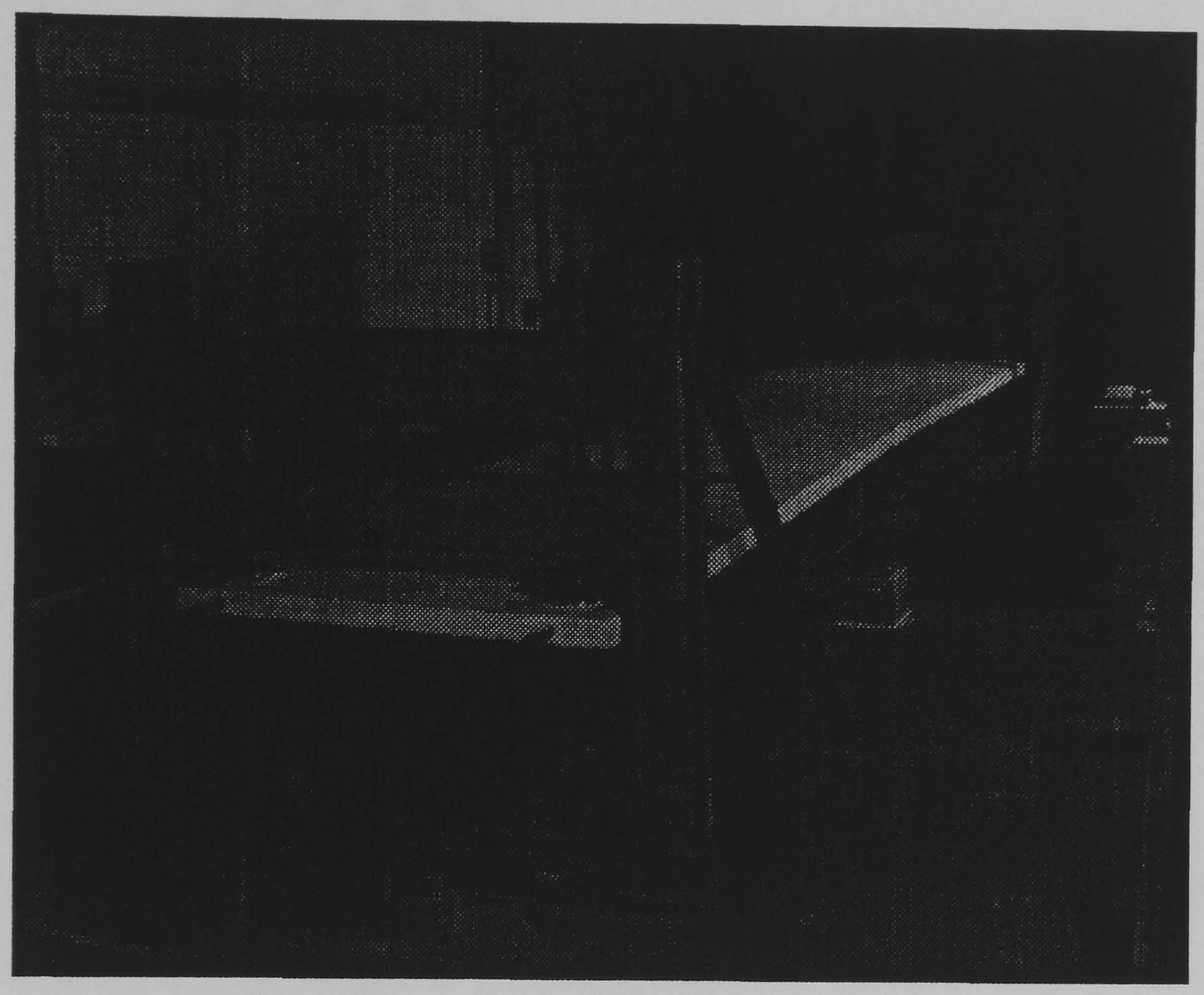

Figure 5.9: Loading arrangement

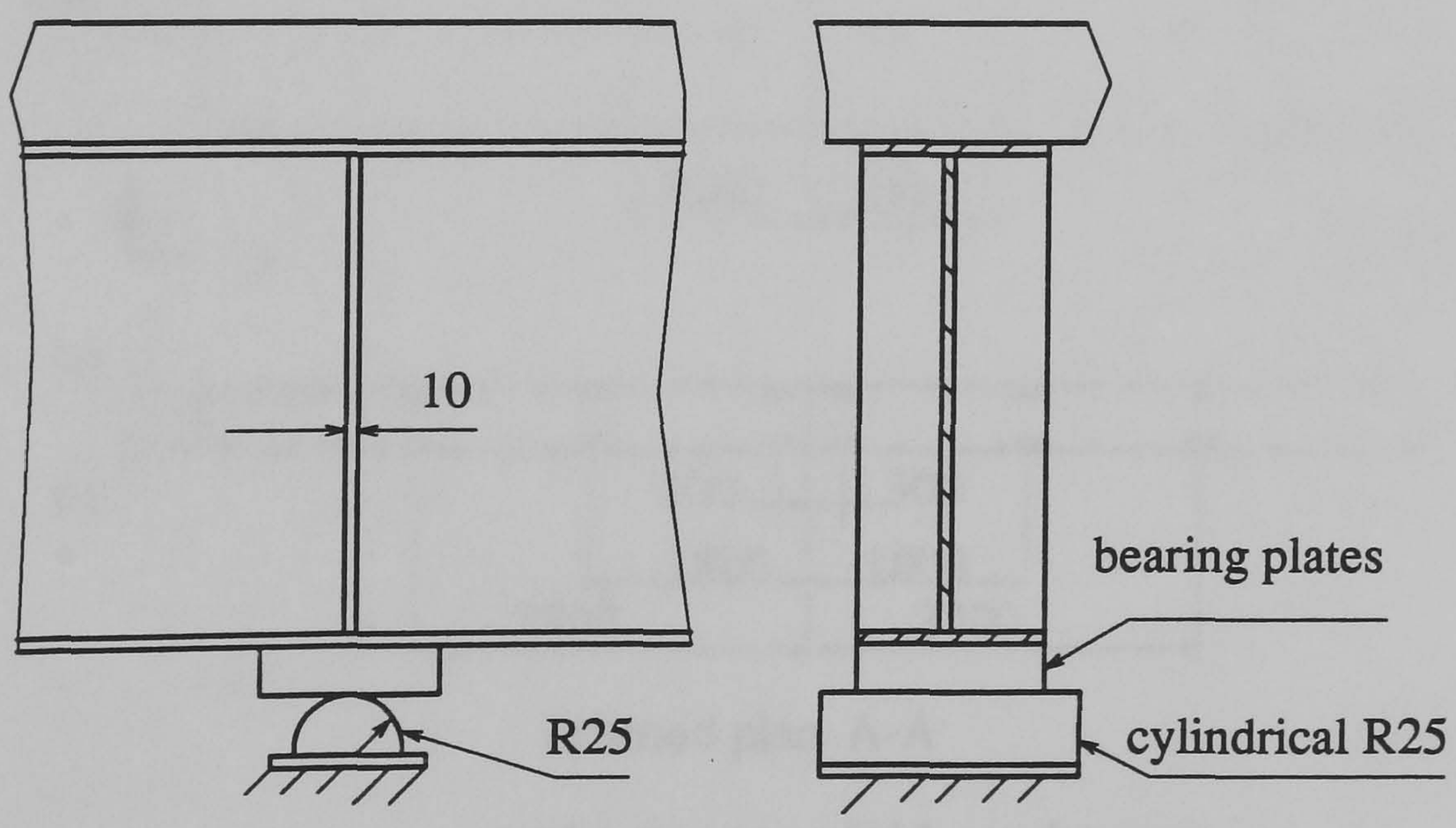

Figure 5.10: Cylindrical roller bearings

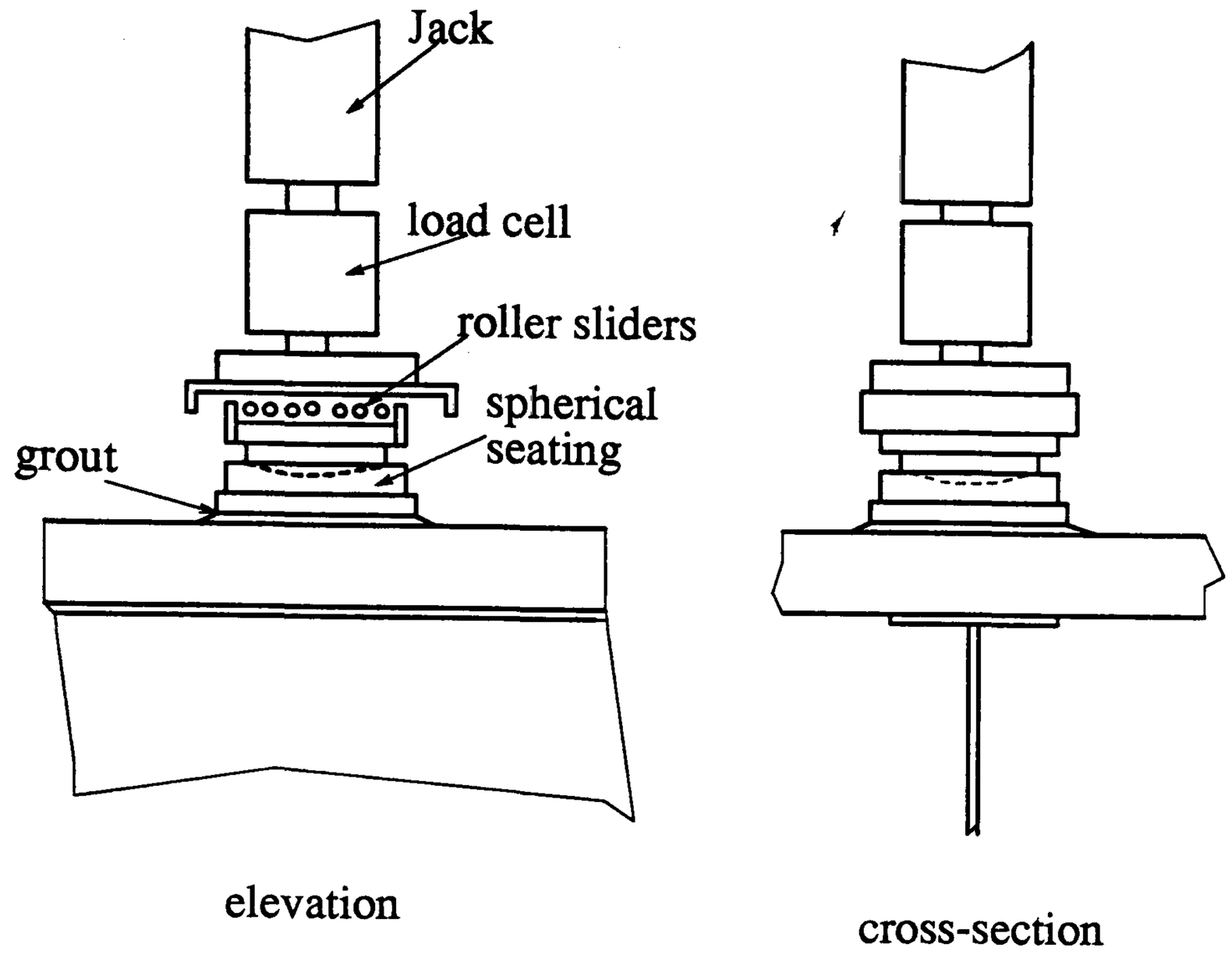

Figure 5.11: End reaction sets

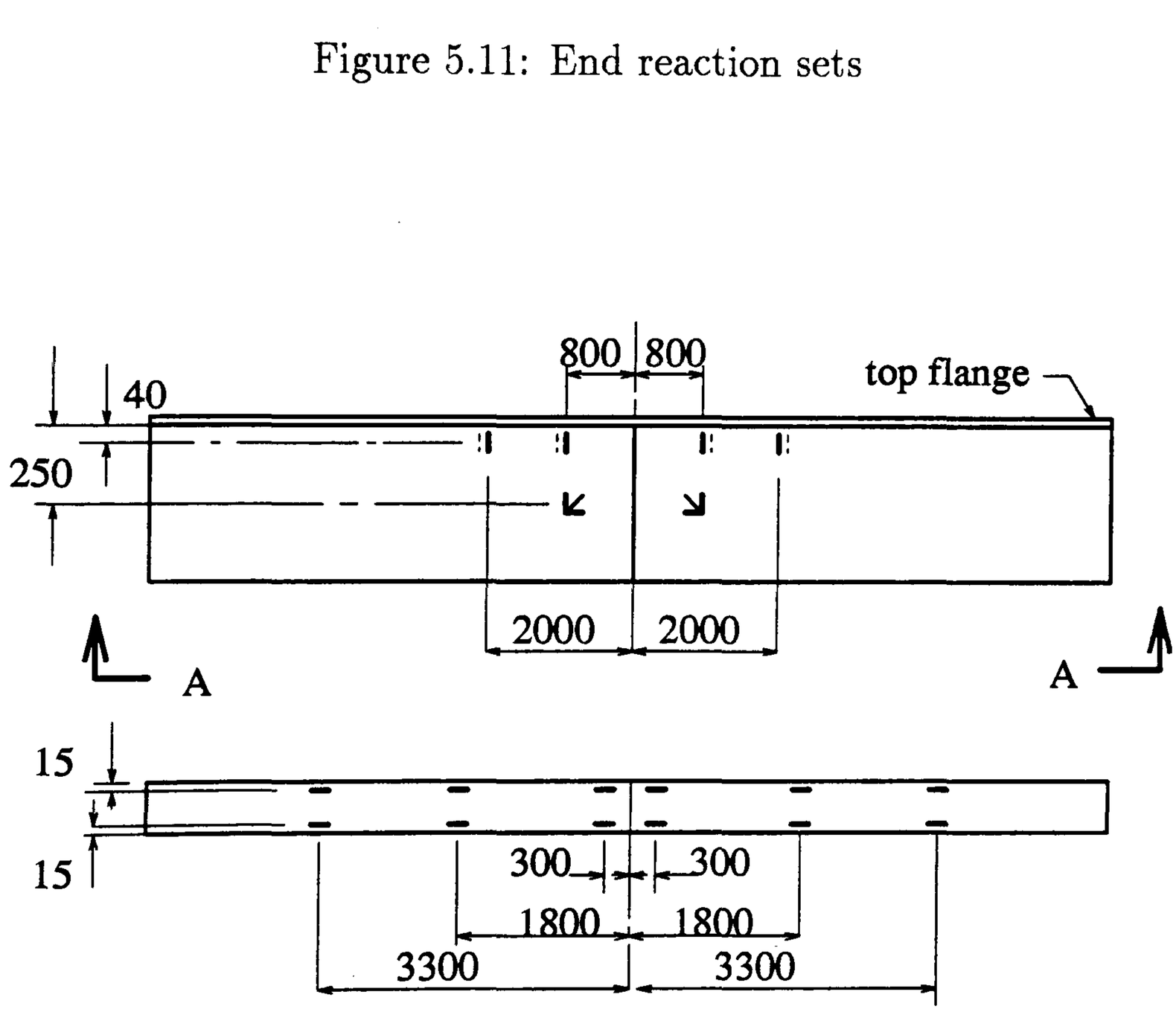

Figure 5.12: Strain gauge positions(U4B)

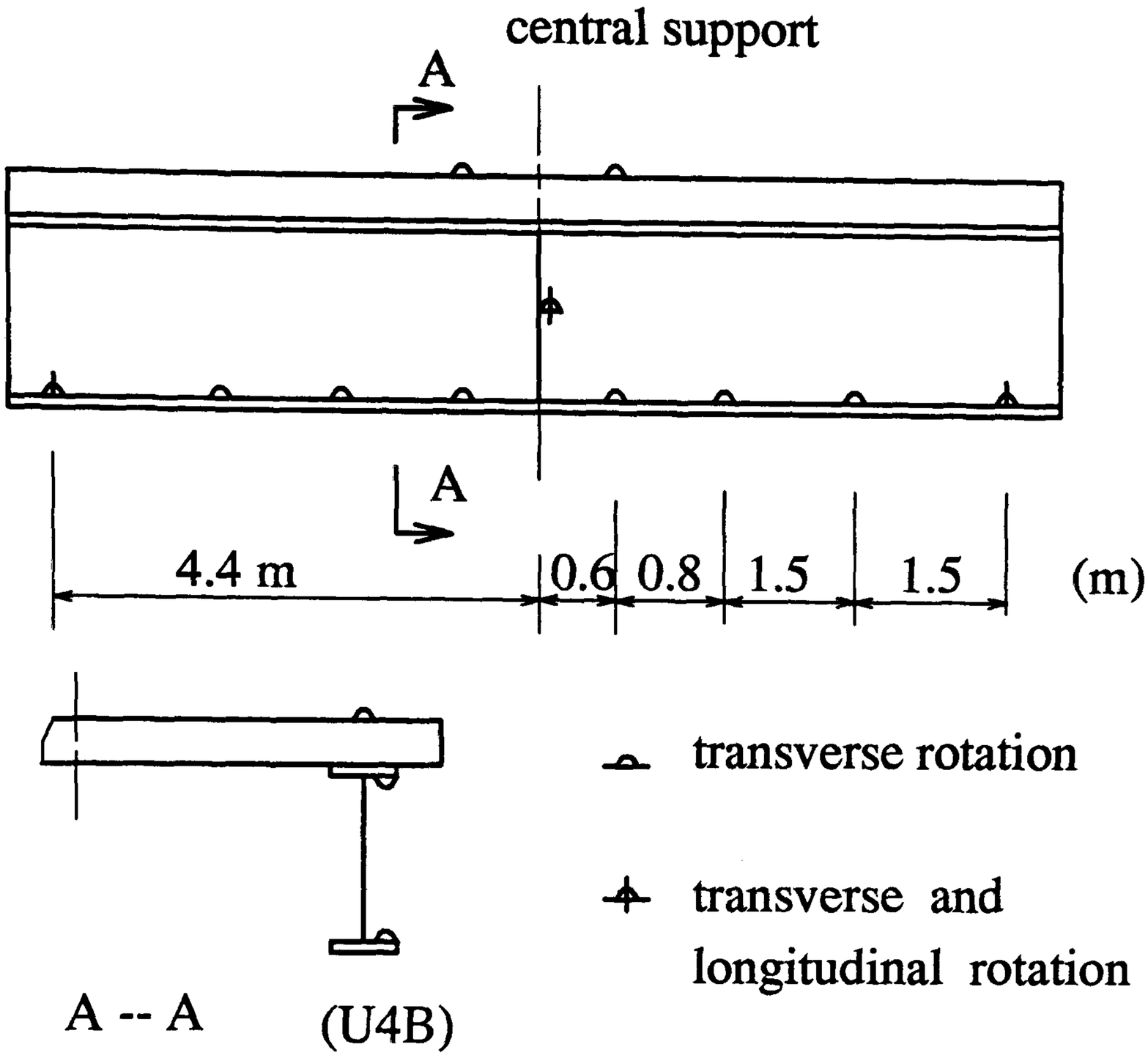

positions on U4A are the same

Figure 5.13: Inclinometer positions(U4)

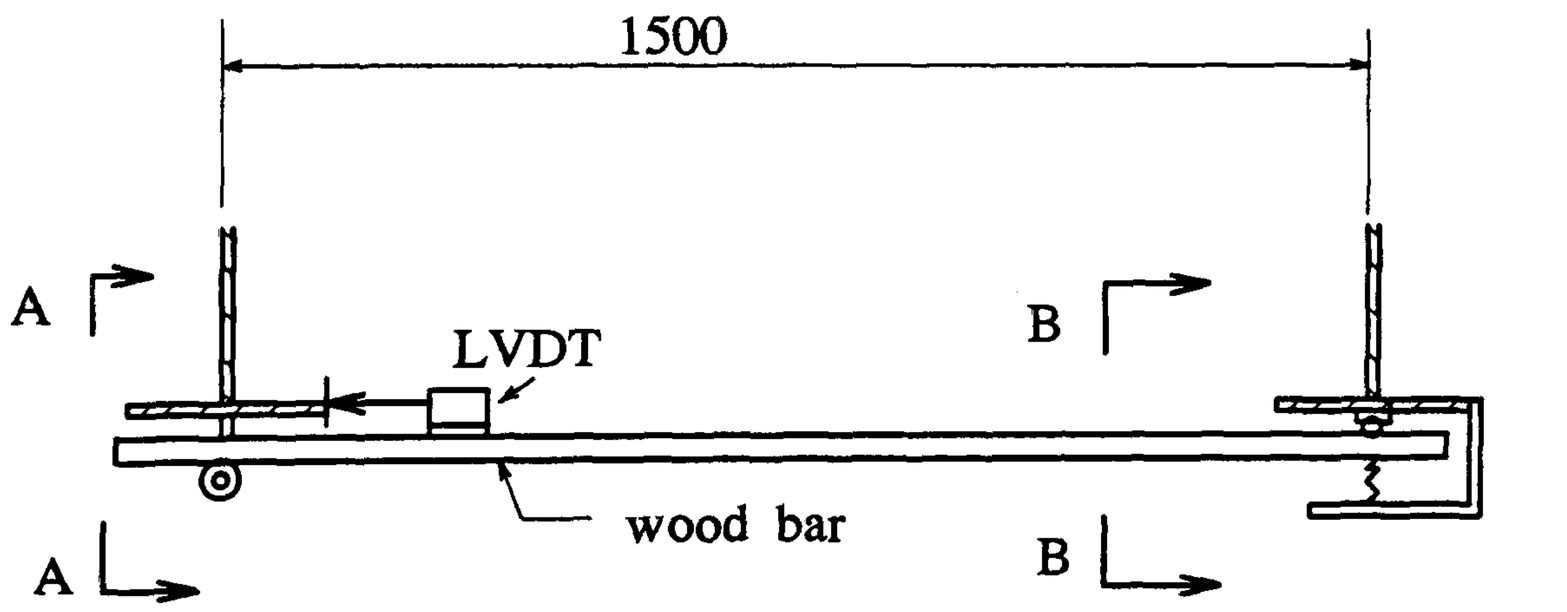

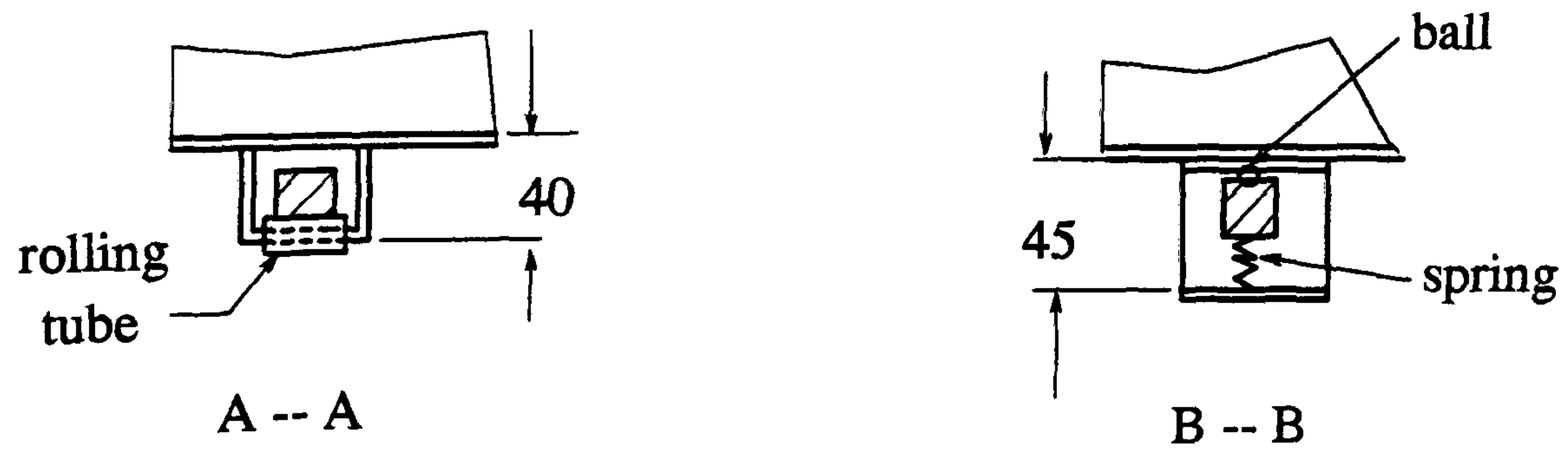

Figure 5.14: Relative lateral movement measurement(U5)

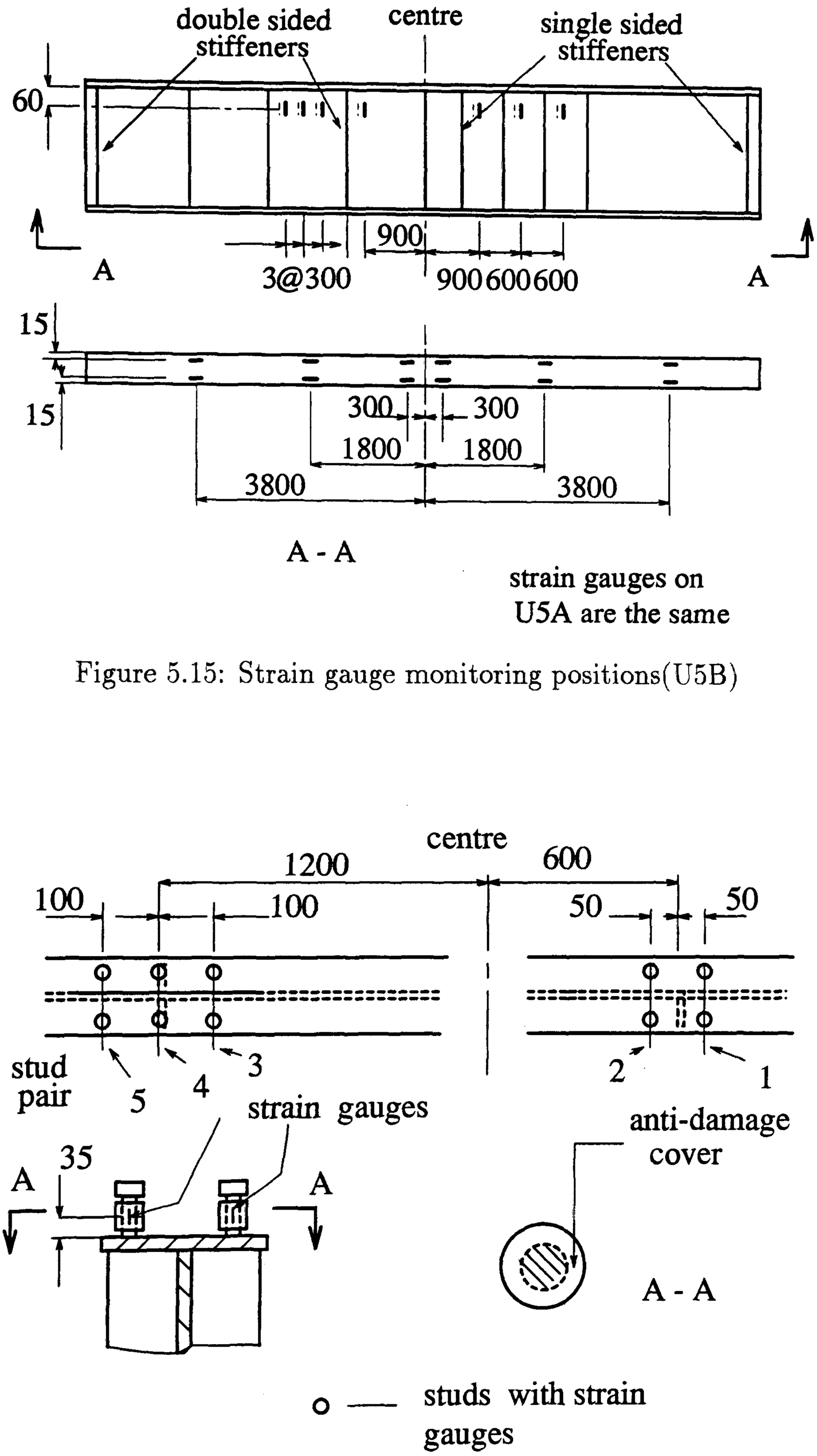

Figure 5.15: Strain gauge monitoring positions(U5B)

Figure 5.16: Strain guages on the studs(U5B)

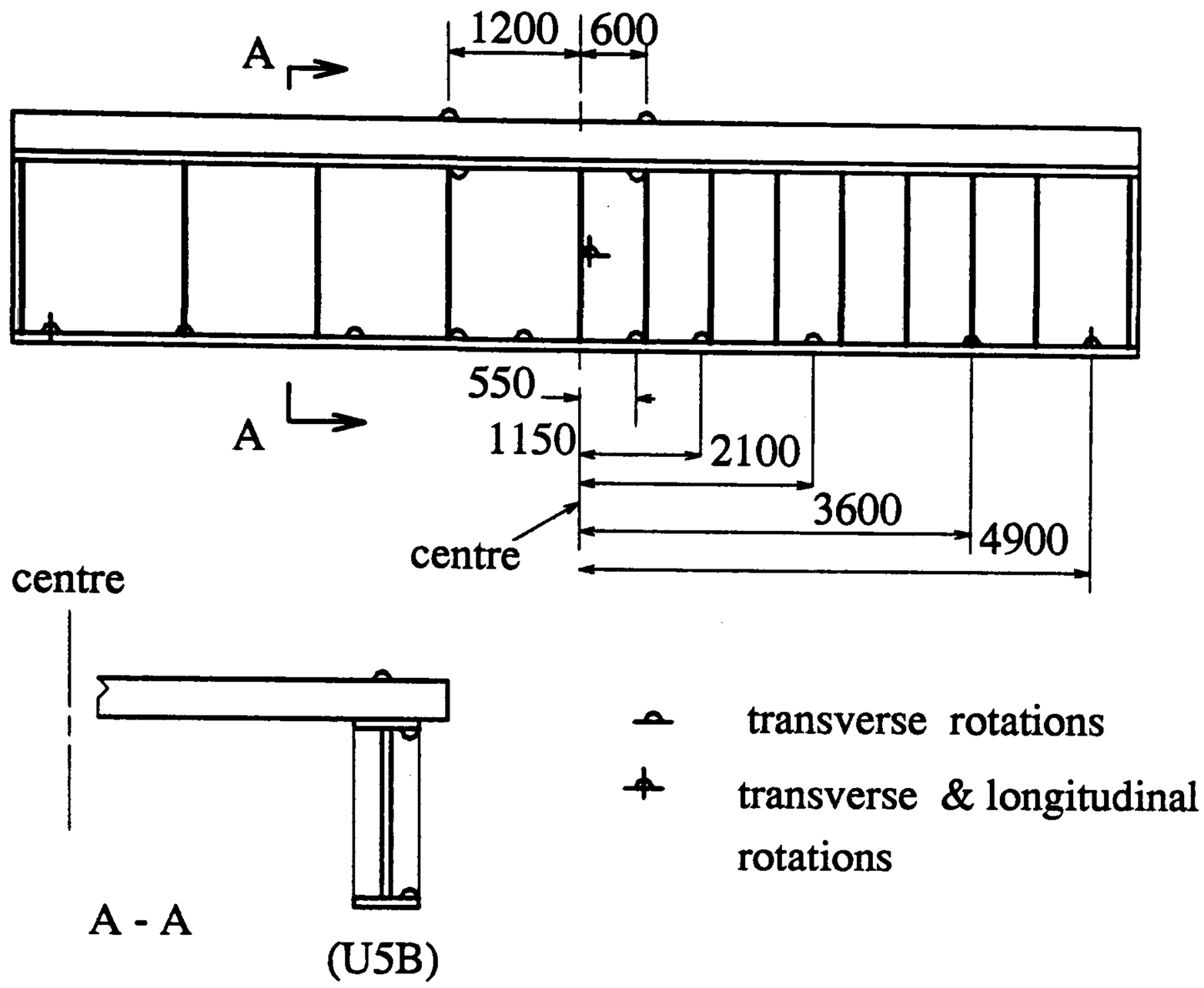

Figure 5.17: Inclinometer positions(U5)

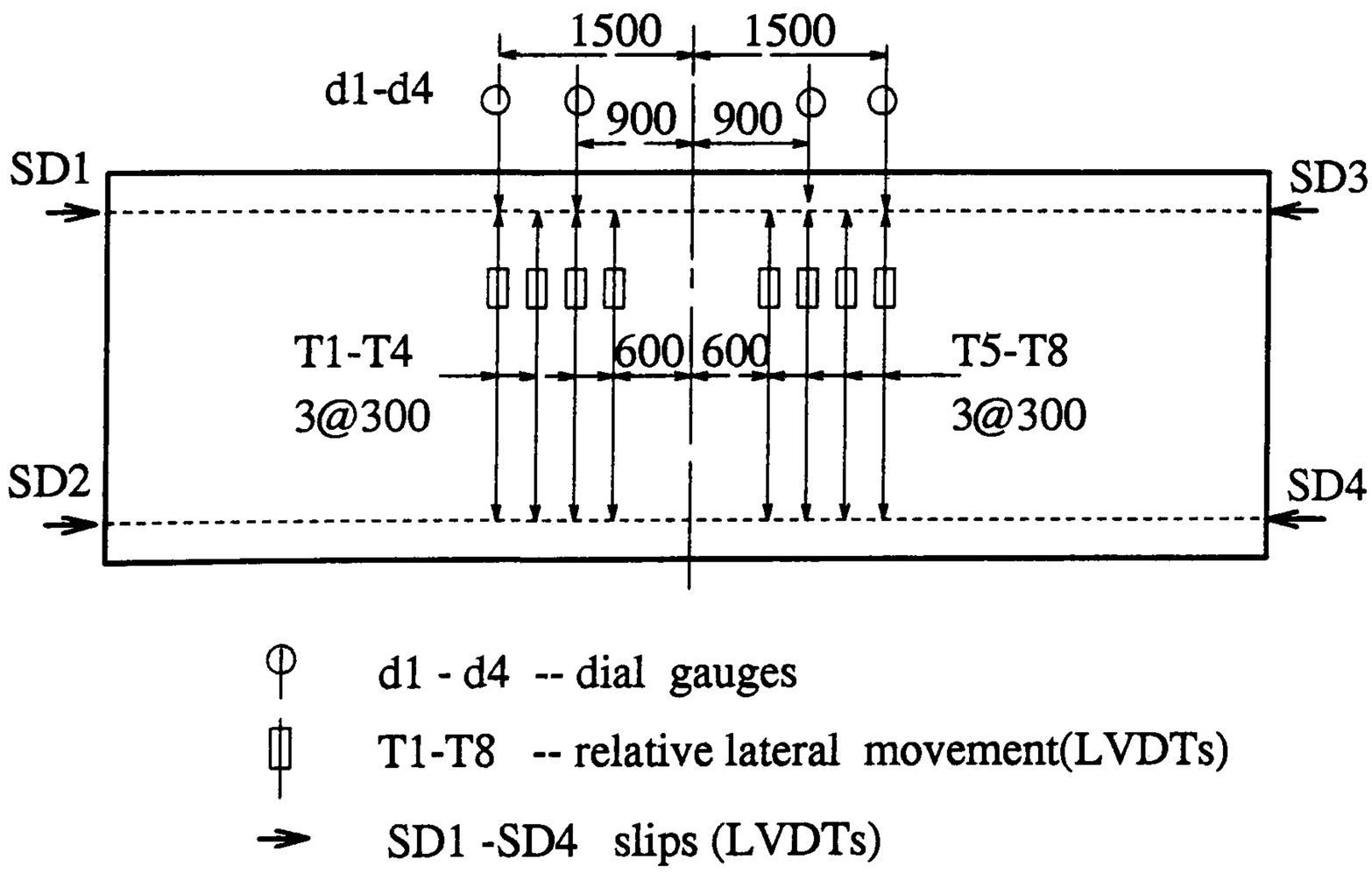

Figure 5.18: Lateral displacement measurement arrangements(U5)

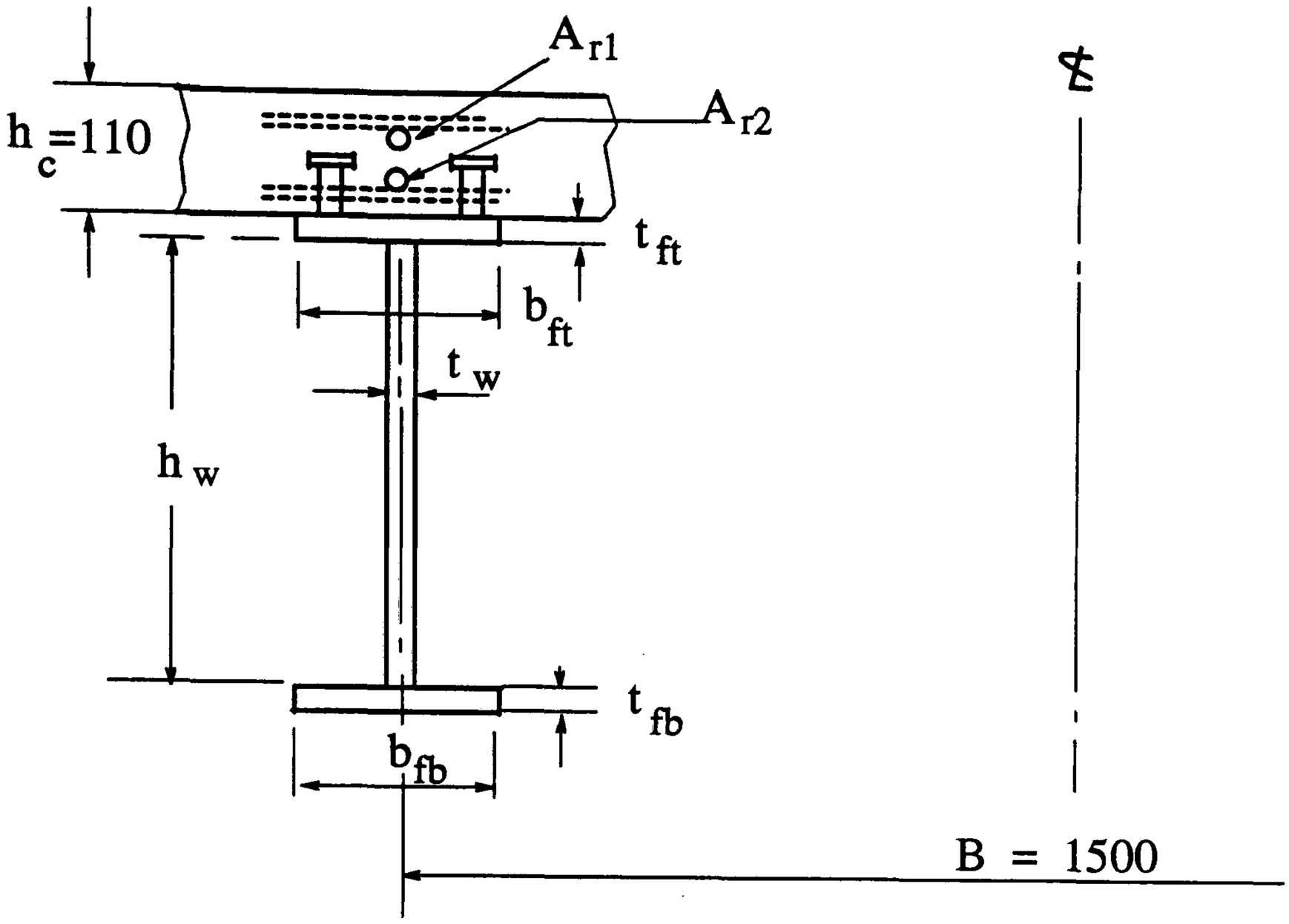

Figure 5.19: Notations of the cross sections(U4 and U5)

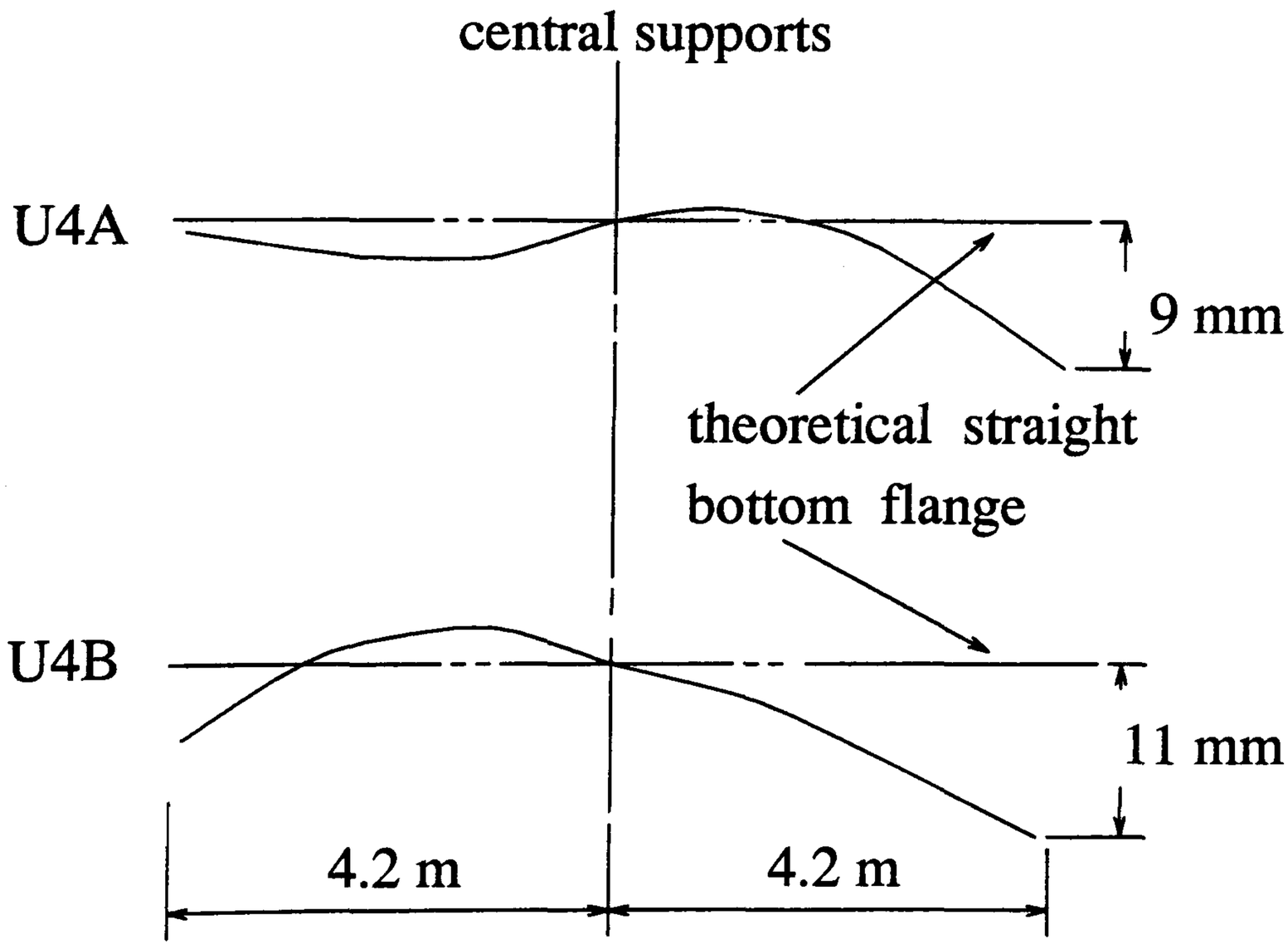

Figure 5.20: Initial lateral imperfections of bottom flanges(U4)

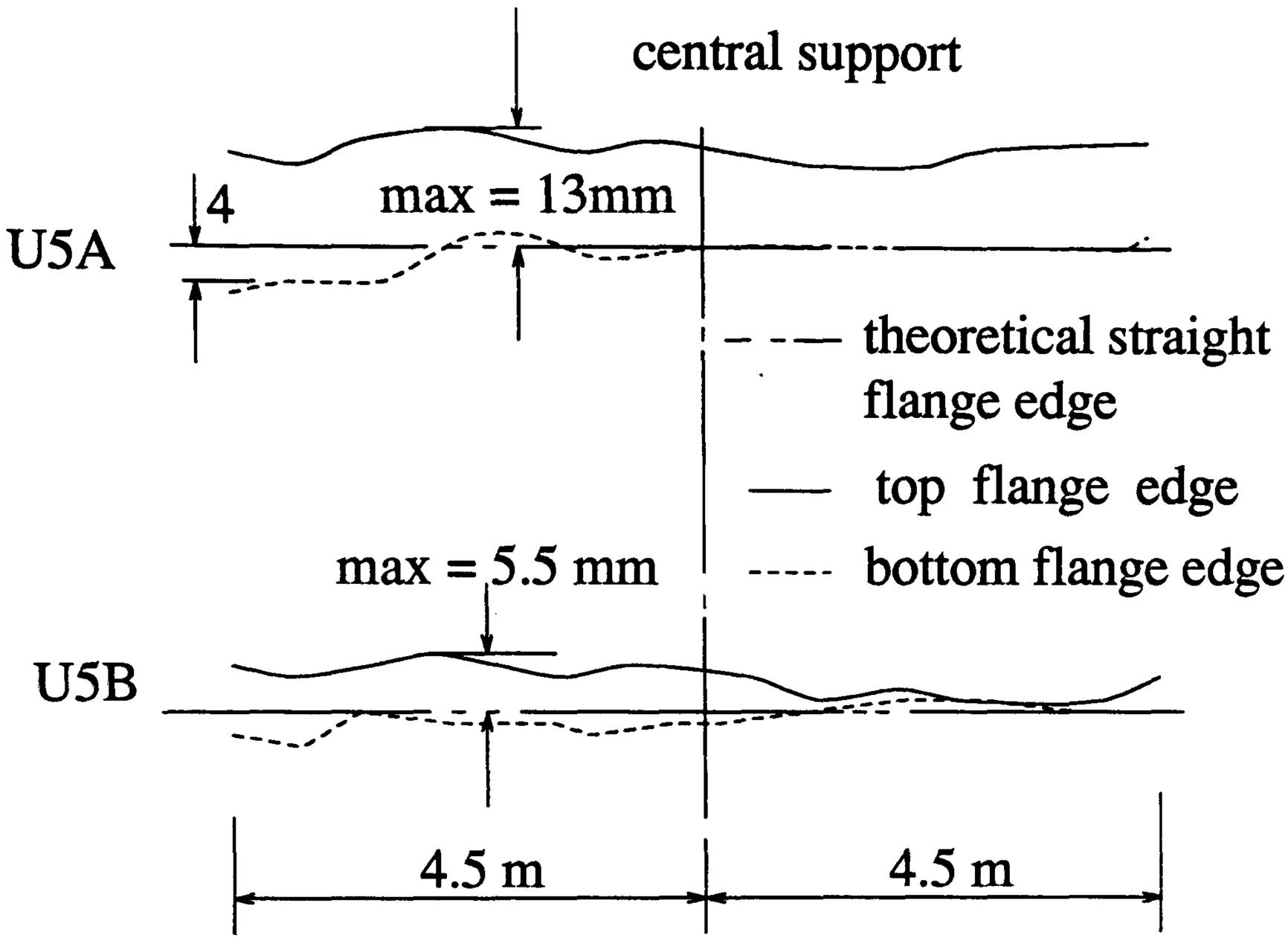

Figure 5.21: Initial lateral imperfections of bottom flanges(U5)

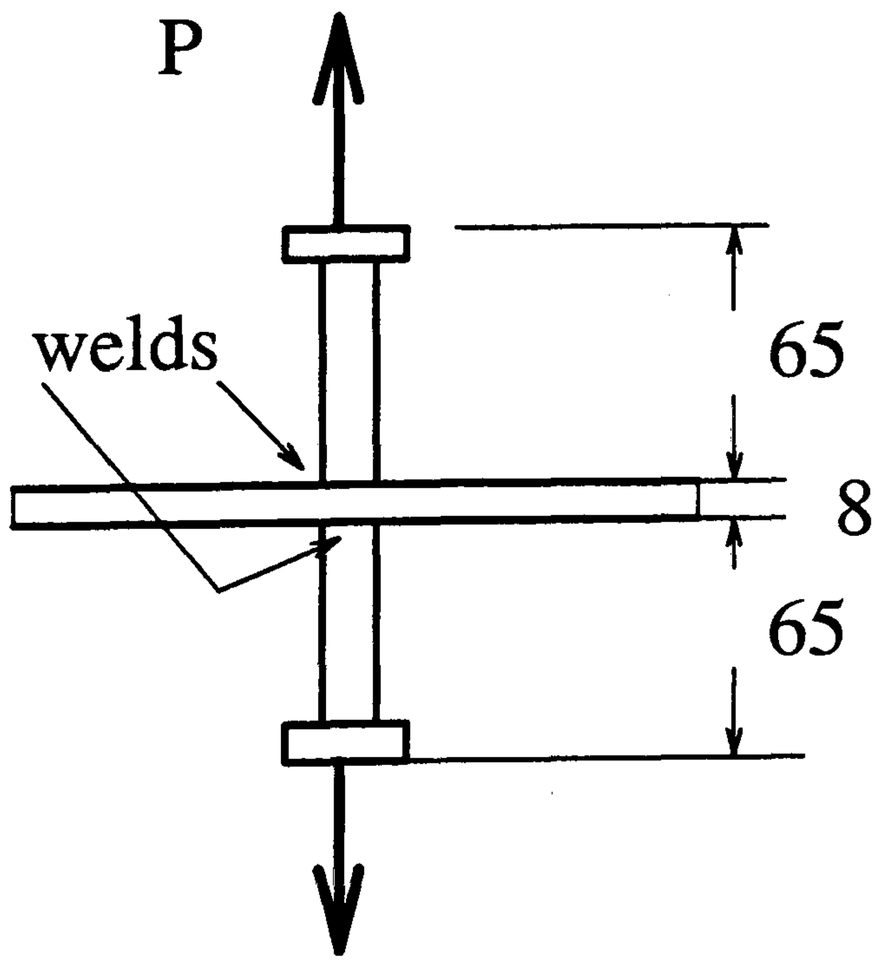

Figure 5.22: Welded stud tests

Chapter 6

Results of tests on specimens U4 and U5

6.1 Introduction

In this chapter, the results from the tests on specimens U4 and U5 are presented. Among the extensive strain and rotation data recorded in the tests, only these essential values and these representing significant changes in behaviour have been reported.

The slenderness and resistance of the specimens are also evaluated based on the relevant codes and design methods.

6.2 Slenderness and resistance of the beams

6.2.1 Slenderness

Design procedures for both steel and composite beams are linked to a classification based on the slenderness of steel elements in compression. As specimens U4 and U5 have identical cross-sections, the slendernesses are the same for both specimens. Since web and flange yield strengths differ by 20%, relevant mean ratios of the strength and mean values of the dimensions were used in calculations of slendernesses for the web and for the flange. In accordance with the draft Eurocode 4, the slendernesses of flange and web, λ_f and λ_w are defined by:

$$\lambda_f = \frac{c}{t_f \epsilon} \tag{6.1}$$

$$\lambda_w = \frac{d}{t_w \epsilon} \tag{6.2}$$

The notations of cross-sections are given in Fig.3.6, where c is the outstand flange in compression, and $\epsilon = \sqrt{235/f_y}$. Table 6.1 gives the web and flange slendernesses

for specimens U4 and U5. In the table, λ_{f1} and λ_{w3} are the slenderness limits of class 1 and 3 for flange and web, respectively.

6.2.2 Resistance of the specimens

Table 6.2 gives the yield and plastic moment resistances of the two specimens.

In the Table, the hogging yield and plastic moment resistances, M_y and M_p, calculated neglecting shear lag in the slab, were about 1% below and above the mean values. The material partial factors γ_m were all taken to be 1.0.

The slight differences in the resistances are attributed from the differences in dimensions and yield strengths.

Lateral buckling resistance for the unstiffened specimen, U4, is also given based on the relevant design methods. These design methods are only for composite beams with continuous U-frame action, and have been described in chapter 2. The Weston method [44] is based on a beam with uniformly distributed loading, so that there will be some error applying this method to specimen U4, in which the bending moment is a linear distribution. The EC4 method [1] and SCI method [49] provide more options of moment gradients, so that in the calculation of the lateral buckling resistance by these two methods, specimen U4 was assumed as a hogging region between two contraflexure points near an internal support, with a linear bending moment gradient. However, for stiffened beams with discrete U-frame action, no methods are available for prediction of the lateral buckling resistance.

6.3 Results of tests

6.3.1 Specimen U4

Fig.6.1 shows the moment-rotation curves of U4A and U4B beams. The similar curves of moment-deflection are given in Fig.6.2. The numbers in the Figures represent corresponding load stages. The two dash point lines represent deformations (deflections or longitudinal rotations respectively) based on the elastic analysis by using cracked (EI_{cr}) and uncracked (EI_u) flexural stiffnesses [1]. The longitudinal rotation is the change in the angle between the tangents at the two ends of each

beam and the end deflection is a mean value of deflections at the two ends of each beam.

Distortional lateral buckling initiated near to stage 12 when in-plane bending strains at bottom flanges tended to increase fast as shown in Fig.6.3. The positions of these strains are at 300 mm away from the central support section. The in-plane bending strain is represented by the difference of strains between two strain gauges of a pair on the bottom flanges. Variation of plane bending strains in the bottom flanges of test 1 are shown in Fig.6.4 and the corresponding lateral movement of the bottom flanges is illustrated in Fig.6.5. Test 1 was stopped at stage 16 and the support moments are 317.9 kNm for U4A and 316.8 kNm for U4B. The lateral deformations measured at this stage show the obvious distortional lateral buckling modes nearly symmetrical about the central section for U4A, as shown in Figs.6.4 and 6.5. The difference of strength between the two beams results mainly for differences in their initial imperfections.

Figs 6.6 and 6.7 show the curves of transverse rotations against the support moments of beams U4A and U4B in test 1 when the specimen was unbraced except at the support section. The positions of the measurements are at sections 600 mm away from the central support section. One can find that the transverse rotations of the top flanges and the slab are much smaller than those of the bottom flanges.

In test 2, the beams were stabilized by cross bracings at two sections each side of the central support section. The ultimate strength of the beams is governed by a complex interaction between distortional lateral buckling and local web buckling. At load stage 21 U4A had more loading then U4B, which caused a discrete gap between U4A and U4B in moment-rotation and moment-deflection curves (Figs.6.1 and 6.2). Possible reasons for this may be by mistakes in loading sequence and also the beginning of yielding in the steel. Buckling initiated at load stage 23, and the maximum recorded support moments are 405.7 kNm for beam U4A and 405.4 kNm for beam U4B at load stage 24.

Fig.6.8 shows the variation of in-plane bending strains in the bottom flanges along beams U4A and U4B.

The measurement of strains in the bottom flanges also illustrates compression forces of the bottom flanges and in-plane bending induced by lateral buckling.

Figs.6.9 and 6.10 show the curves of mean compression strain in the bottom flanges of specimen U4 against the support moment and Figs.6.11 and 6.12 show the curves of in-plane bending strains against the support moment in the same places of beams U4A and U4B. They were measured from the same strain gauges from which, the bending strains in Fig.6.3 were measured, positioned at 300 mm away from the support section and arranged in pairs as shown in Fig.5.12.

Lateral movements of the bottom flanges were restrained at the braced positions, and lateral deformations were distributed in four regions separated by the braced sections as shown in Fig.6.13. Compared with beams without cross bracings(Fig.6.5), the length of buckling region is reduced because of lateral restraints to bottom flanges.

Similar to Figs. 6.6 and 6.7, Figs.6.14 and 6.15 show the curves of the transverse rotations against the support moment in beams U4A and U4B, at the positions 600 mm away from the supports in test 2.

Local web bucklings were observed near the support regions for both beams at stage 24. For beam U4A, there was inward web buckling in the left side and outward buckling in the right, and for beam U4B, the web buckled outward in the left and inward in the right side.

Development of web distortion is shown in Figs.6.16 and 6.17, in which the web distortion is defined as difference of strains of a pair of strain gauges bonded onto the each side of the web, positioned at 40 mm from the top flange and 800 mm and 2000 mm from the central support. The effect of local buckling is eliminated at this position. It is found that large web distortion started at stage 23 or 24, nearly as the same as when lateral buckling occurred.

Fig.6.18 illustrates the lateral buckling shape of the bottom flange and the local web buckling near the support section of the beam U5B.

The initial cracks of the slab appeared near the central support ,at an early stage in test 1, and the subsequent parallel cracks developed with a spacing about 150 mm, which was the spacing of the transverse reinforcement. This reveals that formation and positions of the cracks are related to the reinforcement arrangement. The crack pattern is also illustrated in Fig.6.18.

6.3.2 Specimen U5

Fig.6.19 shows the moment-rotation curves of U5A and U5B. The numbers in the figure represent the corresponding load stages.

The dash point line represents predicted deformation by the cracked (EI_{cr}) method. At the calculated yield moment, the predicted rotations agree well with the test results.

In the first part of the test, lateral buckling initiated at stage 10, in beam U5B, when the support moment was 315.9 kNm (0.9 M_{yb}) as illustrated in Fig.6.20, in which the in-plane bending strain increased fast at the bottom flange close to the support. The beams were loaded up to stage 12 when the support moments were 362 kNm in U5A(1.0 M_{ya}) and 358.7 kNm in U5B(1.02 M_{yb}) at which local web buckling was observed near the support in the both beams. However no lateral buckling was found in U5A in the first part of the test.

In the second part of the test, because the web panels near the support section were strengthened by equally spaced vertical steel angles in a way as shown in Fig.5.7, the resistance to local buckling in the web panels was therefore enhanced, and the beams were loaded starting from stage 20 up to stage 29 when yielding occurred at the sections near the central support. The lateral buckling initiated at stage 26, about the same value of the moment as before in U5B as shown in Fig.6.20, accompanied by severe out of plane deformation of the strengthened web panel near the support. The local flange buckling was also observed at U5A, near the support, which involved a mixed interactive buckling mode with lateral flange buckling.

The mean values of the maximum deflections at the ends of the beams reached at the tests were 100.33 mm for U5A and 100.34 mm for U5B. The mean values of the deflections at the maximum loading (stage 34) were 70.27 mm and 70.17 for U5A and U5B respectively, compared with the values of 47.3 mm and 47.8 mm at stage 12, when yield moment was reached at the support. The mean values of the corresponding longitudinal rotation θ (Fig.6.19) were 36.6 mrad and 36.2 mrad at stage 34 and 48.1 mrad and 46.9 mrad at stage 46. The relevant values are given in Tables 6.3 and 6.4.

Transverse rotations of the bottom flanges of the beams are illustrated in Fig.6.21. The lateral buckling in U5A was concentrated only in the left side of the beam adja-

cent to the central support section. The half buckling wavelength of U5A is shorter than that of U5B and it is an interactive buckling mode of local flange buckling and overall buckling, in which the local flange buckling dominates. The obvious local flange buckling was observed at stage 34. The relevant values of the transverse rotations in the bottom flanges of beams U5A and U5B are given in Tables 6.5 and 6.6. The positions R1 to R10 are illustrated in Fig.6.22.

Fig.6.23 shows separately the moment-rotation curves of the four cantilevers, to distinguish failure modes of different parts of the U5 beams. The moment-rotation curve of the right side of U5A, where the web has single sided stiffeners at spacing of 0.6 m, shows that the rotation increased with the support moment up to the maximum value attained in the test, then reduced elastically as the moment decreased, leaving a permanent rotation caused by the slab cracks and steel yielding. There is no sign of buckling on this side of the beam. On the other hand, the moment-rotation curve of the left side of the beam(U5A), where the web has double sided stiffeners at spacing of 1.2 m, shows that the rotation still increases when the moment drops from its maximum value so that it corresponds to a characteristic beam failure. The curves are consistent with the transverse rotation patterns of the bottom flanges shown in Fig.6.21, with lateral buckling concentrating at the first stiffened panel adjacent to the central support on the left side and no sign of lateral buckling on the right side.

The moment-rotation curve of the right side of U5B, where the web has single-sided stiffeners at spacing of 0.6 m, appears stiffer than that for the other side of the beam,with double sided stiffeners at spacing of 1.2 m. The difference may be caused by the fact that the strengthened web panel on the left side is weaker than on the right side. As shown in Fig.5.7, the strengthening angle at distance of 0.6 m from the central section on the left side is weaker than the stiffener at the same distance on the right side, and hence, yielding develops faster on the side with the weaker panel. The rotation flexibilities of the two sides of U5B beam are different, which reflects the different failure buckling. For the left side of the beam, the web panel was not strong enough, and the strengthening angles cannot prevent severe out-plane deformation developing further towards to the rest of the web panel, while for the right side of the beam, the local web buckling is effectively stopped by the

first stiffener at 0.6 m from the central section, and hence the out-plane deformation is basically within the first stiffened panel. This is well illustrated in Fig.6.24, which shows the contours of the web panel near the central support section(U5B). The contours of out-plane deformation for U5A are given in Fig.6.25, which shows that there is no sign of local web buckling on the right side (very small out-plane deformation as compared with the left side). The out-plane deformation pattern on left side is also different from that of left side of U5B, although they are all stiffened doubly sided at spacing of 1.2 m.

The measurements of lateral displacement were obtained from eight LVDTs spaced at 0.3 m near the central section each side. Fig.6.26 shows the results. It represents the relative lateral movement of bottom flanges of the two parallel beams(U5A and U5B). Corrections were made to eliminate the errors introduced by the transverse rotation of the bottom flanges. The absolute lateral movements of the beams are illustrated in Fig.6.27, in which the lateral displacement of U5A is based on the reading of four dial gauges near the central section.

The slip between the slab and the top flanges of the steel beams was everywhere less than 0.05 mm.

Fig.6.28 show the relative transverse rotation between slab and top flange at four locations above the stiffeners closest to the central section of the U5 beams. At stage 29 (or initially at stage 27), there developed a great transverse rotation at the connection between the slab and the steel for beam U5B.

Table 6.7 gives the measured strains in the studs above the stiffeners in beam U5B. The positions of the strain gauges are illustrated in Fig.5.16.

A better illustration of the transverse rigidity of the shear connection for this U-frame is shown in Fig.6.29, in which the difference of strains in the two studs of the pair 4 (directly above the double sided stiffener shown in Fig.5.16) is plotted against the relative transverse rotation between the slab and the top flange (transverse shear connection). Prior to stage 27 the rotation is very small. From stage 27 to stage 35, it increases in proportion with the transverse bending increment, represented by the difference of the strains in these two studs, while at stage 36, the rotation increases very very fast up to stage 42. The sudden increase in the flexibility of the connection shows that failure of concrete occurred around the shear connectors. As

stage 36 was after the maximum loading, the moment-rotation curves go into the falling branches. No further full set of readings was taken until stage 42, when the moment at the support section had dropped from 1.2 M_{ya} to 1.1 M_{ya} for U5A and from 1.16 M_{yb} to 1.04 M_{yb} for U5B.

Fig.6.30 shows the strain differences in the three pairs of studs (pairs 3, 4, 5 shown in Fig.5.16) against the support moment for beam U5B. These studs position above the stiffener, which is double sided and closest to the support section. The transverse bending induced by lateral buckling of the bottom flange is transmitted via the studs to the slab. Because the studs are fully embedded in the concrete before shear failure of the concrete around the connection, the transvese bending resisted by the studs does not equal to the total transverse bending of the U-frame. The solid line in Fig.6.30 represents the curve for the middle studs (pair 4 in Fig.5.16) and the dash lines represent the curves for the two adjacent pairs of studs (pairs 3 and 5). It is found that at the location of a discrete U-frame, the middle pair of studs subject to much more transverse bending than the adjacent pairs of studs, especially when lateral buckling occurs and thereafter. This is because these studs are right above the position of a stiffener, so that thay are stiffer than the adjacent studs. It agrees with the test results by Molenstra [78], that the closer the studs are to a stiffener, the more transverse bending moment they subject to.

Similarly, the strain differences in the two pairs of studs (pairs 1 and 2) above the single sided stiffened U-frame are plotted against the support moment in Fig.6.31.

The web distortions are illustrated in Figs. 6.32 and 6.33, in which the differences of strain in four strain gauges are plotted against the support moment for each beam. Similar to those in the specimen U4, the strain gauges were bonded beyond the region of local buckling, (0.9 m from the central section for the nearest strain gauges), and 60 mm from the top flanges. The results show that web distortions were accompanied by lateral buckling, and vertical web stiffeners reduced the web distortion compared with the specimen U4, particular at those locations further away from the support sections, and hence improved the lateral buckling strength.

The transverse crack patterns of the slab in the specimen U5 are similar to those for the specimen U4, parallel and with spacing about equal to that of the transverse reinforcement. However, short longitudinal cracks were formed at the

locations above the stiffeners close to the support section in the specimen U5B. This is illustrated in Fig.6.34.

6.4 Summary of the test results

To summarize the test results, Table 6.9 give the support moments at initial buckling M_{ini} and at maximum loading M_{max}. The corresponding deflections, δ_{ini} and δ_{max}, are also given. In Table 6.9, l_b is the length of buckling regions measured in the tests, and it reveals different dominating buckling modes.

Table 6.1: Classification of cross-section(U4 and U5)

method	λ_f	λ_{f1}	λ_w	λ_{w3}
EC4	7.25	9.0	107.0	95.3

Table 6.2: Moment resistances of the specimens(U4 and U5)

specimen mehtod	M_y kNm	M_p kNm	M_d EC4 kNm	M_d Weston kNm	M_d SCI kNm	
U4A	362	503	192	210	184	unbraced
U4B	356	499	189	205	181	unbraced
U4A			256	329	268	braced
U4B			253	317	261	braced
U5A	362	497				
U5B	351	487				

Table 6.3: Support moments and end deflections(U5)

Stage No.	M_a kNm	δ_{al} mm	δ_{ar} mm	M_b kNm	δ_{bl} mm	δ_{br} mm
	0.0	0.0	0.0	0.0	0.0	0.0
0	44.1	1.8	1.4	44.1	1.8	1.4
1	86.2	5.1	4.9	90.9	5.0	4.9
3	141.8	11.6	11.5	141.8	11.7	11.3
6	193.1	19.7	19.5	190.4	20.0	19.8
9	290.8	35.4	35.7	290.1	35.3	35.2
10	319.6	39.7	39.8	315.9	40.1	39.9
11	347.6	44.4	44.2	339.3	44.7	44.5
12	361.8	48.0	48.2	358.7	48.0	47.9
20	46.2	12.9	13.0	44.2	13.2	12.7
23	193.6	30.2	30.4	192.4	30.5	30.3
24	240.6	36.1	36.3	239.9	36.1	36.1
25	292.7	42.4	42.4	290.5	42.3	42.3
26	339.7	48.1	48.5	336.7	48.2	48.2
27	365.2	51.5	52.0	358.3	51.8	51.4
28	385.6	55.3	55.5	378.9	55.3	55.3
29	397.5	57.9	58.0	386.9	57.7	57.8
31	421.0	63.9	64.0	403.7	63.9	63.9
32	428.2	67.2	67.2	404.5	67.3	67.2
34	433.9	70.2	70.2	406.8	70.2	70.1
36	423.9	74.2	74.4	401.3	74.3	74.2
40	412.2	80.3	80.4	389.8	80.4	80.3
42	398.6	85.8	85.7	365.0	85.7	85.7
46	359.8	100.3	100.3	296.5	100.3	100.3

Table 6.4: Longitudinal rotation

Stage No.	θ_{al} mrad	θ_{ar} mrad	θ_{bl} mrad	θ_{br} mrad
	0	0	0	0
0	0.6	0.6	0.5	0.5
6	5.1	5.6	5.2	5.2
9	9.4	9.8	9.5	9.6
11	12.0	12.2	11.9	12.0
12	12.8	13.2	12.9	13.0
19	3.5	3.5	3.3	3.3
20	3.6	3.4	3.4	3.0
24	9.7	9.8	9.9	9.4
25	11.3	11.5	11.5	11.4
27	14.0	14.0	14.3	13.8
29	15.6	15.5	16.1	14.8
31	17.6	16.5	18.1	15.6
32	18.8	16.9	19.1	16.2
34	19.5	17.1	19.8	16.4
36	21.9	17.1	21.2	17.1
40	24.1	16.9	23.1	17.5
42	28.4	16.3	25.8	18.3
46	32.2	15.9	27.7	19.2

Table 6.5: Transverse rotation of the bottom flange (U5)

U5A Stage No.	R1 mrad	R2 mrad	R3 mrad	R4 mrad	R5 mrad
	0	0	0	0	0
6	-0.5333	-0.1000	1.1000	0.0333	3.6333
9	-0.7667	-0.2333	1.3333	-0.2333	2.6333
11	-0.4667	0	1.4333	-0.9000	9.7000
12	-0.7000	-0.1667	1.2000	-1.2667	11.5667
20	-0.9333	-0.7000	-1.1333	-1.3667	0.8000
24	-0.2000	0.1333	1.2333	-0.0333	1.4667
27	-0.4667	0.1000	1.5333	-0.2000	5.0667
29	-0.1333	0.3667	1.7667	-1.0333	7.4000
31	-0.1333	0.4667	1.2333	-2.1667	11.2000
32	-0.1333	0.6000	0.8333	-3.0000	13.9000
35	0.0333	0.7000	0	-3.7333	17.7000
36	-0.1667	0.5333	-0.1333	-3.8000	21.2333
42	0	0.4667	-1.5000	-4.3333	35.7000

U5B	R1	R2	R3	R4	R5
	0	0	0	0	0
6	-0.0233	0.0033	-0.1267	0.0367	-0.0067
9	-0.2667	0.2667	-1.4333	0.5667	0.4000
11	-0.7000	0.0667	-1.9000	0.9000	0.7667
12	-0.5000	0.1667	-1.8333	1.3000	1.4333
20	0.2000	0.2667	0.4000	0.5333	0.9667
24	-0.3333	0.0667	-1.3000	0.4000	-3.8333
27	-0.6000	0.1333	-2.0000	1.9333	-2.6667
29	-0.9667	-0.2333	-1.9333	4.2000	-0.6667
31	-0.7333	-0.5000	-1.1667	4.9333	2.2333
32	-0.8333	-0.7667	-0.3000	10.3000	4.2667
35	-1.1333	-1.1000	0.7333	13.6333	6.1000
36	-0.7333	-1.2000	1.5333	15.7000	7.1000
42	-1.3000	-2.8000	8.4000	30.9000	17.7000

Table 6.6: Transverse rotation of the bottom flange (U5)

U5A Stage No.	Centre mrad	R6 mrad	R7 mrad	R8 mrad	R9 mrad	R10 mrad
	0	0	0	0	0	0
6	0	0.7667	0.3333	1.0667	-0.0333	0.5333
9	0.1000	1.5333	0.4667	1.7333	0	1.0000
11	0.1000	2.2000	0.5333	2.4333	0.3000	1.5333
12	0.1667	2.5000	0.5667	2.6333	0.2667	1.4333
20	0	0.4333	-0.0333	0.1333	0.2000	0.1333
24	0.2000	0.7000	0.3333	0.7667	-0.2333	0.7000
27	0.3667	1.3333	0.4000	2.1333	-0.0333	1.3333
29	0.7333	1.0333	0	2.3333	-0.1667	1.3000
31	0.6667	1.7333	-0.0667	2.4000	-0.2667	1.4333
32	0.8000	1.6667	-0.3667	2.4333	-0.1667	1.6000
35	0.8667	0.4000	-1.7333	1.9667	0.1667	1.7333
36	0.9000	-0.4333	-2.5333	1.7000	0.2333	1.7667
42	1.6333	-5.0667	-6.6333	-0.2667	0.7333	1.7000

U5B	Centre	R6	R7	R8	R9	R10
	0	0	0	0	0	0
6	-0.0100	-0.0467	-0.0700	0.0300	-0.0367	0.0333
9	-0.1333	-1.0667	-1.5667	0.4000	-0.6667	0.2333
11	-0.2667	-1.6667	-2.7000	0.7333	-1.5333	0
12	-0.2333	-2.0333	-2.2667	0.9333	-0.6333	0.1000
20	-0.1000	-0.6333	-0.9667	-0.4667	-0.5000	-0.5000
24	0	-1.1667	-0.7667	0.5667	-0.0667	0.6000
27	-0.1333	-1.6667	-1.8667	1.2333	-0.3000	0.3000
29	-0.1667	-3.8000	-2.7000	2.0667	0.1000	0.5667
31	-0.1667	-7.9333	-4.0333	2.8000	0.4667	0.5000
32	-0.2667	-10.3000	-4.8000	3.1333	0.6667	0.4333
35	-0.3000	-15.7667	-6.0667	3.3333	0.8333	0.3667
36	-0.3000	-18.0000	-6.9667	3.4667	0.9667	0.3667
42	-0.4000	-30.0667	-11.9667	3.4667	1.8333	0.4333

Table 6.7: Measured strains in studs (U5B unit = $\mu\epsilon$)

Stage No.	1	2	3	4	5	6
	0	0	0	0	0	0
0	0.7000	0.1000	1.3000	-5.9000	-4.6000	-0.7000
1	18.8000	7.3000	10.5000	6.5000	-2.5000	4.5000
2	113.1000	56.1000	9.3000	0	-6.4000	10.5000
5	146.9000	63.3000	68.3000	15.5000	-30.7000	12.8000
6	250.5000	169.5000	30.1000	19.3000	-54.7000	22.6000
7	317.3000	224.1000	-7.1000	26.2000	-104.0000	6.4000
9	376.6000	261.1000	-35.4000	39.6000	-146.4000	-18.3000
10	407.1000	279.5000	-40.8000	50.1000	-157.8000	-18.3000
11	432.0000	297.1000	-47.7000	60.2000	-170.9000	-26.8000
12	467.3000	321.1000	-54.8000	70.3000	-185.2000	-35.2000
19	315.3000	163.0000	-7.0000	9.3000	-77.8000	-63.9000
	×1.0e+03	×1.0e+03	×1.0e+03	×1.0e+03	×1.0e+03	×1.0e+03
20	0.3153	0.1630	-0.0070	0.0093	-0.0778	-0.0639
22	0.4893	0.2590	-0.0258	0.0202	-0.1622	-0.0900
23	0.5347	0.2905	-0.0464	0.0207	-0.1942	-0.0958
24	0.5820	0.3244	-0.0708	0.0156	-0.2172	-0.1125
25	0.6305	0.3574	-0.0875	0.0140	-0.2253	-0.0988
26	0.6849	0.3951	-0.1086	0.0139	-0.2307	-0.0997
27	0.7247	0.4212	-0.1126	0.0155	-0.2363	-0.1025
28	0.7813	0.4575	-0.0922	0.0237	-0.2375	-0.1042
29	0.8251	0.4872	-0.0525	0.0377	-0.2380	-0.1070
30	0.8790	0.5199	-0.0046	0.0610	-0.2382	-0.1102
31	0.9419	0.5492	0.0535	0.0902	-0.2345	-0.1071
32	1.0246	0.5811	0.1140	0.1182	-0.2333	-0.1105
34	1.3916	0.6436	0.2841	0.1374	-0.2310	-0.1508
36	1.5200	0.6943	0.4003	0.2102	-0.2269	-0.1281
39	1.8223	0.7638	0.5764	0.2670	-0.2120	-0.1204
41	1.9487	0.8258	0.6925	0.3450	-0.1701	-0.0494
42	2.0298	0.8766	0.7397	0.3833	-0.1453	0.0111
44	2.1721	0.9878	0.8656	0.4756	-0.0653	0.0358

Table 6.8: Measured strains in studs (U5B unit = $\mu\epsilon$)

Stage No.	7	8	9	10
0	-1.6000	-0.7000	1.0000	10.5000
1	-10.2000	11.0000	12.8000	9.5000
2	19.8000	29.8000	42.4000	38.2000
5	47.2000	69.2000	199.8000	166.9000
6	31.6000	73.8000	224.9000	187.1000
7	41.7000	75.8000	249.6000	201.9000
9	60.3000	110.4000	299.4000	232.1000
10	66.2000	152.3000	349.4000	263.8000
11	40.8000	185.3000	370.5000	279.4000
12	-9.7000	278.3000	397.6000	299.6000
19	36.0000	276.7000	425.3000	303.0000
	×1.0e+03	×1.0e+03	×1.0e+03	×1.0e+03
20	0.0360	0.2767	0.4253	0.3030
22	0.0518	0.3304	0.5961	0.4270
23	0.0534	0.3450	0.6216	0.4467
24	0.0478	0.3650	0.6494	0.4685
25	0.0535	0.3807	0.6775	0.4907
26	0.0357	0.4335	0.7050	0.5137
27	-0.0123	0.5222	0.7218	0.5287
28	-0.0809	0.6682	0.7451	0.5477
29	-0.1527	0.7916	0.7598	0.5619
30	-0.2174	0.9323	0.7820	0.5809
31	-0.2859	1.0832	0.8058	0.5974
32	-0.3599	1.2557	0.8178	0.6164
34	-0.3769	1.4627	1.2830	1.0466
36	-0.4518	1.7700	1.3033	1.0632
39	-0.4580	1.9682	1.5689	1.3113
41	-0.4271	2.0691	1.6195	1.3265
42	-0.3854	2.0290	1.6768	1.3437
44	-0.3452	1.9393	1.7871	1.3484

Table 6.9: Test results (U4 and U5)

Specimen	M_{ini} kNm	M_{max} kNm	δ_{ini} mm	δ_u mm	l_b mm	
U4A	218.4		26.0		4000	unbraced
U4B	217.7		26.6			unbraced
U4A	382.6	405.7		67.5		braced
U4B	377.7	405.4		67.2		braced
U5A	412.7	434.4		70.3	1200	
U5B	315.9	407.2	47.8	70.2	2000	

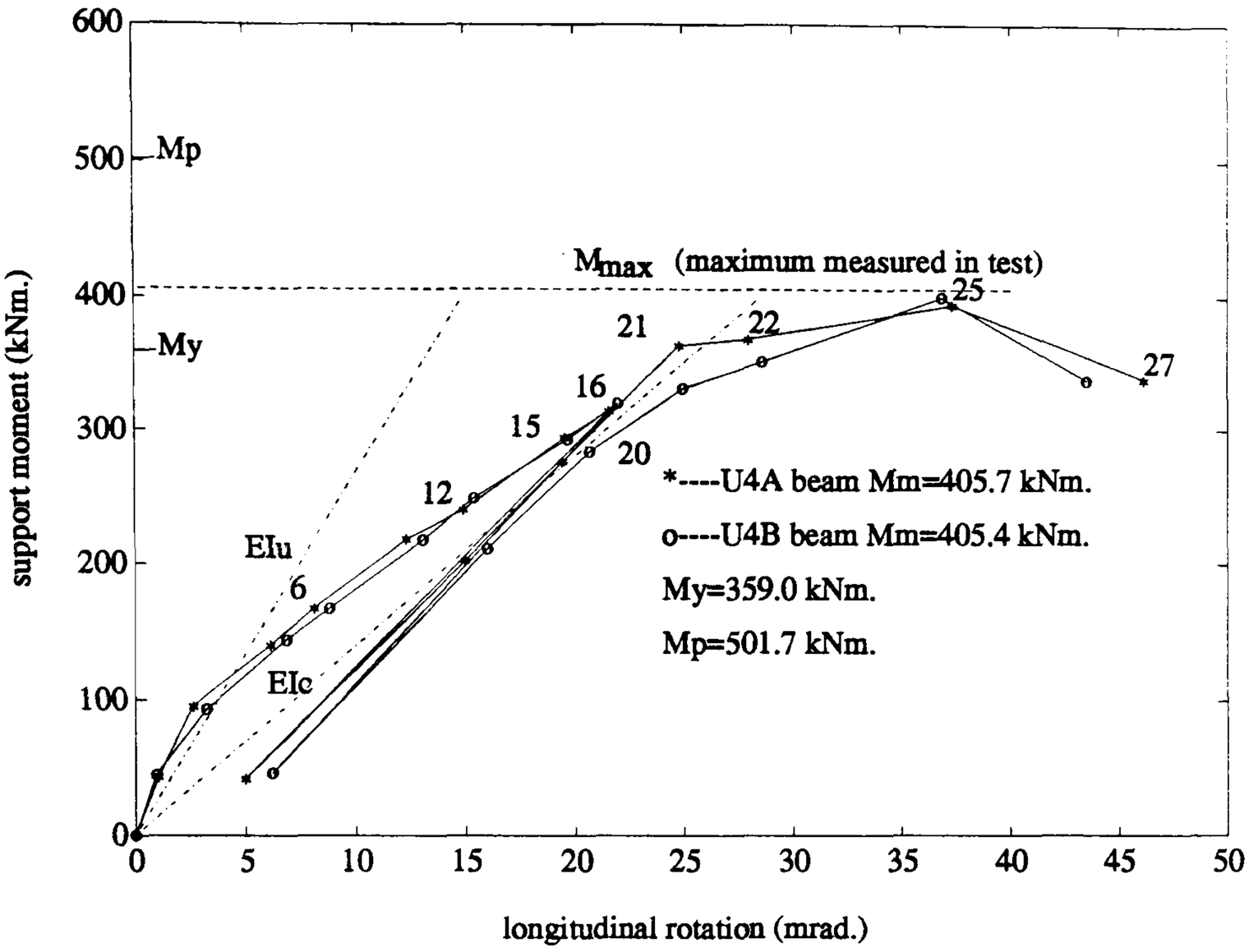

Figure 6.1: Moment-rotation curves (U4)

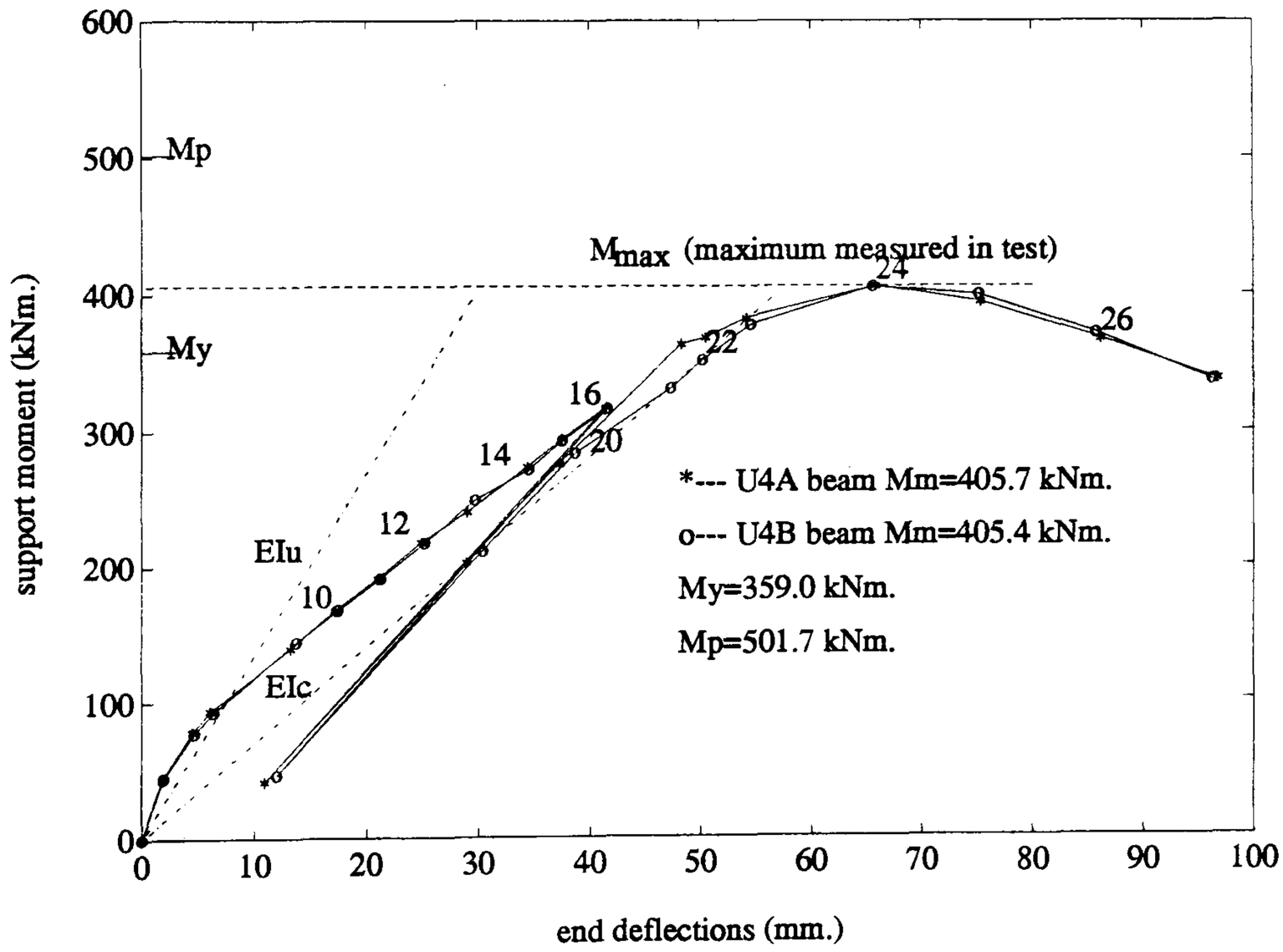

Figure 6.2: Moment-deflection curves (U4)

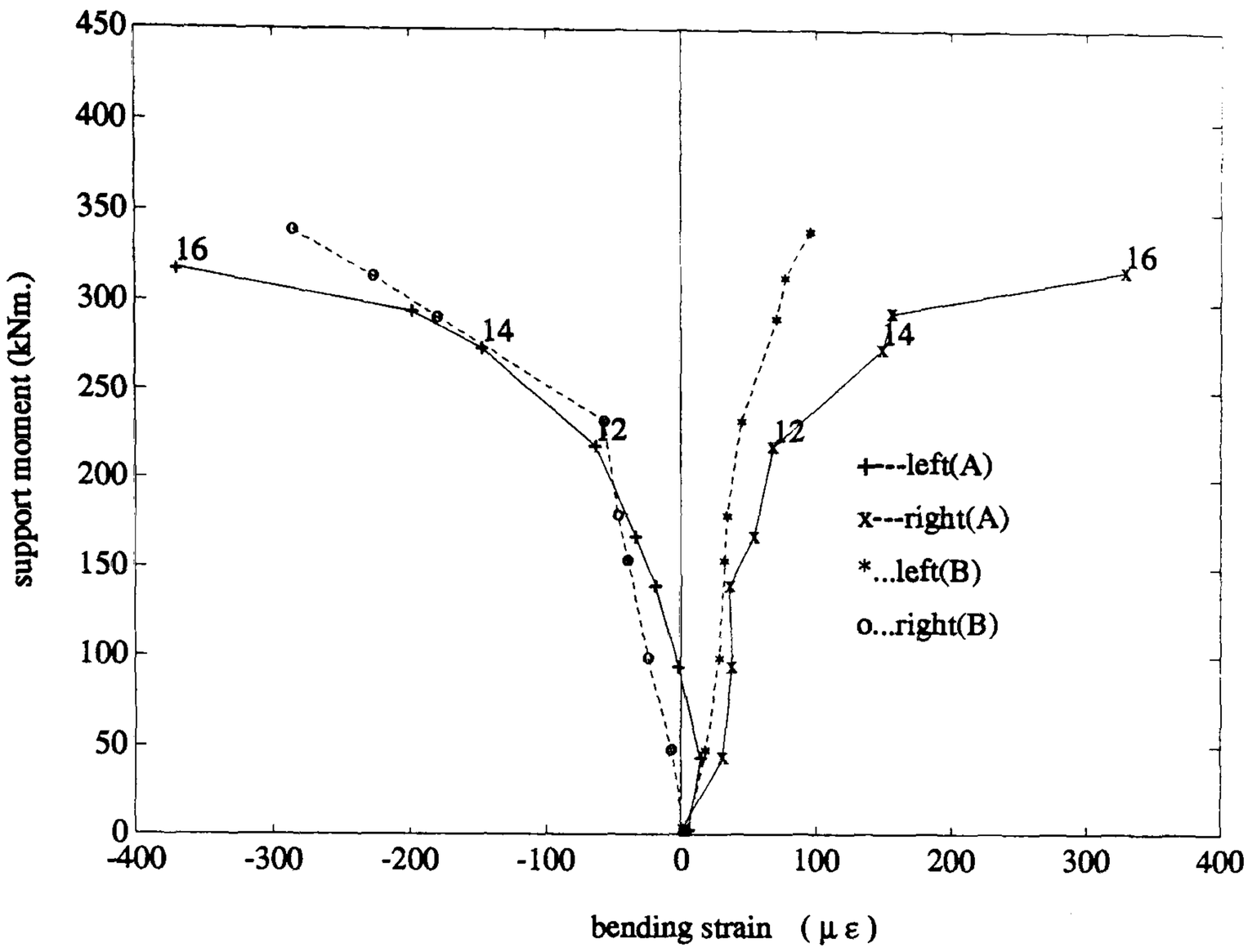

Figure 6.3: Moment-in-plane bending strain(specimen U4)

Figure 6.4: In-plane bending of the bottom flanges (U4 unbraced)

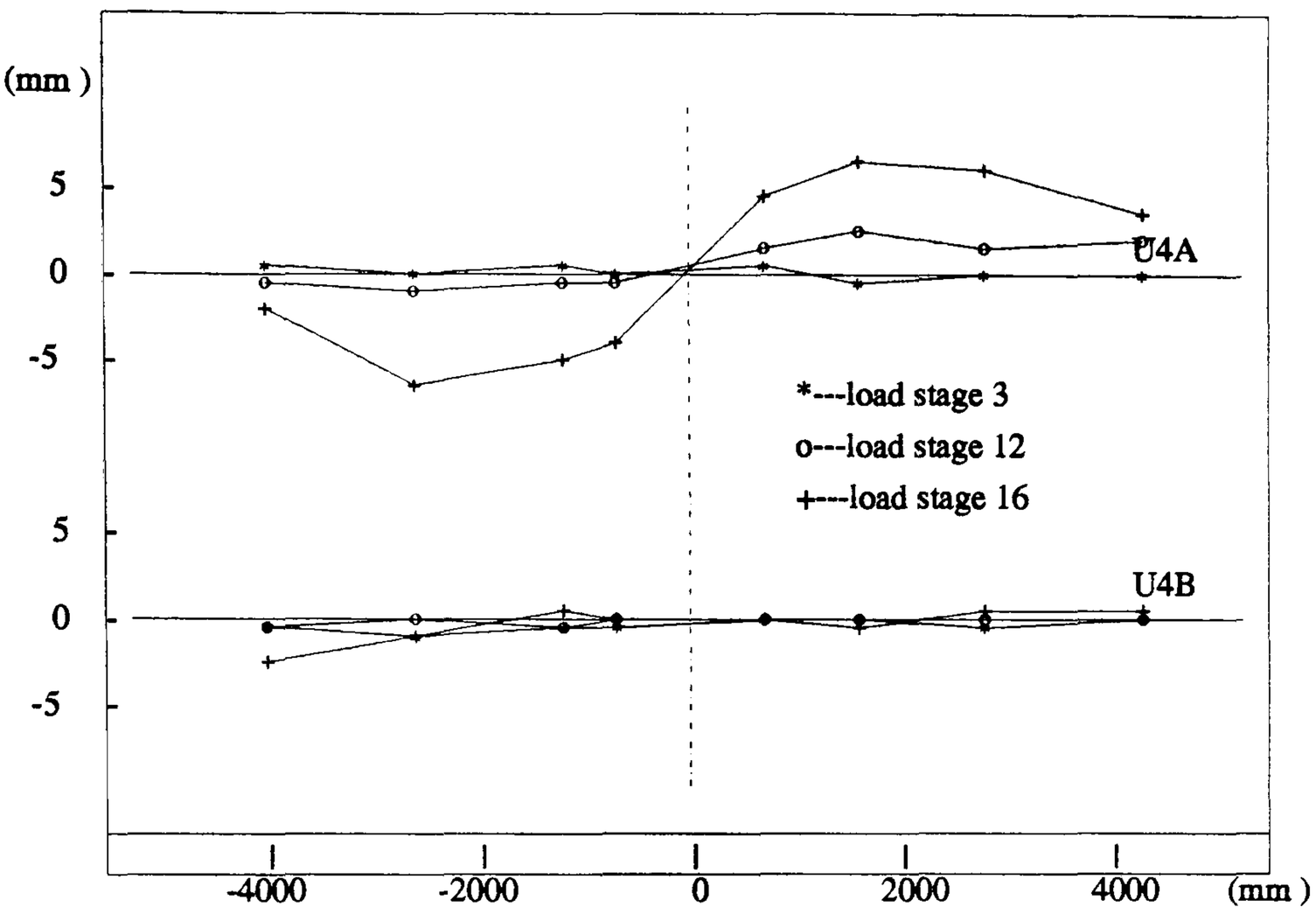

Figure 6.5: Lateral movement of bottom flanges (U4 unbraced)

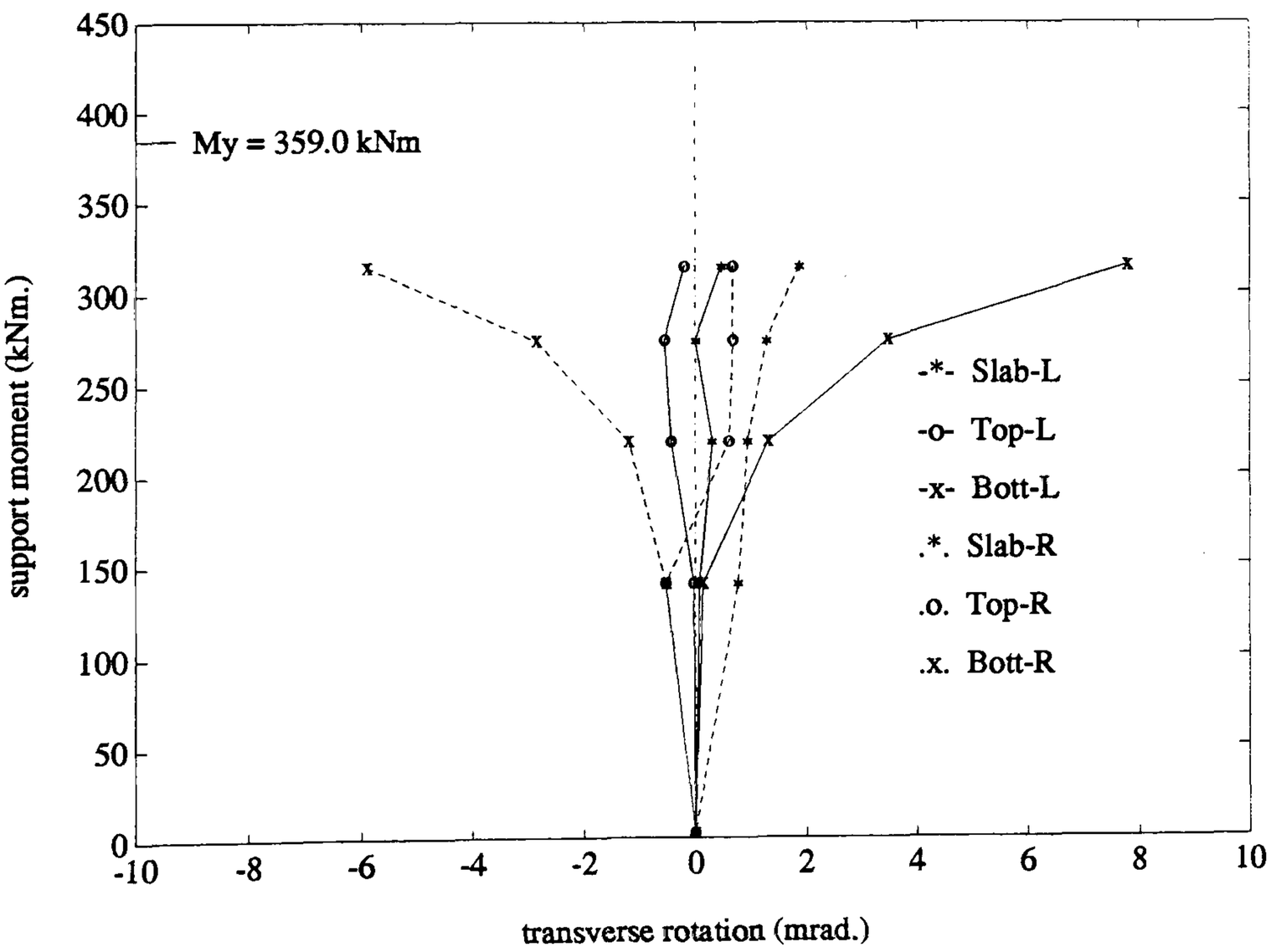

Figure 6.6: Transverse rotations (U4A unbraced)

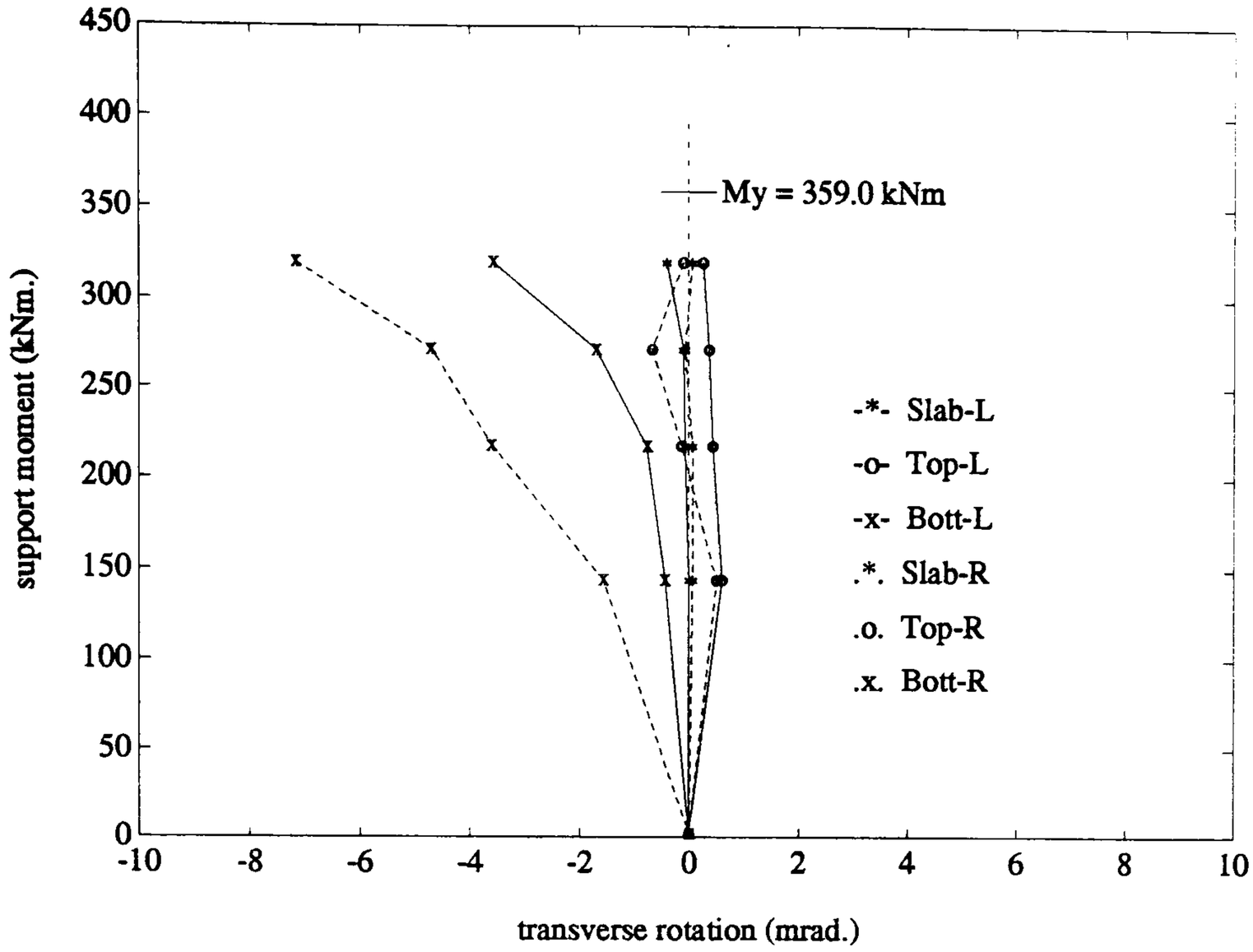

Figure 6.7: Transverse rotations (U4B unbraced)

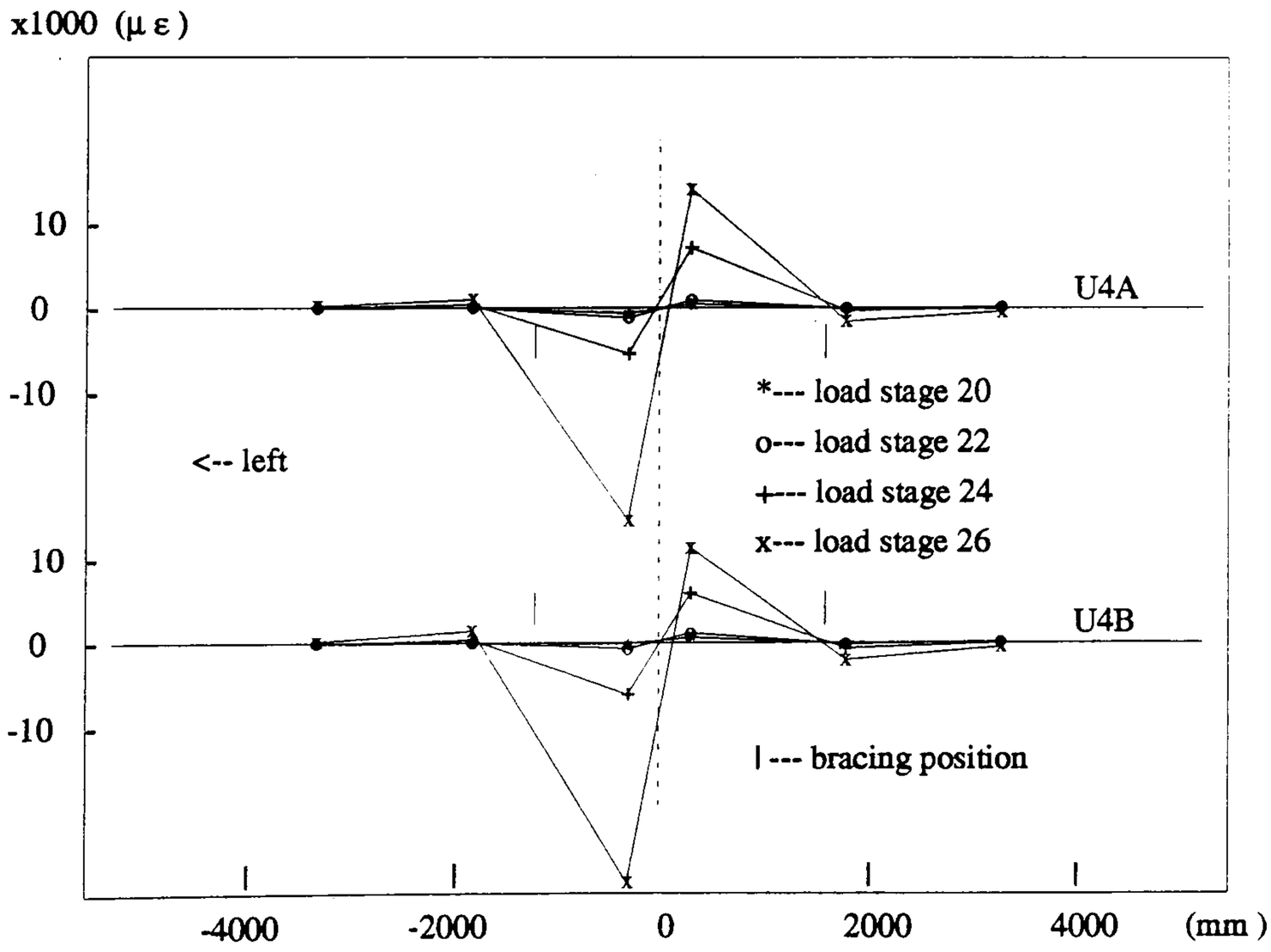

Figure 6.8: In-plane bending of the bottom flanges (U4 with cross bracings)

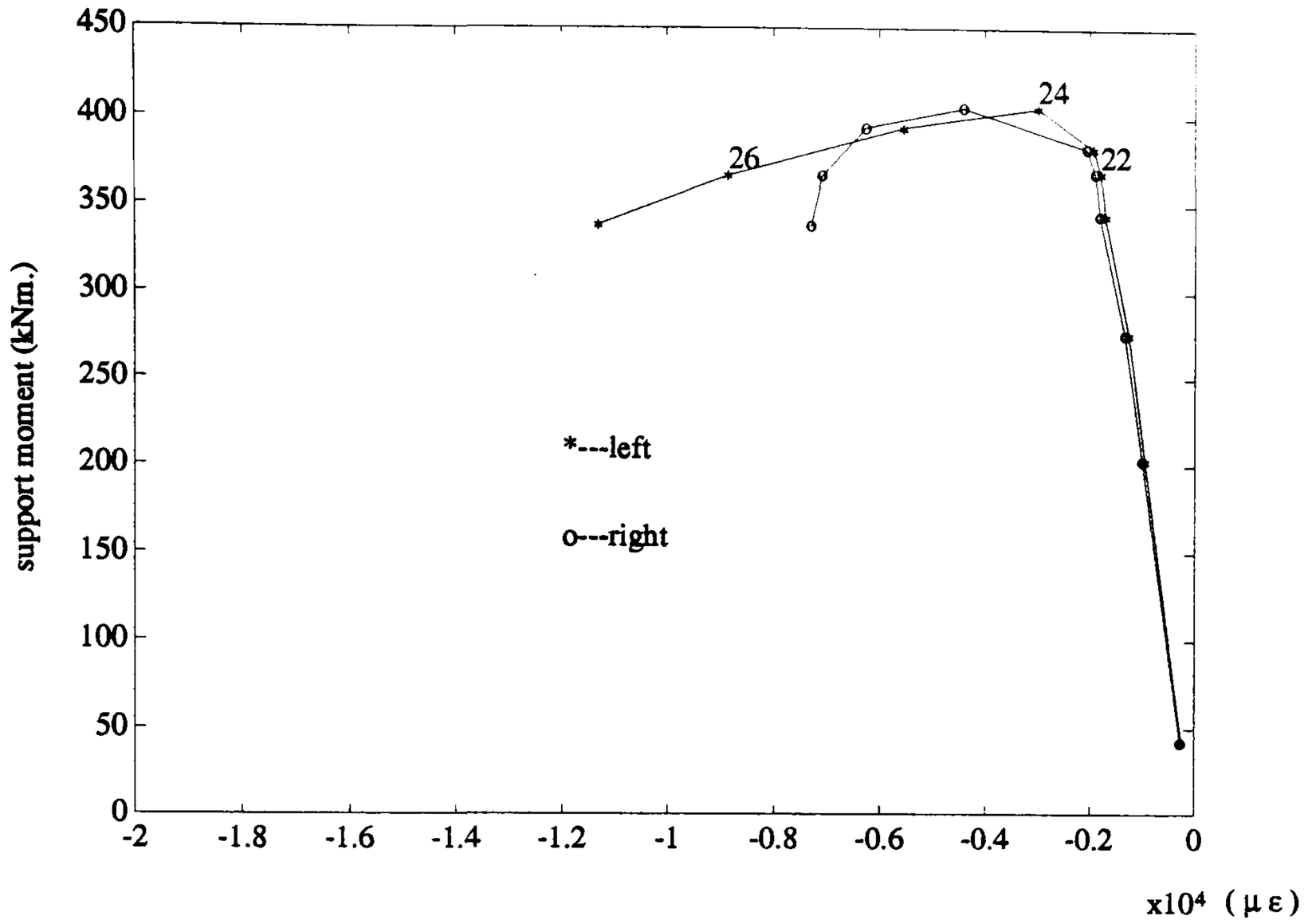

Figure 6.9: Compression strain in the bottom flange (U4A braced)

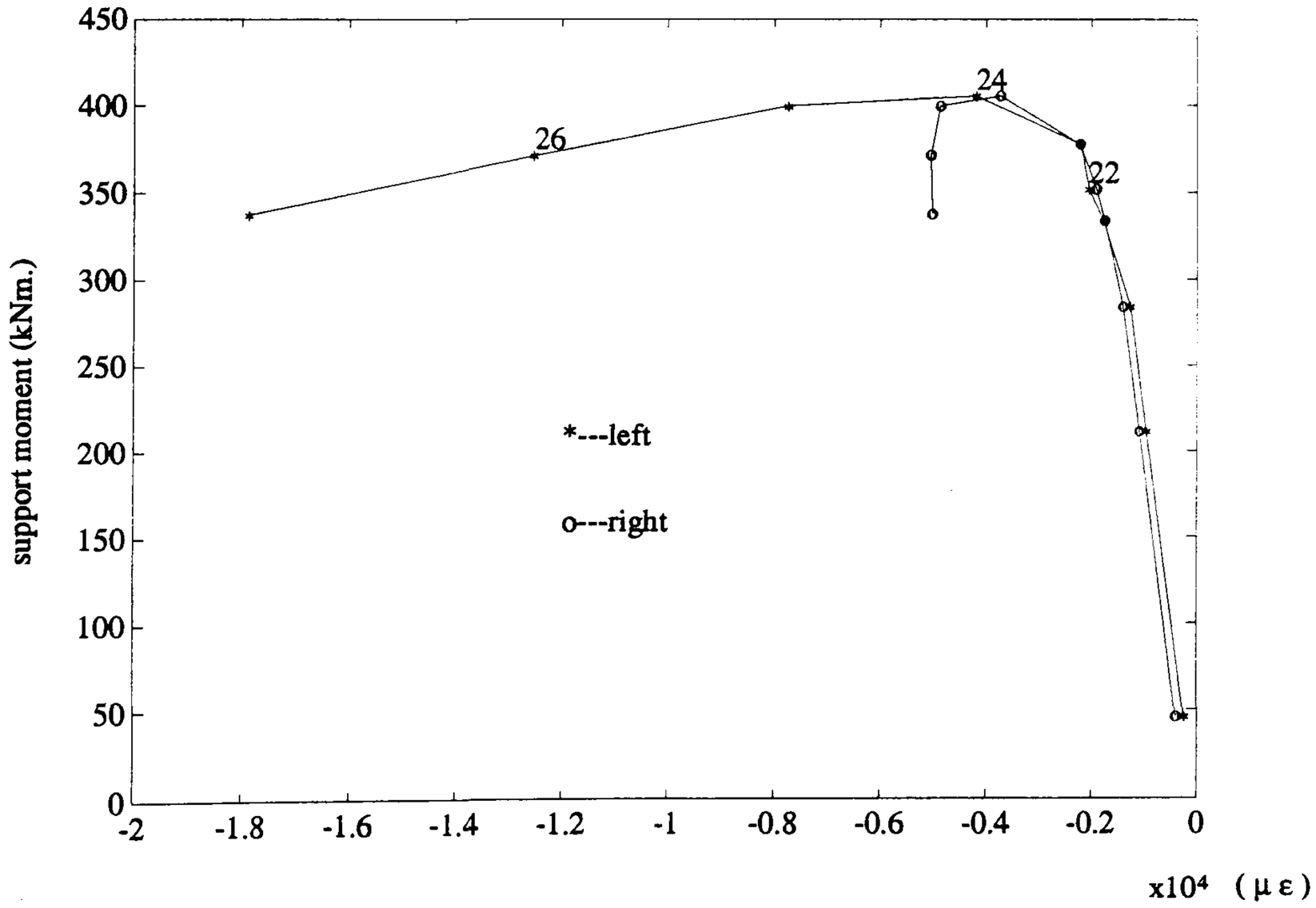

Figure 6.10: Compression strain in the bottom flange (U4B braced)

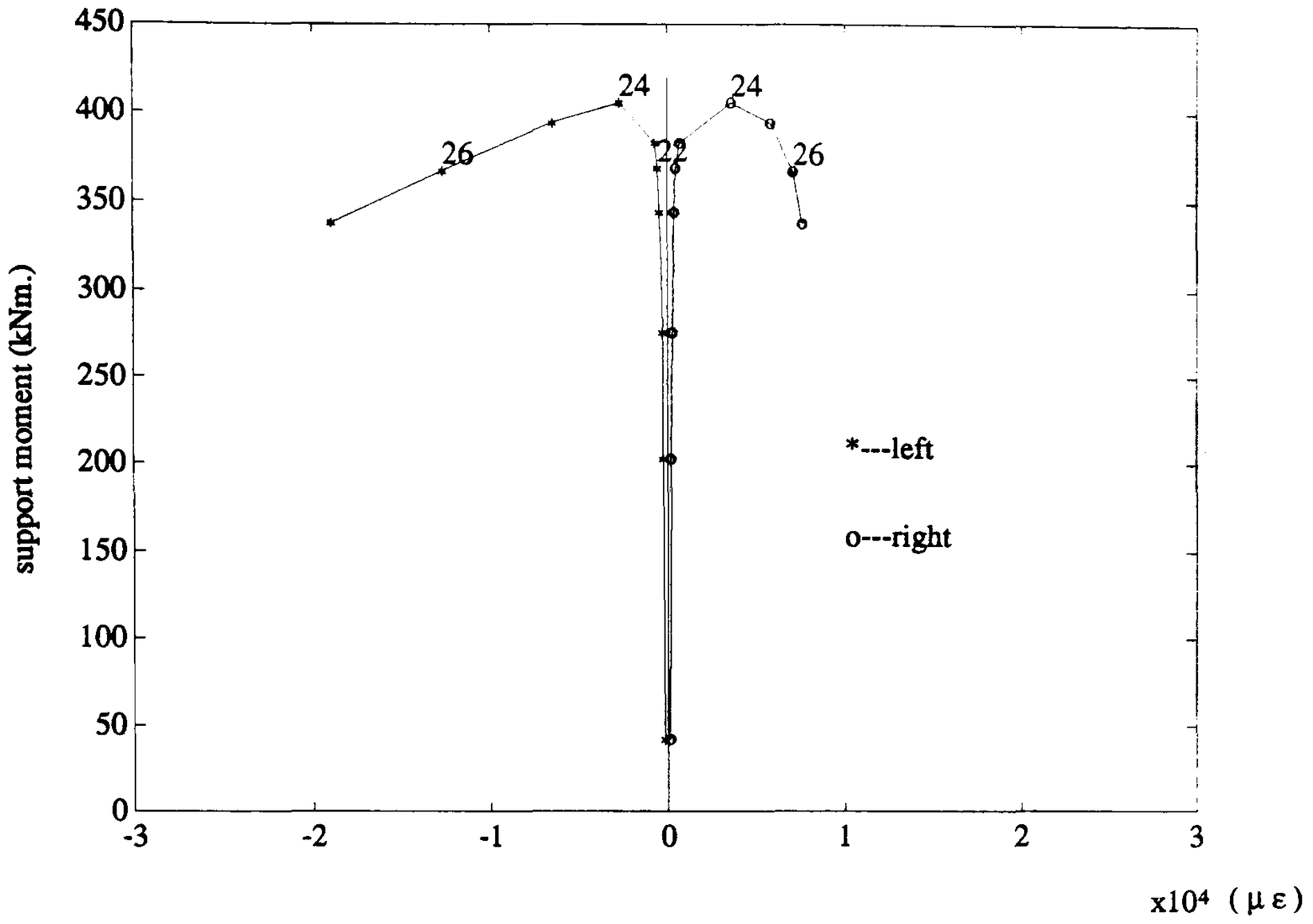

Figure 6.11: In-plane bending in the bottom flange (U4A braced)

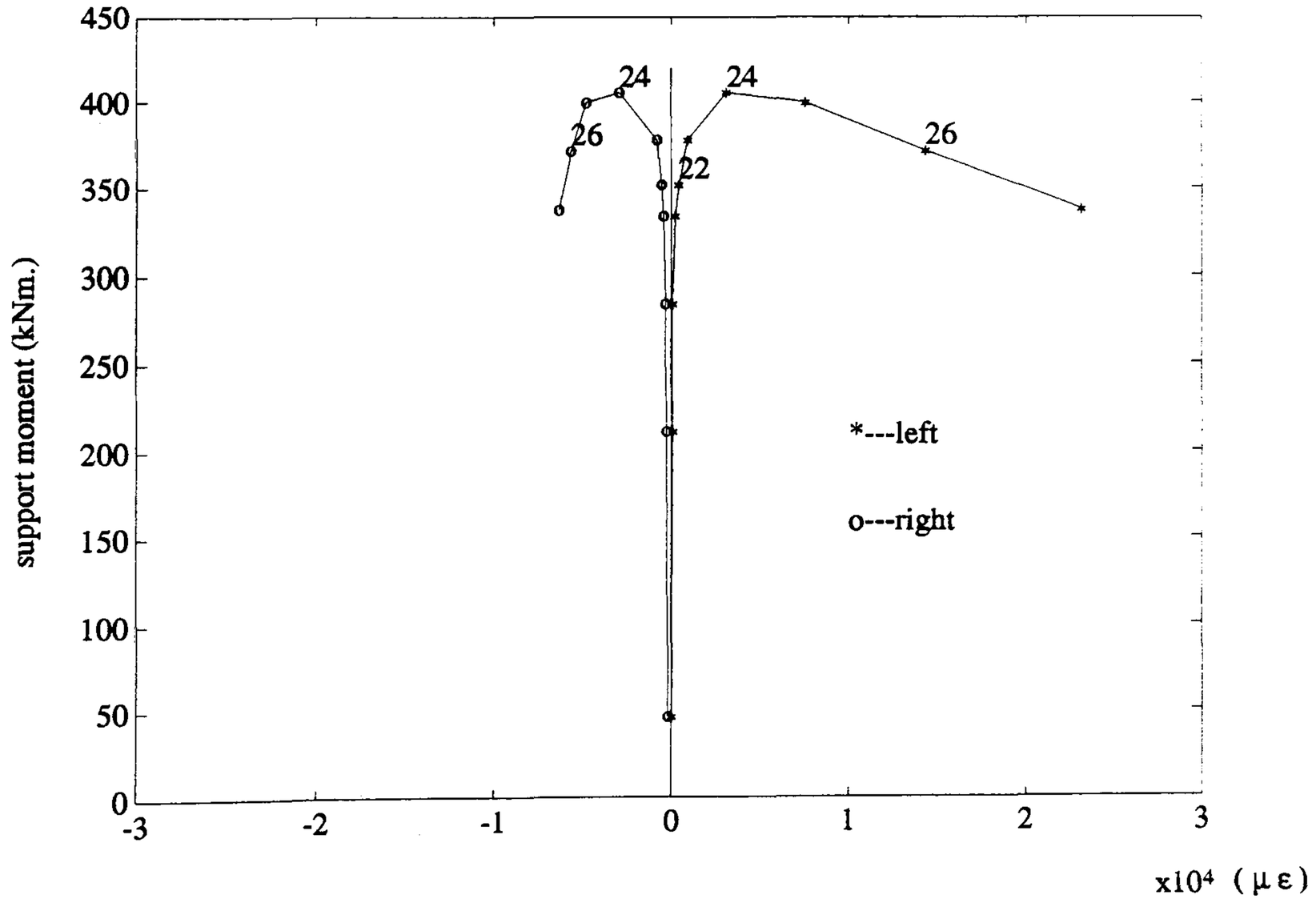

Figure 6.12: In-plane bending in the bottom flange (U4B braced)

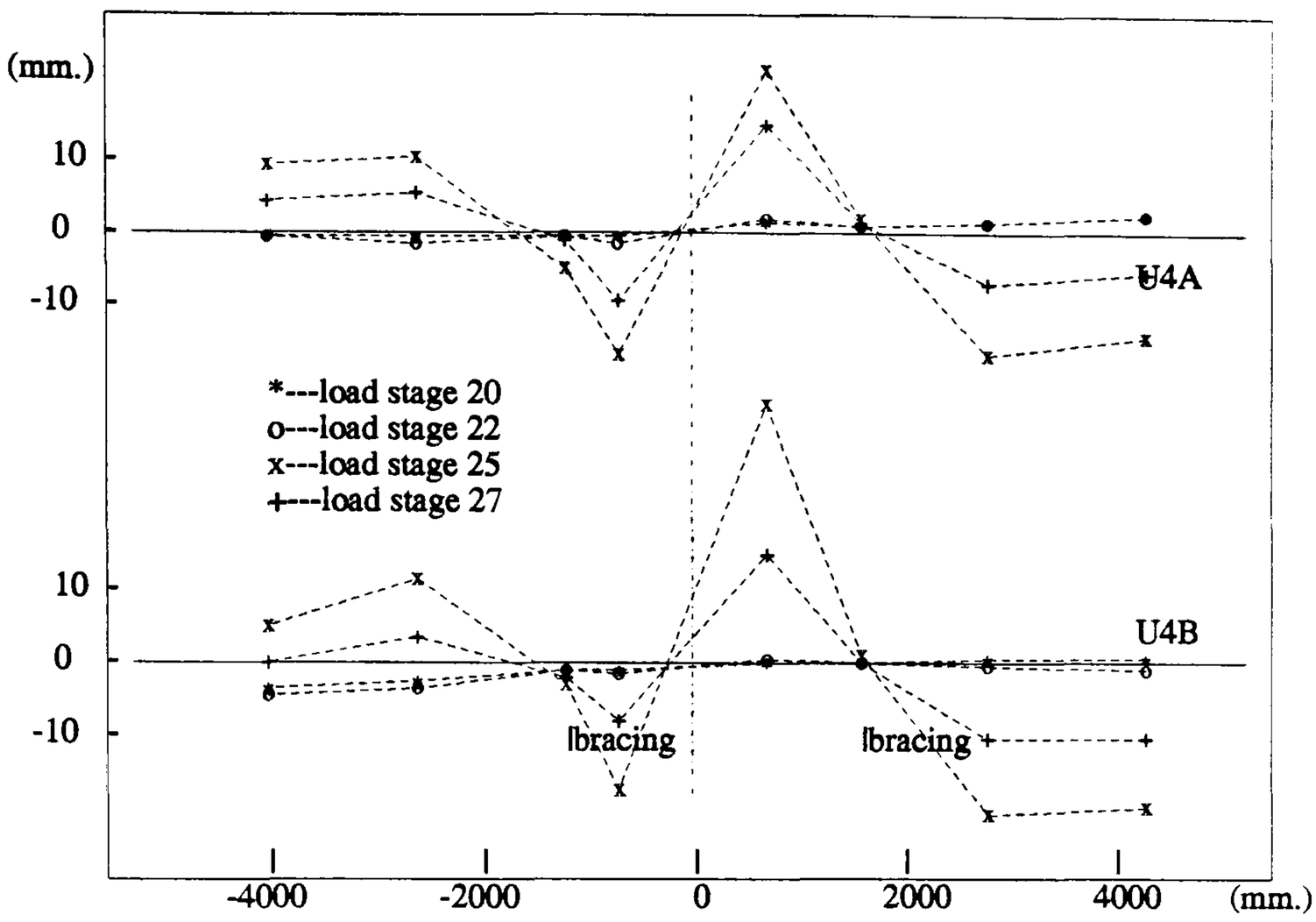

Figure 6.13: Lateral movements of the bottom flanges (U4 with cross bracings)

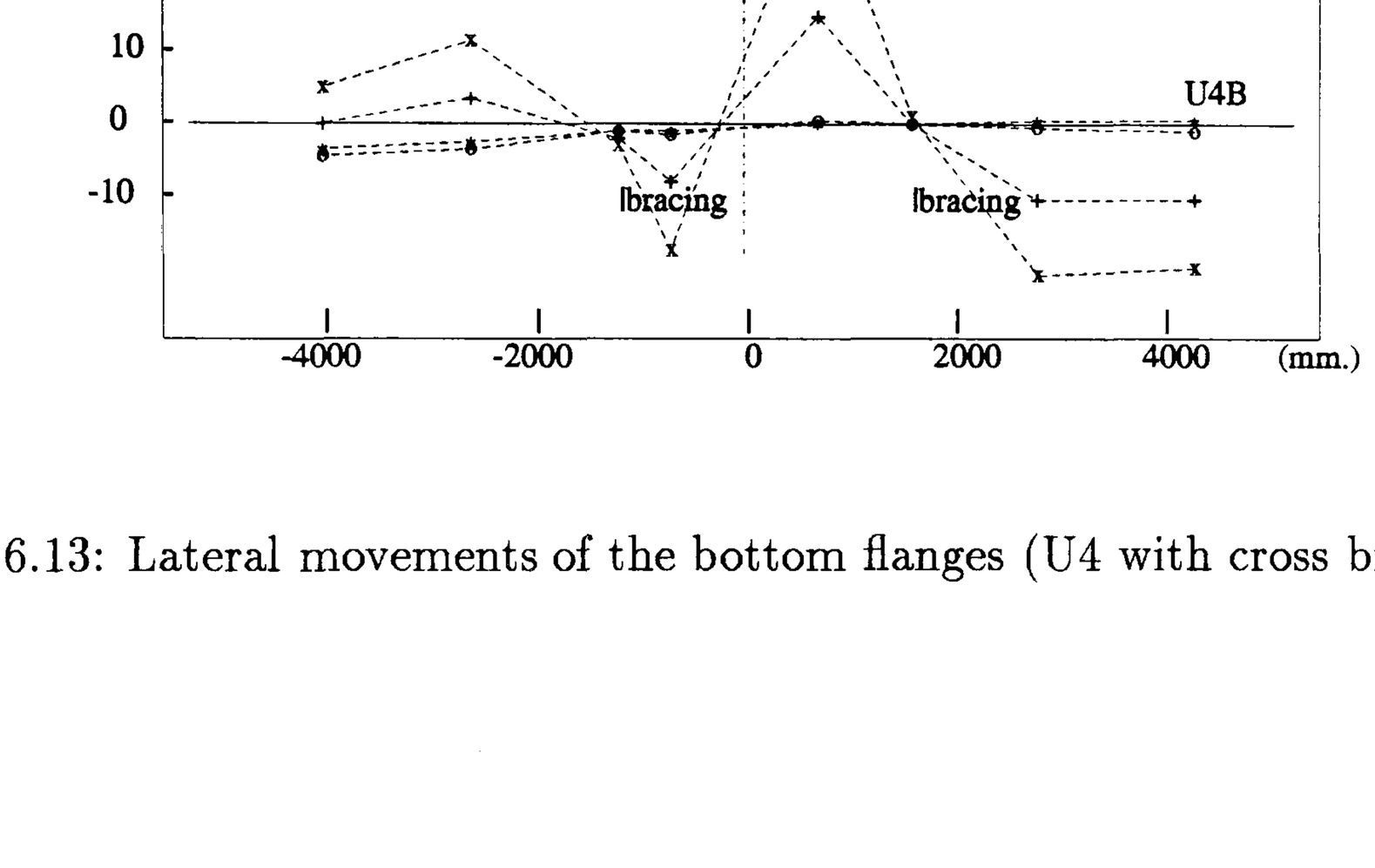

Figure 6.14: Transverse rotations (U4A braced)

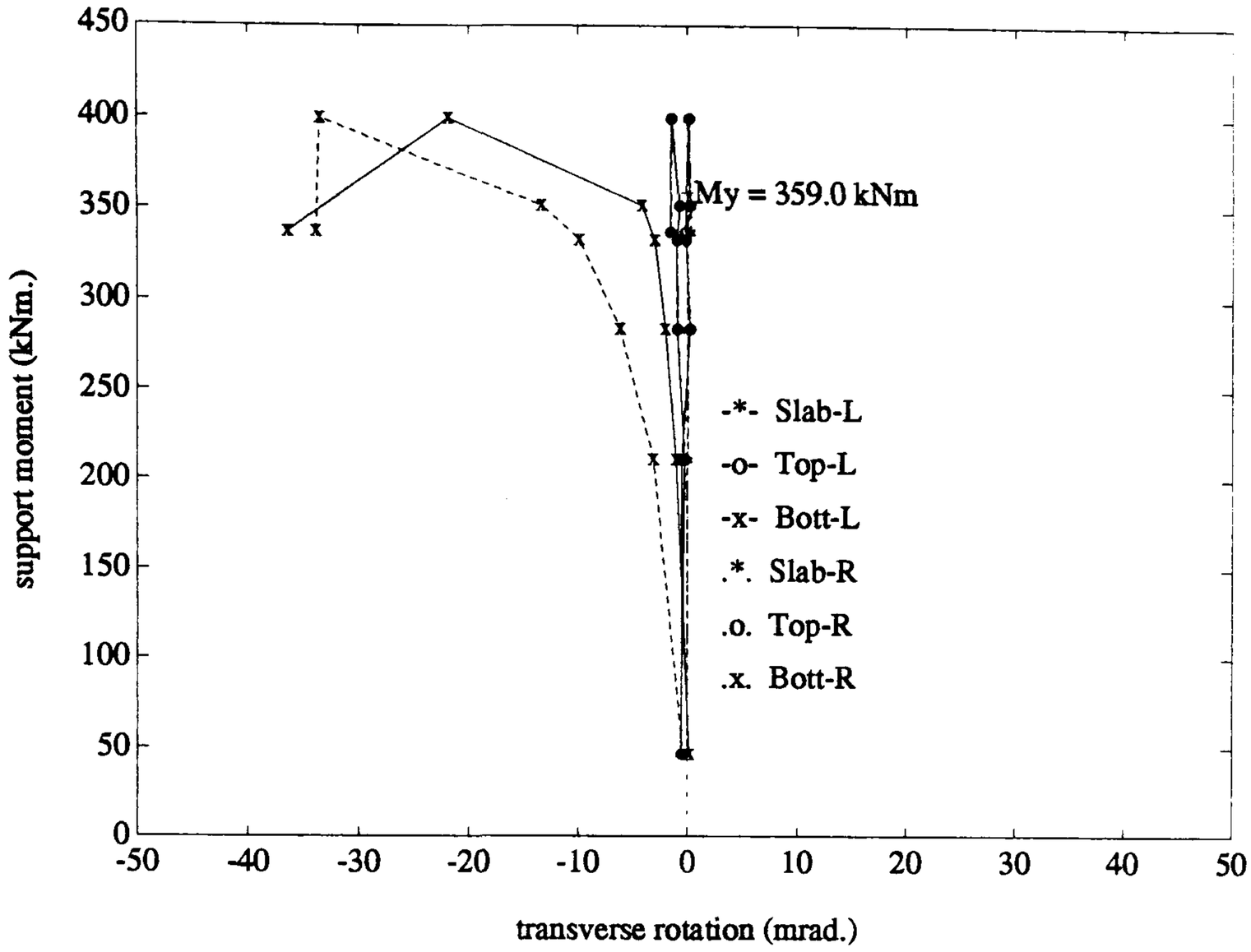

Figure 6.15: Transverse rotations (U4B braced)

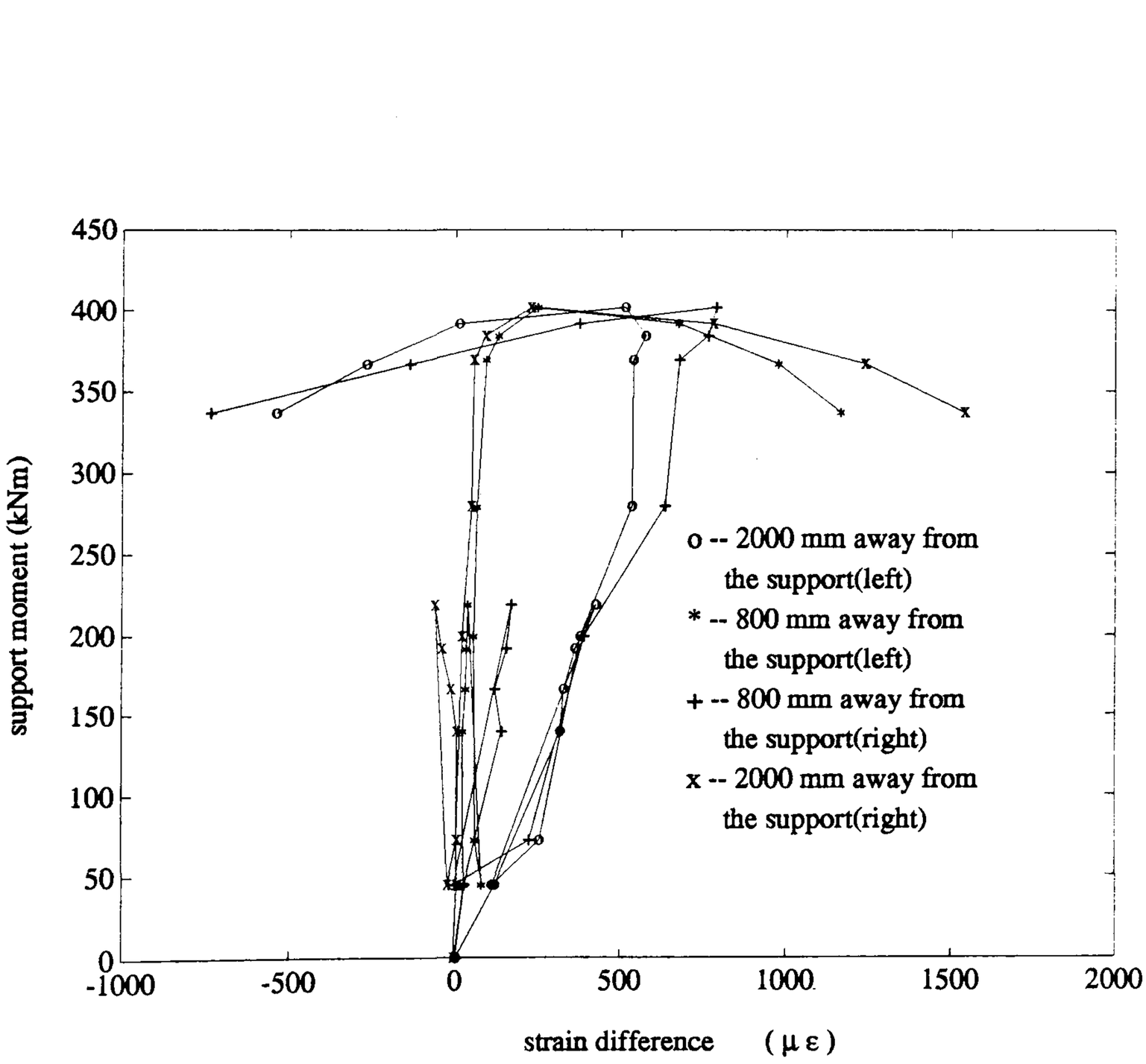

Figure 6.16: Web distortion (specimen U4A)

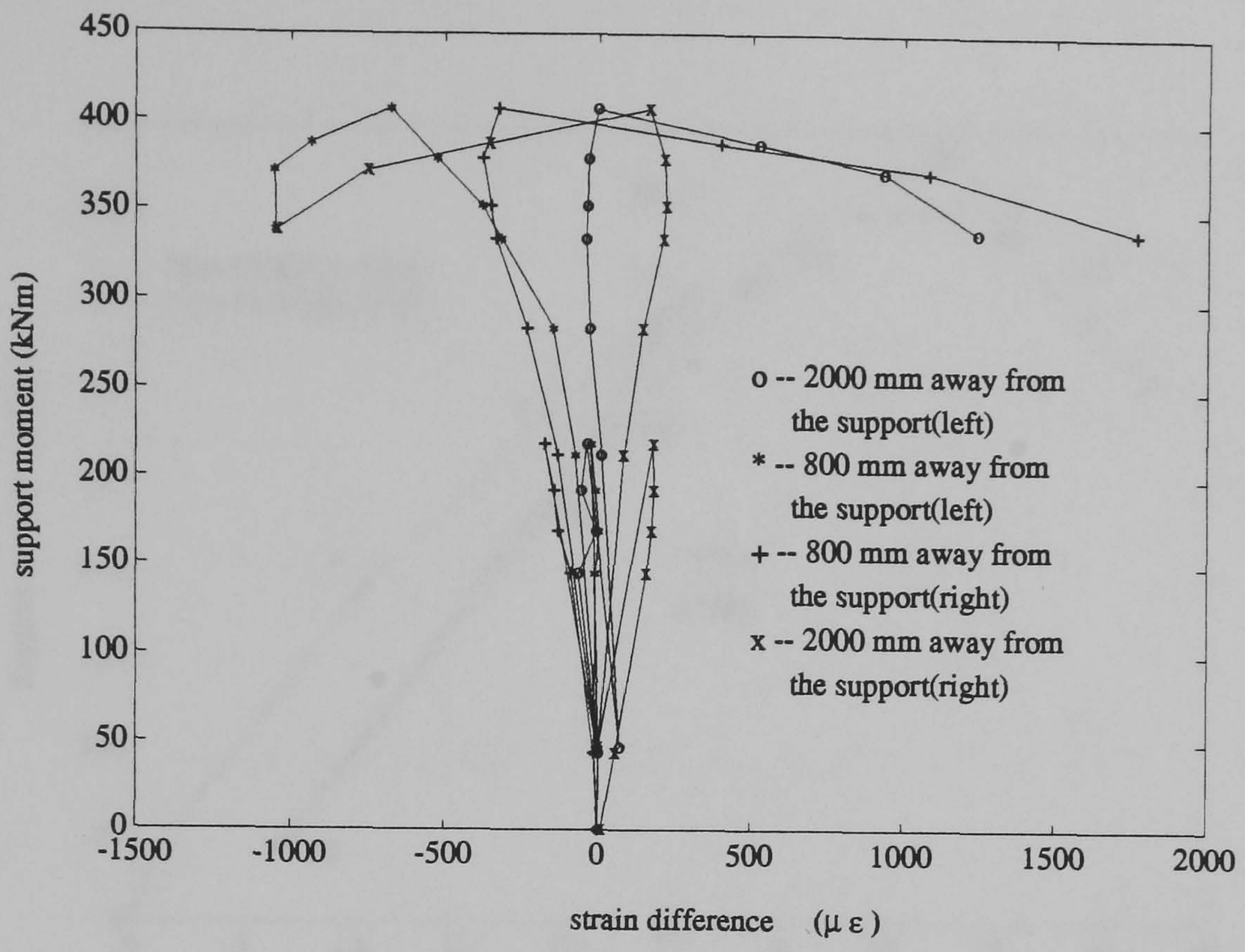

Figure 6.17: Web distortion (specimen U4B)

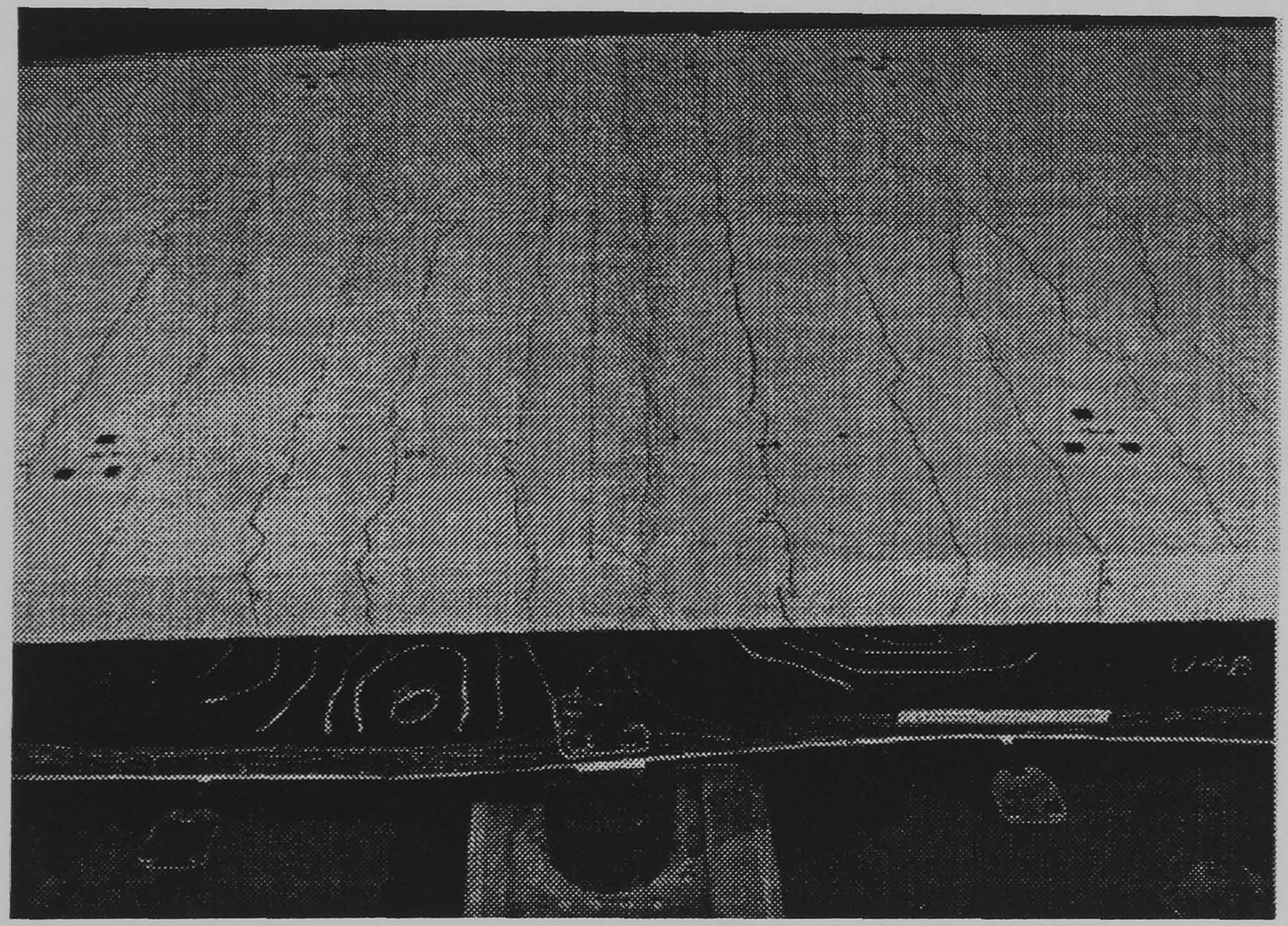

Figure 6.18: Buckling shapes (U4B)

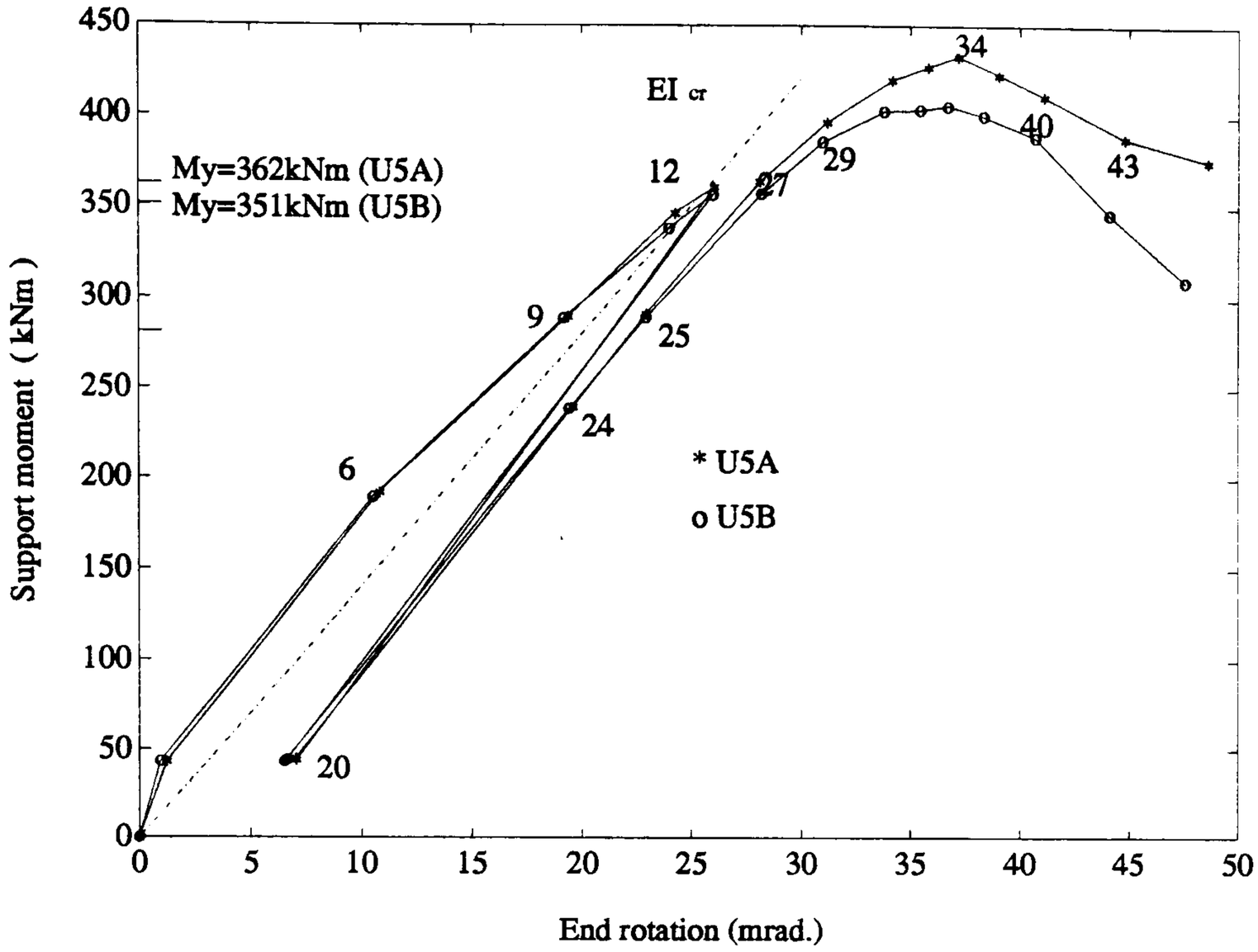

Figure 6.19: Moment-rotation curves (specimen U5)

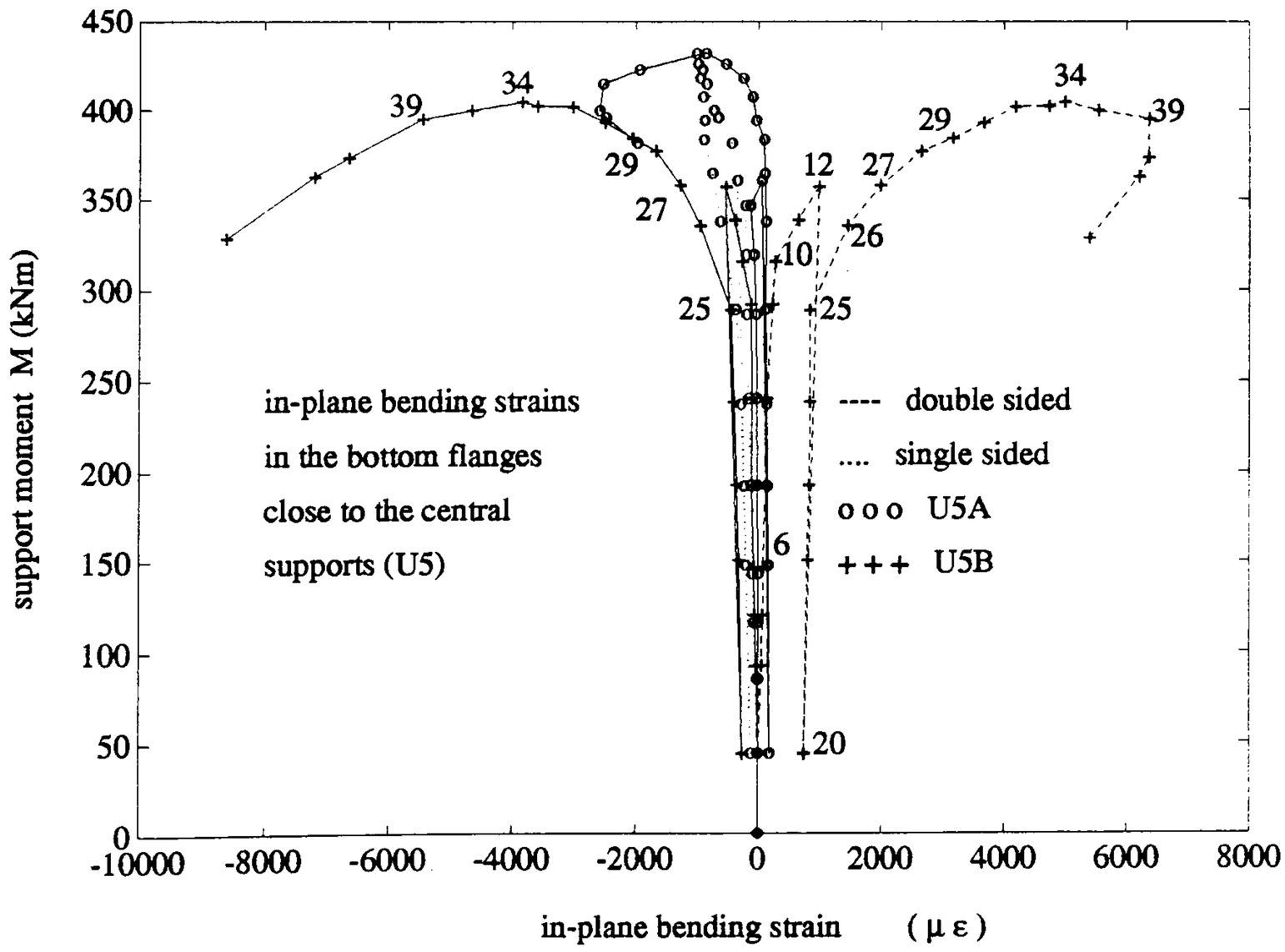

Figure 6.20: In-plane bending strain in bottom flanges (U5)

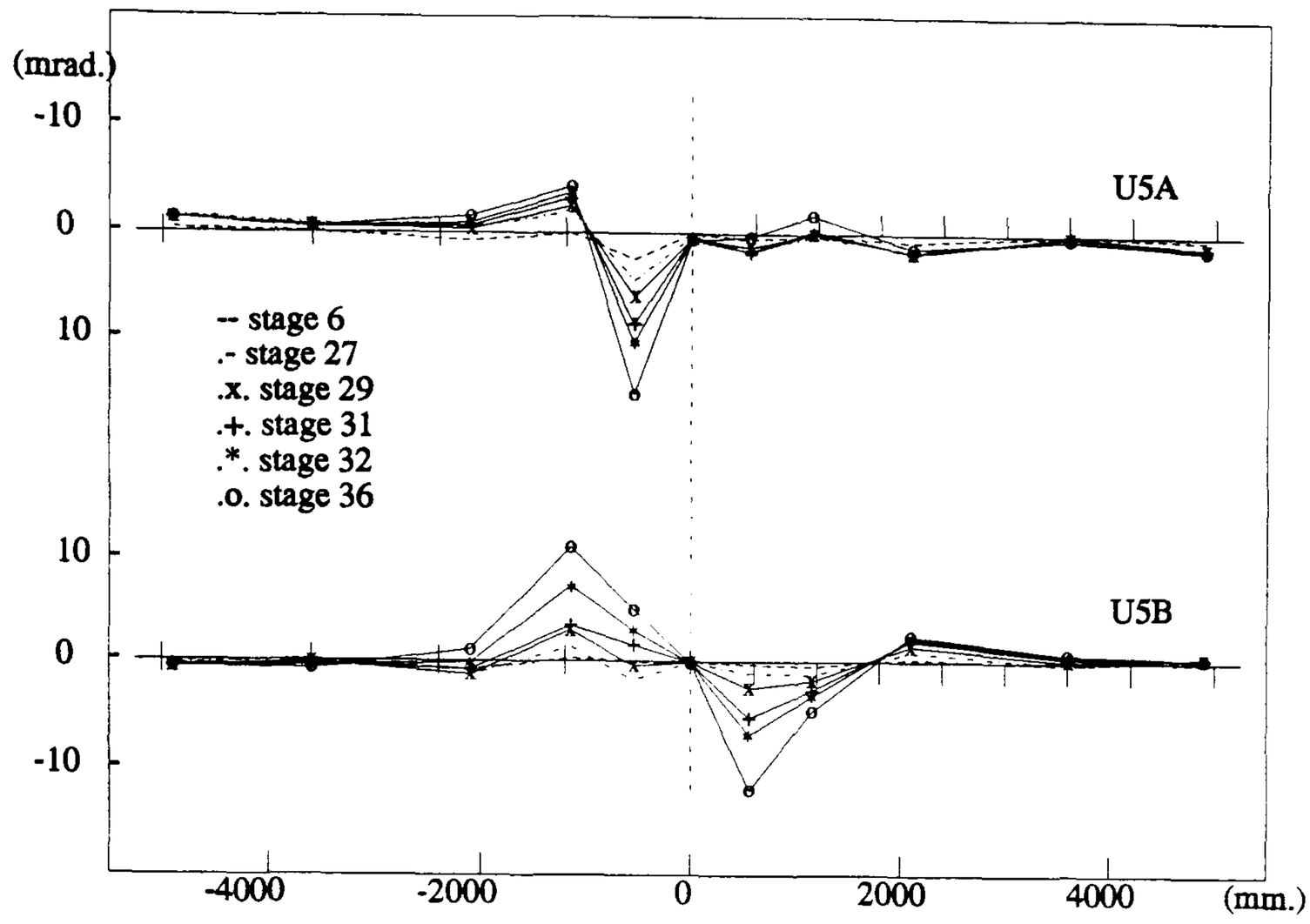

Figure 6.21: Transverse rotation of the bottom flanges(specimen U5)

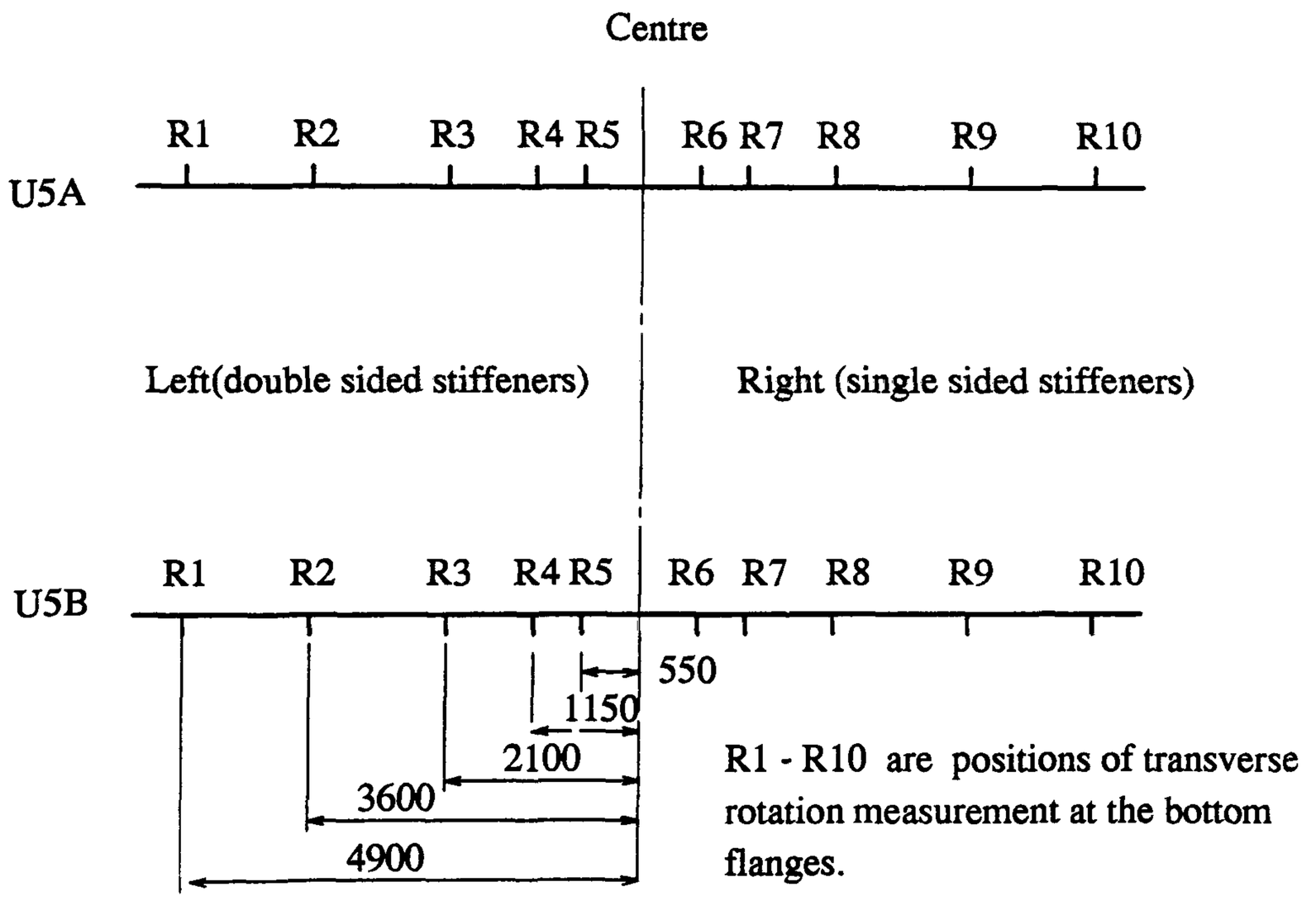

Figure 6.22: Positions of R1-R10 in the bottom flanges (specimen U5)

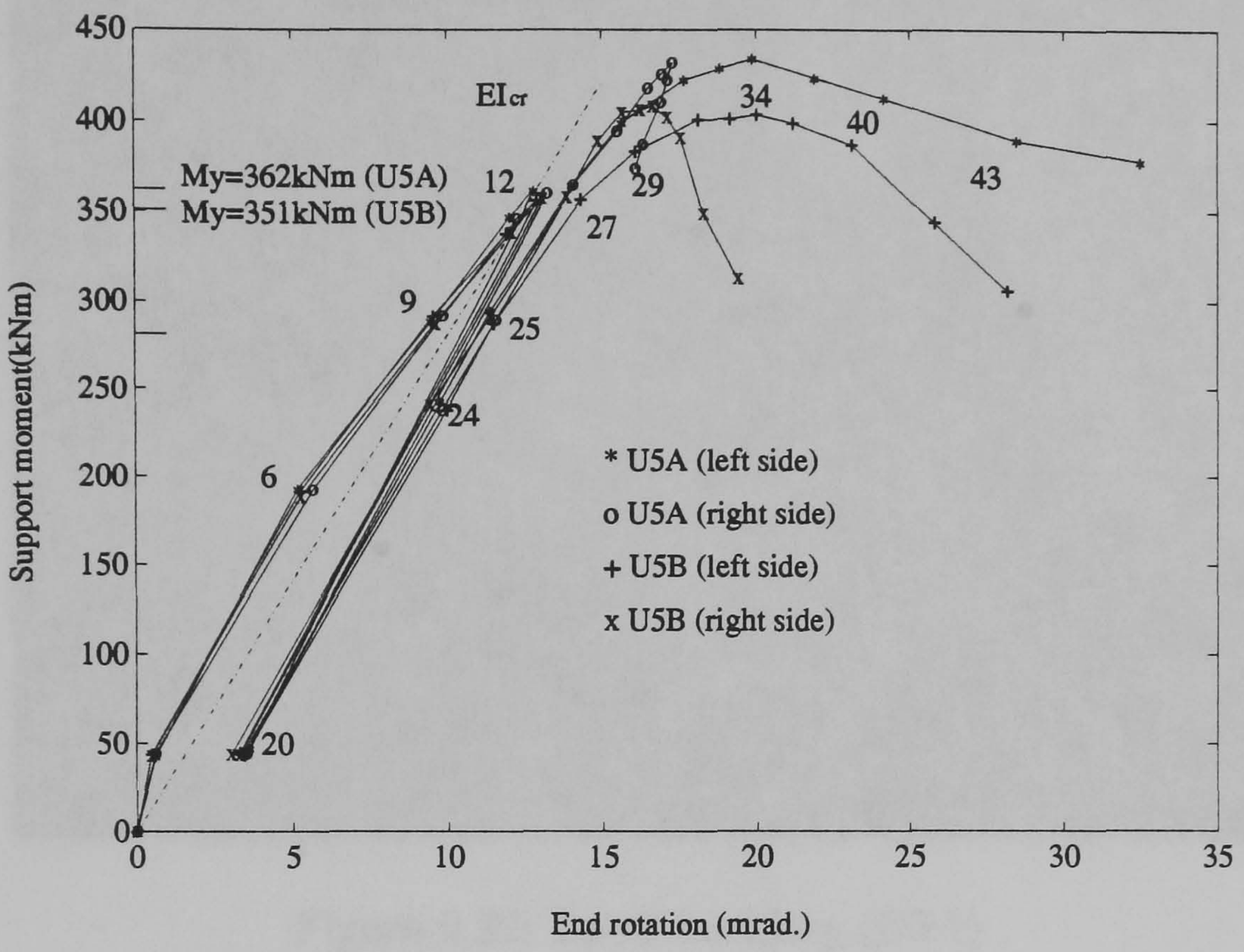

Figure 6.23: Moment-rotation curves(specimen U5)

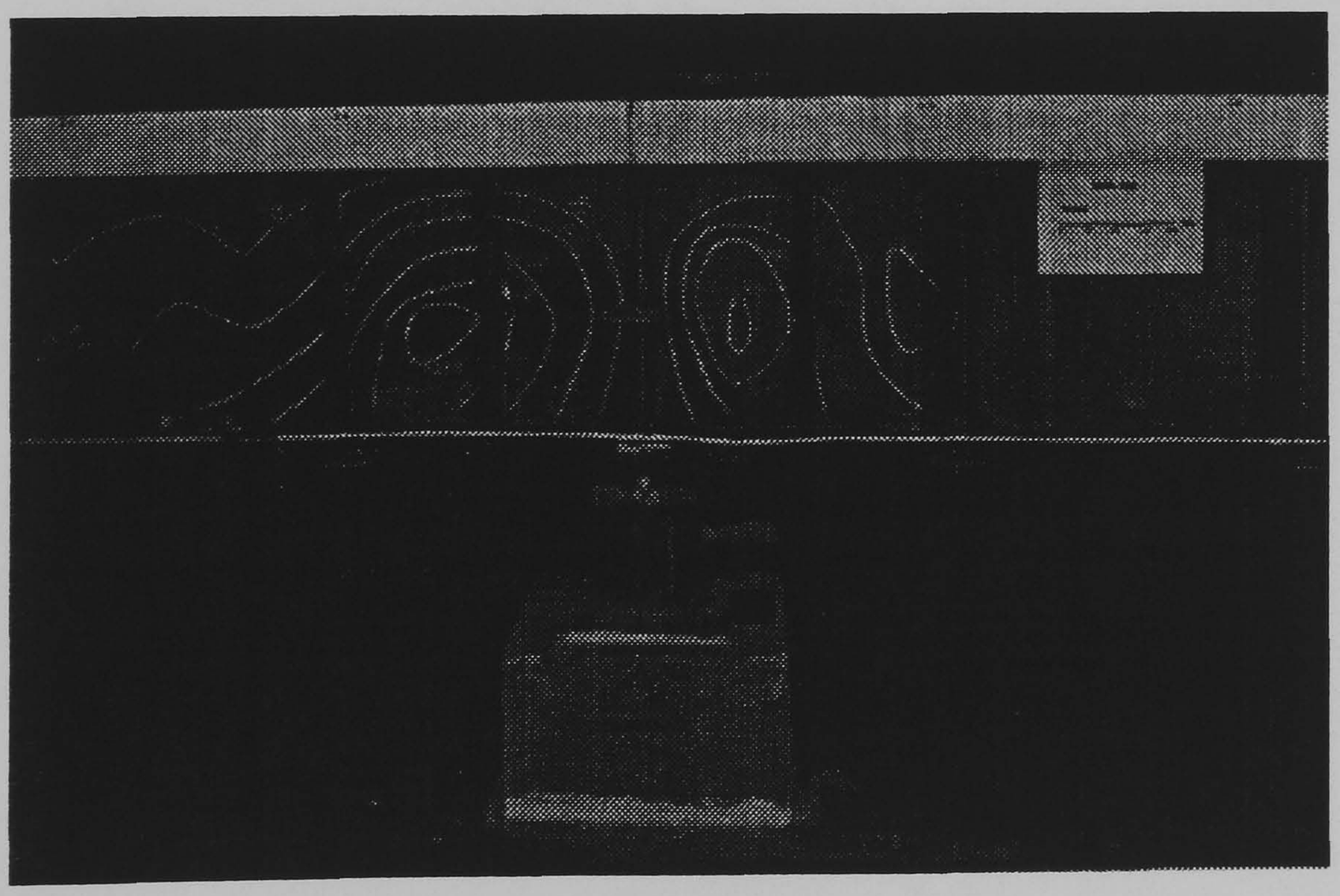

Figure 6.24: Local web buckling (U5B)

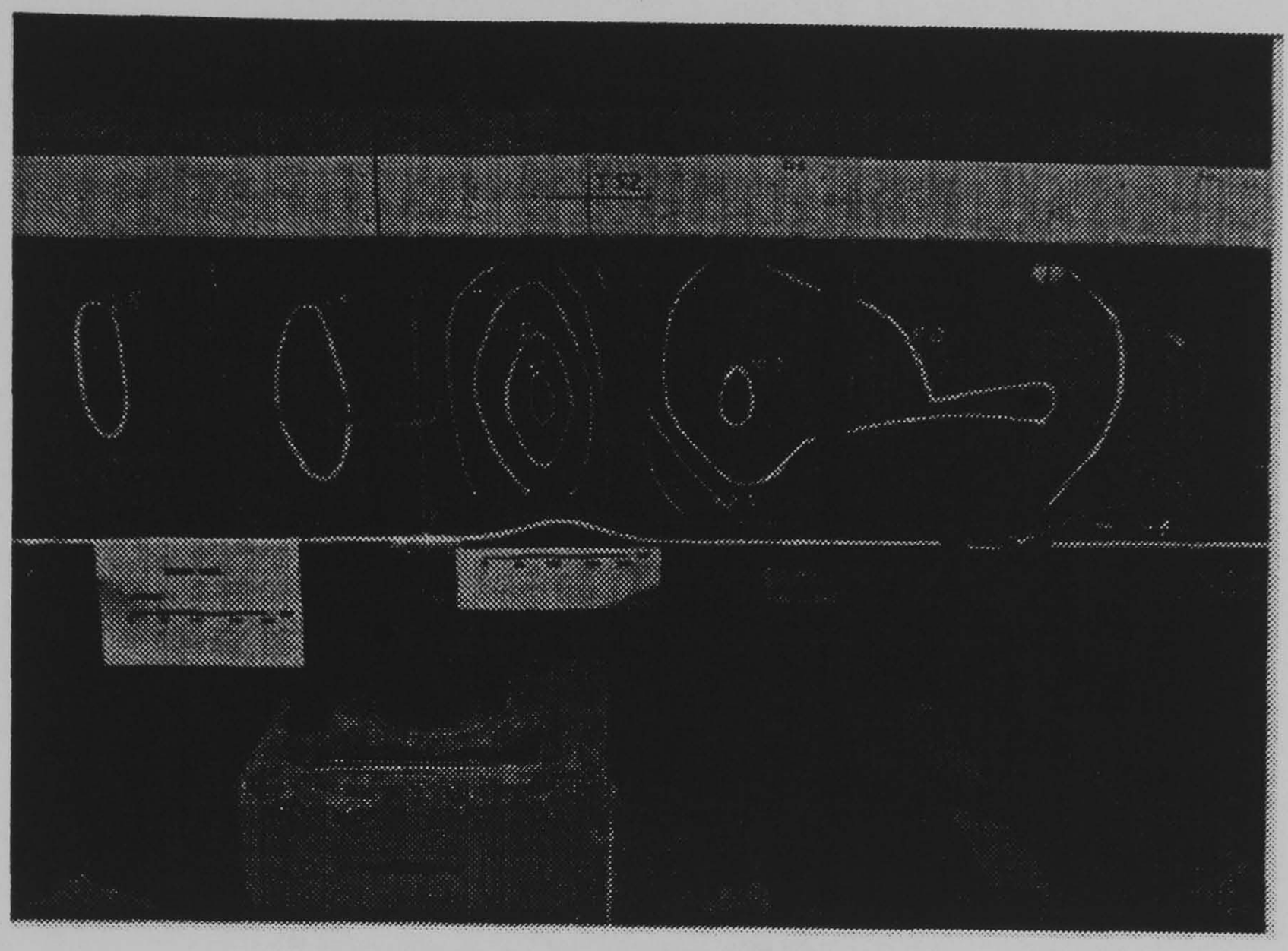

Figure 6.25: Local buckling (U5A)

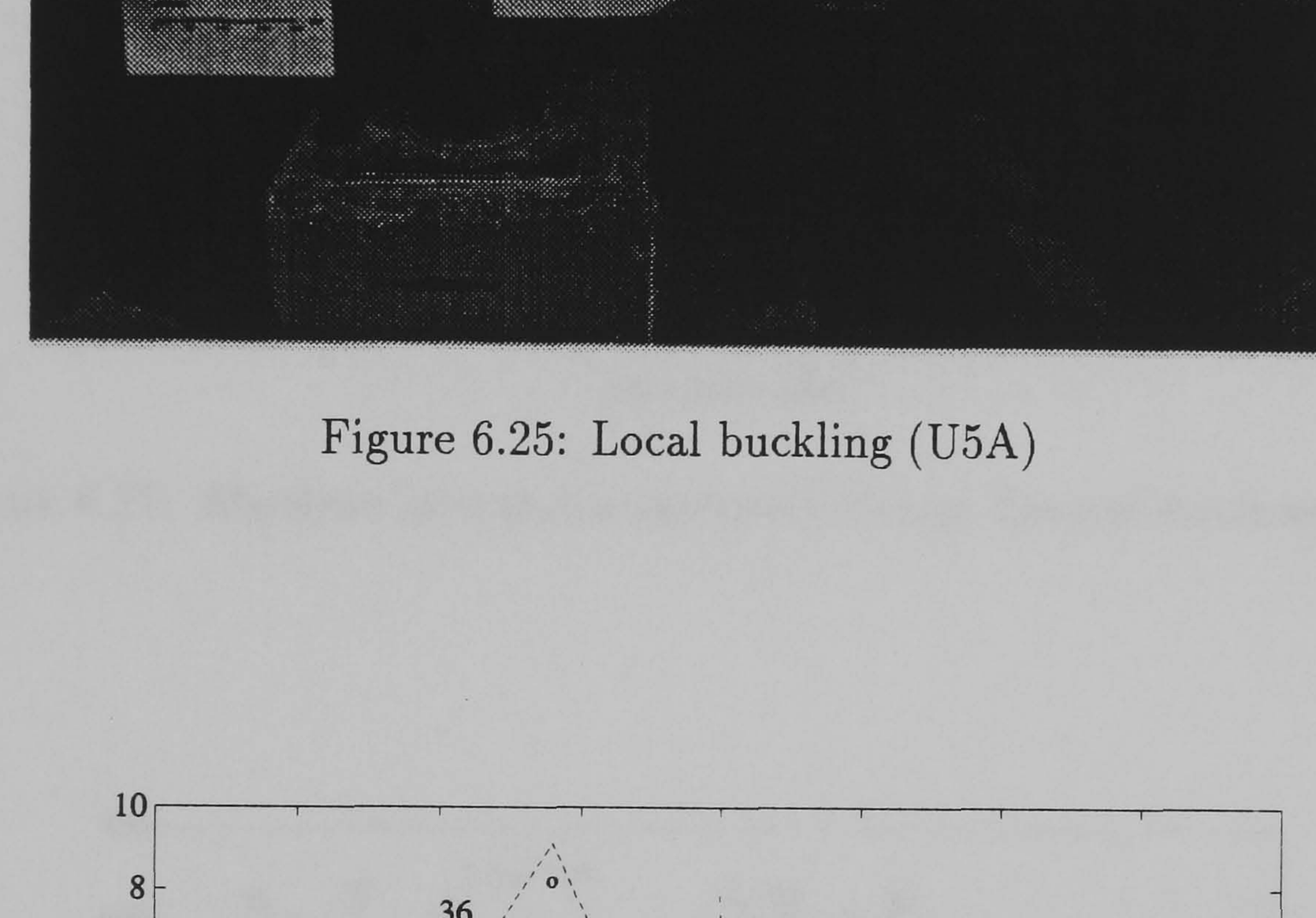

Figure 6.26: Relative lateral movement of bottom flanges(specimen U5)

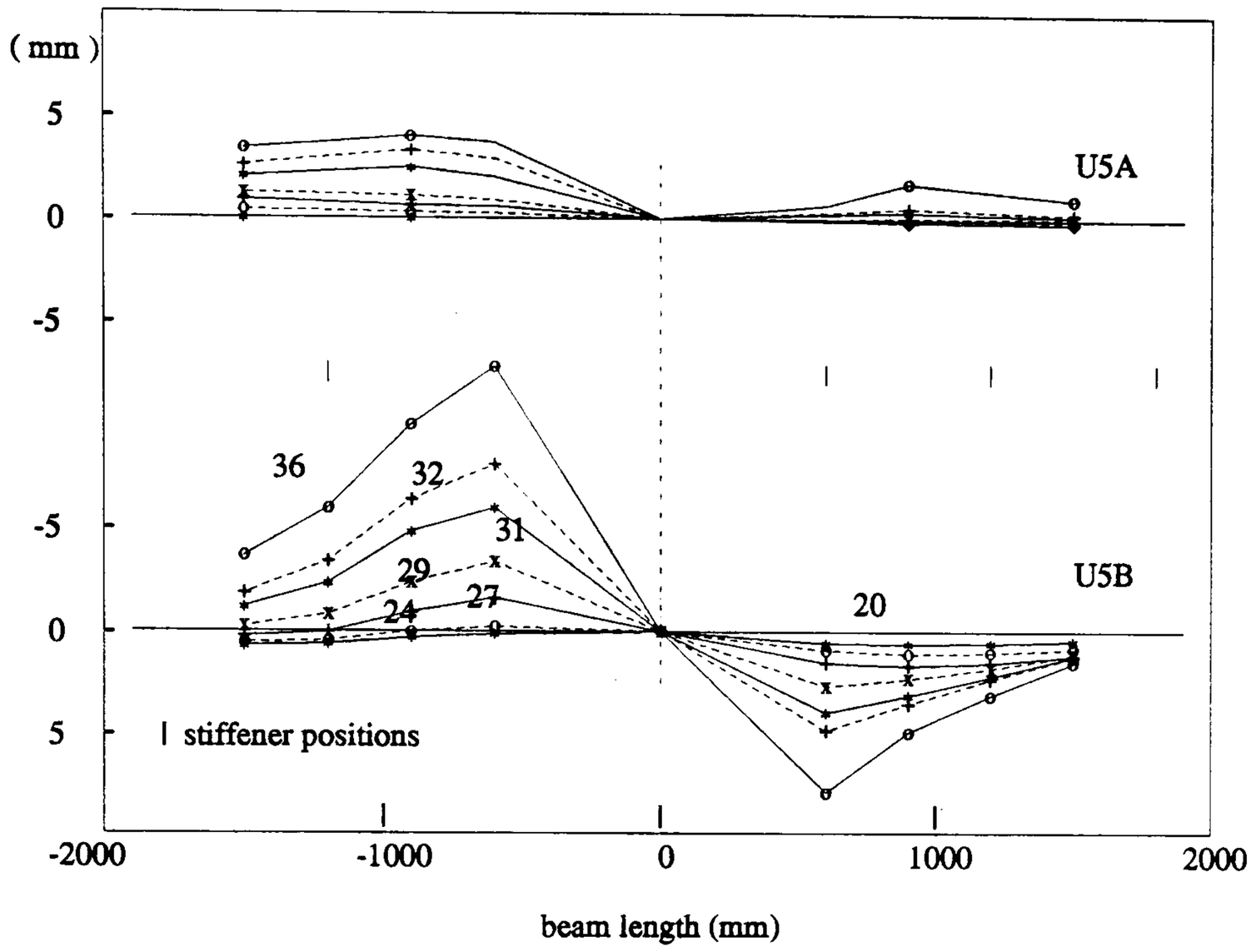

Figure 6.27: Absolute lateral movement of bottom flanges(specimen U5)

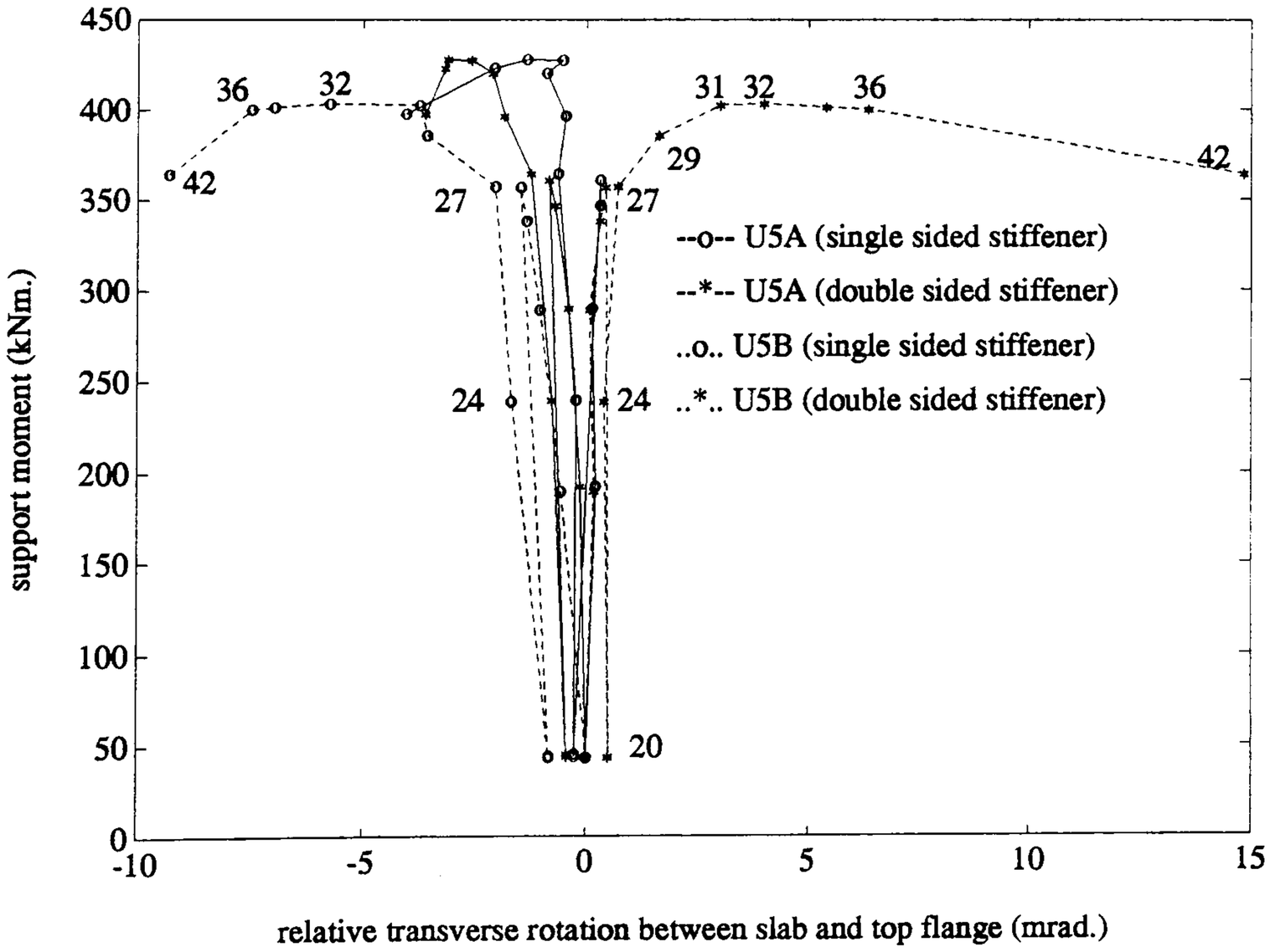

Figure 6.28: Relative transverse rotation (specimen U5)

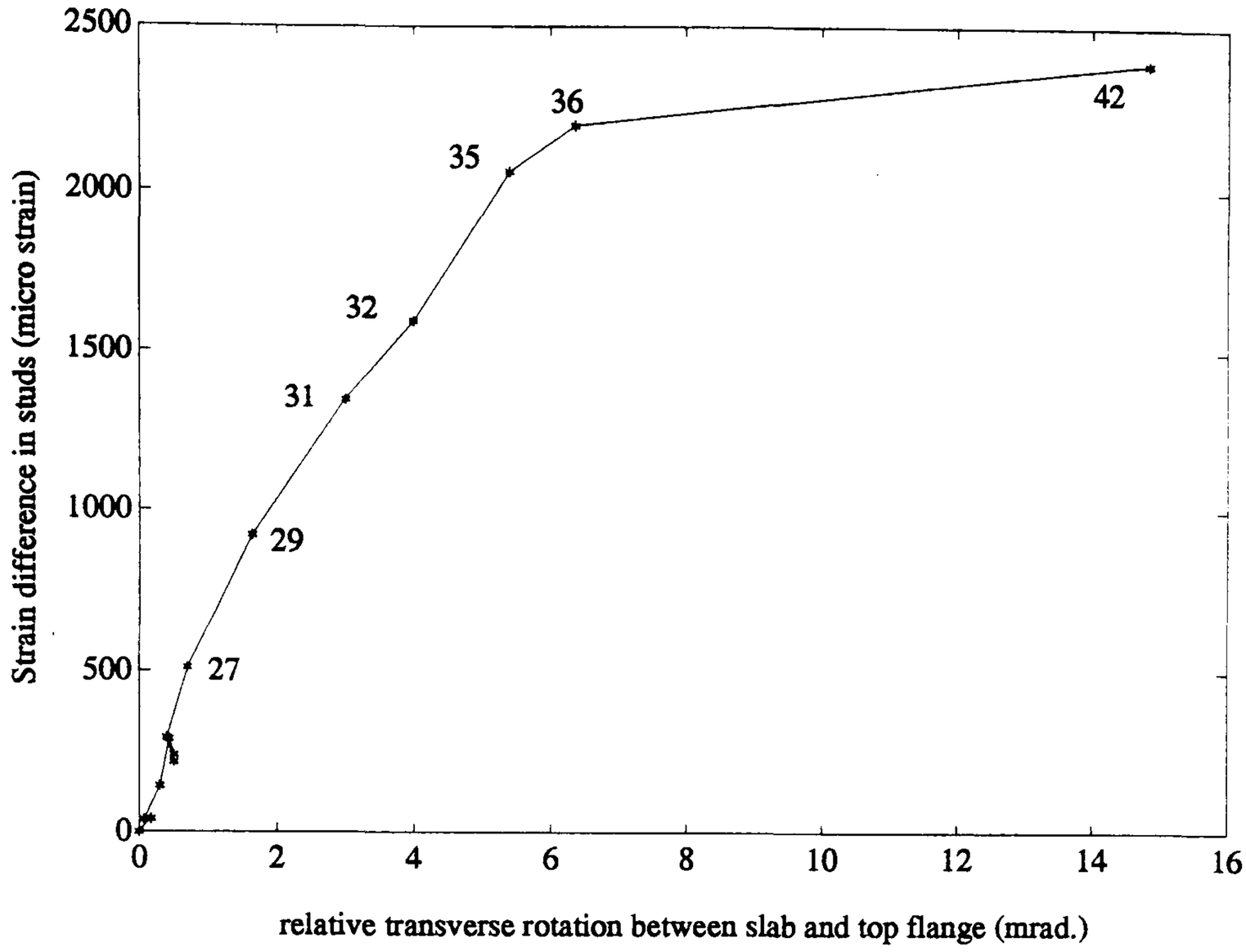

Figure 6.29: Transverse rotation (specimen U5)

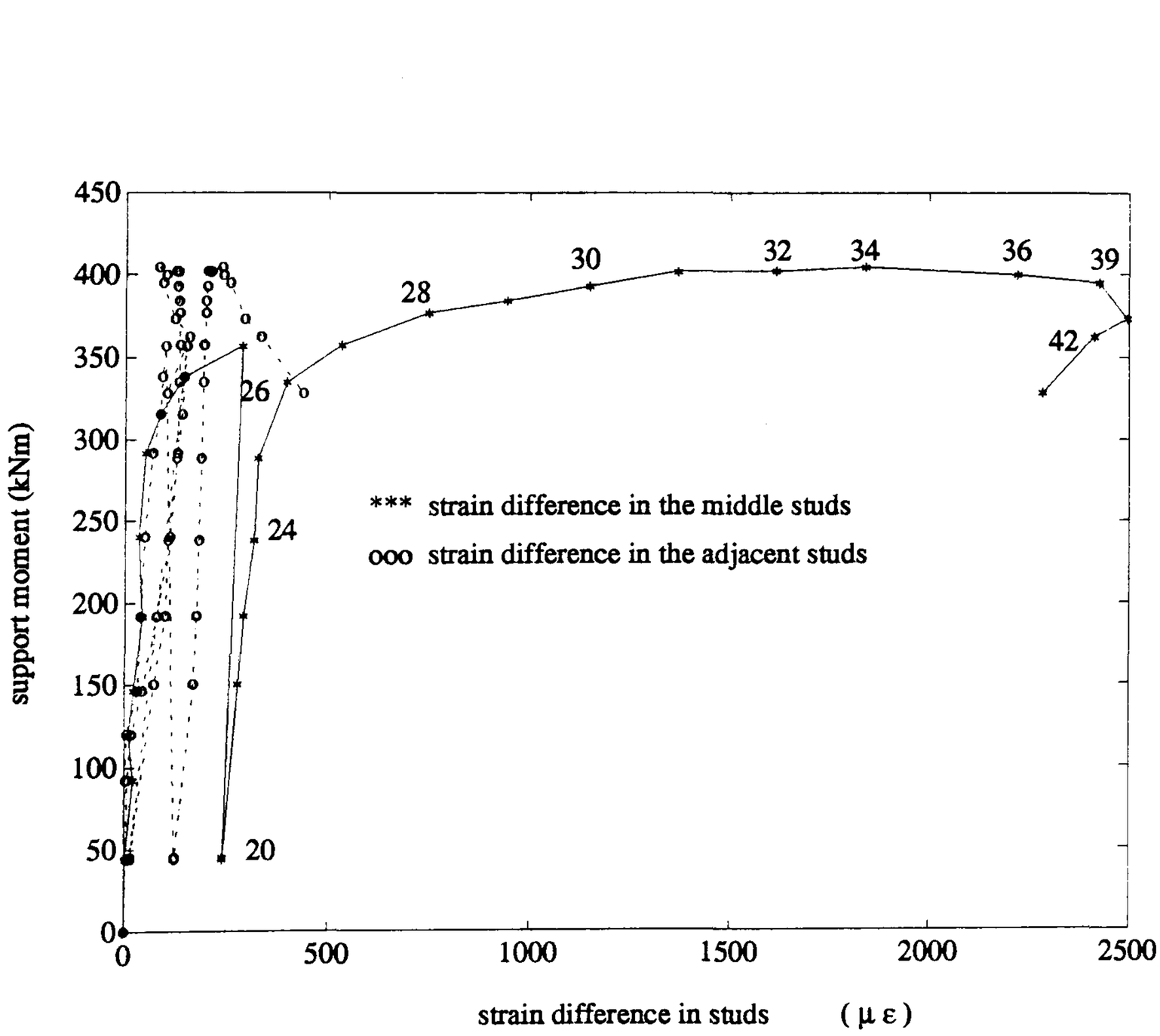

Figure 6.30: Strains in studs (specimen U5B double sided)

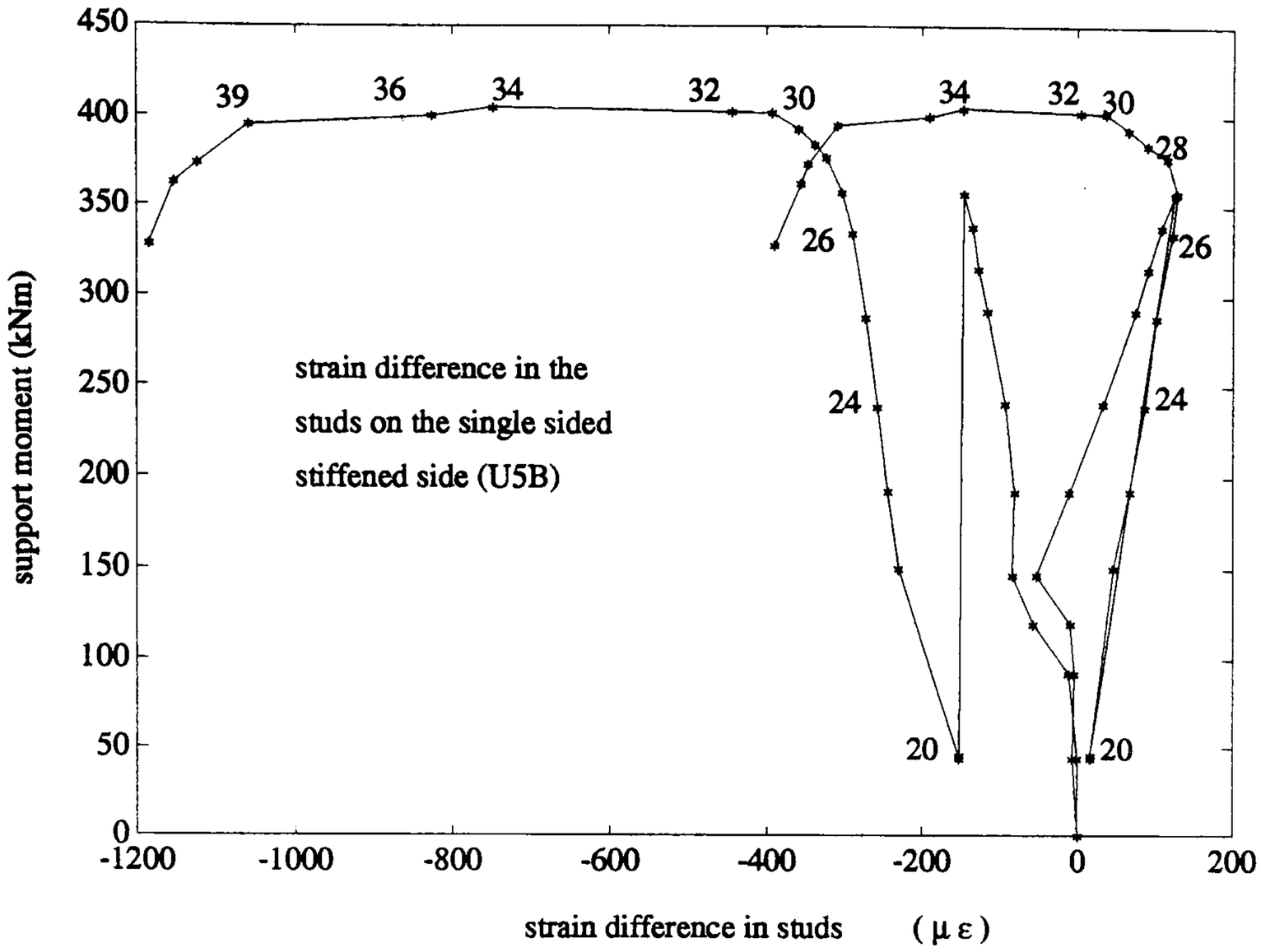

Figure 6.31: Strains in studs (specimen U5B single sided)

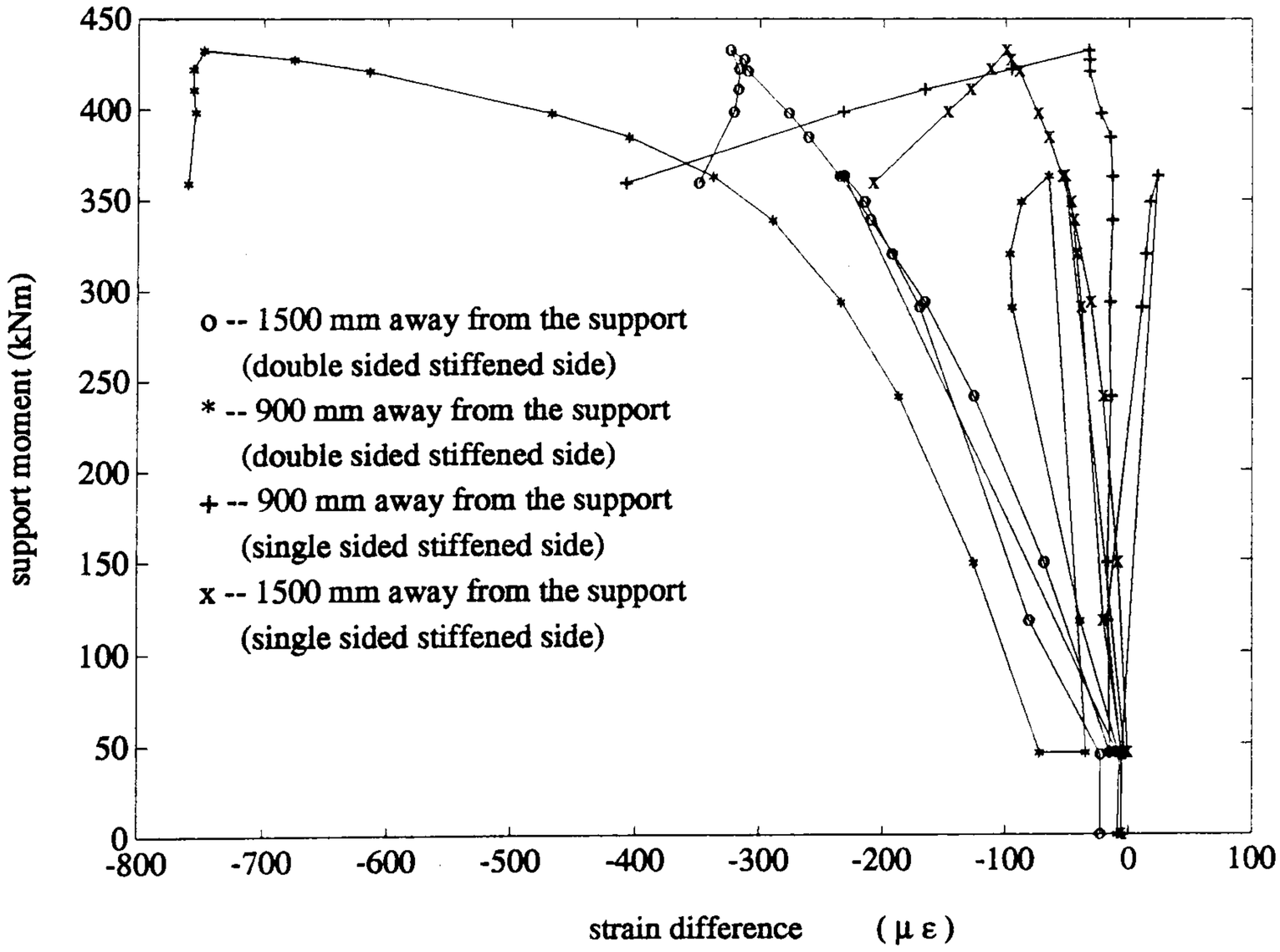

Figure 6.32: Web distortion (U5A)

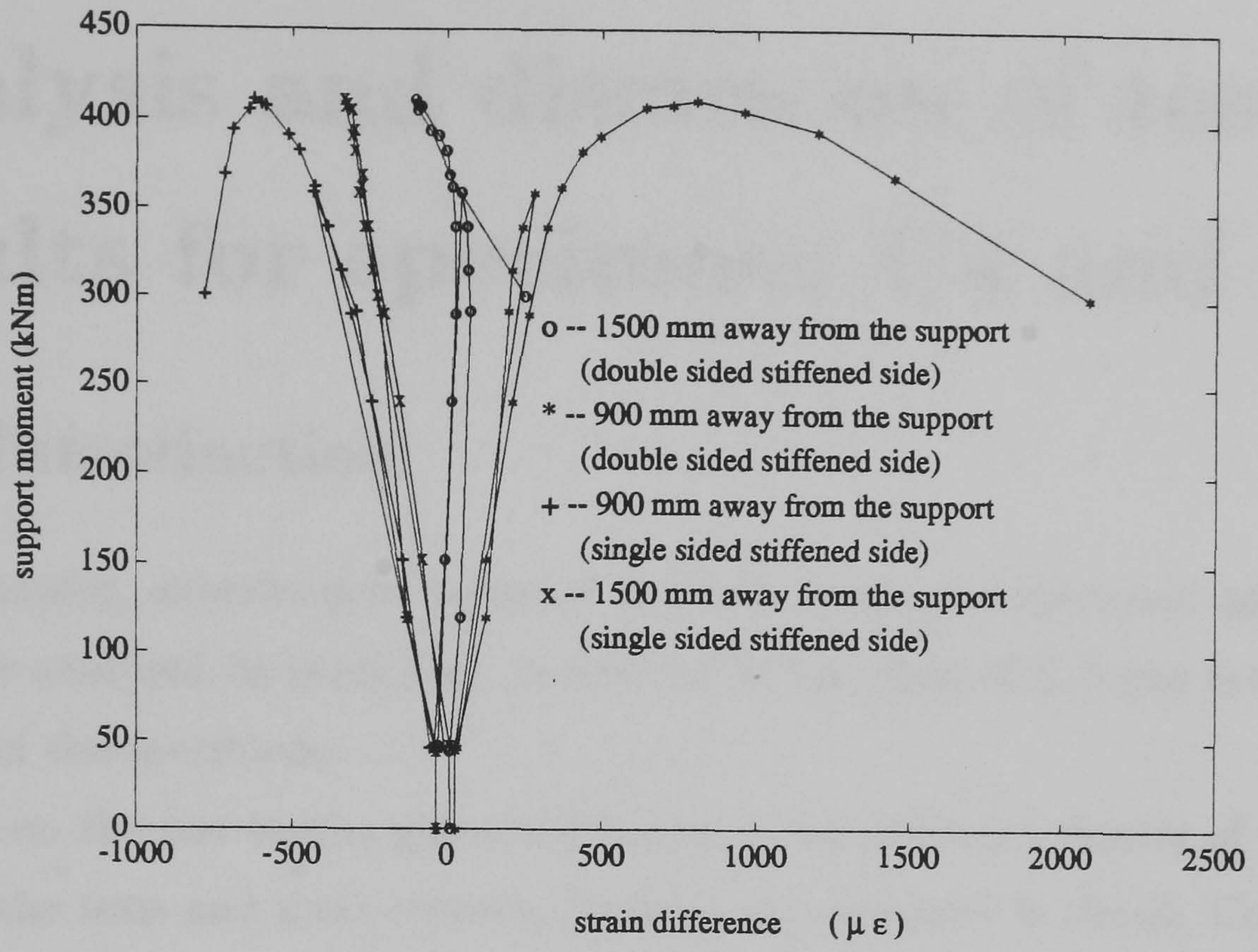

Figure 6.33: Web distortion (U5B)

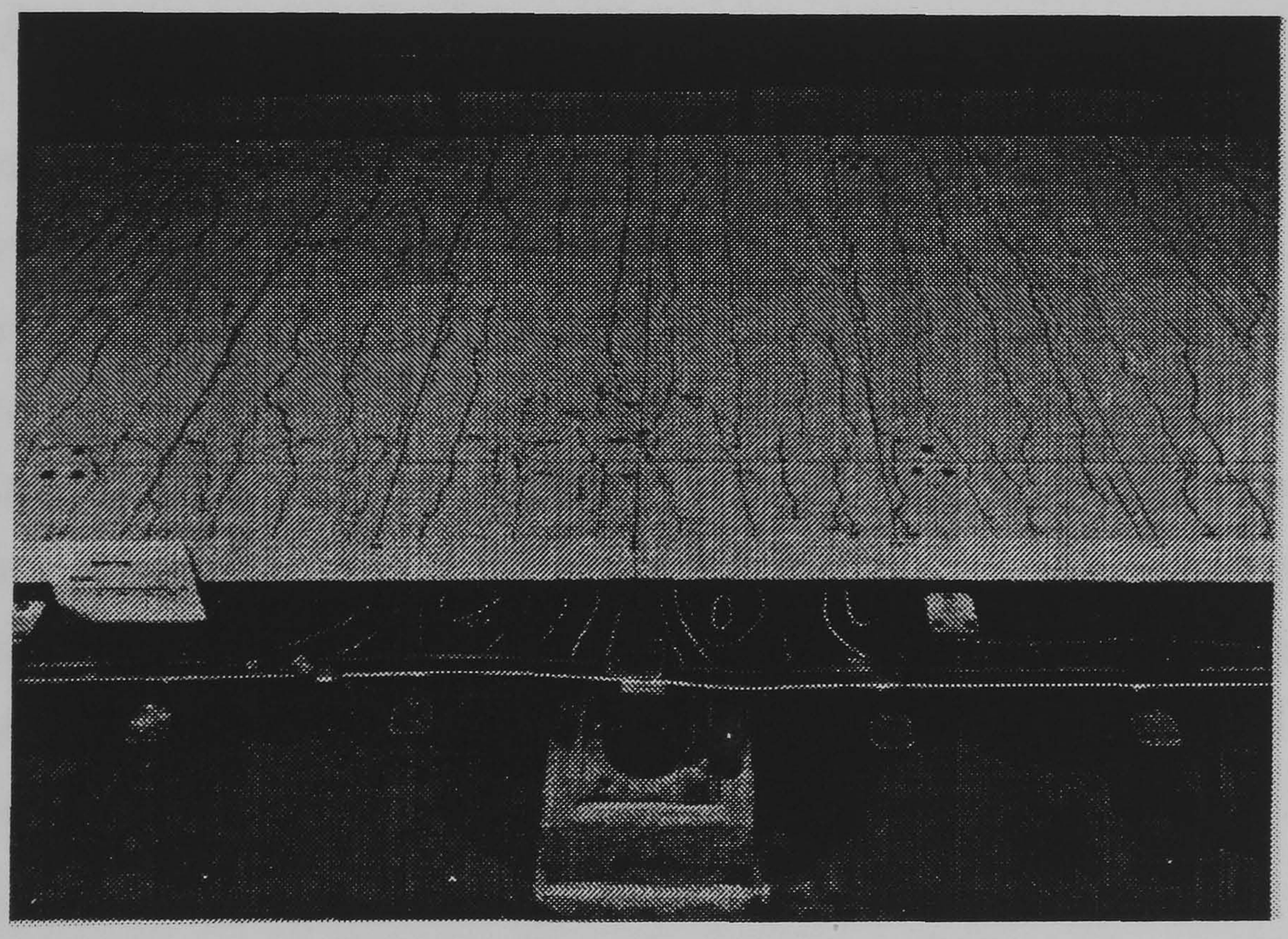

Figure 6.34: Crack in the slab(U5)

Chapter 7

Analysis and discussion of test results for specimens U4 and U5

7.1 Introduction

In this chapter, experimental errors of the test results are discussed and the test results are analysed, in particular, in relation to the effect of U-frame action on the strength of the specimens.

Based on the test results given in Chapter 6, the general behavior of both specimens in the tests and their common features are discussed in detail. Comparisons are made between specimens U4 and U5 in terms of their load-displacement behavior and web distortion. The distinctive features in each test are then summarized and conclusions are drawn.

7.2 Accuracy of the test results

The experimental results presented in Chapter 6 can be divided into two groups: those of which have been derived directly from the test measurements, e.g. rotations, deflections and strains etc., and those of which have been calculated from the test measurements, for instance, moment resistances and support moments.

The applied loads were measured by load cells. Two 100 kN and two 250 kN DATA-sense compression load cells were used in the tests. They were calibrated twice before and after tests, with mean values of loading and unloading. System eccentricities could be attributed to alignment errors resulting in unequal lever arms and loading out of plane. The net effect was believed to be less than 1% of the measured support moments.

The accuracy of the LVDTs, calibrated with standard slip gauges, was found to be ± 0.01 mm, which was about the same as their repeatability.

The accuracy of the dial gauges, measured with slip gauges, was also proved to

be ± 0.01 mm, about the same as the repeatability of these instruments.

The sensitivity of the strain gauges is $\pm 1\mu\epsilon$. The strain gauges used on the steel beams are type PL-10 and PYL-10 (gauge length 10 mm and width 3 mm), and the ones used on the studs are type PL-5 (gauge length 5 mm and width 1 mm). Both types are temperature compensated ($-20°C \sim +80°C$). The strain gauges on the webs to pick the web distortion and the strain gauges on the bottom flanges were all arranged in such a way that the alignment errors of their positions could be minimized, when only the differences and mean values of strains in a pair of the strain gauges were of interest.

The readings of strain and displacement measured by LVDTs were processed via the Schlumberger 3531D data logger. The data logger was claimed that the error is better than 0.15%. A separate check showed that the repetitive error is less than 0.3%. In view of the magnitudes recorded, the system errors (less than 1%) owing to summations of the errors of the data logger and strain gauges, or LVDTs should not have effects on the test results.

The measured sensitivity and accuracy of the 3 inch gauge length inclinometer with slip gauges, became as small as its repeatability in 0.03 mrad (0.03 mrad per division), since it was fairly easy to read the bubble sprit level to much less than 1 division. In view of the magnitudes recorded, the error in the rotation measurement is negligible.

There are two evident sources of error in the measurement of the relative displacements in the bottom flanges: transverse rotations of the bottom flanges and the mismatch distance between the positions of the displacement monitors and the rotation monitors. The transverse rotations introduce errors of lateral displacement measurements. Corrections were made to minimize the errors, however, the transverse rotations used in the correction are interpolated from those of two adjacent positions and adjacent loading stage. Compared with the magnitudes of values, the errors are within 3%.

The displacements picked up by theodolites have a poor accuracy of 0.5 mm, so that they are not reliable until there are large lateral displacements in the bottom flanges. However, the evaluation of initial imperfections are within an error of 2%, because the initial imperfection is divided by the length of a bow, which is about 1

m.

Errors in the calculated values of M_p and M_y are owing to the accuracies of measured dimensions and yield strengths. The yield stresses are believed to be within 1% of the true value, and the dimensions are controlled within 0.3%, so that the calculated values of M_p and M_y are in error about $\pm 1.1\%$.

7.3 Analysis of the results

7.3.1 Specimen U4

Moment rotation characteristic

At low load($M < 0.2M_y$), the moment-rotation curves follow the elastic uncracked stiffness line, and then lie between the elastic uncracked and cracked stiffness lines because of tension stiffening. The maximum moment attained in the tests are beyond the yield moment, and the load began to drop soon afterward. Lateral buckling was found at stage 12 (M = 217.7 kNm(U4A) and M =218.4 kNm(U4B)) when there were no cross bracings other than at the support section. For beams with lateral cross bracings, lateral buckling was observed at stage 23(M = 382.6 kNm(U4A) and M = 377.7 kNm(U4B)).

Load-displacement relationship

The load-deflection curves are similar to the moment rotation curves: elastic deformations at low load stages, large deformation developing beyond the yield moment, and drop of load after the maximum moment.

The lateral displacements of the bottom flanges reveal initiation of lateral buckling. For unbraced beams, lateral buckling occurred at a lower load than local buckling. For braced beams, the interaction of lateral flange buckling and local web buckling was involved. The maximum moment attained was 1.13 M_y.

Transverse rotations

The relationship between load and transverse rotation of a bottom flange is similar to that between load and lateral displacements. Lateral buckling comes with rotation

of the bottom flanges. Stability is improved by using lateral cross bracing to the bottom flanges adjacent to the central section. This is illustrated by comparisons of Figs.6.6, 6.7, 6.14 and 6.15. These Figures show the transverse rotations of the bottom flanges, the top flanges and the slab at the sections 600 mm away from the support section. According to the earlier numerical and experimental investigations [42, 54], lateral buckling of a continuous composite beam is more likely to occur in these regions. When the beams were unbraced (Figs.6.6, 6.7), the bottom flanges initiated a big increase of the transverse rotation at a support moment between 200 kNm and 250 kNm. This value increased beyond 350 kNm (Figs.6.14 an 6.15) when the beams were braced in test 2.

Strain measurement

The measurement of strains in the bottom flanges illustrates both compression strain in the bottom flanges and in-plane bending induced by lateral buckling. Although there were only a few monitoring positions of strain gauges along the length of the beams, the distribution of the in-plane bending, which was caused by lateral buckling, prescribed a clear lateral buckling wave (Figs.6.4 and 6.8).

Comparing the curves of compression strain(Figs.6.9 6.10)against load with the curves of in-plane bending strain (Figs.6.11 and 6.12), it is found that when the specimen was braced, yielding started at nearly the same time as lateral and local buckling.

The strains measured on the bottom flanges also give a value of the maximum compression forces reached in the bottom flanges of the beams with continuous U-frame restraints.

The web distortion is illustrated by the out-plane bending strains of web, in a difference of strains between the two surfaces of the web at the same position. Large web distortion is involved when maximum load is reached. But at early stage of lateral buckling, the distortion is not significant.

Effect of cross bracing

Effective cross bracings are at locations close to the internal supports. This is illustrated in the test when the specimen had cross bracings at two sections adjacent to

the central section. Compared with that of unbraced test(specimen U4), the lateral movement of the bottom flanges at locations of bracing is effectively minimized, and the beams are separated into four regions with shorter buckling wave lengths instead of the two regions with longer buckling wave lengths for unbraced beams.

Basically, when bracing(to the bottom flanges) is introduced, a beam can be divided into several segments, and hence the effective length of the beam is reduced. The buckled shape involves deformation of all segments (see Figs.6.8 and 6.13) and interactive buckling may occur between adjacent segments.

Fig.7.1 shows one span of a multi-span continuous beam, under uniformly distributed loading, w. Besides being fully lateraly restrained at the internal supports, A and B, it is also braced at the sections C and D in its hogging regions. Assuming that the bracings at sections C and D can provide full lateral restraints to the beam, then the beam span is divided into three segments by two lateral braces in the hogging regions. Let L be the span between the two supports, and L_b be the distance between the supports and the braced sections. It is assumed that the design method to distortional lateral buckling in Eurocode 4 [1] is applicable in each of the segments. Clearly, two critical moments M_{cr1} and M_{cr2}, that govern segment 1 and segment 2 will be different, depending upon the spacing of the bracings and the moment gradients. Since the theory, on which the method of Eurocode 4 is based, takes no account of restraint of one segment by the continuity of the bottom flange into adjacent segments, the actual critical moment $M_{cr}{}^*$, that governs the whole span of the beam will be expected to lie between the values M_{cr1} and M_{cr2} for any given location of bracing.

A plot of M_{cr1} and M_{cr2} against L_b is given in Fig.7.2 for a pair of beams with the cross section of specimen U4. The beams are subject to uniformly distributed loading as shown in Fig.7.1. The elastic critical moment M_{cr} is calculated by the Eurocode 4 method [1]. Full lateral restraints at the bracing sections are assumed, so that the span of the beams is divided into three segments by the two cross bracing sections at L_b from the supports. The ratio of the support moment to $wL^2/8$, or ψ referred in the EC4 design method to lateral buckling is 0.889. This is calculated from a span of 15 m, span-depth ratio of 24 (15 m /0.628 m) and a hogging length of 5 m for specimen U4.

The ordinate of the plot gives the maximum moment at the support section, that corresponds to the elastic critical moment, M_{cr}, of either segment 1 or segment 2. The abscissa gives the variation of bracing length, L_b. Two curves of M_{cr}-L_b are given, and they corresponds to segments 1 and 2, of a beam with the cross-section of specimen U4. The two curves intersect at a bracing length about 0.9 m, which means that no interaction occurs between the two adjacent segments. When L_b is smaller than 0.9 m , segment 1 will restrain segment 2 and the effective length of segment 2 will be less L_2 as shown in Fig.7.1. When L_b is greater than 0.9 m, segment 2 will be more stable and hence restrain the segment 1.

Fig.7.2 shows that segment 2 is more stable than segment 1 for specimen U4 with cross bracings at 1.6 m and 1.2 m away from central support each side.

In the above discussion, the bracing is assumed to have sufficient strength and stiffness when the Eurocode 4 method is used.

If L_b is zero, the buckling moment of unbraced beams is obtained. When specimen U4 is unbraced, its elastic buckling moment is given by the horizontal dash line in Fig.7.2. One can find that with increasing of L_b, segment 2 becomes more and more stable, but the buckling moment for segment 1 appears to drop below the buckling moment for unbraced beams. This is due to the conservative approximation made in the derivation of the Eurocode 4 method, that the continuity of the bottom flange at an internal support is not taken into account. Obviously, a beam will be more stable when it is braced than when it is unbraced. Therefore, the elastic critical moment for the whole span of the beam is more likely between the upper curve (M_{cr} for the more stable segment) and the horizontal curve (M_{cr} for the unbraced beam).

Local web buckling

The web is in Class 4, and the flange is in Class 1 in accordance with the draft Eurocode 4 [1].

The moment gradient has less effect on local buckling, because the region of the local buckling is very short as compared with the length of hogging region, i.e. 0.513 m/ 5 m (depth of the steel section/hogging length of U4). Local web buckling only occurred at the web panels near the supports when the support moment was beyond

the yield moment. No local buckling was observed in the flanges.

This test evidence raises the argument that cross-sections with a slender web (Class 4) and compact flanges (Class 1) in composite beams is more likely subject to a yield stress level before local buckling.

7.3.2 Specimen U5

Moment rotation characteristic

The moment rotation curves are similar to those of specimen U4, at low load, following the uncracked stiffness lines and then lying between the cracked and uncracked stiffness lines. The maximum moments attained are beyond the yield moment. Lateral buckling occurred at a moment 40% higher than that of specimen U4 when unbraced, and at about the same bending moment when specimen U4 was cross-braced.

The mean value of rotation at the maximum load, 36.4 mrad(stage 34), is approximately equal to that of specimen U4(at stage 24).

Assume that the specimen is free of lateral buckling, then its strength will be governed by local buckling in the hogging regions near its supports. For a cross-section of Class 4 (near the Classes 3/4 boundary), local buckling would occur when the yield moment is reached at the support sections. Because the maximum moments at the support section were over the yield moment by 10% to 20% in the tests, it is concluded that lateral buckling did not affect the ultimate bending strength of the specimen, and the ultimate strength of specimen U5 was governed by local buckling rather than lateral buckling.

Load displacement relationship

The load deflection relationship is similar to the moment rotation curves, with three distinct states: pre-buckling linear state, buckling-yield state, and post-buckling and post-yield state.

The mean value of deflection at the maximum load is about 70.2 mm, and the maximum deflection is 100.3 mm when the moment drops at 0.89 M_y(U5B).

The load and lateral displacement curves reveal the initiation of lateral buckling.

Compared with those of specimen U4, the lateral instability is improved by adding the vertical web stiffeners along the beam length.

The curves of relative displacement of the bottom flanges of the twin beam against load also reveal the initiation of lateral buckling of the U-frame beams, and the distribution of lateral displacement when buckling occurs. The lateral displacement mainly concentrates close to the support section.

Transverse rotation

The transverse rotations of the bottom flange vary with load in a similar way to lateral displacements. Lateral buckling was found at regions close to the support section. Compared with the test results of specimen U4, the length of lateral buckling shape is greatly reduced.

The difference between transverse rotations of the top flange and the slab of specimen U5 reveals a relatively flexible connection, as compared with that of specimen U4, the beams with continuous U-frames. When lateral buckling occurs, trend of lateral movements of the bottom flange is subject to the restraint of the discrete U-frames, hence inducing a large U-frame force. This is illustrated in the curve of the relative transverse rotation against strain difference in the studs above the stiffeners(Fig.6.29).

The stiffness and strength of the U-frame connection are further investigated in the next chapter.

Strain measurements

Strain measurements of the bottom flanges illustrate the in-plane bending induced by lateral buckling. They are more sensitive than other measurements, and continuous readings by data logger are also available. The in-plane bending strain is the best source of information on the initiation of lateral buckling.

The web distortions are also illustrated by strain differences measurements along the beam length. For specimen U5, large web distortion was involved after lateral buckling only in a region closest to the support section, and this is different from that of specimen U4, the beams with continuous (unstiffened) U-frames. Web distortion was effectively reduced by stiffeners at locations further away from the stiffeners

that are closest to the support section, so that it suggests that the most effective stiffeners are those closest to the support section in the hogging regions.

Local buckling

Basically, local web buckling occurs when the support moment is beyond the yield moment. The web panel may deform either inward or outward when local buckling occurs. However, the welding of angles to the outside surface only may have induced the inward deformation in the web panels between the double sided stiffeners. For the single sided stiffened side, as the stiffener spacing is closer, local web buckling deformation is reduced.

The flanges of specimen are in Class 1 in accordance with the draft Eurocode 4 [1], and in absence of "disturbance" from web and from lateral buckling, they should be able to yield over a significant length (e.g. at least about its width), and also to strain harden a little, before loss strength from local buckling.

However, flange local buckling was observed in the side with double sided stiffeners of beam U5A, so that that flange must be disturbed. The reasons that local buckling of the flange is only in this location may be the differences of geometrical dimensions and stiffener spacing as well as the way of welding. Fig.7.3 illustrates the details at the location of flange local buckling. The out flange is about 15% more slender when a weld is omitted from point A than that of the other side. This has a significant effect on the flange local buckling, since the torsional resistance from one weld is less than than the resistance from two welds. For the side with closer single sided stiffeners, local web buckling deformation is restricted by stiffeners and strengthening angles, but for the side with sparser double sided stiffeners, the strengthening angles restrict the web distortion less and cause a concentrated local stress field, which interacts with the tendency of the bottom flange to move laterally, inducing the flange buckling.

Although U5B would have same situation, the difference in the width of bottom flanges between U5A and U5B is 3.3%, and the alignment in fabrication of beam U5B also made the out flange 10% less slender on the side without weld. This is the reason that no local flange buckling occurred in the beam.

Crack patterns on the slab

The transverse crack patterns are similar for both specimens U4 and U5, parallel at a spacing about 150 mm. However, longitudinal cracks were found in the slab after the maximum loading in specimen U5, at the location above the double sided stiffener, which is closest to the support section. This reveals that concentrated moments induced by U-frame forces occurred at positions of the stiffeners in the beams with discrete U-frames.

7.3.3 Predictions of lateral buckling resistance

From previous chapters, it is found that methods of Eurocode 4 [1], SCI [49] and Weston and Nethercot [44] give good predictions of lateral buckling resistance for specimen U4. This compliments earlier investigations by Johnson and Fan [54], to continuous U-frames with rather compact cross-sections (Class 2) so that these design methods are also applicable to the beams of slender sections (Classes 3/4) with continuous U-frame action. However, no methods are available so far for composite beams with discrete U-frames.

For beams with cross bracings, the method of Weston and Nethercot is not applicable, because it is based on a model with uniformly distributed loadings. The prediction by the method of Eurocode 4 is reasonable, which is based on a beam with full lateral restraint from the bracings. The elastic critical moment M_{cr} lies between the two values of critical moment of the two adjacent segments.

The lateral buckling resistance, or the characteristic moment, M_d is then calculated in accordance with the design curves in Eurocode 4 [1].

7.4 Discussion of test results

In the test on U4 (unbraced), when lateral buckling first appeared at stage 12, the beams could be still further loaded even beyond stage 16, at which test 1 was stopped. When the beams were cross braced to the bottom flanges in test 2, lateral stability was improved, and lateral buckling did not occur until stage 23, at which the support moments were approximately equal to the yielding moment, but the maximum moment (at stage 24) was attained only after severe local web buckling

near the support section.

For the stiffened specimen U5, evidence of lateral buckling at stage 10 (before the web panels were strengthened) did not limit the further loading capacity of the beams. Lateral buckling was observed in beam U5B before the maximum moment was reached.

It is found that for both specimens U4 and U5, although lateral buckling initiates at different levels of loads, and further interacts with local buckling, their moment rotation curves are still very similar. In both specimens, the maximum moment. M_{max} is greater than the yield moment, at which local buckling will occur for a beam with Class 4 cross-sections, and therefore the design to the ultimate strength of both specimens is governed by local buckling.

A comparison of the maximum moments shows that beams U5A and U5B have the ultimate moment strength 0.5%(U5B) and 7%(U5A) over those of specimen U4, which is attributed to the web strengthening angles at the web panels near the support section.

Fig.7.4 shows three basic lateral buckling shapes of the bottom flanges found in the tests.

The first form of lateral buckling shapes is an even sine shape over the whole cantilever length, when beams were unstiffened and unbraced. This is illustrated by the lateral displacement and transverse rotation distributions of the bottom flanges in the test on specimen U4 when it is unbraced. (Fig.6.5 for instance).

The second form of lateral buckling shape is as the four lateral deformation regions separated by three cross bracing sections (including the support section), when the beams were braced to the bottom flanges(Figs. 6.8 and 6.13). The lateral deformations (displacement or transverse rotation) in the two adjacent regions to the support section were large compared with those of other parts of the beams. This reveals the dominent role of buckling in these regions.

The third form of lateral buckling shape is the concentrated lateral deformations close to the support section when beams are stiffened in discrete U-frames along the beam length. Lateral displacement was found to concentrate within the regions of one to two U-frame spacings for the double stiffened side and two to three U-frame spacings for the single stiffened side (Figs. 6.21 and 6.27).

The test on specimen U4 with cross bracings at two sections adjacent to the support, shows that the dominating lateral buckling was in the regions close to the support. The lateral displacement of the bottom flanges in the other regions also contributed to the interactive mode of buckling. But in specimen U5, the intermediate vertical stiffeners together with the slab act as discrete U-frames, which are obviously less stiff at the corresponding positions than the bracings, therefore stiffeners along the beam length minimize the lateral deformation, as compared with that of the unstiffened specimen U4.

Another prominent evidence of the test results is the magnitude of web distortion. Web distortion is involved wherever there is lateral displacement in the bottom flanges, but the significant web distortion was found only when ultimate moment strength was reached. The web distortion is greatly reduced at locations further away from the central support in the stiffened beams U5. But, for the unstiffened beams U4, there is no obvious difference in web distortion along the beam length.

Concentrated transverse moments were found to act on the shear connection above the stiffeners. The measurement of strain in the studs above the stiffeners closest to the support showed that more than 80% of the transverse moment was transmitted via the studs right above the double sided stiffener, which created a worse stress situation in the slab, than if all these adjacent stud pairs had shared the moment equally. A better transmission could be realized by not placing studs right above a stiffener, so that the transverse moment would be shared by the studs adjacent to the stiffener. This arrangement had been used on the side with single sided stiffeners. Although distortional lateral buckling was found on both double and single stiffened sides in U5B, longitudinal cracks, which were the sign of a shear connection failure, were only observed on the double stiffened side.

The measurement of strain in the studs on the two sides of the beam U5B suggests that magnitude of the maximum transverse moments induced by U-frame forces may be proportional to the stiffness of the discrete U-frames. Assuming that the transverse moment at the location of a stiffener is proportional to the summation of the transverse bending strains via the studs, then at the ultimate stage (stage 34), the transverse moment on the double sided stiffener is about twice as that on the single sided stiffener, and this is attributed to the stiffness differences in the

discrete U-frames. The effects of local bending of studs and the lateral restraint force of discrete U-frames in relation to the strains measured on their shanks will be further investigated in the next Chapter.

7.5 Summary of conclusions

The moment-rotation curves are similar for both beams with continuous and discrete U-frames. Basically, the curves can be divided into three distinct parts: pre-buckling, buckling and yield, and post buckling. The vertical stiffeners do not alter the moment-rotation characteristic.

Web distortion is effectively reduced by vertical web stiffeners, and lateral buckling is concentrated in the regions closest to the support section for beams with discrete U-frame action.

For beams with continuous U-frame, bracing to the bottom flange close to the support section in a hogging region is effective in improving the lateral stability. However, the ultimate resistance of the beams with composite U-frame is dominated by local buckling rather than lateral buckling. It was found for both specimens U4 and U5, that lateral buckling preceded the local buckling, but the maximum loads were governed by local buckling.

The connection for a discrete U-frame is more flexible than that of continuous U-frames when lateral buckling occurs. A great U-frame force is induced in discrete U-frame beams, and this force appears to be proportional to the U-frame stiffness.

Design predictions of lateral buckling resistance of continuous U-frames based on Eurocode 4 and other methods are relevant even for the beams with slender cross-sections.

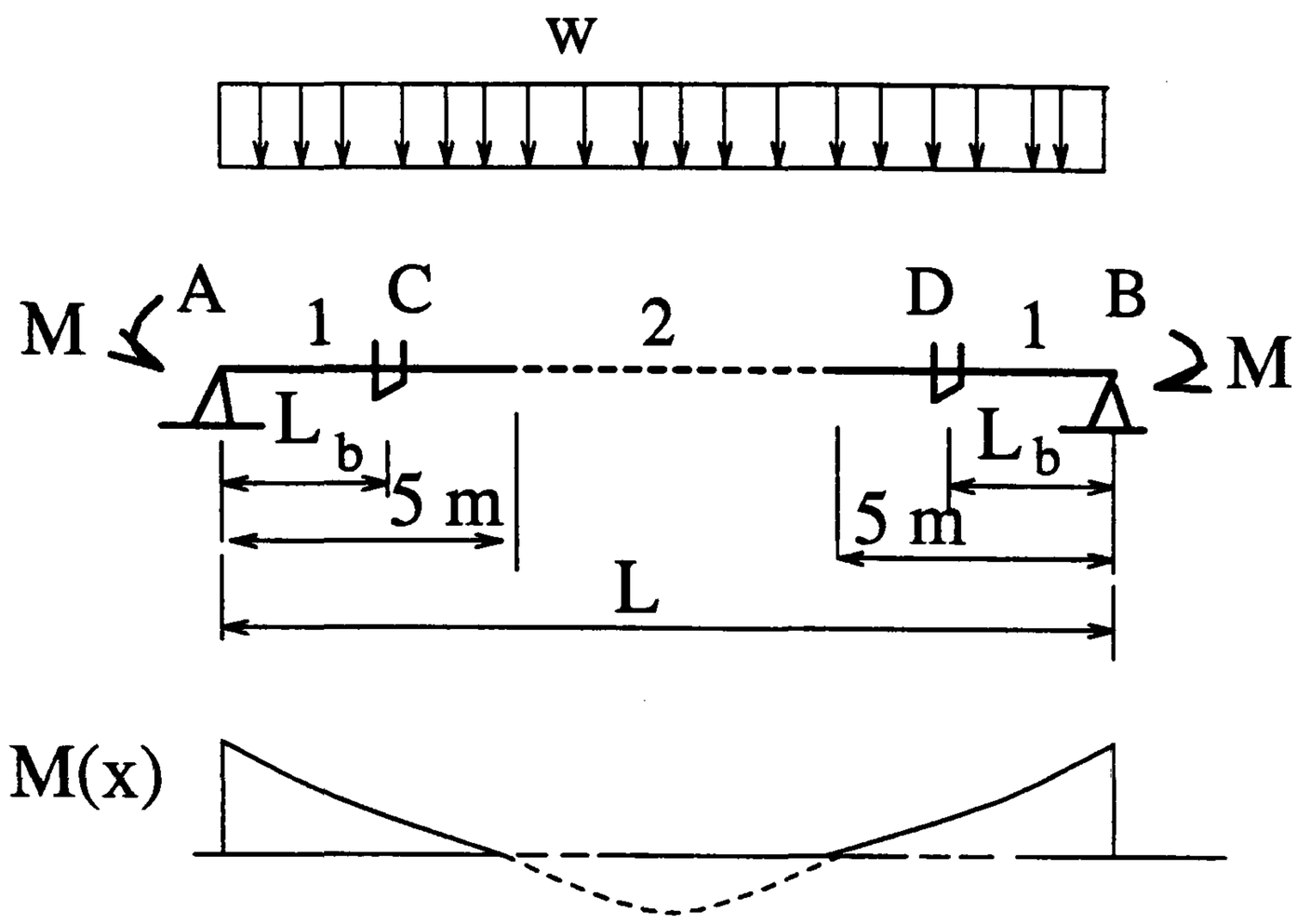

Figure 7.1: Loading and restraint condition

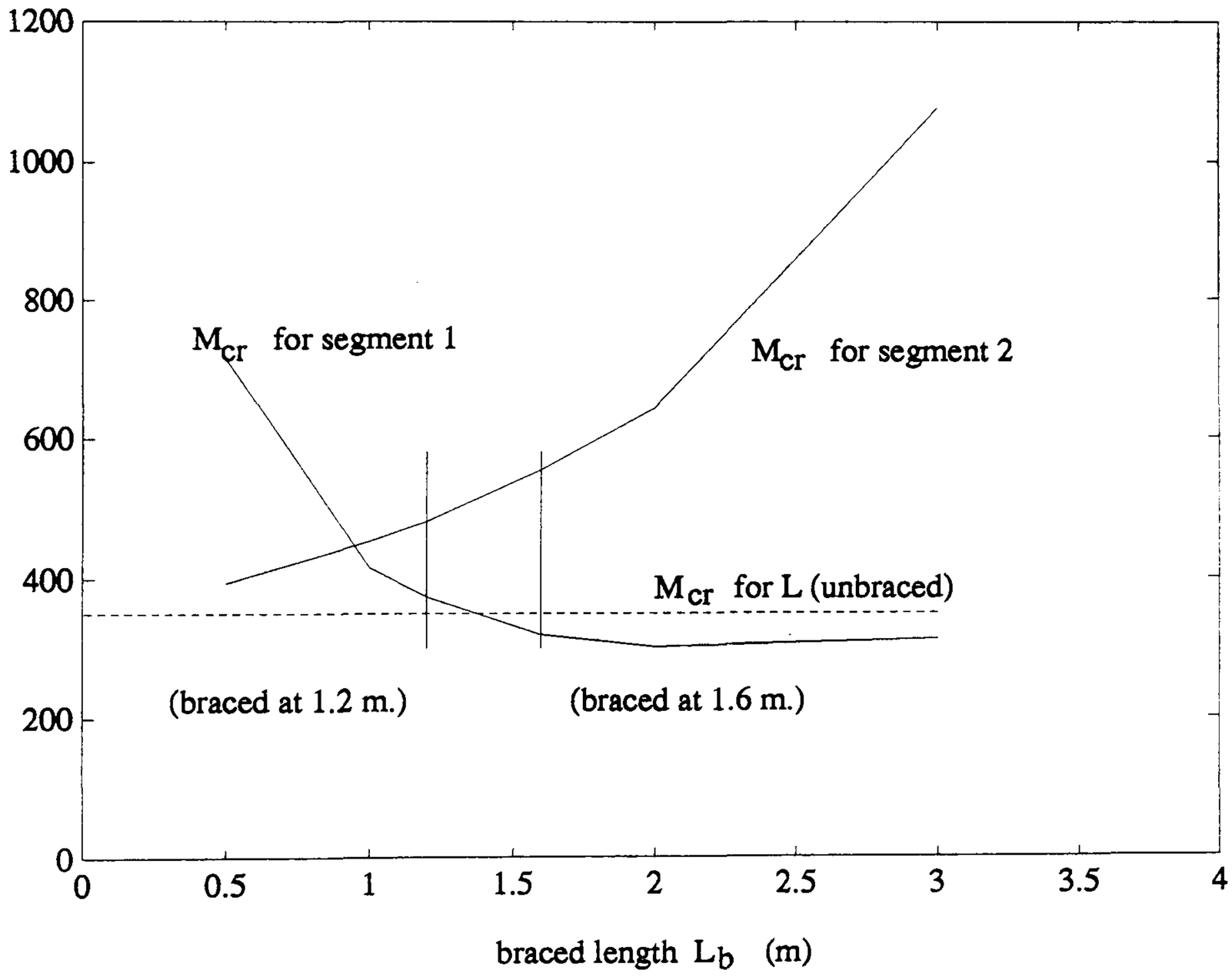

Figure 7.2: Elastic critical moment predictions (U4)

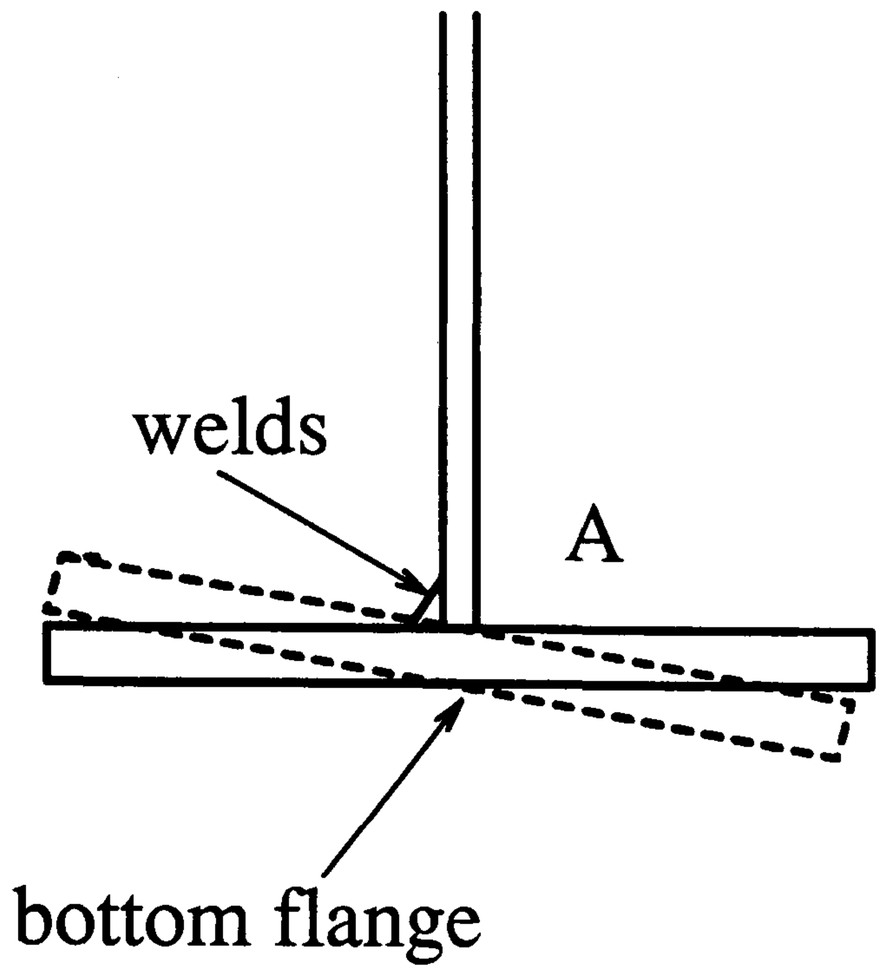

Figure 7.3: Location of local flange buckling (U5A)

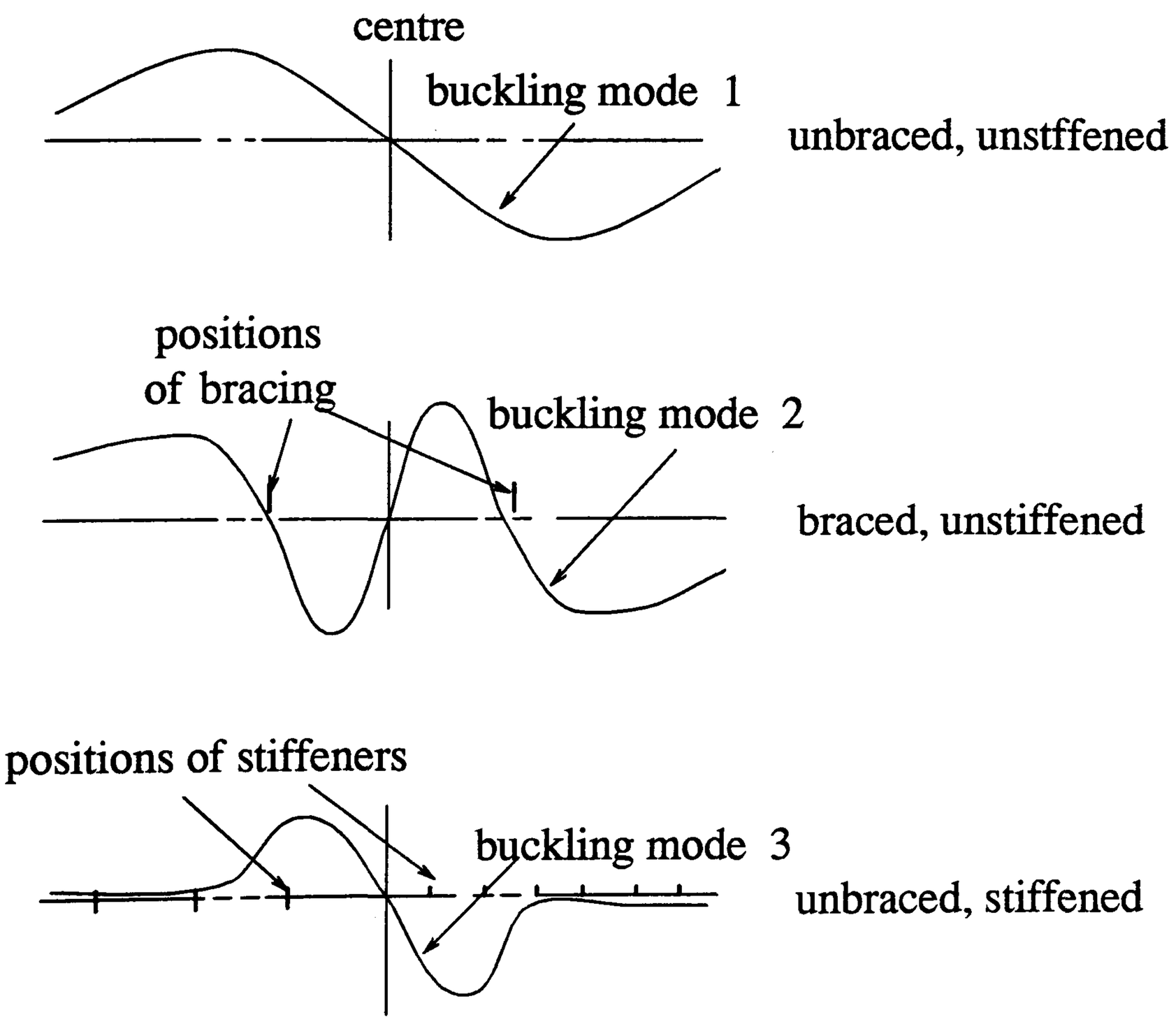

Figure 7.4: Lateral buckling shapes

Chapter 8

Tests to investigate U-frame action

8.1 Introduction

Continuous inverted U-frame action can be effective in stabilizing the bottom flanges of continuous composite plate girders near internal supports, because shear connection usually has sufficient strength and stiffness in transverse bending. However, for discrete U-frames, concentrated moments may act on the shear connections above the stiffeners, so that reliance needs to be placed upon the slab to top flange connections for rigidity via the shear studs.

The limitations of BS5400 when checking bridges, which use U-frame action for compression flange stability, is that it scarcely relates to current configurations of composite connections; but the joint rigidity can be the most critical term in evaluation of the moment resistance relating to the distortional lateral buckling. Besides, the design methods of BS5400:Part 3 [2] for lateral buckling resistance assessments of composite beams are based on the assumptions that the compressive force in a bottom flange is everywhere equal to its peak value at the internal support, and the torsional stiffness is negligible, which make the design very conservative.

Discrete U-frame action was studied by Molenstra and Johnson [71] by a series of tests on six 1:1 scale composite slab-flange connections, under a transverse moment. In a real structure, this transverse moment is caused by a transverse force, applied at the intersection of the compression flange and the vertical stiffener in the hogging bending region of a main bridge girder, which is induced by initial imperfections and lateral deformation tendency in the bottom flange. The research reveals that the significant flexibility of this type of connection would be a vital factor in evaluation of the lateral buckling strength. A limited tentative design formula for transverse flexibility of the relevant stud connections was proposed.

However, general application of the result is limited because only one param-

eter was varied (N, the number of studs in the connection). It is referred to in the formula, whereas other parameters must affect the flexibilities of the connections. Moreover, discrete U-frame action in distortional lateral buckling of composite beams has not been fully assessed, because of the shortage of test evidences.

The tests on specimen U5 show that U-frame forces were induced when lateral buckling occurred; and shear failure in the slab to top flange connections was found after the ultimate load stage (stage 34). To evaluate discrete U-frame action in distortional lateral buckling, tests on isolated U-frames were carried out. The test specimens known as "isolated U-frames" were cut from specimen U5. The stiffness and the strength of the discrete U-frames were investigated. The ultimate U-frame forces in the tests on specimen U5 are assessed based on the results of the isolated U-frame tests.

Two terminologies of tests will be used in the following sections, the global U-frame tests, which are referred to as the double cantilever tests on specimen U5, and the isolated U-frame tests, namely I-UD for the tests on the isolated U-frame with double sided stiffeners, and I-US, for the test on the isolated U-frame with single sided stiffeners.

8.2 Tests on isolated U-frames

8.2.1 Choice of specimen

It was decided that the test specimen would be chosen to be representative of a part of a real bridge plate girder near an internal support, with symmetrical vertical fitted stiffeners, acting as a discrete inverted U-frame.

To interpret the strain measurement of studs above the stiffeners in the previous global tests, the specimens called isolated U-frames were cut from specimen U5, at equal distances from the stiffeners closest to the central support section. The regions included the studs with strain gauges. They were isolated by means of flame cuts through the bottom flanges and web as shown in Fig.8.1.

The length of the specimens was chosen as 400 mm and 1000 mm respectively. This ranged from twice to five times the lengths of web included for stiffness by clause 9.6.5 of BS5400:Part 3 [2].

Specimen I-UD was cut from specimen U5 on the side with double sided stiffeners. Firstly, the specimen was tested with a longitudinal length of 1 m, at a small load, then the specimen was further cut with a reduced length of 0.4 m. The other specimen, labelled as I-US was cut from the specimen U5 on the side with single sided stiffeners with a longitudinal length of 0.4 m.

8.2.2 Test rig and instrumentation

The test rig for the isolated U-frame specimens is shown in Fig.8.2. The U-frames were suspended with continuity only at the slab and the steel top flanges with the remaining parts of specimen U5. A pair of lateral forces was applied to the bottom flanges, equal in magnitude and opposite in direction, using a bi-direction hydraulic jack. To ensure the stability of the test rig, only pulling forces were applied. This direction was also the most adverse loading situation for specimen I-US. This is because the webs of specimen I-US were single sided stiffened, so the studs on the stiffener side could transmit the concentrating pulling forces to the concrete in the U-frame connection more than the studs on the other side. Therefore, the results from specimen I-US should be on the safe side for evaluation of the strength of the discrete U-frame connections. A 2 tonne tension load cell was used to measure the applied force.

The positions of the instruments are illustrated in Fig.8.3. In each test, lateral displacements of the bottom flanges were measured by two LVDTs each side at the locations of the stiffeners. The transverse rotations of the bottom, top and concrete flanges were picked up manually, using an inclinometer.

The strain gauges bonded onto the studs above the stiffeners in U5B were still in use to measure strains in the studs induced by the lateral U-frame force.

8.2.3 Test procedures

Two tests on the isolated U-frames were carried out.

The test on specimen I-UD was divided into two parts. In the first part, the U-frame was tested with a longitudinal length of 1 m. The specimen was unloaded at a lateral force of 5 kN before further increment of lateral displacement in the bottom flanges, which was relative to the floor of the laboratory. In the second

part of the test, specimen I-UD was further cut, with the length reduced to 0.4 m, and loaded beyond the state when obvious nonlinear displacements in the bottom flanges were observed.

Specimen I-US was tested with a longitudinal length of 0.4 m.

A few load cycles were carried out at low loading levels to check the loading rig and the instrumentation.

8.2.4 Test results

The lateral displacements of the U-frames given hereafter are those at the intersections of the stiffeners and the bottom flanges. They are plotted against the U-frame forces in Fig.8.4. There are two curves for each specimen, and they correspond to the measurement on side A and side B. Side A is the side corresponding to beam U5A in the isolated U-frames, and side B corresponds to beam U5B.

The U-frame with single sided stiffeners appears more flexible than that with double sided stiffeners. However, the flexibility of the U-frame is not sensitive to the variation of the longitudinal length. This is illustrated by the curves for specimen I-UD, the double sided stiffened U-frame.

The transverse rotations were measured at the sections of discrete U-frames. The relative rotations between the slab and the steel top flanges are plotted against the U-frame force in Fig.8.5, from which the measured transverse flexibility of the connections is obtained by dividing the relative rotation by the transverse bending moment M_t by

$$f_r = \frac{\theta_r}{M_t} \tag{8.1}$$

- M_t is a product of the U-frame force and the distance h_s (see Fig.8.2) or by

$$M_t = F_u h_s \tag{8.2}$$

- θ_r is the relative transverse rotation between the slab and the steel top flange at location above stiffeners.

Transverse rotation of the connections developed more or less in proportion to the applied moment until failure of the connections occurred, which might be due

either to interior cracks in the slab or excessive deformations in the top flanges. An effective flexibility of the connection is therefore defined and used hereafter, as the linear slope of the moment rotation curves prior to the connection failures.

The measured flexibility of the shear connection is about 1.25 mrad/kNm for specimen I-UD, which is based on the measurement of transverse rotations on the side A because the shear connection had failed in the side B in the previous global tests on specimen U5.

The measured flexibility is about 4.71 mrad/kNm for the connection of specimen I-US.

The strains in the studs at locations above the stiffeners on the side B are plotted against U-frame force in Fig.8.6 and Fig.8.7 for specimens I-UD and I-US respectively. These studs were arranged in a way that strain difference in each pair of studs provided a relevant transverse bending moment. The strain gauges were bonded to the shank of each stud as shown in Fig.5.16. When the strain difference in a pair of studs is used, the effects not relevant to the transverse bending moment can be eliminated.

In Fig.8.6, studs (M.I.) and (M.O.) are the middle pair of studs right above the double sided stiffener (pair 4 in Fig.5.16), where I. refers to the inside, and O. refers to the outside.

In Fig.8.7, strains in studs L.I. and L.O. of specimen I-US are plotted against the lateral U-frame load F_u. The positions of studs are also shown in Fig.5.16, and only the strain gauges on the left pair of studs (L., pair 2) above the stiffener are used, because the other pair of strain gauges were out of working, after previous tests on specimen U5.

8.3 Analysis and discussion of test results

8.3.1 Scope of the test results

Because the specimens known as "isolated U-frames" were cut from the specimen U5, residual deformation in steel and studs as well as the cracks in the slab formed in the previous global tests must have affected the behaviour of the isolated U-frames.

The U-frame forces in the "isolated U-frame" tests were applied to the bot-

tom flanges at the locations of the stiffeners, however, U-frame forces induced by distortional lateral buckling in the global behaviour of U-frame beams would be influenced by lateral buckling shape and the locations of the stiffeners. U-frame forces are evaluated via the measured strains in the studs above the the stiffeners.

The uncut top flanges as well as the slab of the specimen U5 (Fig.8.1) would share parts of the U-frame force in equilibrium, which may slightly reduce the U-frame force transmitted via the studs, but as the slab is much stiffer than the top flange in torsion, the effect is negligible before shear failure of the concrete. However, the test flexibility of the slab would be slightly affected.

In the tests, both specimens I-UD and I-US were subject to inward pulling forces, for which the connection on the single sided stiffened U-frame is the worse loading condition, because the studs above the stiffened side tended to pull down the slab, and there would be greater forces than that if the less stiff side were pulled down. Therefore, the results may lead to safe values for the strength of the connection.

The experimental errors are subject to the instrumentation limits, which have been discussed in the previous chapter.

8.3.2 Stiffness of discrete U-frames

Flexibility of U-frame connection – a semi-empirical analogy

Johnson and Molenstra [71] proposed an empirical formula to predict flexibility of discrete U-frame connection, f_r, based on their tests on six discrete U-frame specimens, as the following expression

$$f_r = \frac{0.7}{N} \quad \text{mrad/kNm} \qquad \text{N} < 12 \tag{8.3}$$

In the formula, f_r is expressed as reciprocal to N, the number of studs included. However, when it is applied for specimens I-UD and I-US, it is found that the values of f_r given by equation 8.3 are about ten times less than those found in the isolated U-frame tests. The reason for this is that it does not include any other parameters, which actually affect flexibility of the connection.

Effective flexibility of a shear connection means the flexibility before failures of the connection , which might be either by interior cracks in the concrete or excessive

deformation of the top flange; so that to model its flexibility behaviour, neither cracks of concrete nor excessive deformation of the top flange should be included. The local deformation of the connection should be proportional to the modulus of the concrete, and dimensions of the studs as well as of the top flange are also relevant.

A semi-empirical analogy for the connection is illustrated in Fig.8.8. The transverse moment M_t is transmitted to the slab via studs above the vertical stiffener. Before shear failures in the slab, the studs are embedded in the concrete. Assume that a typical strain in a cone of concrete, embedding the studs is given by

$$\epsilon_c \propto \frac{T}{h_d^2 E_c} \tag{8.4}$$

As $M_t \propto \mathrm{T}\, b_f$, $\theta_r \propto T/b_f h_d E_c$, and $f_r = \theta_r / M_t$ therefore the flexibility of U-frame connections could be expressed in the form

$$f_r \propto \frac{1}{b_f b_f h_d E_c N} \tag{8.5}$$

b_f is more relevant here than a_{st}, because the studs are fully embedded in the concrete before the concrete fails in connections. Besides, when a_{st} is zero (studs in one row), the transverse bending moment, M_t is still proportional to the width of the top flange.

Compared with double sided stiffened U-frames, a parameter of b_s is introduced to include single sided stiffened U-frame connections. By using the test results, the semi-empirical formula is written as

$$f_r = \frac{300}{b_f b_s h_d E_c N} \tag{8.6}$$

where

- b_f is the breadth of the steel top flange.
- h_d is the overall height of the studs.
- b_s is the breadth of the web stiffener.
- E_c is Young's modulus for the concrete (short-term).

- N is the number of the effective studs at the locations of the stiffeners.

The notations for the relevant parameters are shown in Fig.8.8.

To determine N, the number of effective studs in the connection, a simple rule is proposed for this type of the connection. It is suggested that N be taken as the number of the studs over a length 2 l_n above the stiffeners, where

$$l_n = 28 b_f (\frac{t_f}{b_f})^{1.4} \tag{8.7}$$

- t_f is the thickness of the steel top flange.

The empirical formula (equation 8.7)is based on the two sources of the relevant discrete U-frame tests. Effectiveness of the stud connectors in resisting the transverse bending moment will depend on the transverse distance of the studs(proportional to the width of the flange) and the torsional flexibility of the top flange (t_f/b_f). For the connections referred to [71], eq.8.7 gives l_n = 250 mm, and the value used in the tests is 250 mm. For the connections of specimen U5, eq.8.7 gives l_n = 75 mm, which is a mean value for both single and double sided stiffened U-frames (100 mm for double sided stiffener and 50 mm for single sided stiffener).

Comparisons of the predictions by equation 8.6 with test results are given in Fig.8.9. The predictions by equation 8.6 are more flexible, which are on the safe side in evaluation of lateral buckling resistances.

Table 8.1 gives the dimensions and values for the corresponding specimens used in the assessment of equation 8.6. f_r^* in Table 8.1 refers to test measurements. The Young's modulus of the concrete is taken as 32 kN/mm^2 for simplicity (C30 concrete).

Flexibility of discrete U-frames

An inverted composite U-frame is illustrated in Fig.8.10. The flexibility of a discrete U-frame is defined in BS5400:Part 3 (clause.9.6.5)[2], as the lateral deflection δ (Fig.8.10) due to equal and opposite unit forces at the level of the centroid of the bottom flanges. It is attributed from the deformations of three parts: the stiffened web, the slab and the connection between the steel flange and the concrete slab, or given by

$$\delta = \delta_1 + \delta_2 + \delta_3 \tag{8.8}$$

$$\delta = \frac{d_1^3}{3EI_1} + \frac{uBd_2^2}{EI_2} + f_r d_3^2 \tag{8.9}$$

In the first term of the equation, I_1 is the second moment of area of the effective section of the vertical member about its axis of bending. A width of web plate of up to 16 times the web thickness is suggested to be included on each side of the centreline of its connection in the Bridge Code [2].

In the second term of this equation, u is either 0.50 or 0.33 depending on whether the U-frame is single supported or continuous. For a single span U-frame (single bay), u is taken as 0.5, and for a continuous U-frame (or multi-bay) u is 0.33. Specimen U5 is a single bay(single supported), so that u is taken as 0.5 in the subsequent work. I_2 is the second moment of area of the cross member of U-frame about an axis perpendicular to the plane of U-frame. For a concrete deck, the gross area of concrete within the effective width should be considered. The Bridge Code [2] recommends an effective width of B/8 or $L_u/2$, whichever is less.

The third term δ_3 depends on flexibility of the connection f_r. However, the values of f_r given in Bridge Code only correspond to steel U-frame configurations, and are irrelevant for composite U-frame connections, in which the shear mechanical connectors play an important role of composite actions. For composite U-frame connections, f_r based on equation 8.6 is relevant to the present research and also used in the subsequent work.

The flexibility of a discrete composite U-frame can be determined according to equation 8.9. For specimen U5, there are two values of the flexibility due to the different types of the stiffeners and stud arrangements in the connections. The predicted values of δ and the measured values of δ^* from the relevant tests on specimens I-UD and I-US are all given in Table 8.2.

In Table 8.2, δ is the calculated value for equation 8.9, with the flexibility predicted by equation 8.6, and δ^* is the value based on test measurements of displacements at the bottom flanges.

The flexibility of the connections is found ranging from 0.46 to 0.61 of the total flexibility for the double sided stiffened U-frame and the single sided stiffened U-frame respectively. Therefore, the flexibility of U-frame connections can be a critical term in assessment of lateral buckling resistances of composite U-frame beams.

Flexibility of a discrete U-frame can be also evaluated by its stiffness in transverse direction. Let k_θ be transverse stiffness of a discrete U-frame per unit length, θ be the hypothetical transverse rotation of the bottom flange relative to its original position (Fig.8.10) expressed by

$$\theta = \frac{\Delta}{d_2} \tag{8.10}$$

and M_θ be the concentrated transverse moment on U-frame caused by lateral U-frame force, or by

$$M_\theta = F_u d_2 \tag{8.11}$$

then the transverse stiffness k_θ per unit length is defined by

$$k_\theta = \frac{M_\theta}{L_u \theta} \tag{8.12}$$

where L_u is spacing of U-frames.

Δ is a product of δ and F_u, and k_θ is therefore expressed as three terms, k_1, k_2 and k_3 corresponding to δ_1, δ_2 and δ_3 by

$$\begin{aligned} \frac{1}{k_\theta} &= \frac{\delta_1 + \delta_2 + \delta_3}{d_2^2} L_u \\ &= \frac{L_u}{k_1} + \frac{L_u}{k_2} + \frac{L_u}{k_3} \end{aligned} \tag{8.13}$$

so that

$$k_1 = \frac{d_2^2}{L_u \delta_1} \tag{8.14}$$

$$k_2 = \frac{d_2^2}{L_u \delta_2} \tag{8.15}$$

$$k_3 = \frac{d_2^2}{L_u \delta_3} \tag{8.16}$$

Similar to δ_1, δ_2 and δ_3, k_1, k_2 and k_3 are attributed to the stiffened web, the slab and the connection of discrete U-frames.

8.3.3 Strength of a discrete U-frame

Failure patterns in the U-frame connections

U-frame strength is governed by stability of the stiffeners and the strength of the connection. The comprehensive studies of the stability of stiffeners have led to conclusions given in the Bridge Code [2]. The strength of a U-frame connection is relevant to its flexibility. A connection may fail either in shear failure of the slab or in yield of the top flange caused by the U-frame force.

Before shear failure in the slab, the studs are fully embedded in the concrete, however, whenever interior cracks form in the slab, there may be a strain redistribution in the studs above the stiffeners. This phenomenon was observed in the test.

The strains in the studs are plotted against the U-frame force F_u in Fig.8.7. It is found that the connection with single sided stiffeners failed at a U-frame force of about 7.5 kN, at which a great increase in strain was observed in the studs, resulting from the strain redistribution, when interior cracks were formed in the connection. No evidence of strain redistribution could be traced in Fig.8.6 for the connection with double sided stiffeners, because the shear failure had already occurred in the previous global U-frame tests.

On the other hand, evidence of connection failure is present in the moment rotation curves for the connections, shown in Fig.8.5. Being related to its effective flexibility, the connection with a double sided stiffener (A-side) began to fail at F_u about 8 kN, which is close to the value when a strain redistribution was observed in the connection with single sided stiffeners. The strength of the connection with single sided stiffeners was however, governed by excessive nonlinear deformation in the steel top flange, not by shear failure in the slab. It is well illustrated in Fig.8.5, when the moment rotation curves become obviously non-linear, at a force of about

2.5 to 3 kN, which is much lower than the value when the strain redistribution in the studs occurred. This excessive nonlinear rotation is characteristic of another type of connection failure, basically governed by the excessive deformation in the steel top flange. This was also observed in the tests on the isolated U-frame specimens (I-U specimen), at the intersection of the slab and the top flange, especially for the single sided stiffened I-U. It is believed that this deformation is due to the yield in the local region of the top flange above the stiffener. Fig.8.11 illustrates the deformation shape of the top flange in the test. The maximum gap between the top flange and the slab is 2.3 mm, and even after removal of the U-frame force, the residual gap is about 1 mm.

Strains in studs and U-frame force

Before shear failure of the connection, the studs are fully embedded in slab, and the U-frame force is transmitted via the studs to the slab. An estimate of the bending moment, based on the product of the strain difference and the distance between the inner and external studs is used.

For the side with double sided stiffener, the concrete near the shear connection had cracks already formed in the previous global test. Because the cracks could not come back to the original positions, residual strains were induced in the studs. Fig.8.6 shows the residual strains in the shank of the studs when F_u is zero, and this is also the state when the global tests stopped. Therefore, these residual strains are attributed from two parts; the inelastic yield of the studs, and the mismatch of the concrete due to the interior cracks in the connection. The difference of these residual strains in each pair of studs is equivalent to an interior transverse bending moment acting on the U-frame connection. This residual transverse bending has contribution to the transverse bending caused by the U-frame force.

On the other hand, the permanent remaining buckling shape also contributes to the residual strains in the studs. The residual tension strain of the studs on the single stiffened side is caused by this permanent remaining shape, as shown in the out of plane web deformation in Fig.6.24.

To calculated M_{st}, the bending moment through the studs prior to the shear failure of the connection, the following formula is used

$$M_{st} = \Sigma \Delta \epsilon_i A_{st} a_{st} E \tag{8.17}$$

where

- $\Sigma \Delta \epsilon_i$ is the summation of the strain differences at the location above a stiffener.
- A_{st} is area of the cross section of a stud ($\pi d_{st}^2/4$,).
- a_{st} is the distance between the two rows of studs.
- E is the modulus of steel ($E = 205000$ N/mm^2).

From Fig.8.7., when F_u, the applied force is 6 kN, the bending moment using the product of strain difference and distance between the two studs is 2.5 kNm, which corresponds to a value of 4.87 kN (about 80% F_u). Assume that the transverse bending moment resisted by the studs is about 80% of the total bending moment induced by the applied U-frame force. Then the lateral U-frame force is

$$F_u = \frac{M_{st}}{0.8\ h_s} \tag{8.18}$$

where

- h_s is the distance between the interface of the slab and the steel top flange and the centroid of the bottom flange.

Though it is based on the isolated U-frame with single sided stiffeners, it is assumed that this also applies to the double sided stiffened U-frames in the global tests.

Shear strength of discrete U-frame connections

The strength of a U-frame connection would be governed by either shear failure of the slab or yield of the top flange caused by the U-frame force. No model so far has been found, for the strength dominated by the interaction between the slab, the studs and the top flange, because many parameters are involved. However, the investigation to the problem can be commenced by dealing with the two separate problems; the strength of the slab and the strength of the steel top flange.

The strength of the slab was studied by Johnson and Molenstra [71] and they found that the shear failure of a U-frame connection can be predicted by their proposed design formula. However, the strength of the top flange was excluded, because no evidence was ever observed in their tests.

Fig.8.12 shows the truss model used by Johnson and Molenstra [71] in predictions of the shear failure of the slab. In the truss analogy, the internal forces are represented approximately by a truss of tension members (full lines in Fig.8.12) and compression members (dashed lines). The weak links are the diagonal tension along UQ and the tension along UV below the heads of the studs at point U. The transverse bending strength M_{pr1} is relevant to the shear strength of the slab V_{cr} , the spacing of parallel beams B and the equivalent width a_c. The formula is given as the following

$$M_{pr1} = \frac{V_{cr} a_c}{1 - a_c/B} \tag{8.19}$$

The notations and relevant parameters are given in Fig.8.11. The prediction of the shear strength of the slab for specimens I-UD and I-US by this equation is 3.68 kNm, for M_{pr1}, corresponding to a U-frame force of 7.2 kN. In the prediction, B was taken as 1.5 m, the distance between the centers of the two steel webs. The value agrees well with the test values of 7.5 kN for the connection with single sided stiffeners in specimen I-US (when strain redistribution occurred) and 8 kN for the connection with doubled sided stiffeners.

Upper-bound plastic limit theorem

Difference in failure patterns is found between specimens I-UD and I-US. For the double sided stiffened specimen (I-UD), shear failure was found in the slab, and for the single sided stiffened specimen (I-US), the connection fails owing to the excessive deformation in the top flange.

For the failure governed by excessive deformation in the steel top flange, the warping normal stress will be additional to the torsional stress. The strength would be relevant to the stud arrangement above stiffeners, the torsional rigidity of flange and the dimensions of the stiffeners.

A simple rule could be used when checking the top flange by preventing yield

at the intersection of the top flange and the stiffeners. It is derived from the upper bound plastic limit theorem.

Fig.8.13 shows a U-frame connection, with the excessive deformation, θ. The mechanism used in the upper bound plastic analysis is illustrated in Fig.8.14. Elastic deformation is neglected, because it is so small as compared with the plastic yield deformation. The upward movement of the steel top flange is restrained by the slab.

In Fig.8.14, AB, BC, BD′ are the the plastic hinge lines, and the relevant unit moments along the hinges are m_1, m_2 and m_3, are determined by plastic theory. When the simple rigid plastic theory is applied, unit moments are given by

$$m_1 = m_2 = m_3 = \frac{t_f^2 f_y}{4} \tag{8.20}$$

where t_f and f_y are the thickness and yield strength of the top flange. The geometric relationships and plastic rotations along hinges AB, BD and BC (α_1, α_2 and α_3) are written as the follows

$$\theta = \frac{e}{B_f} \tag{8.21}$$

$$\alpha_1 = \alpha_3 = \frac{e}{D'O} = \frac{2e}{0.5b_f cos\Phi} = \frac{2B_f}{0.5b_f}\frac{\theta}{cos\Phi} \tag{8.22}$$

$$\alpha_2 = \frac{2e}{DC} = \frac{4B_f}{0.5b_f}\theta tan\Phi \tag{8.23}$$

Corresponding to a rotation increment $d\theta$ the work done by the moment M_f is by

$$dW_f = M_f d\theta \tag{8.24}$$

The work done by the unit moment along the hinges

$$dW_{AB} = dW_{BC} = m_1 AB\alpha_1 = \frac{1}{4}t_f^2 f_y \frac{d\theta}{sin\Phi cos\Phi} B_f \tag{8.25}$$

$$dW_{BD'} = \frac{1}{2}t_f^2 f_y tan\Phi B_f \tag{8.26}$$

Then the energy equation of the system is by

$$dW_f = dW_{AB} + dW_{BC} + dW_{BD'} \tag{8.27}$$

By simplification, it leads to

$$M_f = \frac{B_f}{2}(\frac{2}{sin2\Phi} + tan\Phi)t_f^2 f_y \tag{8.28}$$

The angle Φ is calculated by minimizing M_f or letting $\frac{\partial M_f}{\partial \Phi} = 0$, which leads to

$$\Phi_m = arcsin\frac{1}{\sqrt{3}} = 35.28^o \tag{8.29}$$

Substitute Φ_m into the equation 8.28, then the moment M_f is obtained as

$$M_f = 1.414 B_f t_f^2 f_y \tag{8.30}$$

Equation 8.30 gives a upper bound value of M_f when the top flange fails. The application of the expression is based on the following discussions.

- The mechanism described by Φ_m is obstained based on the minimum total energy of the system. When there are studs within the region of ABC, the energy absorbed by the studs to be considered. Before the yield of the studs, a possible mechanism is bounded by the hinge lines not beyond the studs, as shown in Fig.8.15. When the studs yield, the work absorbed by the studs is included.

- For connections with a single sided stiffener, B_s is the width of the stiffener, because M_f is concentrated in the side of the top flange with the stiffener, which is much stiffer than the other side. For connections with double sided stiffeners, taking B_f as $b_f/2$, a half of the total width of the stiffeners is conservative, because, the side where the top flange moves upward is restrained by the slab. The possible mechanism would be similar to that given in Fig.8.14.

- For connections with a single sided stiffener, the mechanism given in Fig.8.14. prescribes a worse situation. When the stiffer side of the top flange (with stiffener) moves upward (other than shown in Fig.8.11), because of the restraint

of the slab, the deformation on this side is very small, and the other side being less heavily loaded, does not form a mechanism.

- When the mechanism forms, the stress σ in the top flange is transmitted to the mechanism via the unit moments along the plastic hinges, but has been neglected in the energy calculation.

Table 8.3 gives a comparison of M_f with the predicted M_{pr1}, the moment when shear failure occurs in the slab, based on the work by Johnson and Molenstra [71]. As discussed in the previous section, when Φ is smaller than Φ_m, the studs are all beyond the region, where the mechanism has minimum energy potential, and Φ_m is used in calculation of M_f. When Φ is greater than Φ_m, before the yield of the studs, the possible mechanism forms with Φ, as shown in Fig.8.15.

In Table 8.3, specimen BM2 to BM7 are from Johnson and Molenstra's tests. B_f is taken 2/3 of the width of the top flange (distance from the edge of the flange to the positions of the studs, which are on the other side of the web). Specimen IU1 is the isolated U-frame (U5) with double sided stiffeners and IU2 is the U-frame with single sided stiffeners. For IU1, there is a pair of studs right above the stiffener, and the mechanism forms only when the stud in tension, yields, so that the M_f has to include the contribution from the stud, which is a product of yield force($A_s f_{ys}$, where A_s and f_{ys} are area of cross section and yield strength for the stud) and B_f.

The predicted values of M_f are consistent with the test results. For specimen IU1 and all specimens from [71], M_f is more than twice of M_{pr1}, so that the U-frame connections are governed by the shear failure in the slabs, and no evidence of the top flange yield has ever been found for these specimems. For specimen IU2, M_f is about half value of M_{pr1}, and the failure pattern of the connection is found in the excessive deformation in the steel top flange (shown in Fig.8.11).

Obviously, the actual strength of the connection is smaller than M_f, because M_f is based on an upper-bound plastic approximation. Being converted to U-frame force F_u, specimen IU2 fails at a predicted value about 3.8 kN (F_u). Test result shown in Fig.8.5, is about 3 kN, when obvious nonlinear deformation is found in the rotation curves, which is about 80% of the value from the upper-bound plastic approximation.

In design procedures, the strength of a U-frame connection can be checked ac-

cording to its shear strength of the slab (Johnson Molenstra's formula [71]) and its strength of the top flange (equation 8.30).

In chosing the layout of stud and stiffener arrangement, S_l/S_t and B_f are relevant.

8.4 Evaluation of U-frame action in tests on specimen U5

8.4.1 Test evaluations

Further tests on the isolated U-frame specimens showed that before shear failure of connections, the transverse bending via the studs (expressed as the strain differences between the inside and outside studs above the stiffeners) is about 80% of the total transverse bending caused by lateral U-frame force.

The lateral U-frame force is calculated from the measured strains in the studs at the locations above the stiffeners, in accordance with equations 8.17 and 8.18. The measured strains in the studs recorded in the global U-frame tests are given in Tables 6.7 and 6.8. The positions of the studs are above the stiffeners as shown in Fig.5.16. Stage 20 is when the specimen U5 was supported at the central section with the jacks free of forces at the four corners. The lateral buckling initiated at the bottom flange of beam U5B, at about stage 26. The maximum moments were reached at stage 34, and interior cracks occurred at about stage 36 in the slab above the double sided stiffener.

In the tests on specimen U5, the U-frame force increased when lateral buckling initiated and developed fast thereafter. From Fig.6.29, a jump in the rotation of the U-frame connection is observed at stage 36, which was after the maximum moments reached in the global test, revealing a shear failure in the slab above the double sided stiffener closest to the central support for U5B. According to equation 8.18, the converted U-frame force is about 13.34 kN. This value is higher than the transverse shear strength of the connection found in the isolated U-frame tests, about 7.5 kN for single sided stiffened U-frame connection, when strain redistribution occurred as shown in Fig.8.7; and 8 kN for double sided stiffened connection, at which the

effective flexibility of the connection was defined as shown in Fig.8.5. The reason for this is that in the U-frame, force would be shared by adjacent concrete and steel locations of the stiffeners, and account should be taken of the continuity of slab and top flange.

Table 8.4 gives calculated values of F_u based on the measurement of strain in the studs. At the maximum loading stage (stage 34), the bottom flange is fully yielded close to the support. The ratios of the U-frame force to the compression force in the bottom flange are 2.6% in the double sided stiffened U-frame and 1.1% in the single sided stiffened U-frame.

8.4.2 Design assessment of the U-frame force

In the design methods of BS5400:Part 3, the U-frame force is assessed based on a laterally restrained Euler strut with initial bow. According to clause 9.12.2.2 of BS5400:Part 3 , F_u is given by

$$F_u = \frac{l_e}{667\delta}\frac{\sigma_{fc}}{\sigma_{cr}-\sigma_{fc}} \tag{8.31}$$

$$\leq \frac{\sigma_{fc}}{\sigma_{cr}-\sigma_{fc}}\frac{EI_c}{16.7L_u^2}$$

where σ_{fc},σ_{cr} are compressive stress and elastical critical stress of the flange, l_e and δ are effective length and U-frame flexibility, and L_u is spacing of U-frames, respectively, as defined in BS5400:Part 3.

However, for continuous composite plate girders, with intermediate vertical stiffeners acting as inverted U-frames, the assumptions made in deriving equation 8.31 are not valid and lead to an overconservative design. The factor $\sigma_{fc}/(\sigma_{cr}-\sigma_{fc})$, defined in this equation reaches its peak value at the support section but decreases very rapidly away from the support due to the high moment gradient. The value of this factor is also conservative as only distortional buckling can occur in these types of girders and the Bridge Code does not provide expressions for elastic critical distortional buckling stress.

To evaluate F_u for specimen U5 by using equation 8.31, the following assumptions

are made.

1. Elastic critical buckling stress: $\sigma_{cr} = \pi^2 E_a I_c / l_e A_{bf}$ (A_{bf} is the area of bottom flange).

2. The maximum stress: $\sigma_{fc} = f_y$ (f_y is yield stress of the flange).

3. Effective length: $l_e = 2.5(E I_c L_u \delta)^{0.25}$.

4. Initial lateral imperfection: $x_0 = l_e/667$.

Table 8.5 gives the relevant values in the calculation of F_u, in which, δ is referred to Table 8.2, and L_u is the U-frame spacing.

8.4.3 Discussion

The design assessments of the U-frame forces are by coincidence close to the values found in the tests when lateral buckling occurred, however, its validation has to be clarifed.

Firstly, it is based on an Euler strut with an initial bow, and a multiwave wrinkle buckle shape of the bottom flange is also assumed. The initial imperfection x_0 is related to the multiwave length (l_e). According to equation 8.31, F_u is proportional to x_0 ($l_e/667$), so that the smaller the imperfection, the smaller F_u.

Secondly, the elastical critical stress σ_{cr} does not take any account of web distortion and torsional rigidity of the steel beam, which leads to a conservative amplification factor $\sigma_{fc}/(\sigma_{cr} - \sigma_{fc})$.

For specimen U5 with discrete U-frame action, lateral buckling occurred in the regions close to the internal support other than in a multiwave wrinkle buckle shape. The relevant initial imperfection x_0 over that buckling regions of the specimen is about 5 mm, and it is greater than that calculated from $l_e/667$, recommended by BS5400 [2]. Therefore, if the real initial imperfection is used instead of $l_e/667$, the design values in table 8.5 will be more than double.

Thirdly, equation 8.31 reveals that the U-frame force F_u is proportional to the U-frame stiffness k (or $1/\delta$), and this agrees with test results, in that F_u on the double sided stiffener is approximately twice that on the single sided stiffener.

The second formula in equation 8.31 indicates that the maximum F_u should be limited to a value proportional to $EI_c/16.7L_u$, however, is too conservative and does not agree with the test results. According to this formula, F_u is basically relevant to U-frame spacing L_u, without taking account of its stiffness. The derivation of this form is based [72] on the assumption that

$$l_e = L_u \tag{8.32}$$

But it is wrong, because, the BEF (beam on elastic foundation theory) model assumes that U-frames are replaced by uniform restraint over their spacing L_u, and the assumption is no longer valid when $l_e \leq L_u$.

For braced I-beams, Wang and Nethercot [62] found that there is an interrelationship between the bracing forces and the loading on the beams, initial imperfection, bracing stiffness, bracing types, number of restraints and positions of the restraint. For multiple brace systems, bracing forces are not shared equally, and a value of 2% of the force in the compression flange is proposed for the bracing strength requirement at the ultimate state.

Compared with the beams with full bracing, U-frames provide rather flexible lateral restraints to the compression flanges. The U-frame forces are expected to be greater than the bracing forces when full brace is achieved.

At the ultimate state(stage 34), the U-frame forces were 2.6% and 1.1% for double and single sided stiffeners respectively.

8.5 Conclusions

The flexibility of a U-frame is governed by the U-frame connections, which could fail either in shear failure of the slab or in yield of the steel top flange. To ensure the effective flexibility of U-frames, the strength of the U-frame connections can be predicted using the shear strength of the slab in the U-frame connection (M_{pr1} in equation 8.19), besides a check of the yield of the steel top flange based on the upper bound plastic mechanism (M_f in equation 8.30).

Flexibility of a U-frame connection is a vital factor in evaluation of the U-frame stiffness. A semi-empirical formula (equation 8.6) is proposed to predict the effective

flexibility of U-frame connection.

U-frame force F_u is found proportional to the U-frame stiffness (k or $1/\delta$). At the ultimate state, the U-frame force F_u is found as 2.6% and 1.1% of compression force in the bottom flanges for double and single sided stiffeners respectively, at locations of the U-frames closest to the support section.

The design assessment of U-frame forces in the Bridge Code is not appropriate for composite U-frame beams, because, either it gives a value based on a multi-wave buckling shape, which does not cover the U-frame at the ultimate state, or it gives a limit based on a wrong assumption.

Table 8.1: f_r and relevant parameters of discrete U-frame connections

specimen	b_f mm	b_s mm	h_s mm	E_c kN/mm^2	N	f_r^* mrad/kNm	f_r mrad/kNm
BM2	330	330	125	32	4	0.134	0.172
BM3	330	330	125	32	8	0.088	0.086
BM4	330	330	125	32	8	0.086	0.086
BM5	330	330	125	32	4	0.135	0.172
BM6	330	330	125	32	12	0.063	0.057
BM7	330	330	125	32	12	0.058	0.057
U5(double)	125	116	65	32	6	1.250	1.658
U5(single)	125	58	65	32	4	4.710	4.970

Table 8.2: Flexibility of the U-frame(U5)(unit: mm/kN)

specimen	δ_1	δ_2	δ_3	δ	δ^*	$\delta_1 : \delta_2 : \delta_3$
U5(double)	0.330	0.180	0.436	0.946	0.834	0.35:0.19:0.46
U5(single)	0.660	0.180	1.308	2.148	2.106	0.31:0.08:0.61

Table 8.3: Predicted strength of U-frame connection

	S_l/S_t	Φ DEG	M_{pr1} kNm	B_f mm	t_f mm	f_y N/mm^2	M_f kNm
BM2	0.9	42^o	30.9	270	25	245	60.2
BM3	1.0	45^o	28.6	270	25	245	62.1
BM4	1.8	60.9^o	33.1	270	25	245	85.9
BM5	0.5	26.6^o	35.1	270	25	245	58.5
BM6	0.9	42^o	16.1	270	25	245	60.2
BM7	2.7	69.7^o	32.1	270	25	245	119.3
IU1			3.68	105	8	360	8.12
IU2	0.85	40.4^o	3.68	55	8	360	1.82

Table 8.4: U-frame force

stage No.	double sided stiffener F_u kN	F_u/F_c	single sided stiffener F_u kN	F_u/F_c
26	3.75		2.15	
34	11.23	2.6%	4.66	1.1%
36	13.34	3.1%	5.32	1.2%

Table 8.5: Assessment of U-frame force

item	double sided U-frame	single sided U-frame
δ	0.946 mm/kN	2.148 mm/kN
l_e	1961 mm	2024 mm
l_u	1200 mm	600 mm
σ_{cr}	684 N/mm^2	642 N/mm^2
$\sigma_{fc}/(\sigma_{cr}-\sigma_{fc})$	0.90	0.79
$\frac{\sigma_{fc}}{\sigma_{cr}-\sigma_{fc}}\frac{l_e}{667\delta}$	3.43 kN	1.79 kN
$\frac{\sigma_{fc}}{\sigma_{cr}-\sigma_{fc}}\frac{EI_c}{16.7l_u}$	15.33 kN	70.48 kN

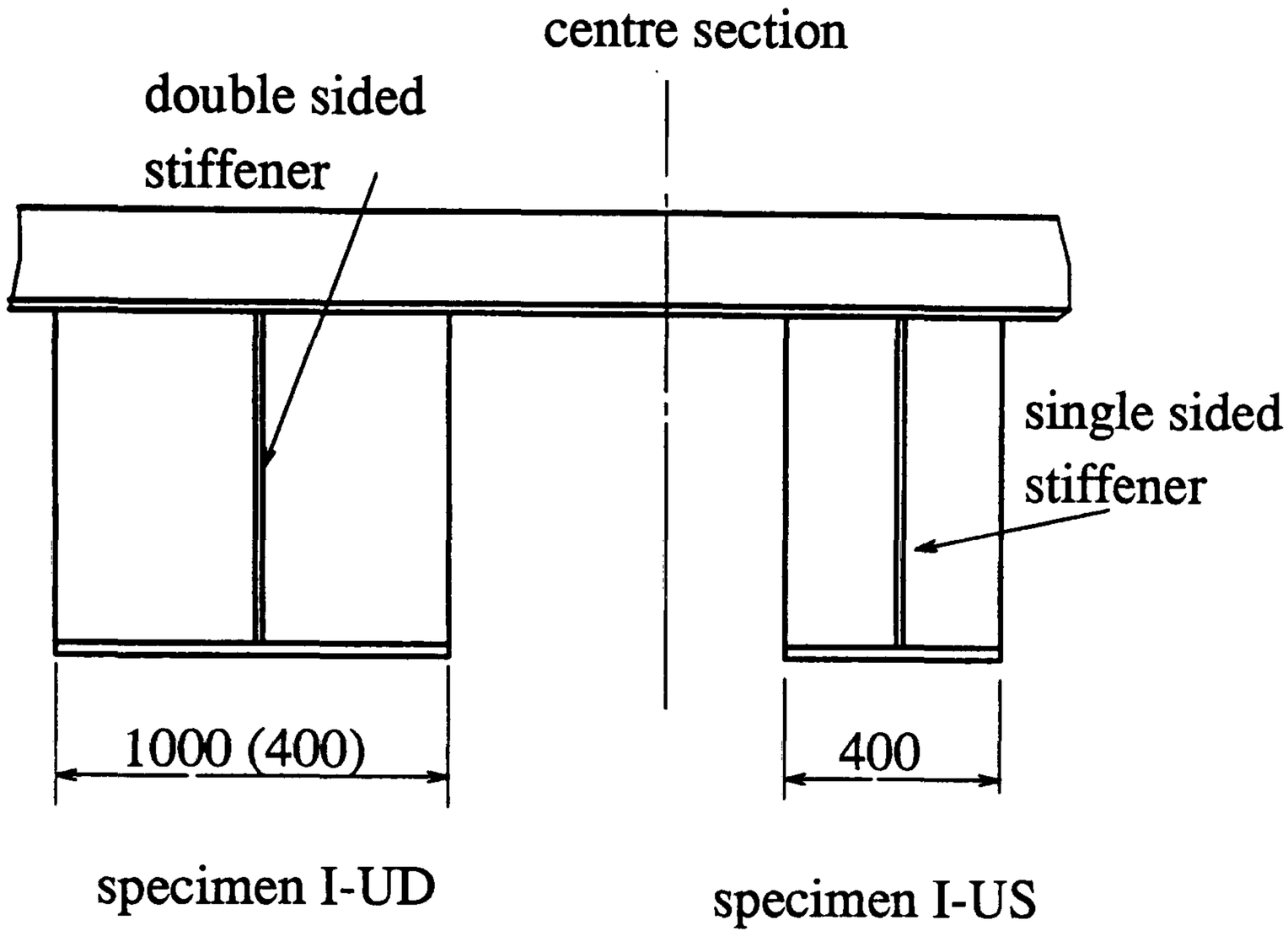

Figure 8.1: Isolated U-frame specimens

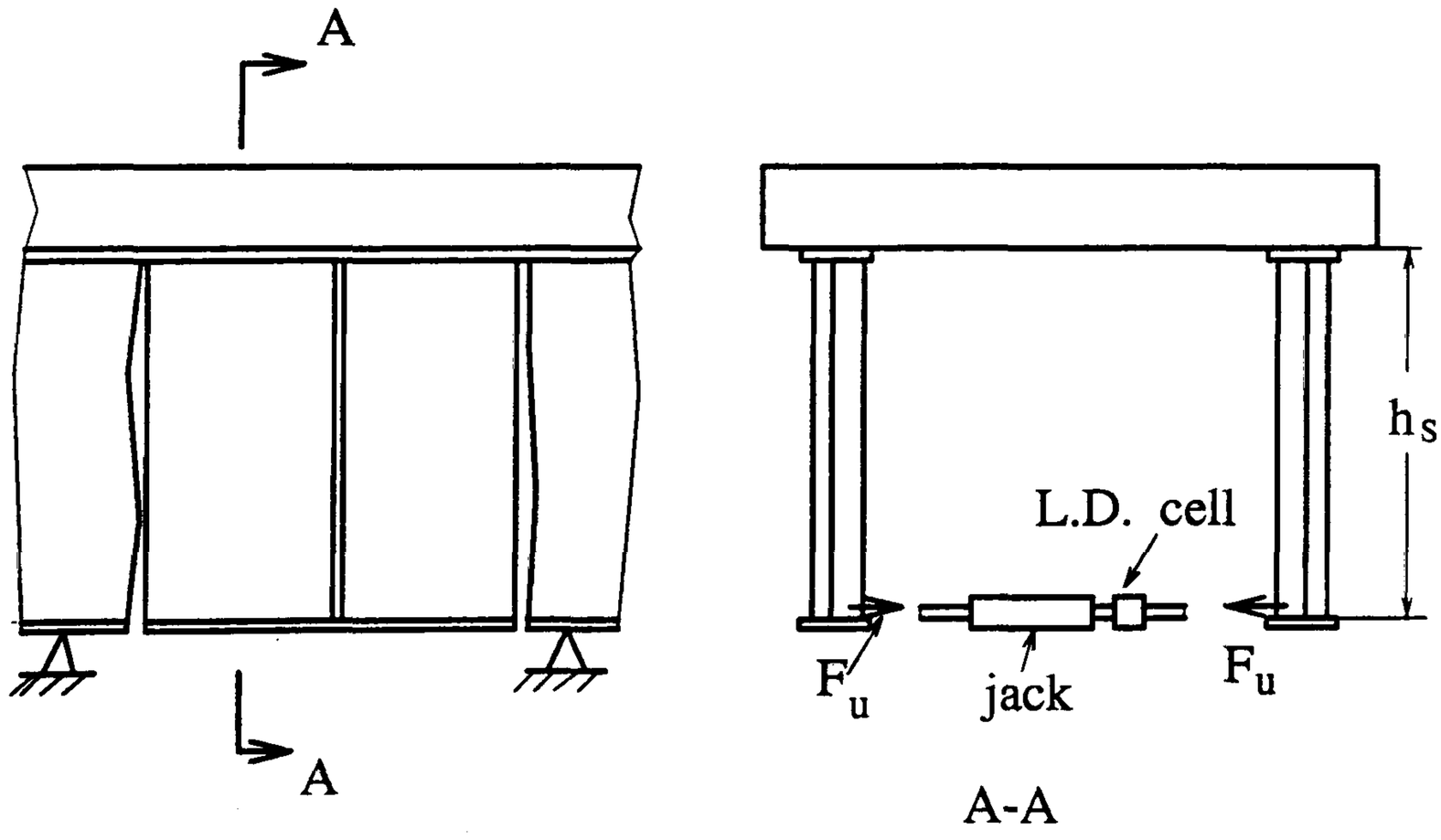

Figure 8.2: Test rig for isolated-U frames

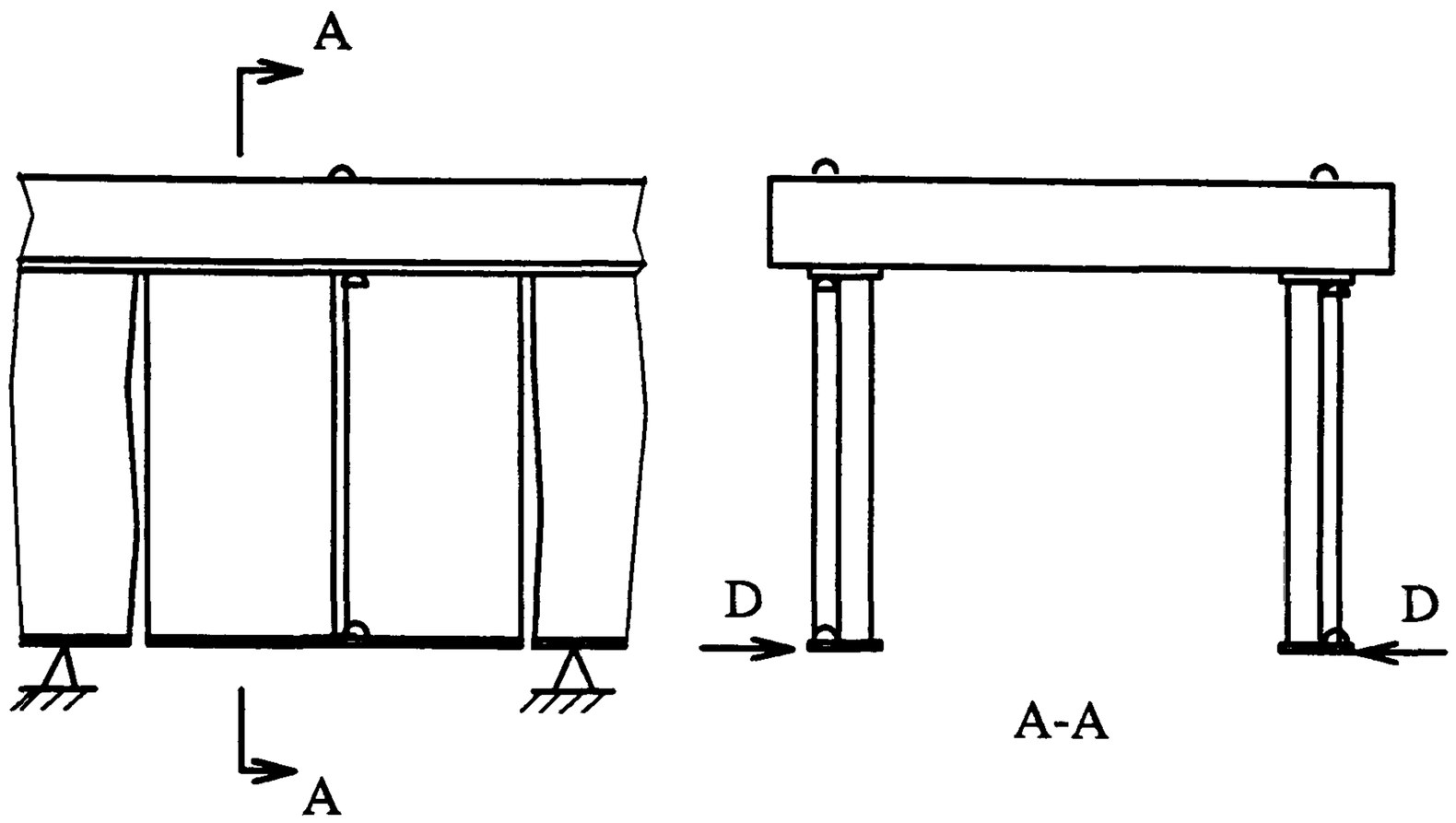

Figure 8.3: Monitor positions of instrumentation

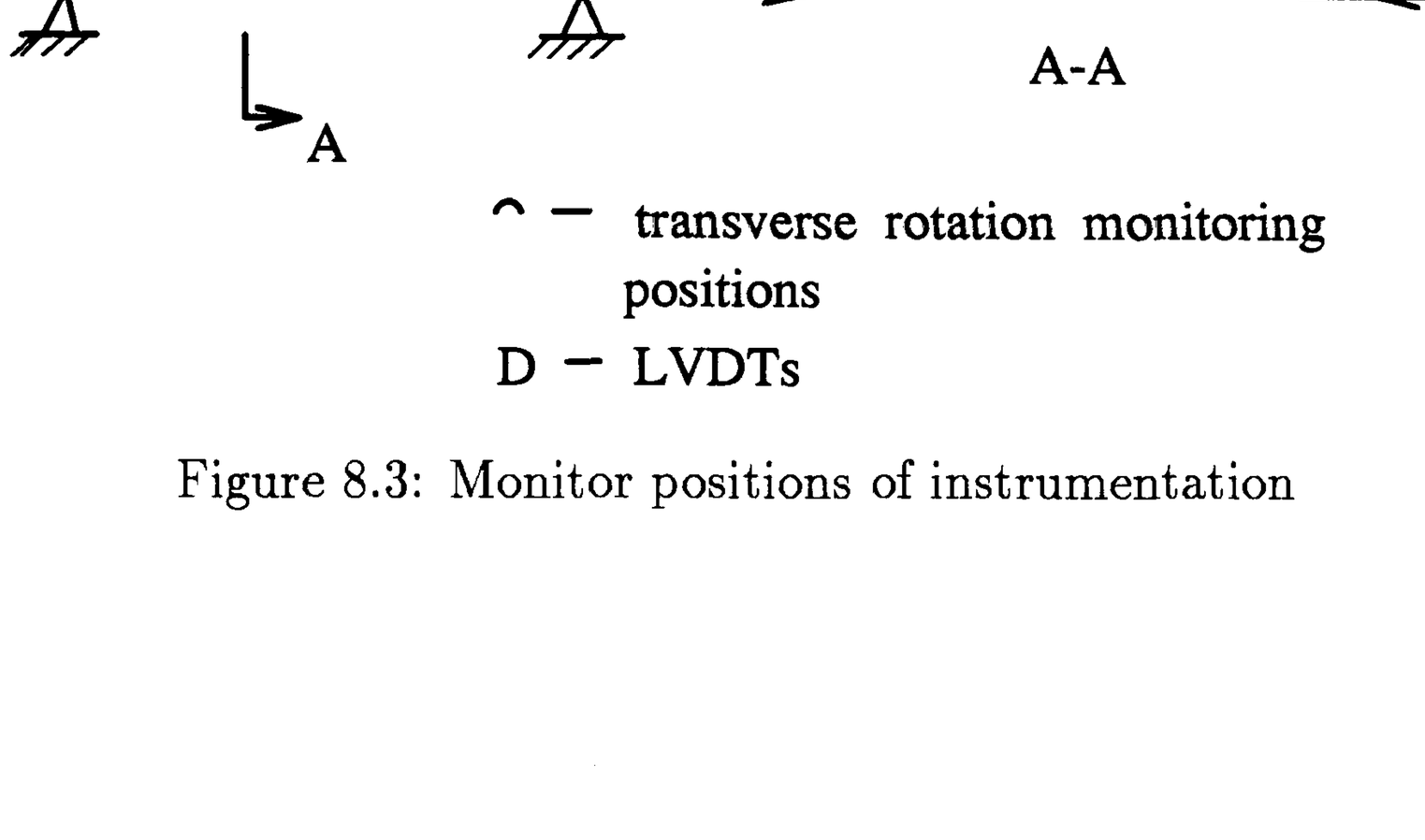

Figure 8.4: Lateral displacements at the bottom flanges

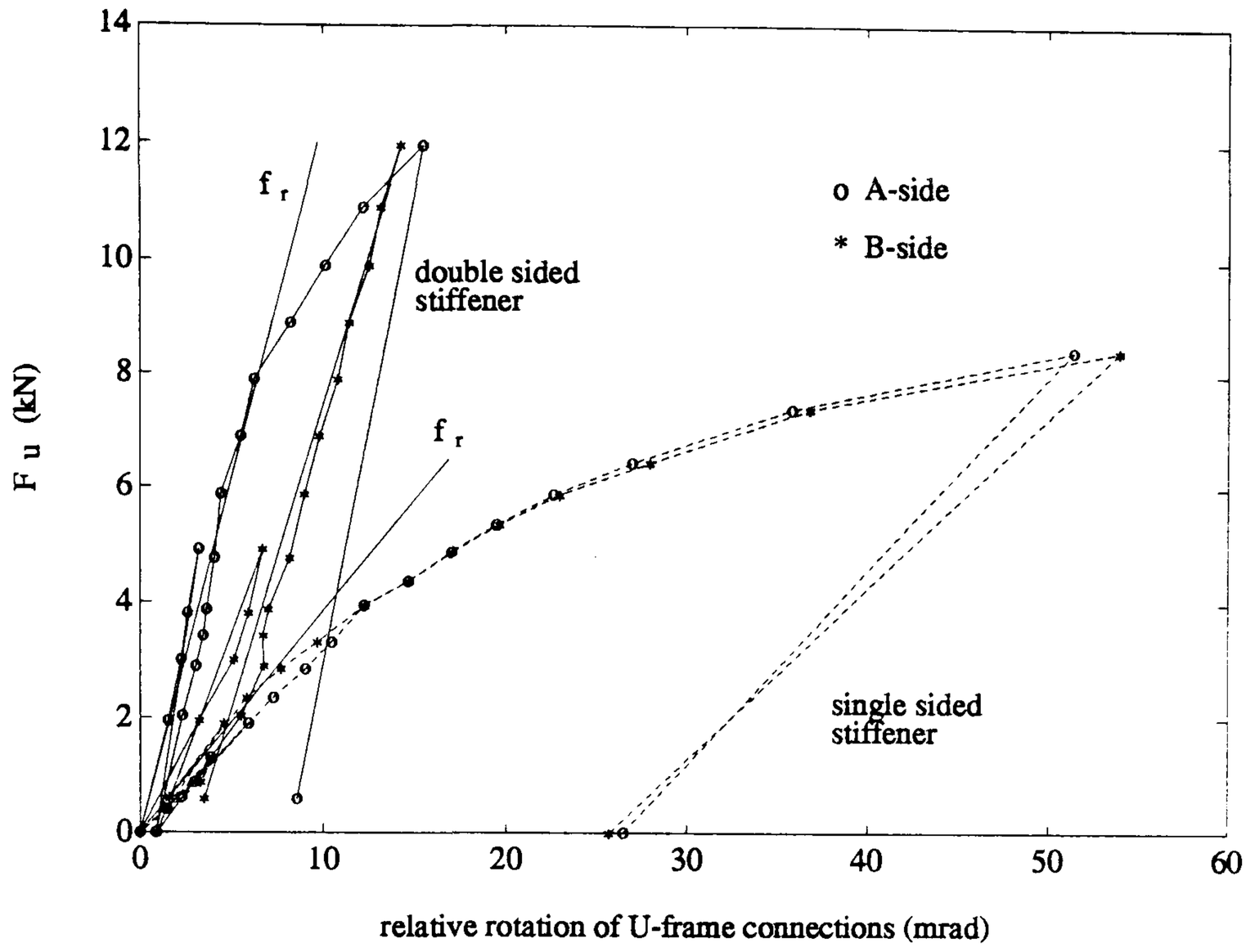

Figure 8.5: Flexibility of the U-frame connections

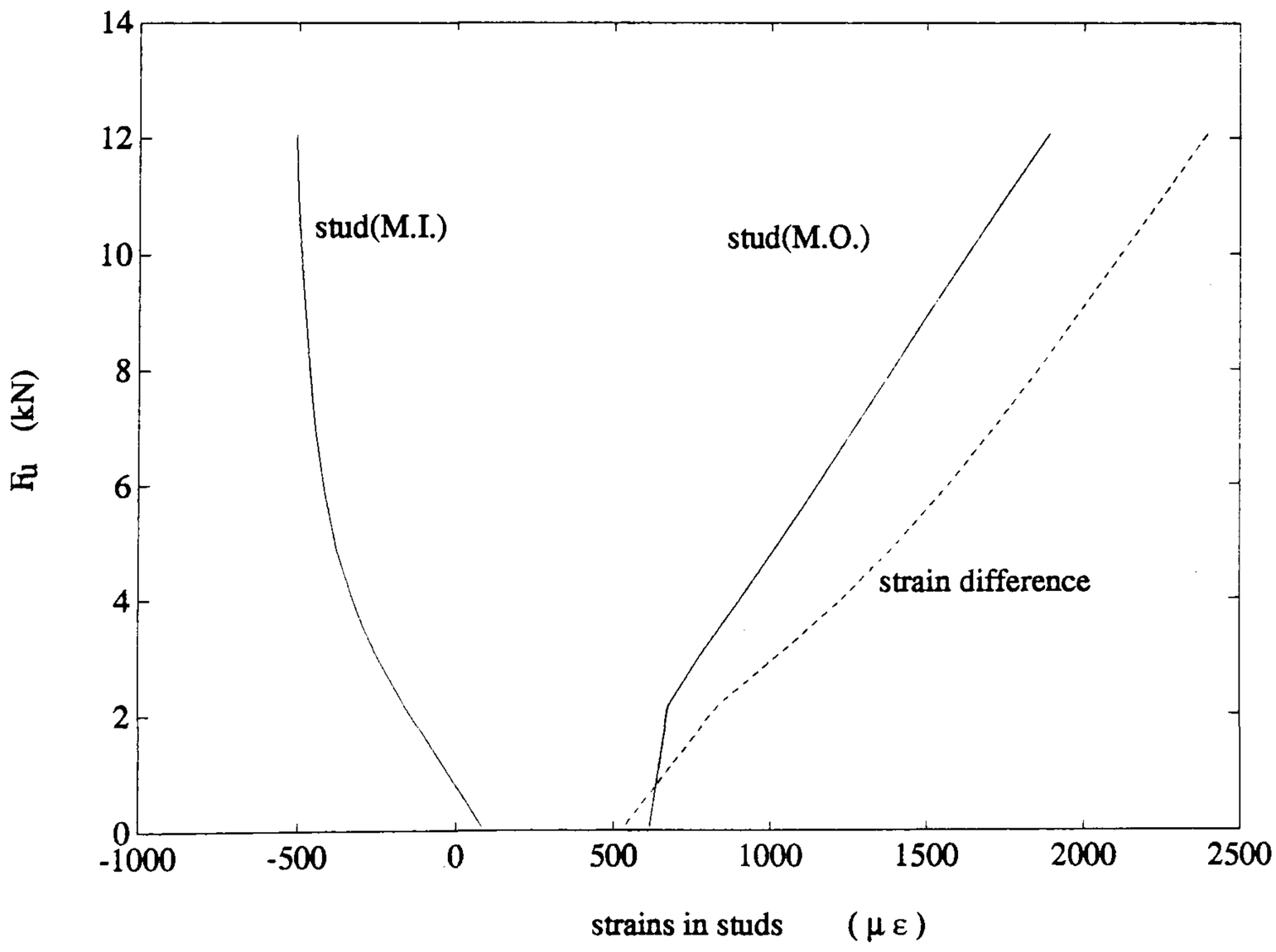

Figure 8.6: Strains in studs above the double sided stiffener(U5B)

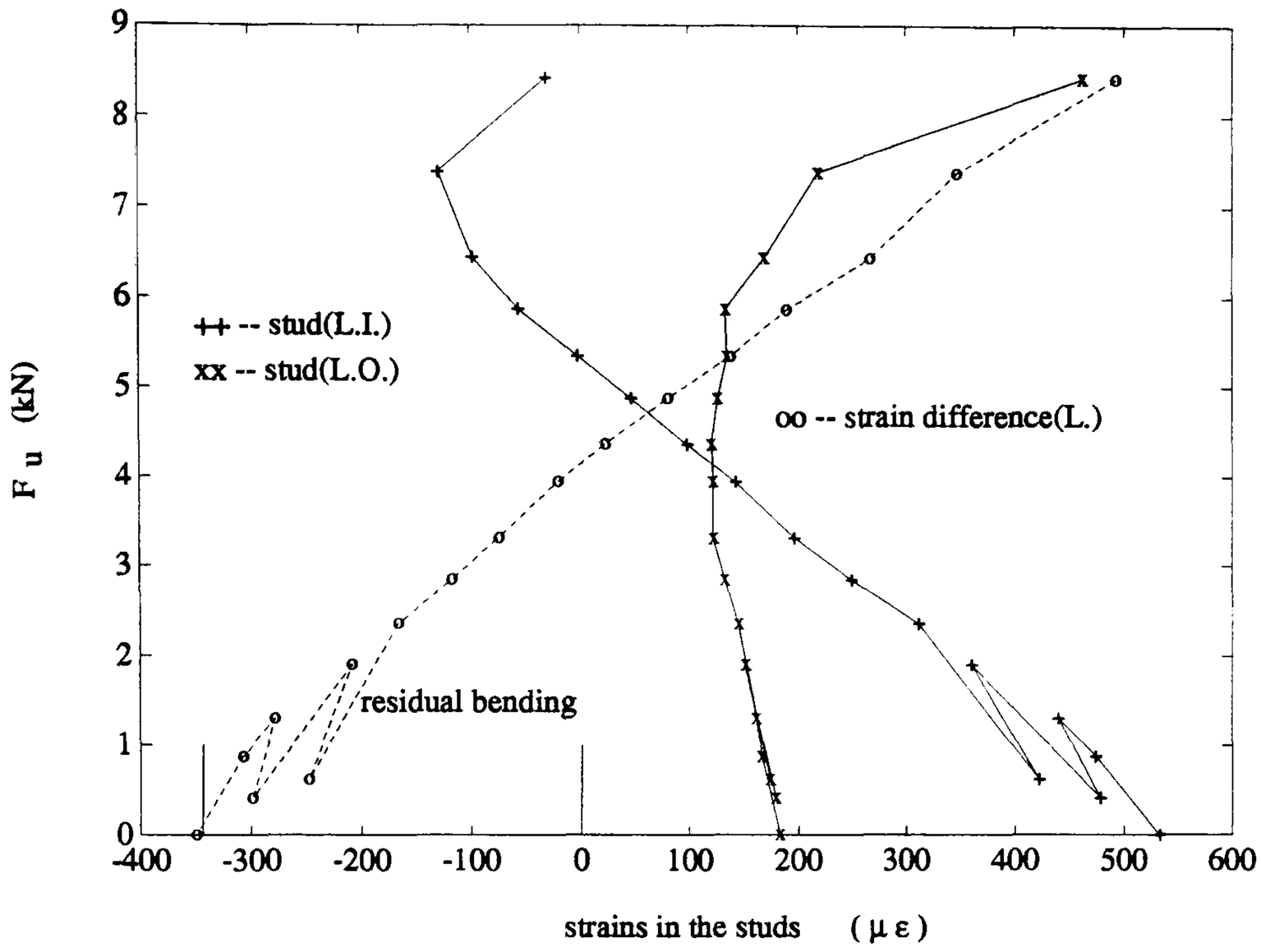

Figure 8.7: Strains in studs above the single sided stiffener(U5B)

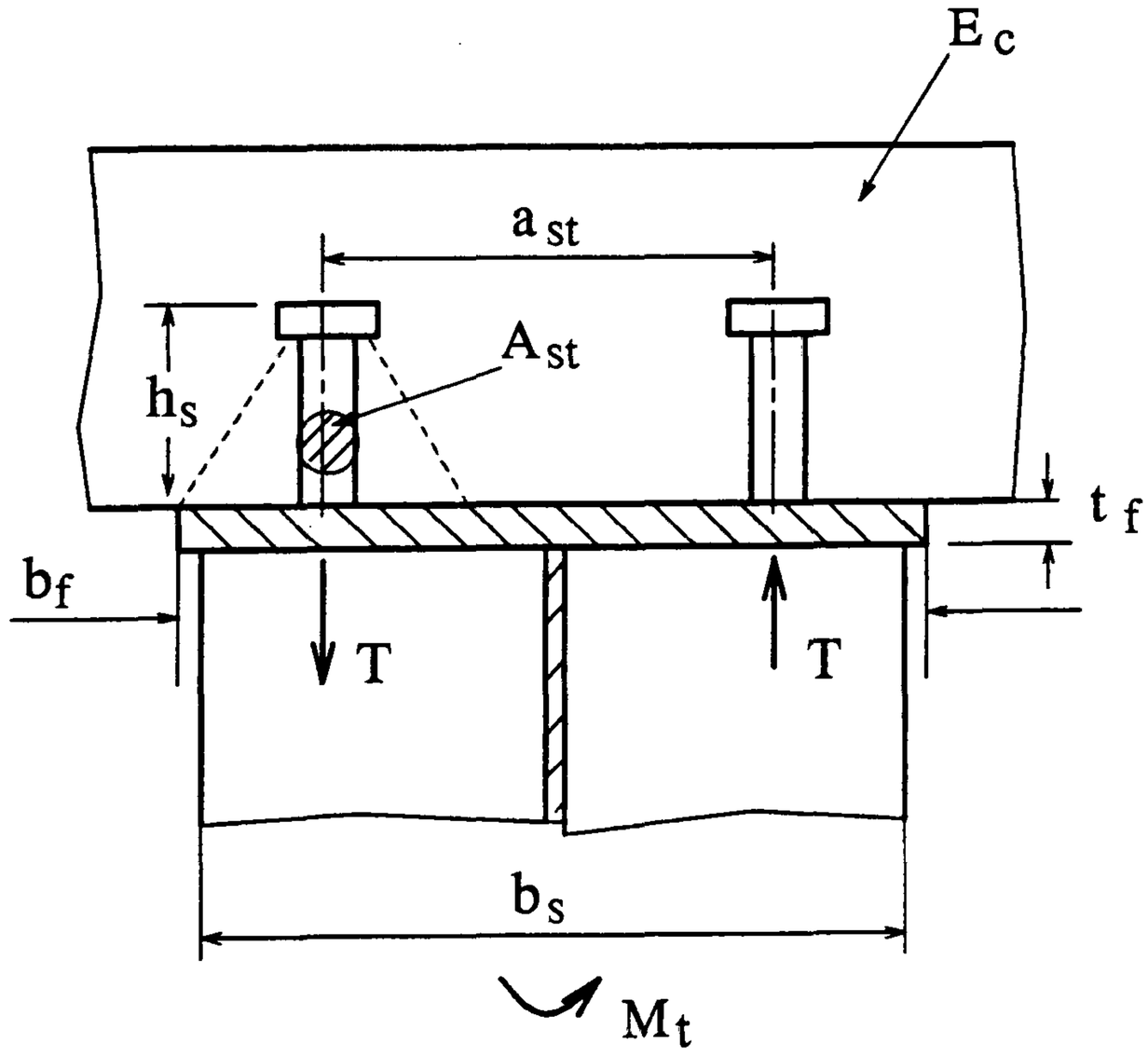

Figure 8.8: Semi-empirical flexibility analogy

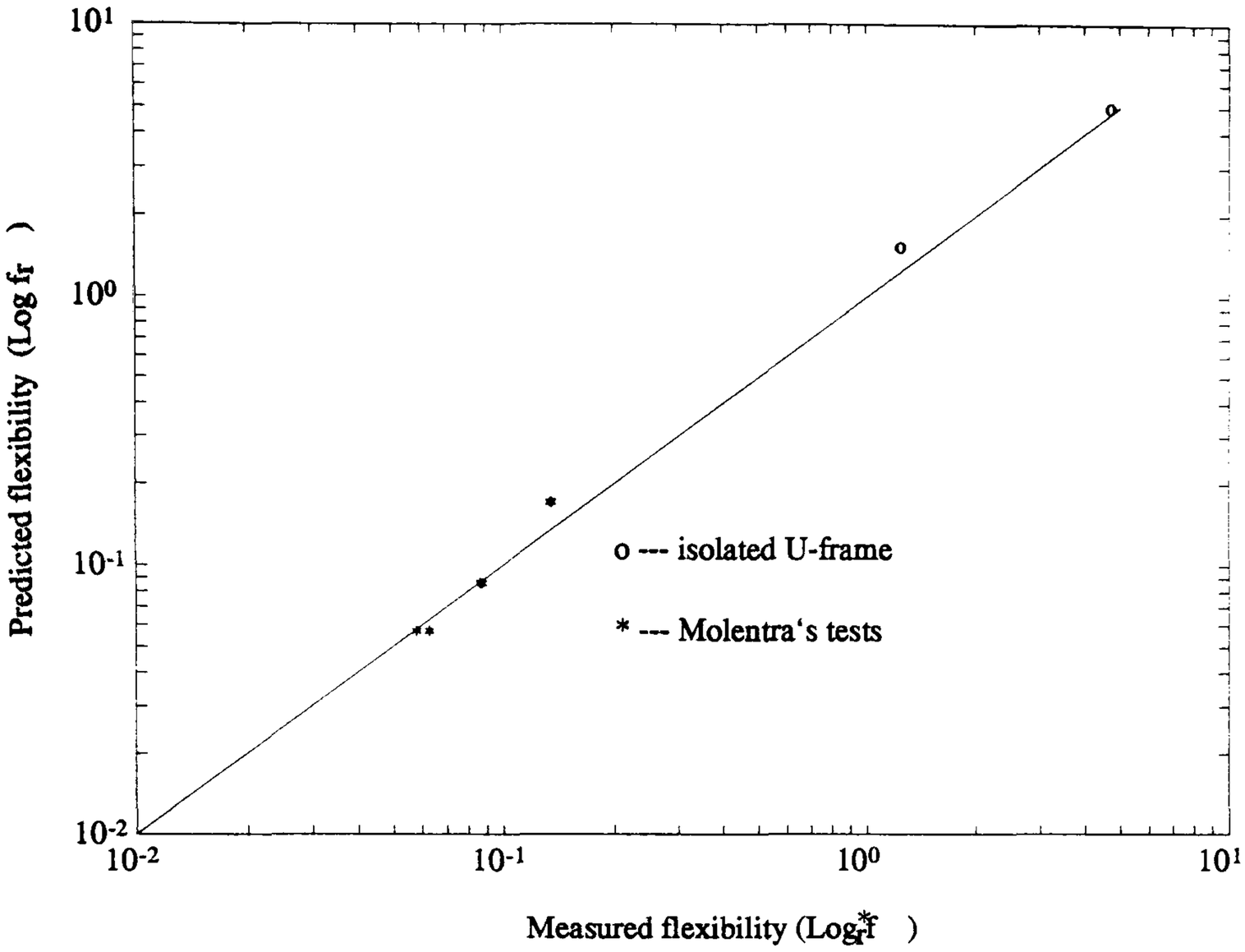

Figure 8.9: Comparison of Equation 8.4 to test results

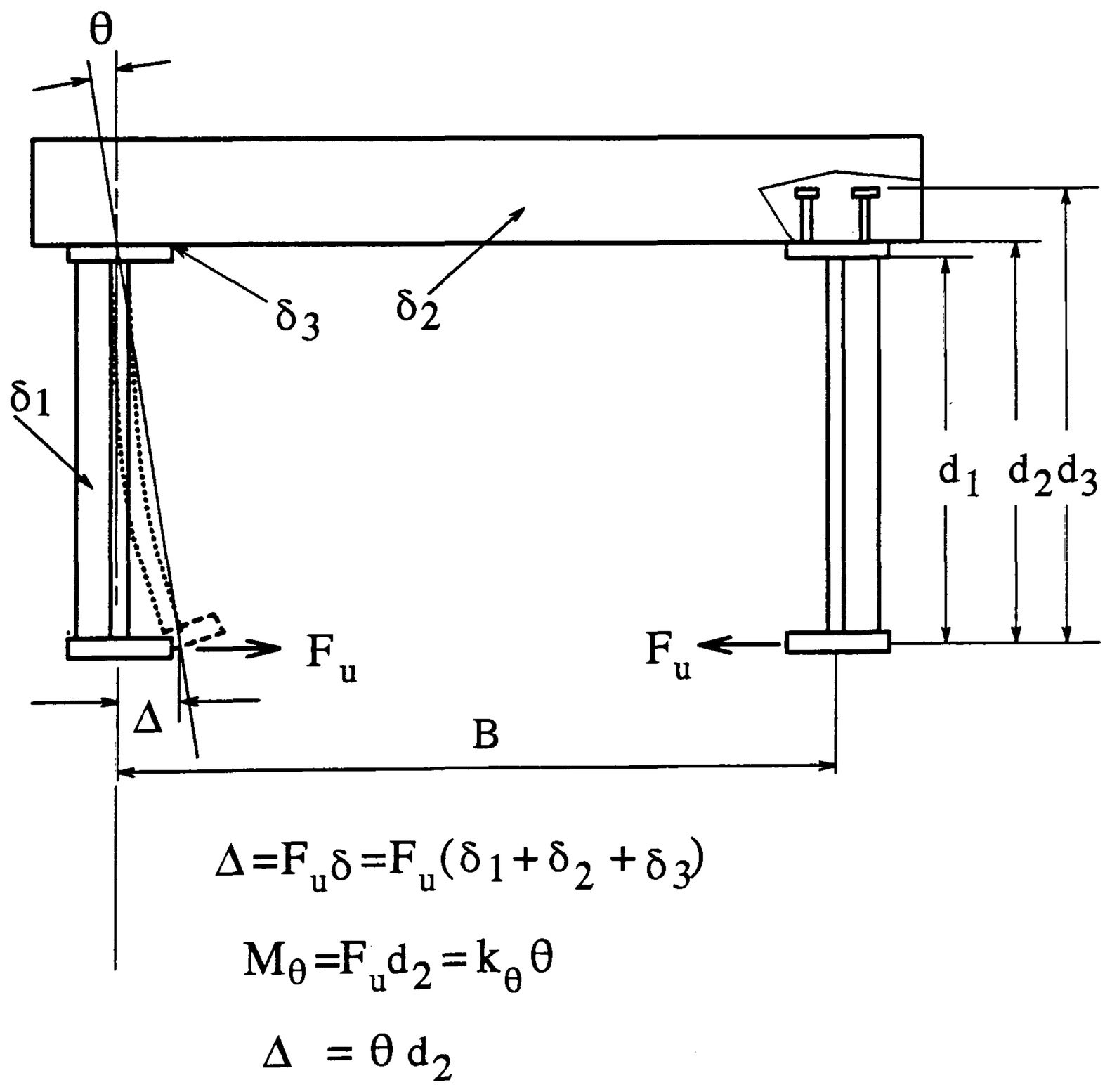

$$\Delta = F_u \delta = F_u(\delta_1 + \delta_2 + \delta_3)$$

$$M_\theta = F_u d_2 = k_\theta \theta$$

$$\Delta = \theta\, d_2$$

Figure 8.10: An inverted composite U-frame

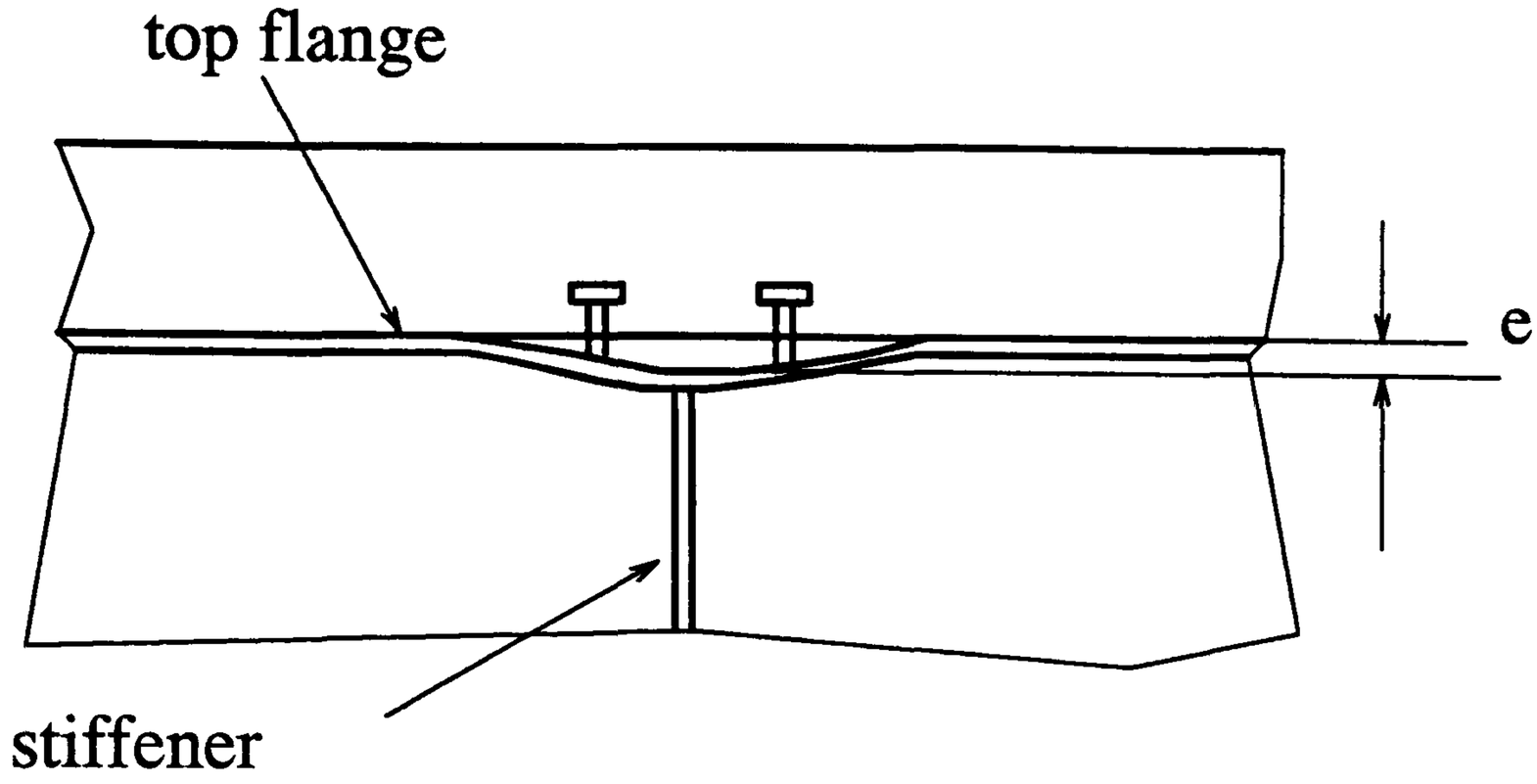

Figure 8.11: Deformation shape of the top flange(single sided stiffened I-U)

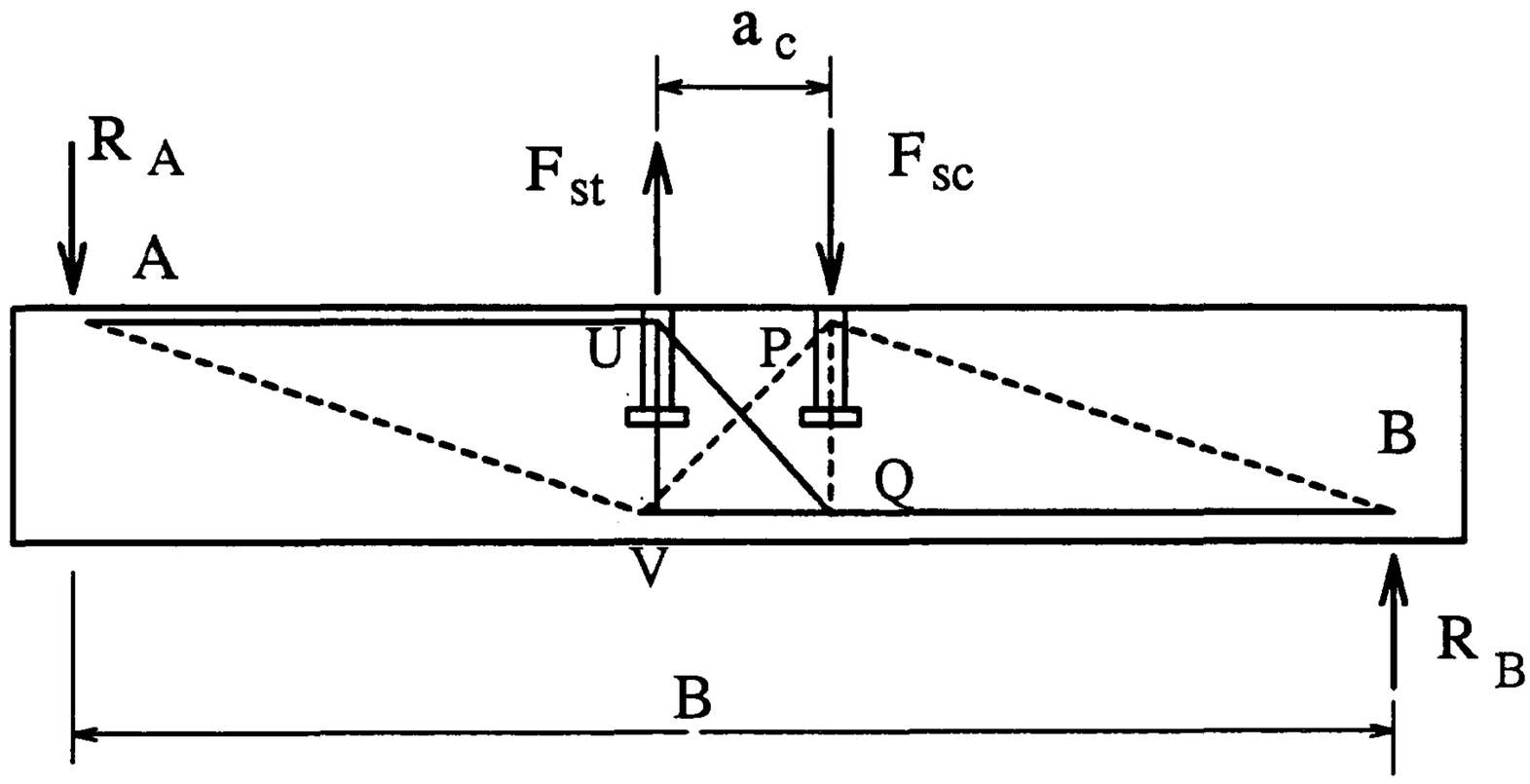

Figure 8.12: A truss model of shear failure of the slab

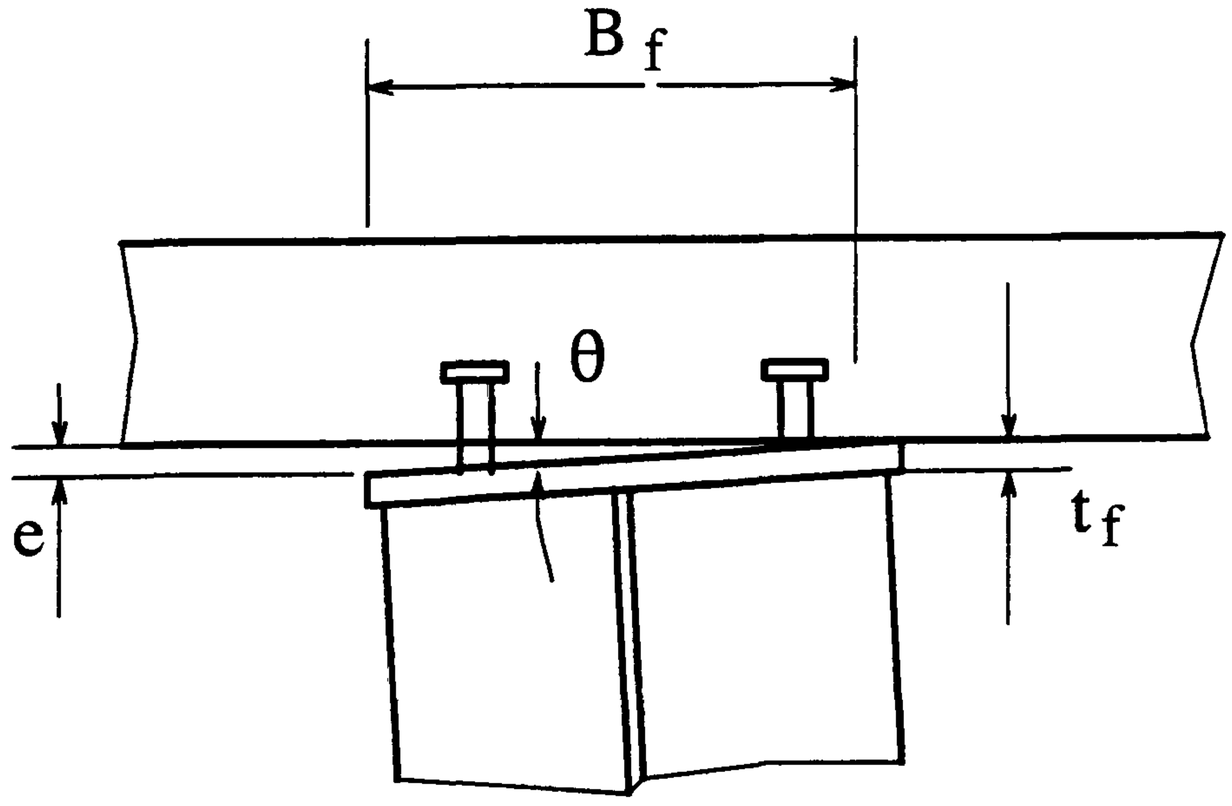

Figure 8.13: U-frame connection

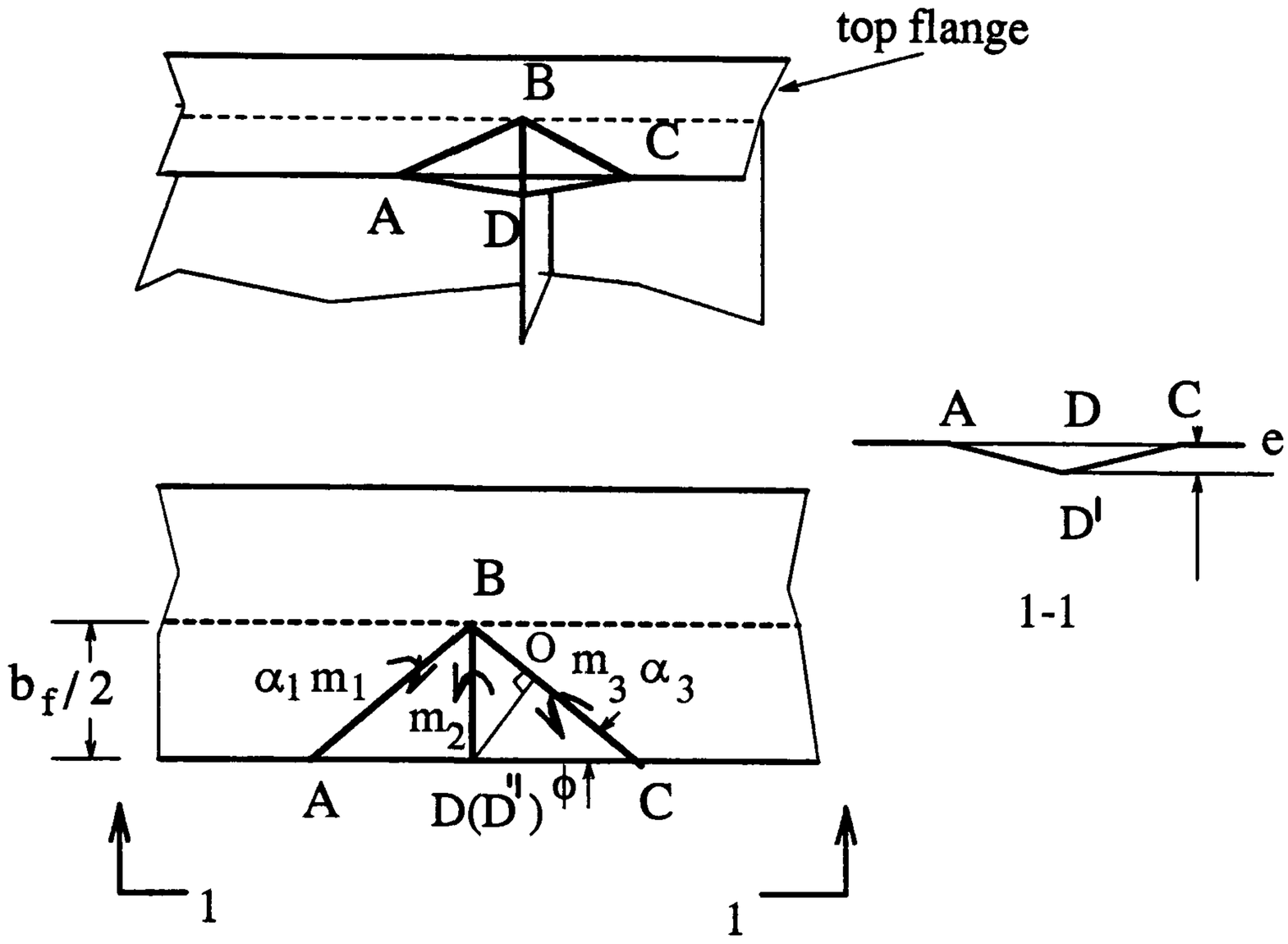

Figure 8.14: Mechanism of the top flange

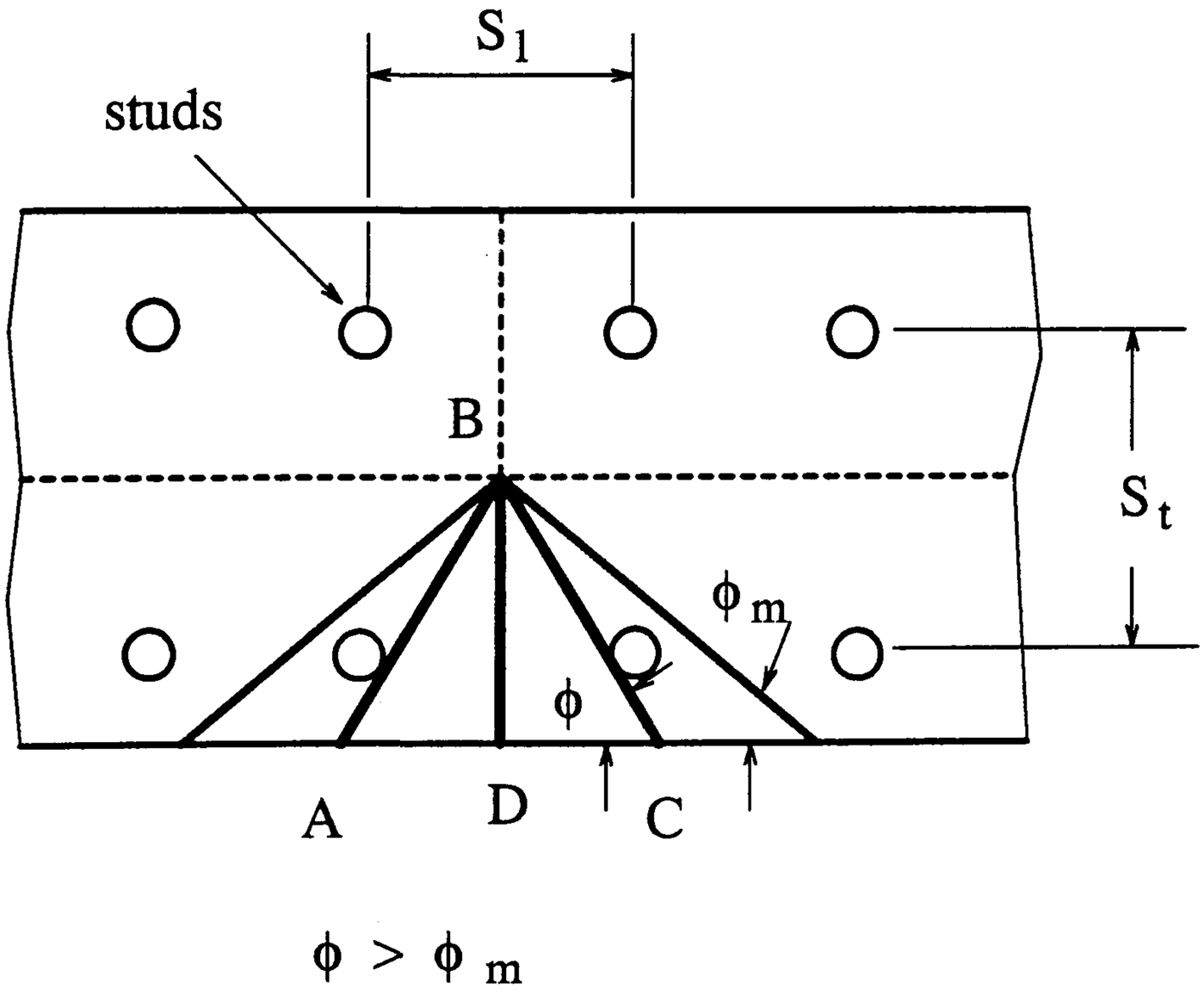

$$\phi > \phi_m$$

Figure 8.15: Possible mechanism of the top flange

Chapter 9

Theoretical investigation of U-frame action

9.1 Introduction

When rolled or welded steel I-section members are used in continuous composite beams, distortional lateral buckling can occur in hogging moment regions adjacent to internal supports. For structures with parallel main composite girders, 'U' frame action is used to stabilize the bottom flange in design practice. Continuous restraint is provided to the compression flange by the slab and the web for unstiffened plate girders. Discrete restraint is provided to the compression flange by the intermediate vertical stiffeners which act as discrete inverted U-frames together with a part of the web.

The U-frame restraint to the bottom flange is tackled in the Bridge Code (BS5400) [2] in a similar way to the earlier code (BS153) [65]. The code, based on a strut analogy from the BEF (beam on elastic foundation) theory makes the U-frame design very conservative. Besides, the flexibility of the U-frame connections suggested in BS5400: Part 3 is irrelevant to the composite configurations.

The design method adopted for recent redrafting of the EC4 [1] is based on an approximation for the elastic critical value of a uniform hogging bending moment, taking account of continuous U-frame restraint. By introducing parameter C_4, which is based on finite element analyses for non-uniform distributions of bending moment, the method is applicable both to complete spans and to short lengths of hogging moment regions between points, at which the bottom flange is laterally restrained.

It has been experimentally verified, that the latter method gives a better prediction of lateral buckling resistance for unstiffened continuous U-frame beams, of either compact [54] or slender section (specimen U4 described in chapters 5,6, and 7). However, no appropriate method is available so far for discrete U-frames of composite construction, and U-frame action, as far as it is concerned, has not been well

assessed.

The scope of the present chapter is to provide a theoretical approach to develop a design method to cover composite beams with discrete U-frame action. It begins with comments and reviews of the application of the BEF theory in dealing with beams with discrete lateral supports. The validation of the theory is discussed. The effect of distributed compression is also studied, based on the numerical results of columns with continuous restraint, subject to varying compression force along the length. It leads to a modification of the design method for lateral buckling in BS5400, taking account of variations of the moment gradient.

Using the distortional buckling model adopted in EC4 is a rational approach to assess the critical moment of beams with U-frame actions. It originated in the work by Lindner [83], who solved beams of I-section with continuous lateral and torsional restraint in the top flange (tension flange). The motivation for using the model to cover beams with discrete U-frame restraint is further prompted with a handful of test data from discrete U-frame beams(U5). Based on the buckling shape observed in the U-frame beam test, the strain energy in transverse bending of a U-frame beam is evaluated, and then a lower bound energy method is proposed, using the similar approach for beams with continuous U-frames. The effect of moment gradient on the elastic critical moment is also studied and the validation of the new method in assessment of the elastic critical moment for beams with discrete U-frame action is discussed.

Interactive U-frame force and stiffness are also studied and the U-frame force at the ultimate state of the beams is evaluated based on an upper bound mechanism for the bottom flange.

9.2 Distortional buckling investigations based on the BEF theory

9.2.1 Bifurcation solution for compression members with intermittent lateral supports

The fundamental principles to determine the bifurcation load of a compression strut with intermittent lateral supports are well established [84]. In practice, the difficulties are that the true unknown, i.e. the lowest bifurcation load, appears as a variable in trigonometrical functions, or buckling shape functions.

Engesser [85] treated the problem as a strut supported on a continuous elastic medium, with the assumptions:

- uniform cross-section, and constant compression force through the length,
- pinned and rigidly supported at the ends of a strut,
- equally spaced elastic supports having the same stiffness and assumed 'smeared' over the support spacing L_u.

Fig.9.1 shows the simplifying assumptions on which the analysis is based.
The critical load N_c is obtained as

$$N_c = \frac{n^2\pi^2}{L^2}EI + c\frac{L^2}{n^2\pi^2} \tag{9.1}$$

where

- E is Young's modulus.
- I is the second moment of area of the cross-section.
- c is stiffness of lateral restraint per unit length (C/L_u).

The determinate number n of half waves corresponds to the minimum N_{cr} or

$$n^2 = \frac{L^2}{\pi^2}\sqrt{\frac{c}{EI}} \Rightarrow N_{cr} = 2\sqrt{EIc} \tag{9.2}$$

For design purposes, an effective length l_e is introduced by

$$l_e^2 = \frac{\pi^2 EI}{N_{cr}} \tag{9.3}$$

and it leads to

$$l_e = 2.22(\frac{EI}{c})^{0.25} \tag{9.4}$$

The effective length l_e does not correspond to the buckle wavelength L/n of the strut (but $L/n = \sqrt{2}l_e$), where n is the number of half buckling waves within the span L. It is found that the accurate solution is obtained [84] only when there are at least three supports per half wave of the buckled strut, using the continuous elastic medium model, to deal with the strut with discrete lateral supports. This can be expressed

$$4L_u \leq \frac{L}{n} = \sqrt{2}l_e \tag{9.5}$$

Equations 9.2, 9.4 and 9.5 can lead to a more useful expression for L_u when the assumption of smearing discrete restraints is still valid ($\sqrt{2}l_e \geq 4L_u$)

$$L_u \leq (0.38\frac{EI}{C})^{1/3} \tag{9.6}$$

On the other hand, L_u is also expressed by

$$L_u = \lambda \frac{l_e}{2\sqrt{2}} \tag{9.7}$$

where λ (≤ 1) is a multiple of the maximum lateral spacing L_u ($l_e/2\sqrt{2}$).

From equations 9.2, 9.4 and 9.7, the minimum lateral stiffness C_{min} at that spacing ($\lambda l_e/2\sqrt{2}$) is found as

$$C_{min} = 0.278\lambda(\frac{N_{cr}^3}{EI})^{\frac{1}{2}} \tag{9.8}$$

9.2.2 Beams on elastic mediums subject to varying axial compression

Considering the effect of moment gradient, Svensson [46] modelled the free flange (relative to the top flange restrained by slab) as a beam subject to a varying axial force, resting on an elastic foundation, as shown in Fig.9.1.

The stability problem is then mathematically represented by the differential equation and boundary conditions as

$$\frac{d^4y}{d\xi^4} + \pi^2\lambda\frac{d}{d\xi}[n(\xi)\frac{dy}{d\xi}] + (\beta L)^4 y = 0 \tag{9.9}$$

and

$$\xi = 0, \qquad y = 0, \qquad \frac{d^2y}{d\xi^2} = 0 \tag{9.10}$$

$$\xi = 1, \qquad y = 0, \qquad \frac{d^2y}{d\xi^2} = 0 \tag{9.11}$$

The non-dimensional quantities used in the equations are given by

$$\xi = \frac{x}{L} \tag{9.12}$$

$$\beta L = (\frac{c}{EI})^{0.25} L \tag{9.13}$$

$$N(\xi) = n(\xi)N_0 \tag{9.14}$$

where

- $N(\xi)$ is axial force along beam length.
- $n(\xi)$ is unit distribution function of the axial force.
- N_0 is the maximum force at the support.

The Fourier expansion, whose single terms satisfy the boundary conditions, is used, and with a Galerkin approach, the elastic critical load can be expressed as λ_{el} by [46]

$$\lambda_{el} = \frac{N_{el}}{N_E} \tag{9.15}$$

where

- N_E is Euler load of the beam, expressed as

$$N_E = \frac{\pi^2 EI}{L^2} \tag{9.16}$$

- N_{el} is the elastic critical load of the beam(subject to $N(\xi)$), and it can be expressed as

$$N_{el} = \frac{\pi^2 EI}{(\eta l_e)^2} \tag{9.17}$$

- l_e is the effective length defined in equation 9.3, which corresponds to a beam subject to uniformly distributed axial force.

- η is a coefficient regarding to the distributed axial compression.

The numerical values of λ_{el} based on Svensson's work are shown in Table 9.1. Sevesson studied 9 cases of varying axial forces, but four of them are irrelevant to the stability in hogging regions so that only the five relevant cases are given in Table 9.1 [46]. The corresponding varying loadings are shown in Fig.9.2.

In Table 9.1, λ_{el} determines the value of the critical load N_{el}, prescribed in equation 9.15. The assumption is made that the effective length l_e, defined in equation 9.3, can apply to the general situations with varying axial force. As the case 1 in Table 9.1 is for constant compression along a beam, the effect of varying axial force is included by introducing η(equation 9.17), based on the results given in Table 9.1, defined as

$$\eta = (\frac{N_{el1}}{N_{el}})^{0.5} = (\frac{\lambda_{el1}}{\lambda_{el}})^{0.5} \tag{9.18}$$

or simply using effective length

$$l_{el} = \eta l_e \tag{9.19}$$

where

- l_{el} is the effective length corresponding to distribution force $N(x)$.

- subscript 1 means the case 1, for constant compression.

The calculated values of η are given in Table 9.2 for different cases and further illustrated in Fig.9.3. For a comparison, the values(η) obtained from BS5400 (Fig.9 in BS5400:Part 3) for these relevant loadings are also illustrated in Fig.9.3.

BS5400 does not distinguish between cases 2 and 3, and it also gives a higher η than those from Table 9.2. Besides, η given in BS5400 is not consistent with the variation of βL. For cases 4 and 5, BS5400 gives values of 0.53 and 0.78, which correspond to those values (η) when βL are about 16 (case 5) and 3.5 (case 4) given by Table 9.2. The reason for these is that these values (η given by BS5400) are not based on a model that lateral elastic restraints have a significant effect on the elastic critical load.

The increase of η with βL reveals the effect from the lateral stiffness of the continuous restraint. When the lateral restraint gets stiffer, the buckling wave length gets shorter, and the varying compression along the axis will have less effect on bifurcation values of the load.

The results (λ_{el}, hence η) are applicable for the free flange (bottom flange) in composite I sections, because they are all based on a BEF (beam on elastic foundation) model, with full lateral restraints only at supports.

9.2.3 Design to lateral buckling with U-frame action, BEF approach

The lateral restraint from a U-frame is assessed, in BS5400: Part 3, using the U-frame flexibility δ, defined as lateral movement of the bottom flange under unit force. The effective length l_e introduced for U-frame beams is based on the BEF theory, only with constant compression, and is given by

$$l_e = 2.5k_3(EIL_u\delta)^{0.25} \tag{9.20}$$

where

- I is the second moment of the area of the bottom flange in the minor axis of the cross section.
- k_3 is the coefficient regarding support conditions.

- L_u is the U-frame spacing.

- δ is defined as the U-frame flexibility.

The differences between equations 9.20 and 9.4 are that, 2.5(eq.9.20) is adopted instead of $2.2(\pi/\sqrt{2}$ in eq.9.4), which accounts for lateral continuity at internal supports of a continuous beam, and δ is used rather than C. It is known that δ for U-frame is a reciprocal of its stiffness C, and therefore, the two equations are basically the same.

The effect of moment gradient introduced by η in BS5400: Part 3 however is not correctly based on the model with U-frame restraints. It is proposed that by introducing the new η, given in Table 9.2, the effect of moment gradient can be included, because it is based on the relevant investigation of the BEF model.

Fig.9.3 shows a comparison of new η with that given in BS5400: Part 3.

When l_e is determined, the effective length l_{el}, accounting for the effect of moment gradient, can be calculated by equation 9.19. The design to the buckling stress (limit) will follow the design curves for compression members. The shortcomings of the method are that it is based on a non-distortion model, and torsional rigidity is neglected, even if the effect of moment gradient can be compensated by introduction of the new η.

A more comprehensive method based on the distortional buckling model will be presented in the next section.

In general, BEF results are based on the assumption of U-frames smeared over L_u. The applicability of the results is governed by eq. 9.6. The validation of the method is not discussed in BS5400: Part 3, and this leads to an inappropriate assessment of U-frame action.

9.3 Energy assessment of distortional lateral buckling

9.3.1 Distortional lateral buckling model

The distortional lateral buckling of a composite cross section is modelled in Eurocode 4 as an I-section with torsional restraint on the top flange, shown in Fig.9.4. For

single span beams with general bending moment, the elastic critical moment M_{cr} can be determined, using an energy method. The partial action effects results from the cracked composite cross section [52] are

$$M_a = M_{cr}\frac{I_{ay}}{I_y} \tag{9.21}$$

$$N_a = -M_{cr}\frac{z_s A_a}{I_y} \tag{9.22}$$

where

- M_a and N_a are the bending moment and axial force acting on the steel cross section;
- I_{ay} and I_y are the second moments of area of the steel cross section and the composite cross section;
- A_a is steel cross section area;
- z_s is the distance from the centroid of the steel section to its shear centre.

The energy equation of the system is

$$\begin{aligned}\delta^2\Pi = \int_0^L [&EI_{afz}h_s^2\theta''^2 + GI_{at}\theta'^2 + k_\theta\theta^2 + M_a(x)r_{mz}\theta'^2 - 2M_a(x)f\theta\theta'' \\ &+N_a(x)(f^2+i^2)\theta'^2 - 2N_a(x)z_s f\theta\theta'']dx\end{aligned} \tag{9.23}$$

The relevant parameters and notations are shown in Fig.9.4.

where

- h_s is the distance between the shear centres of the flanges of the steel section:
- f is the distance between the rotation centre D and the shear centre of steel section;
- i is radius of gyration of the steel section related to the shear centre;
- r_{mz} is calculated by

$$r_{mz} = \frac{1}{I_{ay}}[\int_A z(z^2+y^2)dA - 2z_s I_{az}] \tag{9.24}$$

- I_{az} is the second moment of area of the steel cross section about axis z.

The solution of the critical moment is obtained by introducing a possible buckling shape θ(x). No specific θ(x) functions are given in [52], however, it refers to the work by Lindner [83], in which, beams with extended cantilevers are studied, using polynomial functions which satisfy the boundary conditions.

Following the same approach, a displacement function is assumed and the effect of bending moment variations is introduced by C_4, based on the FE numerical analysis. The elastic critical moment is then expressed

$$M_{cr} = \frac{C_4 k_c}{L}\sqrt{(GI_{at} + k_\theta(\frac{L}{\pi})^2)EI_{afz}} \tag{9.25}$$

The properties of the cross-section are given as follows [1];

- L is the length of the beam between points at which the bottom flange of the steel member is laterally restrained.

- C_4 is a property of the distribution of bending moment within length L given in Tables B.1 to B.3 of EC4 .

- k_c is a shape factor given in Clause B.1.3 or B.1.4, of EC4.

- G is the shear modulus for steel.

- I_{afz} is the second moment of area of the bottom flange about the minor axis of the steel member.

- I_{at} is the St. Venant torsion constant of the steel section.

- k_θ is the transverse stiffness per unit length of the beam, defined in Eurocode 4.

The variations of C_4 with parameter ξ are given in a series of graphs [52] related to the different moment gradients, where ξ is defined as

$$\xi = \frac{EI_{afz}h_s^2}{[GI_{at} + k_\theta(\frac{L}{\pi})^2]L^2} \tag{9.26}$$

In the parametric study, ξ varies from 0 to 0.3. Only the minimum values of C_4 are given in EC4.

9.3.2 Energy evaluation of the transverse bending of a U-frame beam

When lateral buckling occurs, strain energy by transverse bending via the discrete U-frames is induced, which will tend to increase the potential of the system. This strain energy can be evaluated in two ways:(1)the transverse rigidity of stiffeners are treated as uniformly smeared over the U-frame spacing L_u, (2)the transverse rigidity of stiffeners is considered individually.

Assume the lateral buckling shape y as the following

$$y = a_1 sin\frac{\pi x}{L} + a_2 sin\frac{2\pi x}{L} + a_3 sin\frac{3\pi x}{L} + ... \tag{9.27}$$

where

$$y = 0 \qquad at \qquad x = 0, L \tag{9.28}$$

Let K_s be the transverse rigidity of an individual stiffener. When the first five odd terms in equation 9.27 are used, the transverse strain energy for a uniform stiffness K_s/L_u is written as E_1

$$E_1 = \frac{1}{4}\frac{L}{L_u}K_s[{a_1}^2 + {a_3}^2 + {a_5}^2 + {a_7}^2 + {a_9}^2] \tag{9.29}$$

The transverse strain energy using individual stiffeners is

$$E_2 = \frac{K_s}{2}\Sigma_{n=1}^{m}(a_1 sin\frac{n\pi L_u}{L} + a_3 sin\frac{3n\pi L_u}{L} + a_5 sin\frac{5n\pi L_u}{L} + a_7 sin\frac{7n\pi L_u}{L} + a_9 sin\frac{9n\pi L_u}{L})^2 \tag{9.30}$$

where m is the number of stiffeners within span L.

The ratios E_2/E_1 are plotted against L/L_u in Fig.9.5, in which one curve corresponds to the symmetric buckling mode, and the other three curves are for the asymmetric buckling modes. The buckling shapes illustrated in different line types correspond to the various variations of E_2/E_1 with L/L_u. It is found that ratio E_2/E_1 is relevant to two parameters. One is the ratio of L/L_u, and the other is the ratio of l_b/L, where l_b is the half buckling wave length.

1. Buckling shape: The buckling shapes used in the evaluation are based on the test results of specimen U5, in which the lateral buckling occurred in

the regions close to the internal supports. Both asymmetric and symmetric buckling shapes are simulated.

2. Asymmetric modes: Three curves with different ratios of buckling length (l_b/L) are given. When the ratio is 0.4(dashed line), E_2/E_1 approaches 1 if L/L_u is greater than 5. When the ratio (l_b/L) is 0.25(dashed point line), L/L_u increases to 10, for the same value of E_2/E_1.

3. Symmetric modes: The ratio of buckling length(l_b/L) is between 0.3 and 0.4, E_2/E_1 approaches to 1 when L/L_u is about 7 or 8.

4. The ratio of buckling length (l_b/L) influences the value of L/L_u at which unit value of E_2/E_1 is approached. When l_b/L is 0.4, E_2/E_1 tends to 1 only when $L/L_u > 5$. That means that there are more than two stiffeners within l_b. When l_b/L is 0.25, E_2/E_1 trends to 1 only when L/L_u approaches to 10, which reveals that there are 2.5 stiffeners within l_b. All these results coincide with the requirement for at least three lateral supports within each half buckling wave length, when the BEF theory is applied.

5. It is more likely, that the ratio of buckling length (l_b/L) will vary between 0.2 to 0.4, though only one test of discrete U-frame beams is available (linear moment gradient for U5). For uniform moment, ratio l_b/L will be greater than that for moment gradient. In design practice, L/L_u will vary between 10 and 20,(about 12 and 25 for U5), so that the transverse strain energy of discrete U-frames treated as uniformly smeared over spacing L_u can give a very good approximation to the actual transverse strain energy of the stiffened web. These results only apply to the situations, where U-frames are equally spaced along the beam length.

9.3.3 The effect of C_4 –moment gradients

The energy equation for general moment gradients is given in eq.9.23, for continuous U-frames. When the strain energy of transverse bending via discrete U-frames is treated as uniformly smeared over the beam spacing, the energy equations for both continuous and discrete U-frames are the same. This is achieved by assuming the

transverse stiffness of the stiffened web to be

$$k_1 = \frac{3EI_s}{h_s L_u} \tag{9.31}$$

where

- I_s is the second moment of area of a stiffener about the minor axis of the beam.
- k_1 is the transverse stiffness per unit length of the stiffened web.

Derivation of equation 9.31 is referred back to equations 8.9 and 8.14 in the previous chapter(section 8.3.2), with the lateral deflection δ of a U-frame being converted into a hypothetic transverse rotation θ (shown in Fig.8.10). I_s in equation 9.31 corresponds to I_1 in equation 8.9, and h_s in equation 9.31 corresponds to d_1^3/d_2^2 in equation 8.9.

Subject to the validation of smearing discrete U-frames over their spacing, a discrete U-frame beam can be modelled as a continuous U-frame model, but with great increase in the lateral restraint stiffness.

The effects of moment gradient on the elastic critical moment of beams with discrete U-frames are analysed as follows.

From eq.9.26, it is found that the parameter ξ decreases with the increase of the lateral restraint stiffness k_θ. Since stiffeners greatly increase the lateral stiffness of the web, the lateral restraint stiffness of a stiffened beam (with discrete U-frames) is much greater than an unstiffened beam (continuous U-frames), even with the identical cross section.

Let U-frames be smeared over the beam length, and k_θ be expressed as

$$k_\theta = \kappa k_1 \tag{9.32}$$

where κ is a factor of k_1 for analysis of variation of $\xi(< 1)$.

Usually $GI_{at} \ll k_\theta(L/\pi)^2$, so it can be neglected, and by substituting equation 9.32 into equation 9.26, ξ can be simplified as

$$\xi = \frac{\pi^2}{3\kappa}\frac{I_{afz}}{I_s}(\frac{h_s}{L})^4\frac{L_u}{h_s} \tag{9.33}$$

In practice, the ratio L/h_s ranges from 15 to 25, and L_u/h_s from 1 to 2. Let κ be 1/3 (κ may range from 1/4 to 1, but it is certainly smaller than 1 for discrete U-frame beams), I_{afz}/I_s be 1, and ξ is then from 0.008 to 0.044. Therefore, C_4 in all circumstances for the discrete U-frames is covered by that for continuous U-frames, because ξ ranges from 0 to 0.3 in the numerical study.

Similar analysis can be done for continuous U-frame restraints. It can be found that in practical range, ξ is always smaller than 0.3.

Besides, only the minimum C_4 is recommended for continuous U-frames in EC4, and therefore C_4 also applies for discrete U-frames.

9.4 U-frame force evaluation

The U-frame force is assessed in BS5400 [2], by modelling the flange as a simply supported strut, with an initial bow. The force is proportional to the lateral deflection Δy expressed by

$$\Delta y = y_0 \frac{\sigma_{fc}}{\sigma_{cr} - \sigma_{fc}} \tag{9.34}$$

where σ_{fc},σ_{cr} are compressive stress and elastical critical stress of the flange, and y_0 is the amplitude of the initial bow.

However, the lateral restraint from the U-frame is not well evaluated, because uniform compression force is assumed in the strut, when equation 9.34 is derived. It has been found that elastic critical stress is influenced by the axial force distribution. Besides, axial compression force in the bottom flange of a continuous composite beam usually decreases very rapidly away from its internal supports due to a high moment gradient. This also raises a question that whether equation 9.34 can be still applicable. Furthermore, in BS5400, the lateral U-frame force is considered equal everywhere along the beam length. This is very conservative, and actually, the lateral force also drops away from the internal support regions.

The influence of axial force distribution on the elastic critical stress for columns with elastic restraints was studied by Svensson [46]. But, in his study, Svensson did not include the initial imperfections.

Recent work by Jeffers, of Travers Morgan [73] traced the results from Winter's work [86]. But the shortcoming of the work is that the U-frame forces are based

on a strut with discrete rigid lateral support, which does not cover beams with lateral restraints from discrete U-frames of intermediate stiffness. Also, compression gradients are still not included.

In design, the elastic critical stress is normally above the yield stress, and it is more likely that the U-frame force will be governed by an inelastic collapse load than by the elastic critical stress. These problems are tackled in the following sections.

9.4.1 Flexible U-frames

In this section, the free bottom flange of a U-frame beam is modelled as a strut (or column) with lateral elastic restraints provided by U-frames.

The principles for notation of symbles are follows;

- C —- stiffness of lateral restraints,
- c —- stiffness of lateral restraints per unit length,
- F —- lateral restraint force,
- N_{cr} —- the elastic critical load (uniform compression),
- N_E —- the Euler critical load ($\pi^2 EI/L^2$),
- N_{el} —- the maximum value of elastic critical load at the support (non-uniform compression),
- N_0 —- the maximum axial force at the support,
- N_y —- the axial force when yielding occurs in the bottom flange,
- L —- length of span between the ends of a beam,
- L_u —- spacing of lateral restraints,
- l_e, l_b —- effective length/ buckling wave length,
- ϕ —- factor for the elastic critical load regarding distributed force.

Other symbols are defined in the text where they appear.

Analytical model

Fig.9.6 shows a strut with an initial bow $y_0(x)$, subject to axial force $N(x)$. The assumptions of smearing U-frames over its length still holds. The notations for the parameters are the same for those given in Fig.9.1.

By equilibrium of the small segment dx, following equations are obtained

$$q = \frac{\mathrm{d}Q}{\mathrm{d}x} \tag{9.35}$$

$$Q = \frac{\mathrm{d}M}{\mathrm{d}x} - N(x)\frac{\mathrm{d}y}{\mathrm{d}x} \tag{9.36}$$

From eq.9.35 and eq.9.36, we can obtain

$$q = \frac{\mathrm{d}^2M}{\mathrm{d}x^2} - \frac{\mathrm{d}}{\mathrm{d}x}(N(x)\frac{\mathrm{d}y}{\mathrm{d}x}) \tag{9.37}$$

Considering the effects of the initial imperfection y_0, q and M are written as

$$q = c(y - y_0) \tag{9.38}$$

and

$$M = -EI(y'' - y_0'') \tag{9.39}$$

So that the governing equation of the system is

$$EIy'''' + \frac{\mathrm{d}}{\mathrm{d}x}(N(x)\frac{\mathrm{d}y}{\mathrm{d}x}) + cy = EIy_0'''' + cy_0 \tag{9.40}$$

with the boundary conditions

$$y = 0 \qquad \text{when} \qquad x = 0, \qquad x = L \tag{9.41}$$

$$y'' = 0 \qquad \text{when} \qquad x = 0, \qquad x = L \tag{9.42}$$

Solutions, when $N(x) = N_0$ (constant along the length)

When $N(x)$ is constant along the length, the governing equation is simplified as

$$EIy'''' + N_0 \frac{\mathrm{d}^2 y}{\mathrm{d}x^2} + cy = EIy_0'''' + cy_0 \tag{9.43}$$

This equation is solved with the general solution in a form as

$$y = A_1 e^{\lambda_1 x} + A_2 e^{-\lambda_1 x} + A_3 cos\lambda_2 x + A_4 sin\lambda_s 2x \tag{9.44}$$

where A_1, A_2, A_3 and A_4 are coefficients relating to the boundary conditions, and λ_1 and λ_1 are eigenvalues relating to the elastic critical load.

The specific solution to the initial bow y_0 is also obtained as far as y_0 is known. Assume the initial imperfection is a sinusoid shape over its length L, or by

$$y_0 = a_0 sin\frac{\pi x}{L} \tag{9.45}$$

Then the specific solution is

$$y^* = \frac{1 + (c/EI)(L/\pi)^4}{1 - (N_0/N_E) + (c/EI)(L/\pi)^4} a_0 sin\frac{\pi x}{L} \tag{9.46}$$

where N_E is defined in eq.9.16 ($\pi^2 EI/L^2$).

The solution is a summation of the general solution and the specific solution. By satisfying the boundary conditions, the following equations are derived

$$A_1 + A_2 + A_3 = 0 \tag{9.47}$$

$$\lambda_1^2(A_1 + A_2) = \lambda_2^2 A_3 \tag{9.48}$$

and

$$A_1 e^{\lambda_1 L} + A_2 e^{\lambda_2 L} = A_4 sin\lambda_2 L \tag{9.49}$$

$$\lambda_1^2(A_1 e^{\lambda_1 L} + A_2 e^{\lambda_2 L}) = \lambda_2^2(A_4 sin\lambda_2 L) \tag{9.50}$$

It is found A_1, A_2, A_3 and A_4 are all equal to zero, which leads to y equal to the the specific solution expressed as in equation 9.46.

The initial imperfection of bottom flanges is usually not a simple sinusoid shape as that given by equation 9.45, especially when single sided stiffeners are used. Fig.9.7 shows a plan view of the bottom flange of this type. It is more likely that the initial imperfection curve of the flange has a shorter wavelength, due to welding the stiffeners.

Therefore, more accurate curves of the initial imperfection are expressed as a summation of more than one term of the triangular series, i.e.

$$y_0 = a_{10} sin\frac{\pi x}{L} + a_{20} sin\frac{2\pi x}{L} + a_{30} sin\frac{3\pi x}{L} + ... \tag{9.51}$$

It can be verified that the solution is a sum of a series of the corresponding terms, as

$$y = \Sigma_{i=1}^{n} \frac{1 + (c/EI)(L/i\pi)^4}{1 - (N_0/i^2 N_E) + (c/EI)(L/i\pi)^4} a_{i0} sin\frac{i\pi x}{L} \tag{9.52}$$

The lateral deflection of the strut Δy is

$$\begin{aligned} \Delta y &= y - y_0 \\ &= \Sigma_{i=1}^{n} \frac{N_0/i^2 N_E}{1 - (N_0/i^2 N_E) + (c/EI)(L/i\pi)^4} a_{i0} sin\frac{i\pi x}{L} \\ &= \Sigma_{i=1}^{n} \frac{N_0}{N_E i^2 + N_{cr}(L/l_e)^2/(4i^2) - N_0} a_{i0} sin\frac{i\pi x}{L} \end{aligned} \tag{9.53}$$

where N_{cr} is the elastic critical load corresponding to an ideal straight strut ($N_{cr} = 2\sqrt{EIc}$), and l_e is the effective length defined by Euler formula in eq.9.3,

so that q is expressed as

$$\begin{aligned} q &= c\Delta y \\ &= c\Sigma_{i=1}^{n} \frac{N_0}{N_E i^2 + N_{cr}(L/l_e)^2/(4i^2) - N_0} a_{i0} sin\frac{i\pi x}{L} \end{aligned} \tag{9.54}$$

When the first term is of predominant importance, then q is simply

$$q = \frac{cN_0}{N_E + N_{cr}(L/l_e)^2/4 - N_0} a_{10} sin\frac{\pi x}{L} \tag{9.55}$$

For the continuous U-frame, the U-frame force F_u is therefore

$$F_u = q \leq \frac{cN_0}{N_E + N_{cr}(L/l_e)^2/4 - N_0} a_{10} \tag{9.56}$$

For the discrete U-frame, the U-frame force F_u is a product of the lateral deflection and C,the rigidity of the lateral U-frame restraint

$$\begin{aligned} F_u &= \frac{CN_0}{N_E + N_{cr}(L/l_e)^2/4 - N_0} a_{10} sin \frac{i\pi x_u}{L} \\ &\leq \frac{CN_0}{N_E + N_{cr}(L/l_e)^2/4 - N_0} a_{10} \end{aligned} \tag{9.57}$$

where x_u is the location of the U-frame considered.

The restraint force at the support is also found by integration of q over L

$$\begin{aligned} F_s &= \frac{1}{2}\int_0^L q dx \\ &= \frac{CN_0}{N_E + N_{cr}(L/l_e)^2/4 - N_0} \frac{L}{\pi} a_{10} \end{aligned} \tag{9.58}$$

General solution for non uniform compression $N(x) = N_0 n(x)$

When the compression is not constant along the axis, the governing equation given in eq.9.40 can be solved by the Galerkin method. Assume y as the Fourier expansion, where each term satisfies the boundary condition ($y = 0$, $y'' = 0$ at $x = 0$ and $x = L$)

$$y = \Sigma_{i=1}^{n} a_i sin \frac{i\pi x}{L} \tag{9.59}$$

and the initial imperfection y_0

$$y_0 = \Sigma_{i=1}^{n} a_{i0} sin \frac{i\pi x}{L} \tag{9.60}$$

Substituting the Fourier expansion into eq.9.40, and integrating from 0 to L, then

$$\int_0^L [EIy'''' + \frac{d}{dx}(N(x)\frac{dy}{dx}) + cy] sin \frac{j\pi x}{L} dx = \int_0^L [EIy_0'''' + cy_0] sin \frac{j\pi x}{L} dx \tag{9.61}$$

where $j = 1, n$.

Using the orthogonal properties, the following equation is obtained

$$a_j[(\frac{j\pi}{L})^4 + \frac{c}{EI}] + \frac{2}{l}\int_0^L [N'(x)(\Sigma a_i \frac{i\pi}{L} cos\frac{i\pi x}{L})sin\frac{j\pi x}{L}] - N(x)[(\Sigma a_i(\frac{i\pi}{L})^2 sin\frac{i\pi x}{L})sin\frac{j\pi x}{L}]dx = a_{j0}[(\frac{j\pi}{L})^4 + \frac{c}{EI}] \quad (9.62)$$

When $y_0 = a_0 sin\pi x/L$, the solution for equation 9.62 is found as a form

$$a_j = \frac{[1 + (c/EI)(L/\pi)^4]a_{j0}}{(j)^4 + (c/EI)(L/\pi)^4 - (N_0/N_E)(j^2\phi_j)} \quad (9.63)$$

where ϕ_j is a function of $N(x)$, L, $E\ I$, and c.

When $j = 1$, a_1 is the amplitude of the displacement shape given by eq.9.46. ϕ_j can be found by the numerical analyses for the different distributed functions $n(x)$. When ϕ is 0, the amplitude is its initial one (a_0) or Δy is 0, and ϕ_j of 1 is for the constant N along the axis.

When the first term is predominant, using l_e ($= \pi(EI/c)^{1/4}/\sqrt{2}$ equation 9.4), the U-frame force F_u is simplified as

$$F_u = \frac{CN_0}{N_E/\phi + N_E(L/l_e)^4/4\phi - N_0} a_{10} \quad (9.64)$$

Discussion and evaluation of U-frame force

The solution given in previous sections reveals that the effects of lateral restraints from discrete U-frames and the compression distribution $N(x)$ are prominent. The assumption of smearing U-frames over spacing L_u will govern the validity of the result.

For constant N, the effective length l_e, defined as in BS5400, is relevant to the buckling wavelength. When there are more than three discrete U-frames within the half buckling length, the result by smearing U-frames over L_u is expected to be sufficiently accurate.

To be consistent, let N_{el} be the maximum force at the support that corresponds to the elastic critical load of a beam subject to distributed $N(x)$, and N_{cr} be that when subject to uniform compression. The effect of the distributed $N(x)$ is represented by ϕ as shown in equation 9.64. ϕ is a function of $N(x)$, L, EI, and even c, and the

algebraic expression is complex.

A reasonable approximation to the critical load N_{el} is

$$N_{el} = \frac{N_{cr}}{\phi} \tag{9.65}$$

When equation 9.65 is substituted into equation 9.64, F_u/N_0 is then written as

$$\frac{F_u}{N_0} = \frac{Ca_{10}}{N_{el}[(l_e/L)^2 + (L/2l_e)^2] - N_0} \tag{9.66}$$

Assume that L equals to the buckling length $\sqrt{2}l_e$, then it is

$$\frac{F_u}{N_0} = \frac{Ca_{10}}{N_{el} - N_0} \tag{9.67}$$

The effect of distributed compression force is included in equation 9.67, because N_{el} (hence σ_{cr}) takes account of that effect. It also reveals the effect of contributions from the discrete U-frames, and the jump in F_u/N_0 occurs only when N_0 approaches to N_{el}. For uniform compression force, ϕ is 1, and $N_{el} \Rightarrow N_{cr}$. But when the bottom flange is treated as a free strut, neglecting the lateral restraints from U-frames, N_{cr} reduces to N_E.

For uniform compression, by using eq.9.2 and $c = C/L_u$, equation 9.67 can be simplified as

$$\frac{F_u}{N_0} = \frac{\pi^2 L_u a_{10}}{4l_e^2} \frac{1}{1 - N_0/N_{cr}} \tag{9.68}$$

If $a_{10} = \sqrt{2}l_e/1000$ and $L_u \leq \sqrt{2}l_e/4$, then

$$\frac{F_u}{N_0} \leq \frac{0.00123}{1 - N_0/N_{cr}} \tag{9.69}$$

For a situation with distributed $N(x)$, equation 9.66 provides a general expression of F_u/N_0. Let buckling length l_b in that situation($N(x)$) equal to $\sqrt{2}l_e$ (uniform compression). When $L \Rightarrow l_b$, it leads to an expression of F_u/N_0 by

$$\frac{F_u}{N_0} \leq \frac{0.00123}{N_{el}/N_{cr} - N_0/N_{cr}} \tag{9.70}$$

It also reflects the great increase in F_u/N_0 when N_0 approaches N_{el}. In practice,

if N_{el}/N_{cr} is taken as 2.0, and N_0 as 0.8 N_{el}, F_u/N_0 given by equation 9.70 is 0.003. If N_{el}/N_{cr} is 1.0 (equation 9.69), and N_0 is still 0.8 N_{el}, then F_u/N_0 is 0.0015. They are all smaller than 0.01, the value used in design practice (usually $F_u/N_0 > 0.01$. The reason for this is that both equations 9.69 and 6.70 are only for the elastic range, while in practice, yielding occurs, and the ratio F_u/N_0 will be governed by the yielding rather than the elastic critical load. Further discussion is given in the following section.

Ultimate U-frame force – an upper bound approach

In design, σ_{cr} is usually beyond the yield stress f_y, so that N_0 never reaches N_{el}(or N_{cr}), because of yielding.

An upper bound value of F_u can be found by modelling the bottom flange as a mechanism, in which a plastic hinge develops midway along the buckling wave length ($\sqrt{2}l_e$). This is likely because of the initial imperfection, as shown in Fig.9.8.

The deflections due to flexure of the two halves are neglected in comparison with those due to the rotation of the hinge. The lateral restraint forces induced from the U-frames are neglected too, so that the lateral deflection y is an upper bound value. The stress distribution across the section at the hinge appears also in Fig.9.8. The cross section of the bottom flange at the hinge is divided into three zones. The inner zone 2 is regarded as providing the compression N, and the outer zones 1 and 3 are regarded as providing equal compressive and tensile forces which constitute the bending moment M_{pf} at the hinge.

$$N = f_y t_f (b_f - 2e) \qquad (zone2) \tag{9.71}$$

and

$$M_{pf} = f_y t_f e(b_f - e) = Ny \tag{9.72}$$

The deflection is found as

$$y = \frac{b_f}{4}(\frac{N_y}{N} - \frac{N}{N_y}) \tag{9.73}$$

where $N_y = f_y b_f t_f$.

The upper bound value of F_u is then expressed as

$$F_u = Cy = C\frac{b_f}{4}(\frac{N_y}{N} - \frac{N}{N_y}) \tag{9.74}$$

and the ratio of F_u/N is by

$$\frac{F_u}{N} = \frac{Cb_f}{4N_y}[(\frac{N_y}{N})^2 - 1] \tag{9.75}$$

Fig.9.9 illustrates the variation of F_u/N with the axial force N. The abscissa represents F_u/N, the ratio of the lateral restraint force to the compressive force, and the ordinate represents the N/N_{cr}(or N/N_{el}), the ratio of the axial force and the elastic critical load.

The curve OAB is given by equation 9.69, that is based on the elastic BEF theory. The half buckling wavelength is assumed as $\sqrt{2}l_e$(also related to initial imperfection $a_{10} = \sqrt{2}l_e/1000$). The U-frame spacing L_u is taken as $\sqrt{2}l_e/4$, the maximum spacing of L_u, for which the assumption of smearing U-frames is valid (equation 9.5). Reducing L_u will decrease the ratio F_u/N (equation 9.68), so that the curve corresponds to an upper value of F_u/N.

The curves AC and BD correspond to equation 9.75 from the plastic mechanism. Length of the plastic mechanism is also $\sqrt{2}l_e$. The ratio b_f/a_{10} is taken as 10, and 20 respectively. When $N_{cr} = 2N_y$, F_u/N follows the curve OA, and at point A, $(N \Rightarrow N_y)$, it will increase very fast. For the situation of $N_{cr} = N_y$, the ratio F_u/N follows curves OB and BD.

Theoretically, collapse occurs at the intersection points A and B of the curves. However, because of residual stress and imperfection in the cross sections, the real failure takes place at a level of load lower than the intersection points A and B accordingly. It is found that whenever $N_{cr} > N_y$, large deflection occurs at the collapse loads (A and B) of the mechanism when N approaches to N_y. It is more likely that large lateral force will be induced, although the lateral restraints are neglected in the mechanism model. Therefore, when the critical load N_{cr} (or N_{el}) exceeds the yield load(N_y), the lateral force increases when the compression in the flange approaches N_y.

When $a_0 = \sqrt{2}l_e/1000$ and $L_u = \sqrt{2}l_e/4$ (influence from b_f/a_{10} negligible as

shown in Fig.9.9), the values F_u/N at onset of the collapse (A and B) are about 0.25%($N_{cr} = 2N_y$) and 0.7%($N_{cr} = N_y$). If 80% post ultimate bending strength of a beam is considered(on curves BD and AC), the ratio F_u/N ranges from 1.5% to 2.5%.

These values agree with the test results of specimen U5. At the onset of the lateral buckling(yielding also occurred), the ratios of F_u/N (only in the U-frames closest to the central supports) from the test were 0.8% and 0.5%, higher than 0.25%, but lower than 1.5%. This is because initial lateral imperfection in the specimen is larger than that leading to equation 9.69. This ratio increases to 1.2% and 3.1% at the post-ultimate state (stage 36, 90% of the ultimate bending strength).

9.4.2 Rigid U-frames

For a strut with lateral restraints along its length, the minimum stiffness of the lateral restraints, at which the restraints behave as if absolutely rigid is

$$C_i = \frac{\alpha N_u}{L_u} \tag{9.76}$$

where N_u is $\pi^2 EI/L_u^2$, α is a function of n, the number of restraints within its span. The values of α are given in Table 9.3. They are derived from the results reported by Timoshenko(Table 2-3, p76, [84]).

When an imperfect strut is loaded, the lateral restraint force F is found as (appendix 3 in [73])

$$\begin{aligned} F = Cy &= C_i(y_0 + y) \\ &= C_i y_0 \frac{1}{1 - C_i/C} \end{aligned} \tag{9.77}$$

where

- C is the stiffness of the lateral restraints.
- y_0 is the initial imperfection of the strut.
- C_i is the minimum stiffness given in equation 9.76.

When the bottom flange of a beam with discrete U-frame action is modelled as

such a strut that the U-frame restraint to this free flange is sufficiently stiff, equation 9.77 can be used to evaluate the lateral restraint forces. However, for most beams, the lateral stiffness provided by U-frame, is much smaller than C_i (equation 9.76).

9.4.3 Assessment of U-frame force

For composite beams with discrete U-frame action, the flexible U-frame is appropriate.

As the bottom flange is modelled as a strut with lateral restraints along its length, the effects of the torsional rigidity and the distortion of the cross section of a beam can be compensated by introducing the elastic critical stress based on the distortional buckling model described in section 9.3.

For a composite I-section, the stress in the bottom flange can be calculated from the bending moment acting on the section, so that the compressive force in the flange is known (elastic range). Therefore, the compressive force N in the bottom flange is related to the moment on the cross section, M by

$$\frac{N}{N_{el}} = \frac{M}{M_{cr}} \tag{9.78}$$

where

- M_{cr} is the elastic critical moment of the beam.
- N_{el} is the hypothetical elastic critical force for the bottom flange.

Lateral restraint forces actually decrease away from internal supports of a continuous beam, so that assessment of the U-frame force depends not only on the magnitude of M_{cr}, but also on moment gradients. Equations 9.66, 9.67, (or 9.69 and 9.70) and 9.75 provide general expressions of F_u/N_0 in different conditions (elastic and ultimate plastic states), but they do not reflect that variation of lateral restraint forces along the beam length.

Tests on discrete U-frame beams (specimen U5) show that the discrete U-frames (stiffeners) closest to the supports were subject to larger lateral forces than those frames further away, because failure of U-frame connections occurred at these sections rather than at the sections far away from the central supports. A test evidence is that lateral deformation of bottom flanges mainly occurred in regions close

to the supports (the maximum hogging bending moment). When lateral buckling initiated(stage 26), at positions of U-frames closest to the supports, the ratios of F_u/N_{max} (N_{max} is the maximum compression force in bottom flanges) were 0.8% and 0.5%, for U-frames with double sided stiffeners and single sided stiffeners respectively(see chapter 8).

Although these test results do not tell the exact distribution of lateral restraint forces in the beams (U5A and U5B), they suggest that advantage be taken in assessment of U-frame force. Therefore, following assumptions are made:

- at each U-frame section, the ratio $F_{u(i)}/N_i$ is proportional to the value of F_u/N_0 given by equations 9.66, 9.67, and 9.75, where $F_{u(i)}$ is the lateral force at the position of U-frames, and N_i is the compression force in the bottom flange at the same position,

- a uniform compression force N_i is assumed between every two U-frames as shown in Fig.9.10. It is taken as a mean value of the compression forces at the locations of the two adjacent U-frames.

- the lateral buckling length is $\sqrt{2}l_e$, so that in the elastic range, equation 9.67 (hence equation 9.70) is generally applicable, with elastic critical load N_{cr} (N_{el}) relevant to its corresponding moment gradient, or with ratio N/N_{el} determined by equation 9.78.

According to these assumptions, the lateral force decreases further away from internal supports of a continuous beam, depending on the moment gradient in the beam. If N_i at the positions of a U-frame is no longer a compression force, it does not mean the lateral force F_u is zero, but suggests that F_u is so small, that strength of U-frames does not govern.

When M_{cr} is smaller than M_y, (the yield moment of the cross section), the ratio F_u/N_0 (hence $F_u(i)/N_i$) is expressed

$$\frac{F_u}{N_0} \leq \frac{0.00123}{1 - N_0/N_{cr}} \tag{9.69}$$

where N_0 is the maximum force expected in the bottom flange, N_{cr}(for uniform compression) or N_{el}(for distributed compression) is the elastic critical load. Although

l_e, which is used in developing the equation, is irrelevant to M_{cr}, the effects of the torsional rigidity and the distortion as well as the moment gradient can be compensated more or less by using M_{cr}, evolved from the distortional buckling model. The lateral U-frame force $F_{u(i)}$ is then determined.

When M_{cr} is greater than M_y, F_u can be evaluated as about 1.5% of the maximum compression force (taken N_y), based on the upper bound approximation. This ratio actually takes account of about 80% post-ultimate bending strength of a beam. The lateral force $F_{u(i)}$ is then calculated according to this ratio.

9.5 Design method for distortional lateral buckling of discrete U-frame composite beams

The design method proposed here is for the composite beams with discrete U-frames equally spaced along the beam length. The moment gradient is also considered, and the ratio of L/L_u should be greater than 10.

9.5.1 Transverse stiffness of U-frames

Fig.9.4 illustrated the cross section of an inverted composite U-frame beam. The transverse stiffness per unit length of the beam, k_θ is defined (referred to equation 8.13) by

$$\frac{1}{k_\theta} = \frac{1}{k_1} + \frac{1}{k_2} + \frac{1}{k_3} \tag{9.79}$$

where k_1, k_2 and k_3 are the transverse stiffnesses of the web, the slab and the connection, which comprise the U-frame given by

$$k_1 = \frac{3EI_1}{h_s L_u} \tag{9.80}$$

and

$$k_2 = \frac{4EI_2}{B} \tag{9.81}$$

for a slab continuous across the steel beam or

$$k_2 = \frac{2EI_2}{B} \tag{9.82}$$

for a simply supported or cantilever slab. and

$$k_3 = \frac{1}{f_r L_u} = \frac{b_s b_f h_d E_{cm} N}{300 L_u} \tag{9.83}$$

A similar approach to equations 8.14, 8.15, and 8.16 is used in deriving equations 9.80, 9.81(or 9.82) and 9.83. But in equations 9.80 to 9.83, d_1^3/d_2^2 and d_3^2/d_2^2 are replaced by h_s (Figs.8.10 and 9.4). EI_2 in equations 9.80 and 9.81 based on per unit width is also different that in equation 8.9, which is for per effective U-frame.

The properties used in the above equations are as follows:

- E, E_{cm} are Young's modulus for steel and the short-term elastic modulus for the concrete,

- I_1 is the second moment of area of the effective stiffened section about the vertical axis of bending, including a width of web plate of up to 16 times of the web thickness on each side of the stiffener,

- EI_2 is the 'cracked' flexural stiffness per unit width of the composite slab, and I_2 should be taken as the lower of

  - the value at midspan, for sagging bending;

  - the value at an internal support, for hogging bending.

  with a width of the slab on either side of the U-frame, equal to $B/8$, or $L_u/2$, whichever is less,

- L_u is the distance between U-frames,

- h_s is the distance between the shear centres of the flanges of the steel member,

- B is the distance between centers of adjacent beams,

- b_f and t_f are the breadth and thickness of the steel flange,

- b_s is the breadth of the web stiffener,
- h_d is the overall height of the studs,
- N is the number of the effective connectors within a longitudinal distance $2l_n$ of the nearest part of the web stiffener. where

$$l_n = 28 b_f (\frac{t_f}{b_f})^{1.4} \tag{9.84}$$

9.5.2 Strength of U-frame connections

The strength of a discrete U-frame connection should be checked both for shear failure and the top flange failure.

The shear strength of the U-frame connection is

$$M_{pr1} = \frac{V_{cr} a_c}{1 - a_c/B} \tag{9.85}$$

and the strength of the top flange is

$$M_f = 1.414 b_f t_f^2 f_y \tag{9.86}$$

where V_{cr} is the characteristic shear resistance of the concrete slab, which is calculated from [71]

$$V_{cr} = \gamma_c h_c b_{eff} \tau_{Rd} (1.2 + 40\rho) \tag{9.87}$$

with the properties of the parameters

- h_c,b_{eff} are the effective depth and breadth of the slab.
- τ_{Rd} is the basic shear strength, given in Eurocode 2, including a partial safety factor $\gamma_c = 1.5$.
- ρ is the tensile reinforcement ratio in the slab.

and a_c is effective distance between the studs, which is proposed to be two-thirds of the width of flange that is stiffened [71].

9.5.3 Elastic critical moment – a lower bound energy approach

As discussed in section 9.3.2, the potential energy of a discrete U-frame beam can be modeled as that for a beam with continuous U-frame, provided that the assumption of smearing U-frames over their spacing is valid. In the notation of EC4 [1], the elastic critical moment is found as in eq.9.25.

The notations of the parameters are the same as those for continuous U-frame beam, except that k_θ is the transverse stiffness of the discrete U-frame, calculated by eq.9.79.

9.5.4 Design curves for distortional lateral buckling

For design, the effects of inelasticity, residual stress and imperfections are represented by a curve of Perry-Robertson type, which gives a design stress or resistance as a function of the relevant slenderness parameter, based on the elastic critical stress.

The design curves based on non-distortional lateral buckling of steel I-sections are well authenticated in current and draft codes of practice. However, not enough test results are available for distortional lateral buckling, to enable a design curve to be deduced, so that it is assumed that the design curves for non-distortional lateral buckling are valid also for the distortional lateral buckling. This is checked against the few available tests on distortional lateral buckling, with the elastical critical moment based on the distortional buckling model.

9.6 Discussion and comparison

The transverse stiffness of U-frames k_θ is related to the stiffness of lateral restraint to the bottom flange (BEF theory), c by

$$k_\theta = ch_s^2 = \frac{Ch_s^2}{L_u} \tag{9.88}$$

The final expressions of the bifurcation load from the BEF theory and from the distortional buckling model are quite similar.

When the beam length is very long, or $GI_{at} << k_\theta L^2/\pi^2$, eq.9.25 is simplified as

$$M_{cr} \approx \frac{k_c C_4}{\pi}\sqrt{k_\theta E I_{afz}} \tag{9.89}$$

On the other hand, introducing η, the distributed compression compensation factor, the critical load N_{el} from the BEF theory, is written as

$$N_{el} = \frac{2}{\eta^2}\sqrt{EIc} = \frac{2}{\eta^2 h_s}\sqrt{EI_{afz}k_\theta} \tag{9.90}$$

where the relationships of $I = I_{afz}$ and $c = C/L_u = k_\theta/h_s^2$ are used.

For uniform compression in the bottom flange(or constant bending), $\eta = 1$ and $C_4 = 6.2$, and this leads to

$$M_{cr} \approx 2k_c\sqrt{k_\theta E I_{afz}} \qquad \text{(distortional buckling model)} \tag{9.91}$$

and

$$N_{el} = \frac{2}{h_s}\sqrt{k_\theta E I_{afz}} \qquad \text{(BEF theory)} \tag{9.92}$$

This similarity of the buckling loads is owing to the similar treatment of the lateral restraints from the U-frames. However, the distortional buckling model is much more comprehensive, because it includes the cross section shape factor k_c and web distortional effect, which is reflected in C_4, especially when non-uniform bending is considered.

The effect of moment gradient is introduced by C_4 in Eurocode 4 method. It is similar to factor η, introduced in section 9.2. When these two theories are used, it (the effect) is expressed

$$\frac{M_{cr}}{M_{cr0}} = \frac{C_4}{6.2} \tag{9.93}$$

where M_{cr0} and 6.2 are elastic critical moment and value of C_4 under uniform bending moment, and

$$\frac{N_{el}}{N_{cr}} = \frac{1}{\eta^2} \tag{9.94}$$

Assume that moment M on a composite beam is proportional to axial force N

in its bottom flange, then it leads to an equivalent η based on C_4:

$$\eta_{ec4} = \sqrt{\frac{6.2}{C_4}} \tag{9.95}$$

Comparison of the two η is shown in Fig.9.11. For each corresponding loading, the Eurocode 4 method gives a higher value of η (from C_4). They all correspond to a βL between 2 and 3 on the curves based on the BEF theory. The reason is that the former method(EC4) takes account of web distortion, torsional rigidity, cross-section shape etc, while the latter method(BEF) only models the bottom flange. Therefore, the EC4 method is more rational, and less conservative.

The application of the BEF theory to the discrete U-frame beams is governed by eq.9.6 (or $\sqrt{2}l_e > 4L_u$), so that whenever the lateral stiffness of the U-frame at the bottom flange level(a strut in the BEF model) is less than the minimum stiffness required (a variation of equation 9.6, $C \leq C_i = 0.38\ EI_{afz}/L_u^3$, I=$I_{afz}$), accurate results can be obtained from the BEF model. The stiffness C (U-frame) consists of three parts contributed from the slab, the stiffened web and the U-frame connection. For a specific U-frame, suppose the stiffness C is one third of that of the stiffened web C_w, which is written as

$$C = \frac{C_w}{3} \approx \frac{EI_s}{h_s} \tag{9.96}$$

then it leads to

$$\frac{I_s}{I_{afz}} \leq 0.38(\frac{h_s}{L_u})^3 \tag{9.97}$$

The approach of using distortional buckling model reveals a criterion of $L/L_u > 5 \sim 10$ for the validation of smearing U-frames over their spacing. $L/L_u > 10$ for the validation of smearing U-frames over their spacing. In design practice, the span/depth ratio of a beam (L/($h_s + h_c$)) ranges from 15 to 30, and assuming h_c is 1/4 h_s (h_c is depth of the concrete slab), then the range for L_u/h_s is

$$\frac{L_u}{h_s} \leq 1.875(L_u/h_s + h_c = 15) \sim 7.5(L_u/h_s + h_c = 30) \tag{9.98}$$

In design practice, L_u/h_s ranges from 1 to 2.5 (considering shear), so that the condition of smearing U-frames is usually satisfied.

9.7 Summary of conclusions

The validation of using BEF theory is governed by the transverse stiffness of U-frames.

The elastic critical loads benefit from the distributed compression. A parameter η based on the relevant numerical studies of struts with varying compression is introduced to modify the present BS5400 method for the prediction of critical buckling stress.

The design method for continuous U-frames is developed to cover the discrete U-frame beams. The transverse stiffness of a U-frame is assessed in accordance with the relevant contributions from the slab, the stiffened web and the connection.

The U-frame force is influenced by the U-frame stiffness, the moment gradient, and the magnitude of the elastic critical stress in the bottom flange. When the stress in the bottom flange is beyond yield, the ultimate U-frame force is found, based on an upper bound plastic mechanism.

Table 9.1: Elastically supported column subject to a varying axial force(λ_{el})

	Case				
βL	1	2	3	4	5
0	1.000	1.881	2.355	5.824	2.835
1	1.010	1.899	2.376	5.856	2.860
2	1.164	2.166	2.694	6.309	3.235
4	3.628	5.472	6.450	11.06	8.044
6	7.326	10.91	12.86	20.06	19.48
8	13.67	18.06	20.91	30.99	33.16
10	20.41	26.92	30.75	43.62	47.21
12.5	31.66	40.41	45.51	61.89	66.65
15	45.79	56.56	63.00	82.97	88.86
17.5	62.75	75.35	83.20	106.8	113.9
20	81.63	96.78	106.1	133.5	141.7

Table 9.2: Calculated η for varying axial force

	Case			
βL	2	3	4	5
0	0.729	0.652	0.414	0.594
1	0.729	0.652	0.415	0.594
2	0.733	0.657	0.430	0.600
4	0.814	0.750	0.573	0.672
6	0.819	0.755	0.604	0.613
8	0.870	0.809	0.664	0.642
10	0.871	0.814	0.684	0.658
15	0.900	0.853	0.743	0.718
20	0.918	0.877	0.782	0.759

Table 9.3: Values of α

n	1	2	3	4	5	6	∞
α	2	3	3.41	3.63	3.73	3.80	4

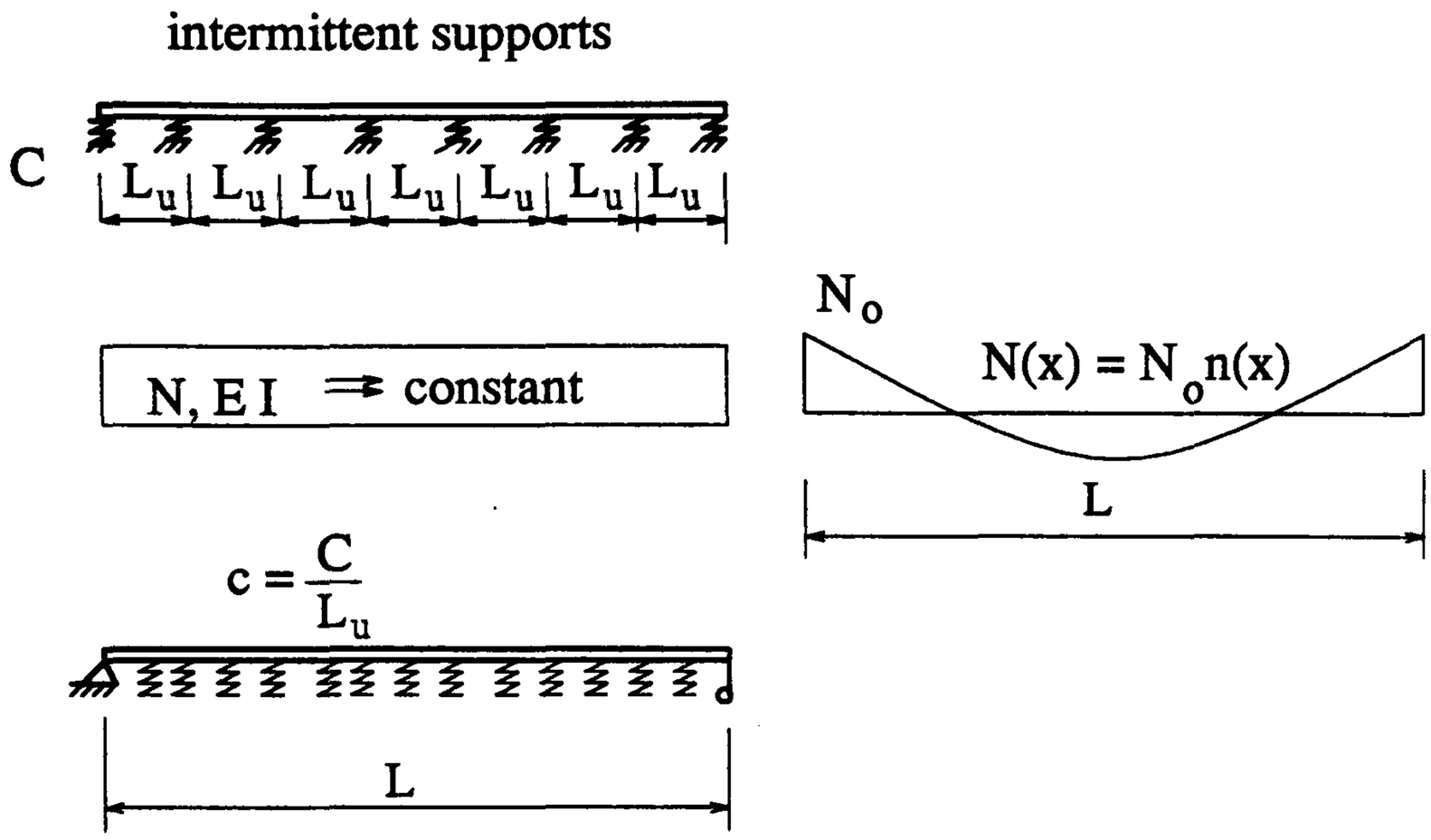

Figure 9.1: Elastically supported beams

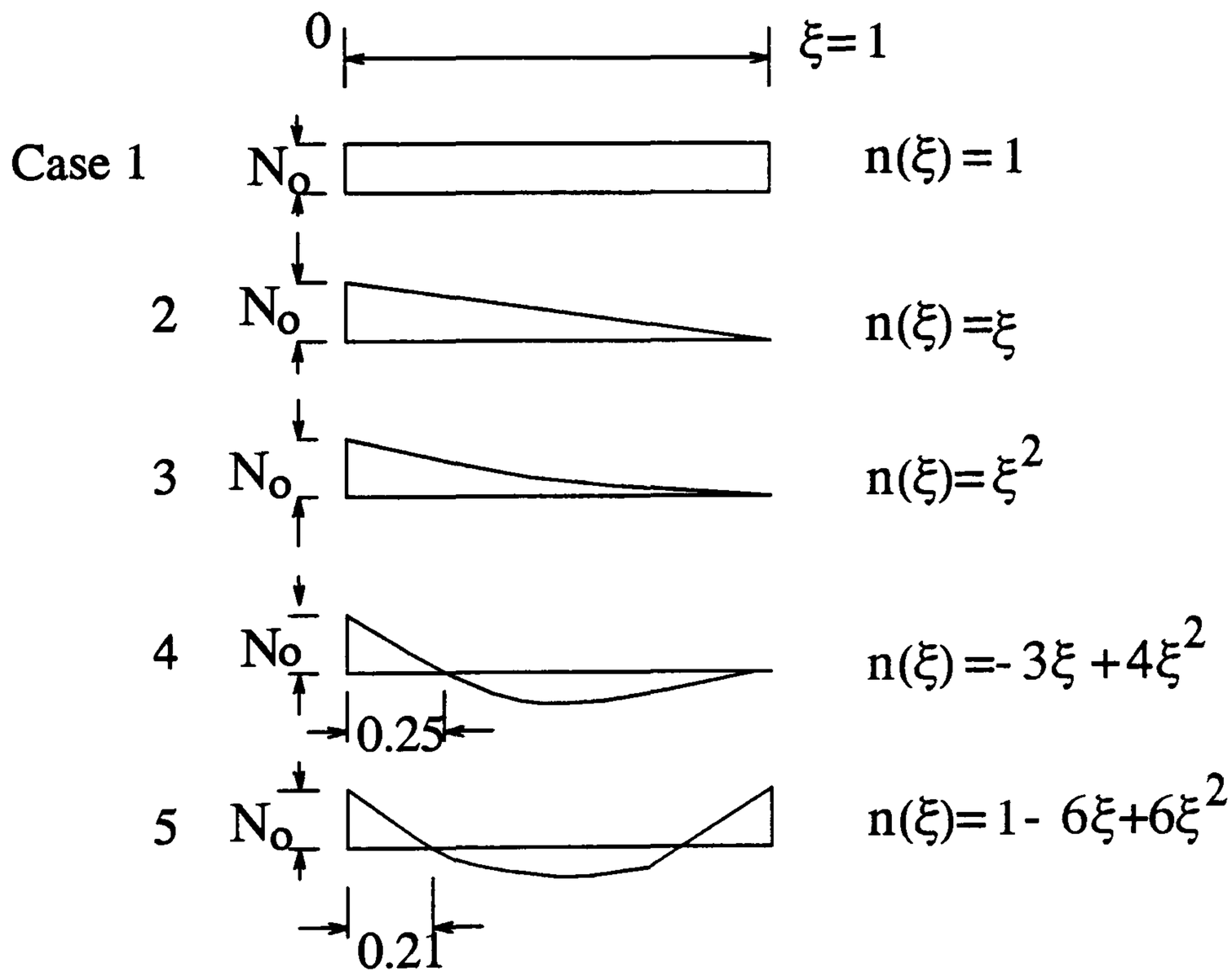

Figure 9.2: Cases of varying axial force N(x)

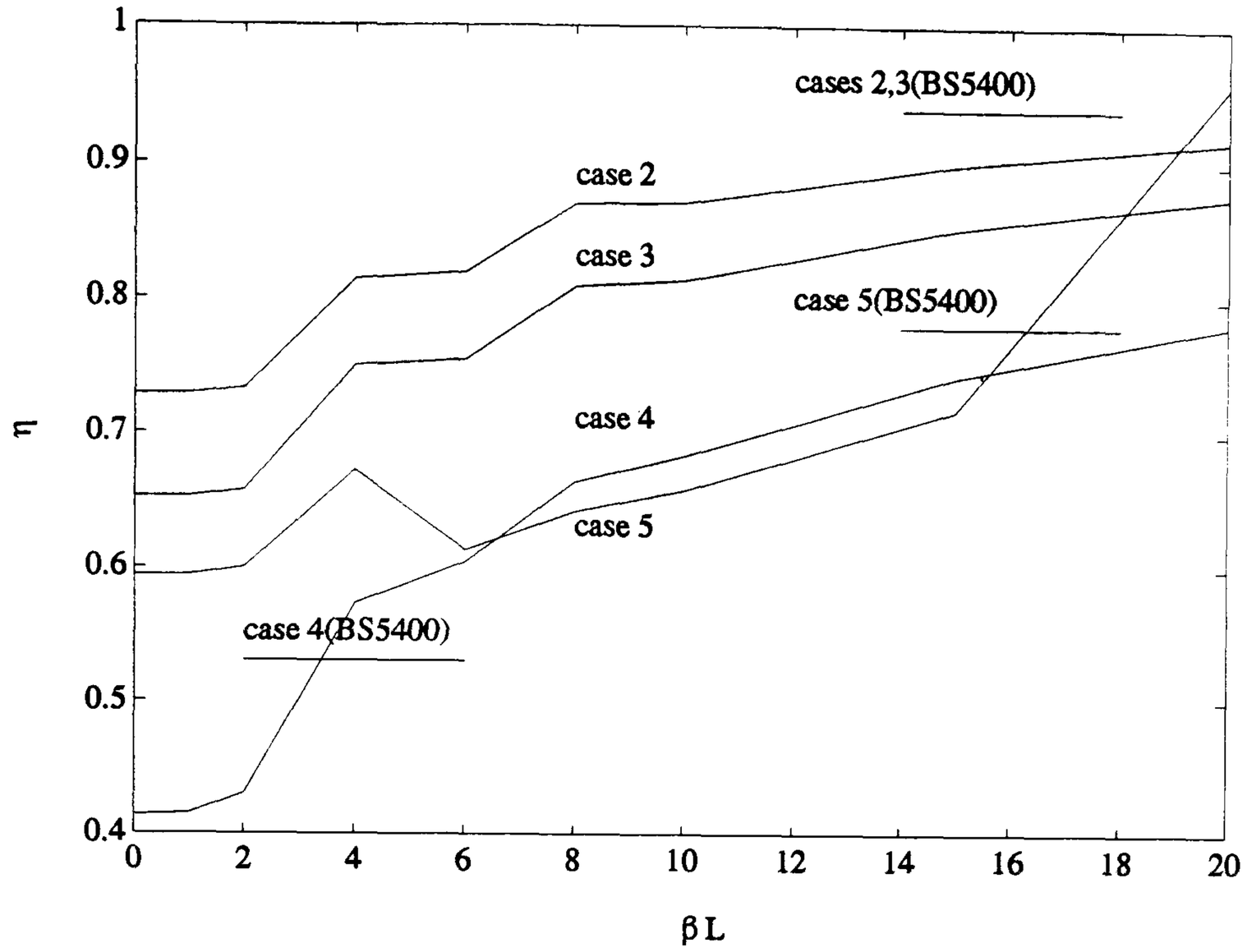

Figure 9.3: Influence of βL

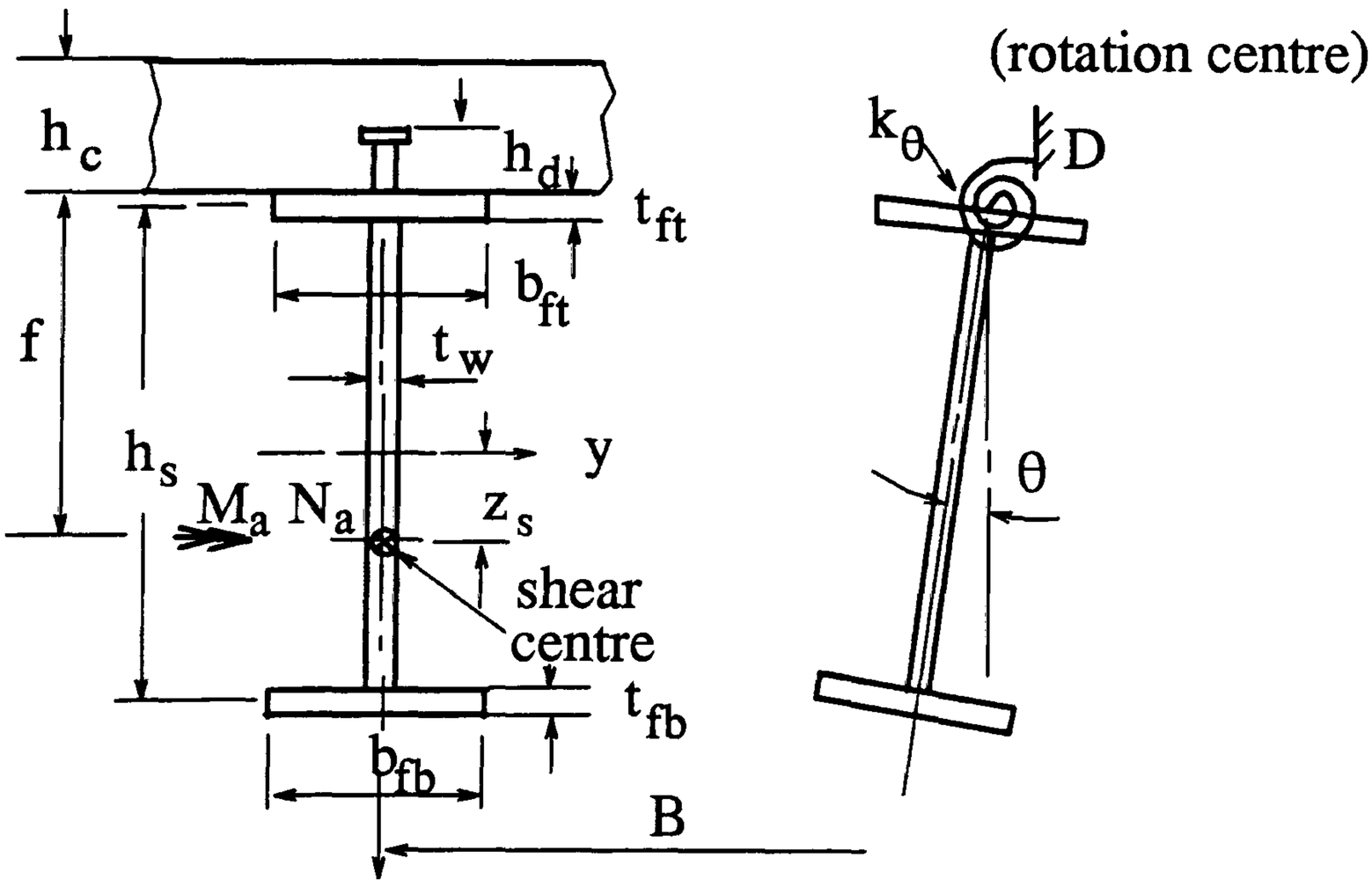

Figure 9.4: Notation of distortional buckling model

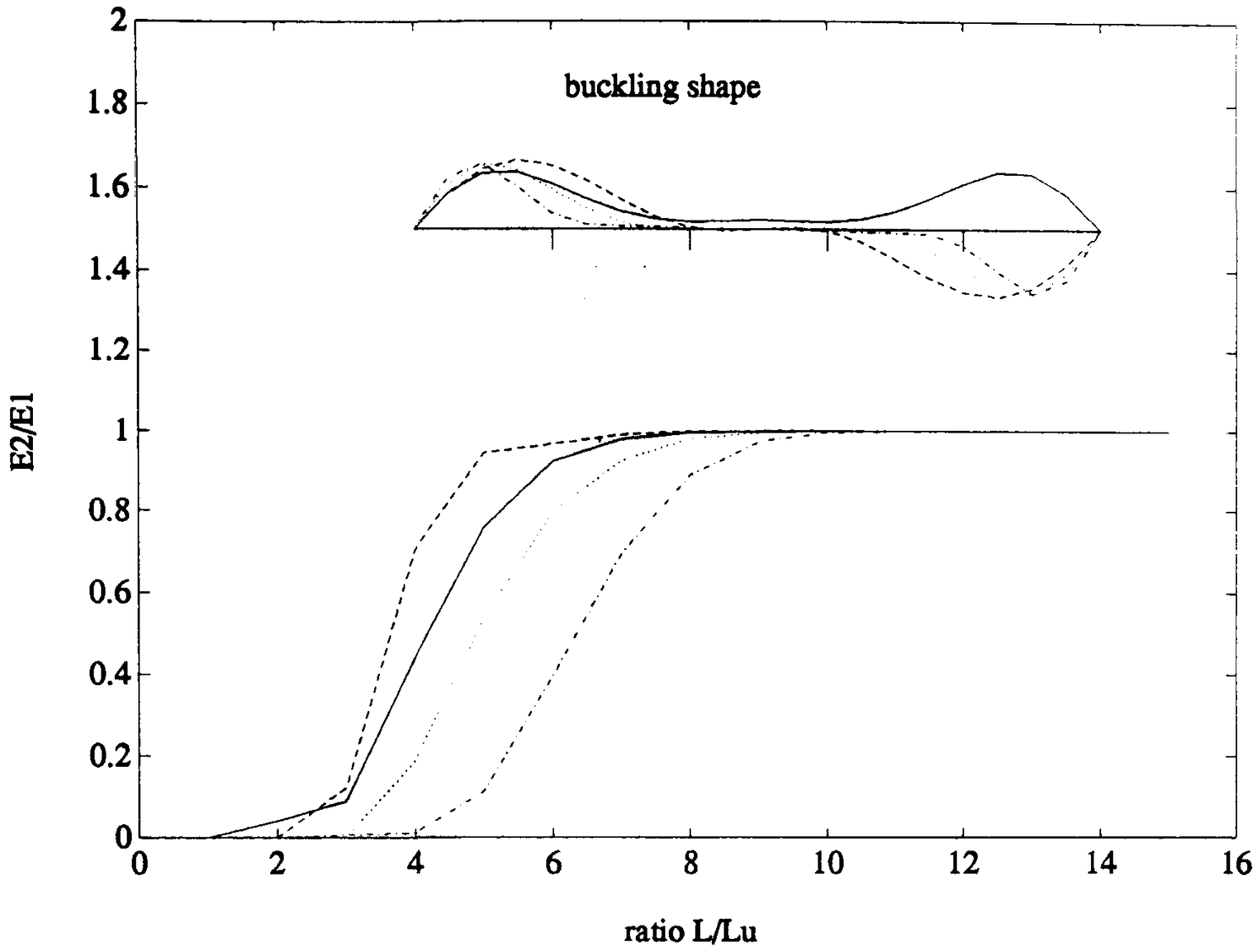

Figure 9.5: Energy evaluation

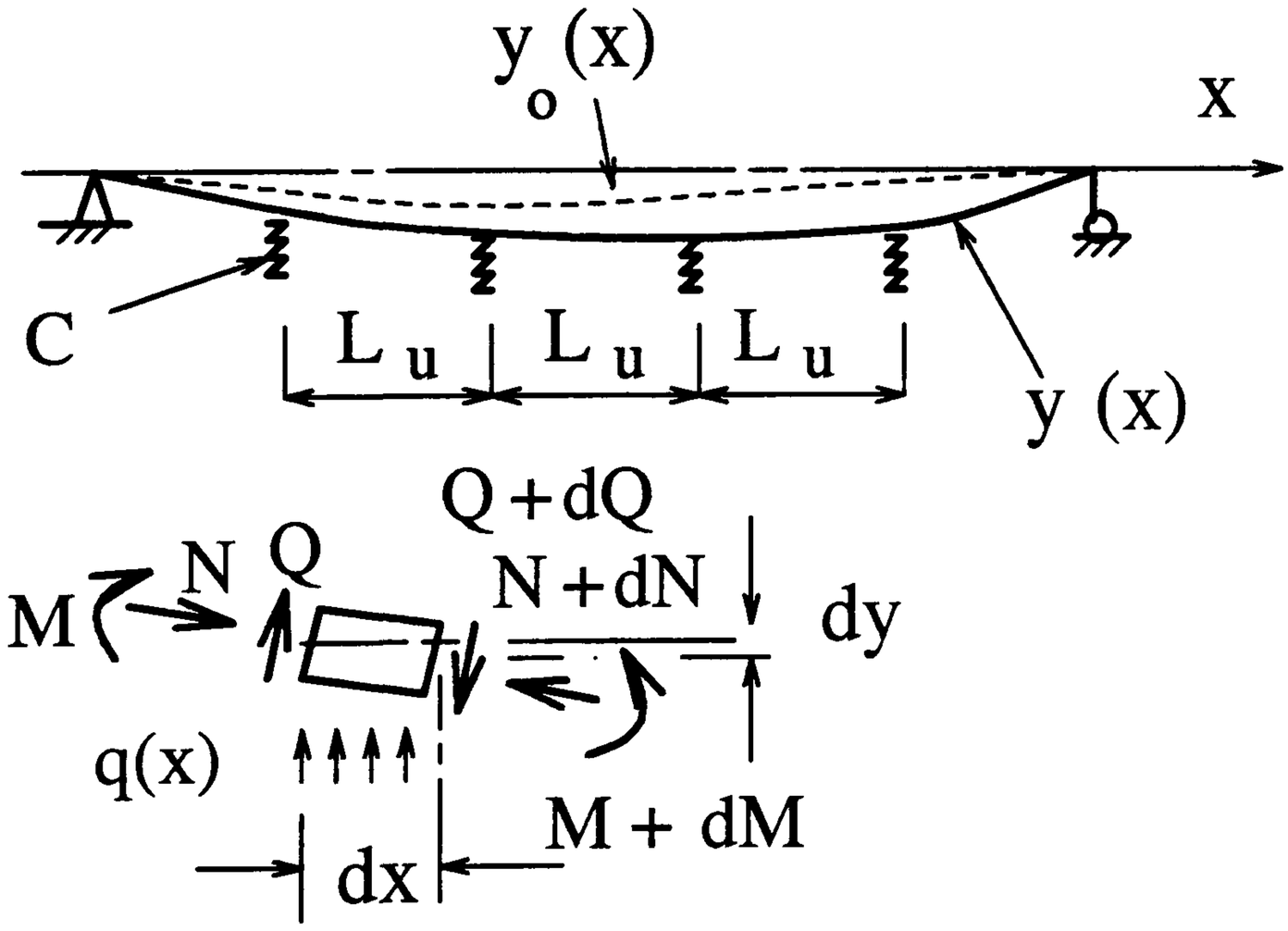

$$q = (y - y_o)\, c$$

$$c = C / L_u$$

Figure 9.6: Modeling the bottom flange

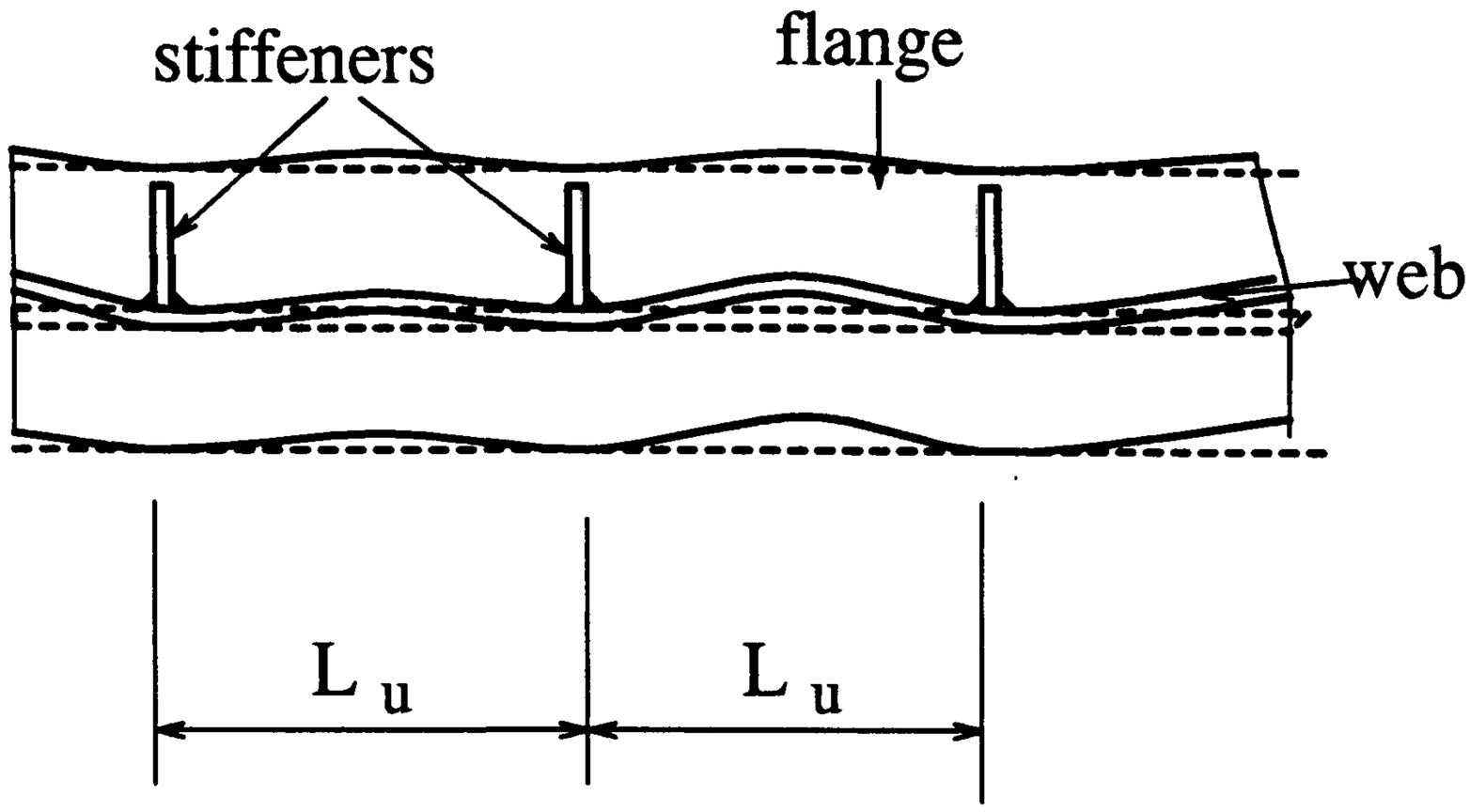

Figure 9.7: Initial imperfection in a welded bottom flange

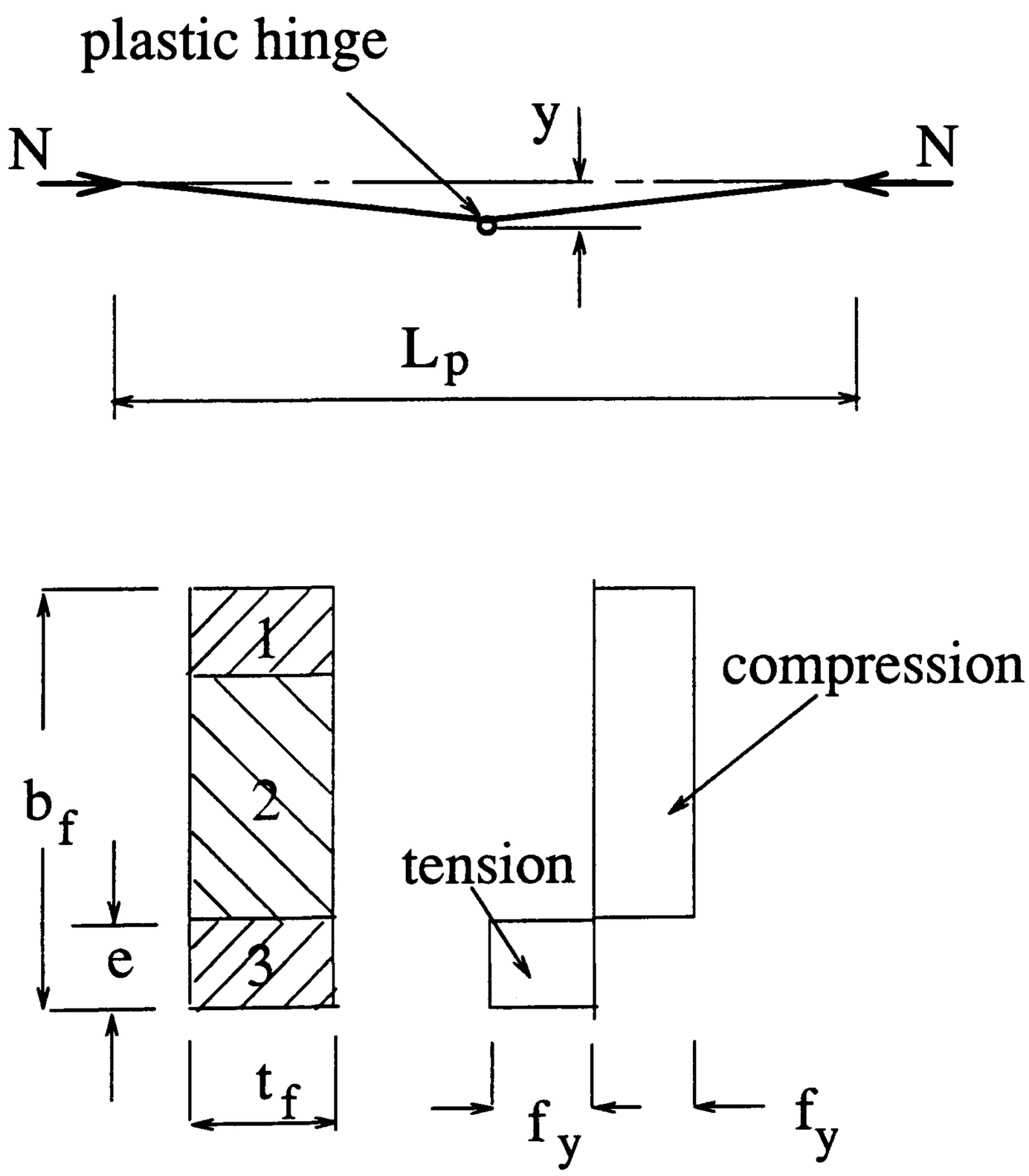

Figure 9.8: An upper bound mechanism of the bottom flange

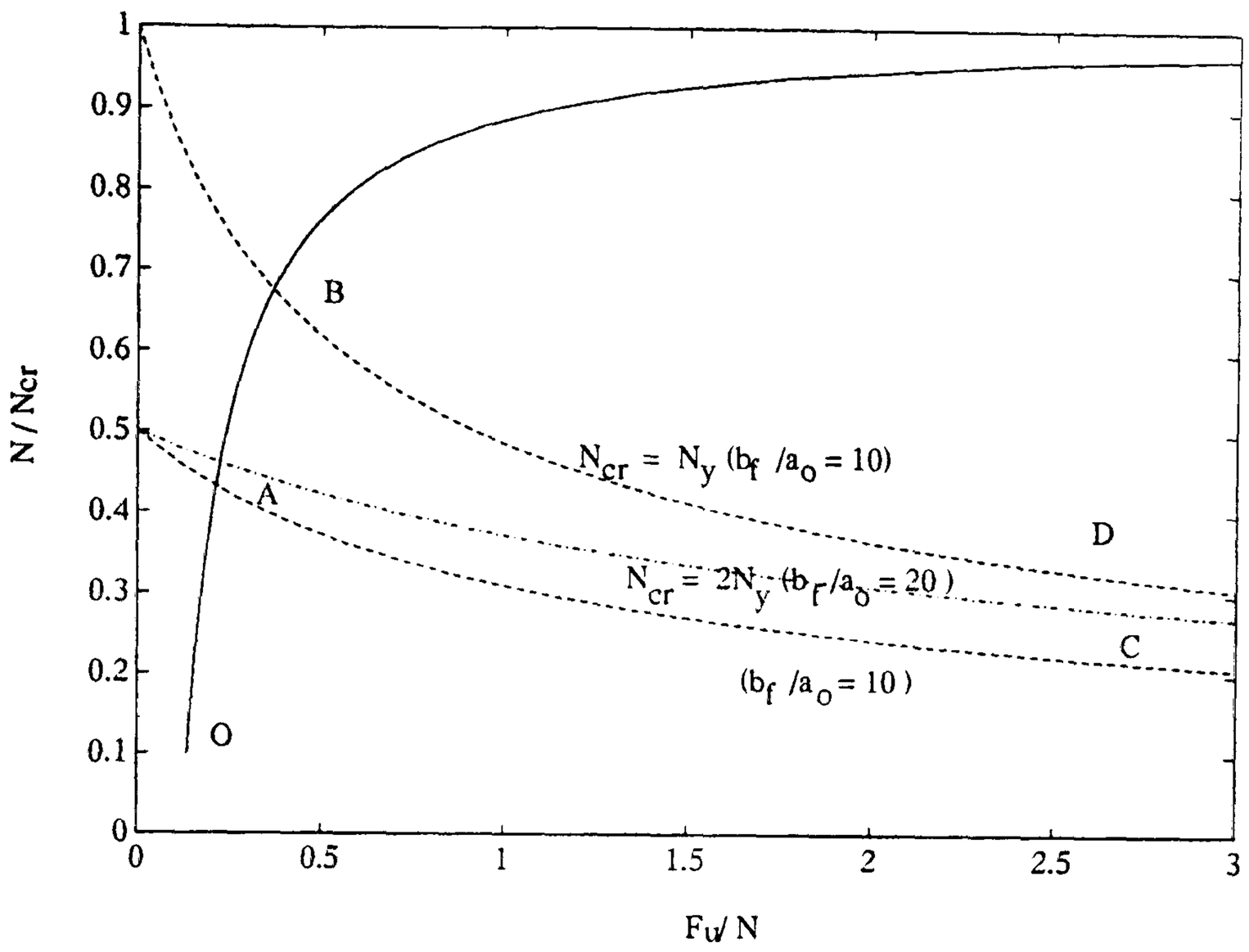

Figure 9.9: Variation of lateral restraint force

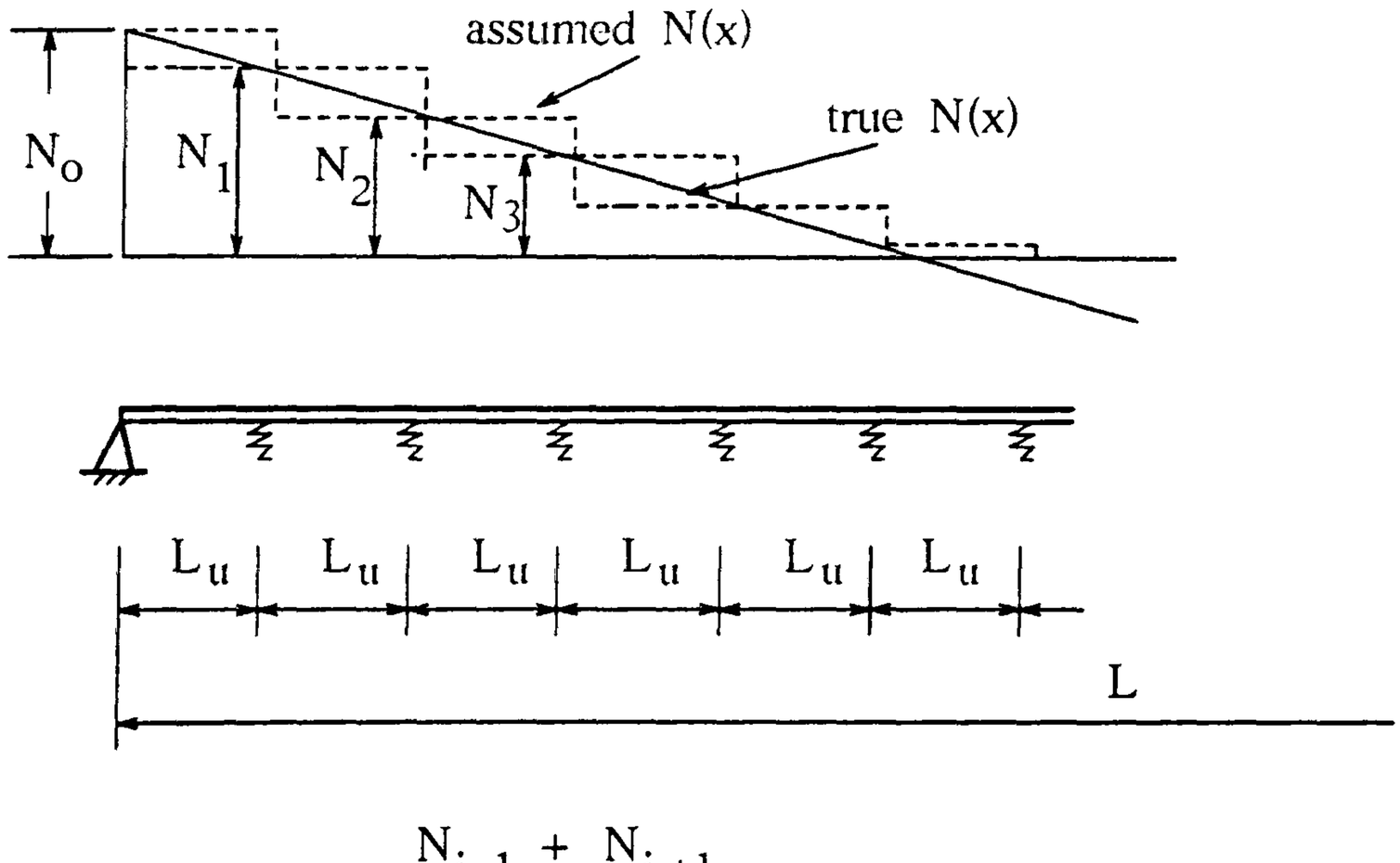

$$N_i = \frac{N_{i-1} + N_{i+1}}{2}$$

Figure 9.10: Assement of lateral U-frame force

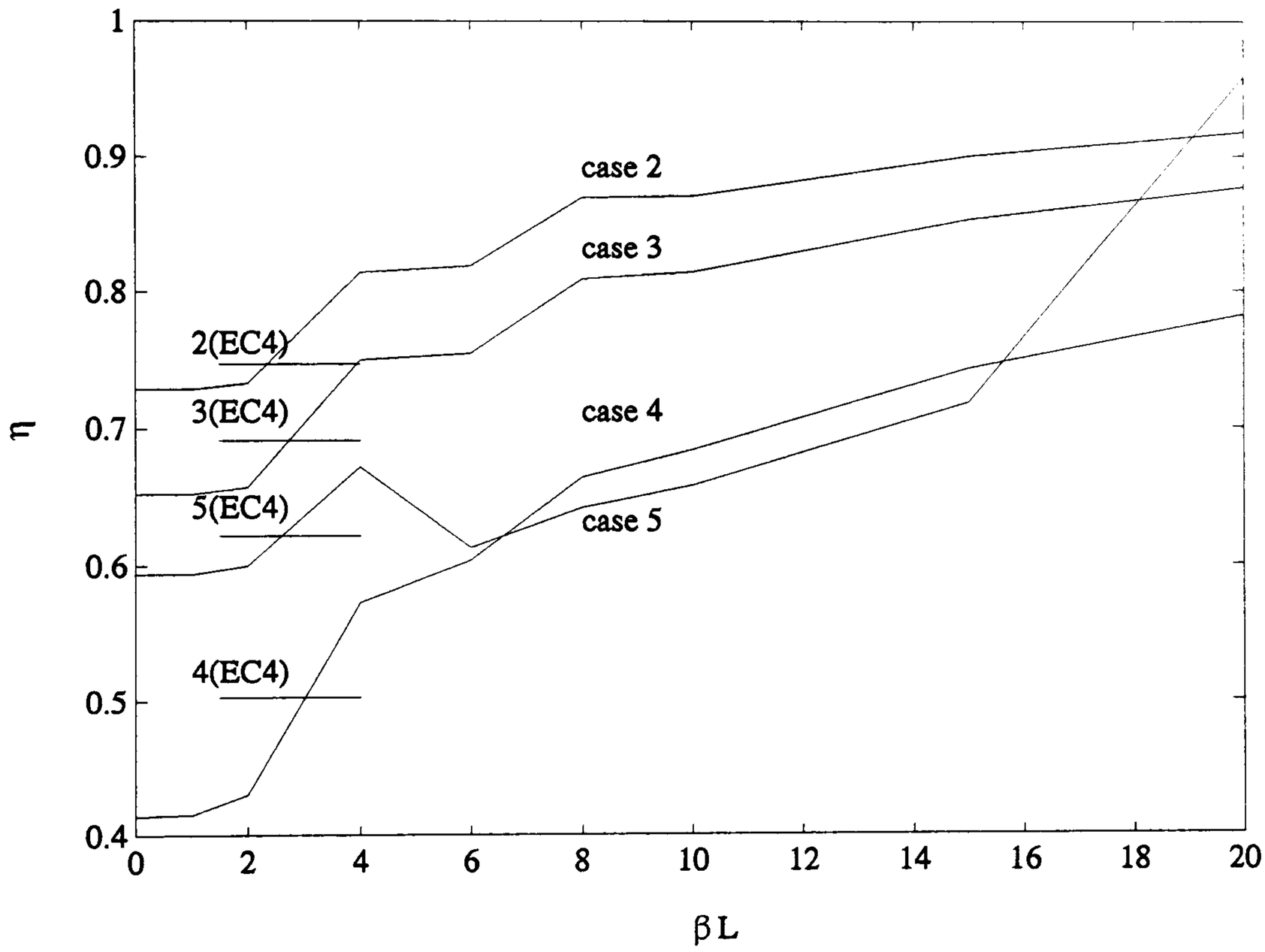

Figure 9.11: Comparion of moment gradient effect

Chapter 10

Conclusions and design recommendations for composite beams with U-frame action

10.1 Summary of conclusions

Distortional lateral buckling was found in the tests of the two composite beams with U-frame action. Web distortion was effectively reduced by the vertical web stiffeners, which form a part of discrete U-frames together with the reinforced concrete slab and the shear connection between the steel top flange and the slab, so that the stability of a beam against the lateral buckling was much enhanced.

For specimen U4, a composite beam with continuous U-frame action, distortional lateral buckling was found prior to local buckling. The cross bracing to the bottom flange in the hogging moment regions are proved to be effective.

When the beams (U4A and U4B) were not braced, lateral buckling initiated (support moment = 218 kN/mm^2 U4B) before local buckling, but it did not govern failure of the specimen, because the beams were still capable of further loading up to a higher support moment (316 kN/mm^2 U4B) before the specimen was unloaded. Slight web local buckling was also observed before the beams were unloaded near the support regions. Therefore, the ultimate bending strength of the specimen is believed to have been governed by local buckling, relating to the slenderness of the cross section, rather than lateral buckling.

For braced beams, lateral buckling is governed by the interaction between the two adjacent segments separated by the braced cross section. It is suggested that in design for distortional lateral buckling of a braced beam, account should be taken of the upper and lower bounds of buckling resistance of each segment.

For specimen U5, a composite beam with discrete U-frame action, distortional lateral buckling was mainly concentrated within a length about three times the

depth of the steel section close to the internal support. The measurement of strain in the studs above the steel top flanges of stiffeners that are close to the support section and comprise discrete U-frames, shows that the U-frame restraint force increased proportionally with the support moment M (and hence with the main load) before buckling failure of the beam. No significant U-frame force was found even at the onset of the buckling (lateral or local), however, the force was observed to be increasing steeply when the ultimate bending strength of the beam had been reached. The lateral restraint force provided by a U-frame is also influenced by the stiffness of the U-frame. It was found in the tests that the less stiffer the U-frame has, the smaller the U-frame force is. The U-frame connection between the slab and the top flange failed after maximum moment had been reached.

Similar to specimen U4, the ultimate strength of specimen U5 is governed by local buckling rather than lateral instability, although these two buckling modes may associate with each other. The moment rotation curves of the two specimens are so similar that it is likely that local buckling governs the design of composite beams in hogging bending.

Both specimens U4 and U5 have the identical cross section, which is classified as Class 4 cross-section in accordance with Eurocode 4: Part 1 [1], or specifically, Class 1 for flange and Class 4 for web. The web is more vulnerable to local buckling than the flange, and this was confirmed in the tests. Local buckling did not occur in either specimen until after the yield moment was attained at the support section, so that the cross-sections behaved better than Class 4 cross-sections.

The strength of a discrete U-frame is influenced by both shear failure in the U-frame connection and torsional rigidity of the steel top flange. The interactive mode of the two failures is complex. However, a simple rule to assure the strength of the connection is proposed by checking the two different failures separately. The prediction of the shear failure of a U-frame connection is based on a truss model [71], and the prediction of failure in the steel top flange is based on a rigid plastic mechanism, and they were all checked against test results.

The stiffness of a discrete U-frame depends on the three parts of the frame, i.e., the transverse flexure of the concrete slab, the shear connection (or U-frame connection) between the slab and the steel beam, and the stiffened web. The flexibility

of a U-frame connection can be predicted by a semi-empirical formula.

Theoretical study of the lateral force applied by a U-frame restraint shows that although the U-frame force is likely to be influenced by the elastic critical stress in the bottom flange, it is governed by the yielding in the flange when the elastic critical stress exceeds the yield stress, especially in the U-frames that are close to an internal support. The lateral U-frame force is also influenced by the distribution of the compression force in the bottom flange, hence by the shape of the moment diagram.

When lateral buckling occurred (stage 26), at the locations of U-frames that are closest to the support, the ratio of the lateral restraint force to the axial force in the bottom flange, is 0.8% and 0.5% for double sided stiffeners and single sided stiffeners, respectively, in specimen U5.

At the ultimate state(stage 34), when yield governs in the regions of the bottom flange, where U-frames are close to the supports, the ratio of the lateral restraint force from the U-frames to the axial force in the bottom flange at the location of U-frames is 2.6% for the double sided stiffeners used in specimen U5, and 1.1% for the single sided stiffeners. This only occurred in these regions because stress there exceeded the yield stress. Outside these regions, the U-frame force is influenced by elastic critical stress.

The fact that lateral restraint force is greater in U-frames with double sided stiffeners than that in frames with single sided stiffeners also reflects influence from spacing of U-frames. These two types of stiffeners on specimen U5 have the same magnitude of moment of area about their major axises (parallel to axis of the beams) over U-frame spacing (L_u = 1.2 m and 0.6 m for double and single sided stiffeners, respectively), so the conclusion that the less the stiffness a U-frame has, the smaller lateral force the U-frame is applied with, is subject to this condition.

The longitudinal cracks on the slab were also found at the positions above the stiffeners closest to the central section. They not only reveal failure of the U-frame connections, but also suggest that the further away a U-frame is from an internal support, the smaller lateral force the U-frame subjects to.

10.2 Improvements suggested for the current design method of composite beams with U-frame action in BS5400

Design procedures for composite beams with U-frame action include determination of the elastic critical moment in hogging bending, and of the U-frame stiffness and U-frame spacing, and assuring the strength of the U-frame connections.

The limiting stress σ_{li} is used for design to lateral buckling of U-frame beams in the Bridge Code [2], in which the free bottom flange is modeled as a strut on an elastic foundation, with constant compression along its length. As the effective length l_e is only relevant to a situation of constant compression, the effect of the non-uniform compression caused by moment gradient is neglected. The factor η used in the Code [2] to modify the slenderness λ (Clause 9.7.1) is based on a steel I-section beam, with both top and bottom flange unrestrained, so that it is not suitable for composite beams with the top flange restrained laterally and torsionally by the slab.

In order to obtain a less conservative and more realistic method for design of composite beams with inverted U-frame action, a new η is proposed, which is based on a column with elastic lateral restraint and varying compressive force along the axis [46, 48], to include the effect of moment gradient of the beam. The new η is given in Fig.9.3, or Table 9.2, in terms βL, which can be interpreted as the ratio of the span of the beam to its effective length l_e.

l_e is relevant to the buckling wave length when the compression force in the bottom flange is constant. Let us assume that it also applies to the situation of varying force in the bottom flange. When the hogging bending moment of a beam with U-frame action is designed within elastic range (i.e. the maximum hogging bending moment is lower than the yield moment), the lateral force from U-frame restraint is expressed by

$$F_u = \frac{l_e}{667\delta} \frac{\sigma_{fc}}{\sigma_{cr} - \sigma_{fc}} \tag{10.1}$$

where

- l_e is the effective length (Clause 9.6.5, BS5400:Part 3),

- δ is the flexibility of the U-frame (Clause 9.6.5), but with a flexibility of the U-frame connection f_r given by

$$f_r = \frac{300}{b_s b_f h_d E_{cm} N} \tag{8.6}$$

where

  - E_{cm} is Young's modulus (short-term) for the concrete,
  - b_f and t_f are the breadth and thickness of steel top flange,
  - b_s is the breadth of the web stiffener,
  - h_d is the overall height of the studs,
  - N is the number of the effective connectors over a longitudinal distance $2l_n$ above the web stiffener, given by:

$$l_n = 28 b_f (\frac{t_f}{b_f})^{1.4} \tag{10.2}$$

- σ_{fc} is the maximum compression stress in the bottom flange,

- σ_{cr} is the elastic critical stress in the bottom flange which is expressed by:

$$\sigma_{cr} = \frac{\pi^2 EI}{(\eta l_e)^2 A_f} \tag{10.3}$$

- where A_f is the cross section area of the bottom flange.

When compressive strain in the bottom flange is designed to exceed the yield strain, at the locations of U-frames, the lateral force $F_{u(i)}$ from U-frames is determined by:

$$F_{u(i)} = \alpha N_{ci} \tag{10.4}$$

where

- $F_{u(i)}$ is the lateral restraint U-frame force at locations of the U-frames,

- α is coefficient depending on the stiffeners. For double sided stiffeners, α is 0.025, and for single sided stiffeners, α is 0.013,

- N_{ci} is the compression force in the bottom flange at the locations of the U-frames,

At locations of the U-frames where stress in the bottom flange is not in compression, the lateral restraint force $F_{u(i)}$ can be ignored.

Lateral U-frame force should be checked against the strength of the U-frame, in additional to the lateral loading in accordance with Clause 12.2.2 of BS5400 :part 3.

The U-frame force in additional to lateral loading should be also checked against the strength of the U-frame connection, M_{pr1} and M_f, given by:

$$\begin{aligned} \Sigma F_u h_s &\leq M_{pr1} \\ &\leq M_f \end{aligned} \tag{10.5}$$

where

- $\Sigma F_u h_s$ is transverse bending moment acted on U-frames, which are a summation of a U-frame force $F_{u(i)}$ and the additional lateral loading,

- h_s is the distance between the steel top and bottom flanges,

- M_{pr1} is the transverse bending strength when cracks occur in the concrete of a U-frame connection, and it is determined by equation 8.19,

- the M_f is the strength of the top flange given in equation 8.30.

Equation 8.6 must be incorporated into Clause 9.6.5 of BS5400:Part 3 for the transverse flexibility of steel-concrete stud connections for symmetric inverted U-frames, but not for other configurations of U-frame connections. Obviously, the U-frame connection is only effective when it satisfies the strength requirements.

10.3 A tentative design method for distortional lateral buckling of composite beams with discrete U-frame action

The method of Eurocode 4 for distortional lateral buckling of composite beams, (Annex B of Eurocode 4:Part 1[1]) is more rational and versatile in treatment of lateral buckling of composite beams than the other existing design methods. However, it still excludes composite beams with discrete inverted U-frame action. The design method proposed here is an extension of the method of Eurocode 4 to cover discrete U-frame action.

The scope of the method is for distortional lateral buckling in composite beams of uniform sections. The beam could be either one span in a continuous beam, with full lateral restraints at two ends of the span, or a cantilever extension, with full lateral restraint only at the support. Discrete U-frames should be equally spaced along the span length, and ratio of L/L_u should be greater than 10, where L is the span of a beam, L_u is U-frame spacing. The stiffeners, which comprise a part of discrete U-frames are either double sided or single sided. Although in the test specimen(U5), from which, the proposed method is developed, stiffeners were fully welded to the top and bottom flanges (Fig.10.1), the method could also be applicable to those beams when stiffeners are only welded to the top flange, as shown in Fig.10.1. However, in the latter situation, the gap between the bottom flange and the stiffeners should be at least less than a half width of the bottom flange.

Design for distortional lateral buckling of composite beams with discrete U-frame should be checked with respect to the strength of the U-frame connection. The general design criteria relating to the distortional lateral buckling are summarized as follows:

- Choose cross sections initially according to the maximum compressive stress σ_{fc} expected in the steel bottom flange. If hogging bending of a beam is designed up to the yield moment, the cross section should be chosen as Class 3 or Classes 1 and 2. If σ_{fc} is less than the yield stress, Class 4 cross section can be also chosen.

- Calculate the design hogging moment of resistance of the beam. Choose the buckling resistance M_d, taking account of the Class of the cross section, using the relevant design curves for non-distortional lateral buckling, adopted in EC3 and EC4. Then determine $\bar{\lambda}_{LT}$. For Class 1 and 2 cross sections:

$$\bar{\lambda}_{LT} = \sqrt{\frac{M_p}{M_{cr}}} \tag{10.6}$$

- and for Class 3 and 4 cross sections:

$$\bar{\lambda}_{LT} = \sqrt{\frac{M_y}{M_{cr}}} \tag{10.7}$$

  where

  - M_{cr} is the elastic critical moment of a composite beam,
  - M_p is the plastic moment resistance of the cross section in hogging bending,
  - M_y is the yield moment resistance of the cross section in hogging bending.

- Use M_{cr} to determine required k'_θ. As usually, $GI_{at} << k_\theta L^2/\pi^2$, it can be assumed that

$$M_{cr} \approx \frac{k_c C_4}{\pi} \sqrt{k'_\theta E I_{afz}} \tag{10.8}$$

  where

  - C_4 is a property of the distribution of bending moment given in Tables B.1 to B.3 of Eurocode 4 [1],
  - k_c is a shape factor of cross section given in clause B.1.3 or B.1.4 of Eurocode 4 [1],
  - I_{afz} is the second moment of area of the bottom flange about the minor axis of the steel member,
  - I_{at} is the St. Venant torsion constant of steel section,
  - E and G are the Young's modulus and the modulus for steel,
  - k'_θ is the required transverse stiffness per unit length of the beam.

- Calculate the available k_θ, where $k_\theta > k'_\theta$. Choose U-frame details(spacing L_u and size of the stiffeners) to satisfy the above requirement. Transverse stiffness k_θ is defined and expressed as equation 8.13 in the previous chapter by:

$$\frac{1}{k_\theta} = \frac{1}{k_1} + \frac{1}{k_2} + \frac{1}{k_3}$$

  Change the cross section size if necessary, and repeat the procedure.

- Check the strength of U-frame connections. The design lateral force for a discrete U-frame is determined by:

  - When the maximum compressive strain in the bottom flange is designed to exceed the yield strain, at the locations of U-frames, the lateral force $F_{u(i)}$ is

$$F_{u(i)} = \alpha N_{ci} \qquad (10.4)$$

    $F_{u(i)}$, α and N_{ci} are as the same as those described in section 10.2.

  - When the hogging bending strength is designed within elastic range, the U-frame restraint force is expressed by

$$F_u = \bar{\Delta} k_\theta L_u \frac{1}{1 - M_h/M_{cr}} \qquad (10.9)$$

    where

    * $\bar{\Delta}$ is the maximum crockness allowed for beams,
    * L_u is spacing of U-frames,
    * M_h is the maximum hogging bending moment in internal supports,

At the location of the U-frames, where the axial force is tension, F_u is very small, so that in these locations, the strength of the U-frame connections does not need to be checked.

10.4 Further work regarding U-frame action in composite beams

The scope of the work is limited to composite beams of uniform steel cross section and having U-frames equally spaced over beam spans. The normal weight concrete is also assumed.

Proposals for further research regarding U-frame action are as follows:

- **Variable depth and U-frames unequally spaced** Difficulties can arise in assessments of hogging bending strength against lateral stability and lateral restraint force provided by U-frames, when beams have non-uniform cross-section (variable depth in cross-section of steel members as shown in Fig.10.2). Research is also needed to evaluate lateral instability of those beams on which U-frames are not equally spaced over beam spans.

- **Skew half-through decks** In a heavily skewed, simply supported composite deck, the 'half-through' trimmer girders are restrained by U-frames that consists of edge trimmer web stiffeners and composite deck. However, lateral torsional stiffness at two ends of the main girder is much smaller than that in internal supports of a continuous beam, where full lateral torsional restraints are usually provided. Questions also arise in assessments of hogging bending strength and lateral U-frame force by using the present methods (BS5400 and Eurocode 4).

- **Lightweight concrete** Since use of lightweight concrete becomes more and more popular in construction practice, questions may also arise whether the results for U-frames of normal weight concrete can be used for U-frames of lightweight concrete. In principle, both U-frames should be the same. However, attention should be given to criteria of conditions of full shear connections, and strength of discrete U-frame connections.

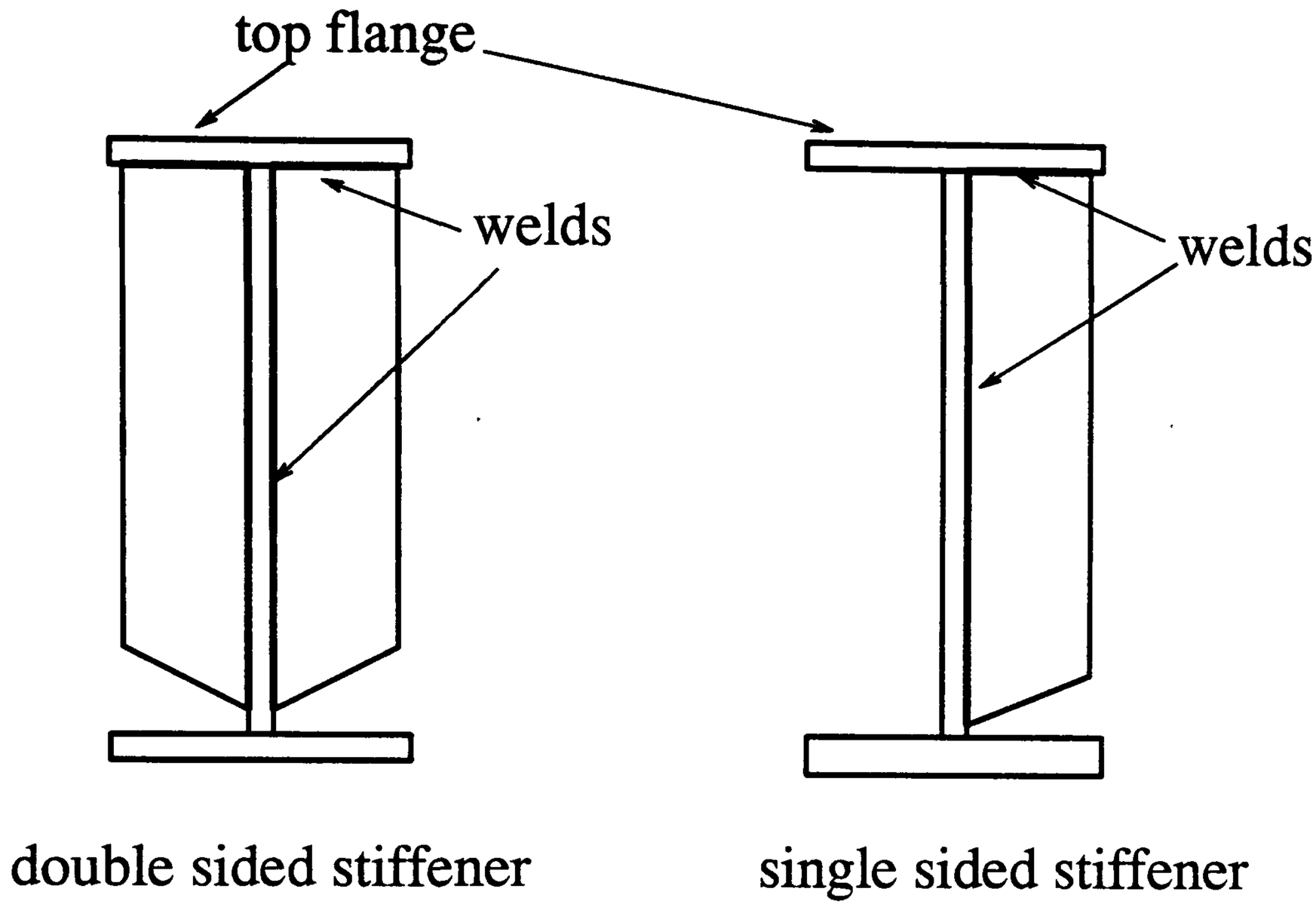

Figure 10.1: Web stiffeners

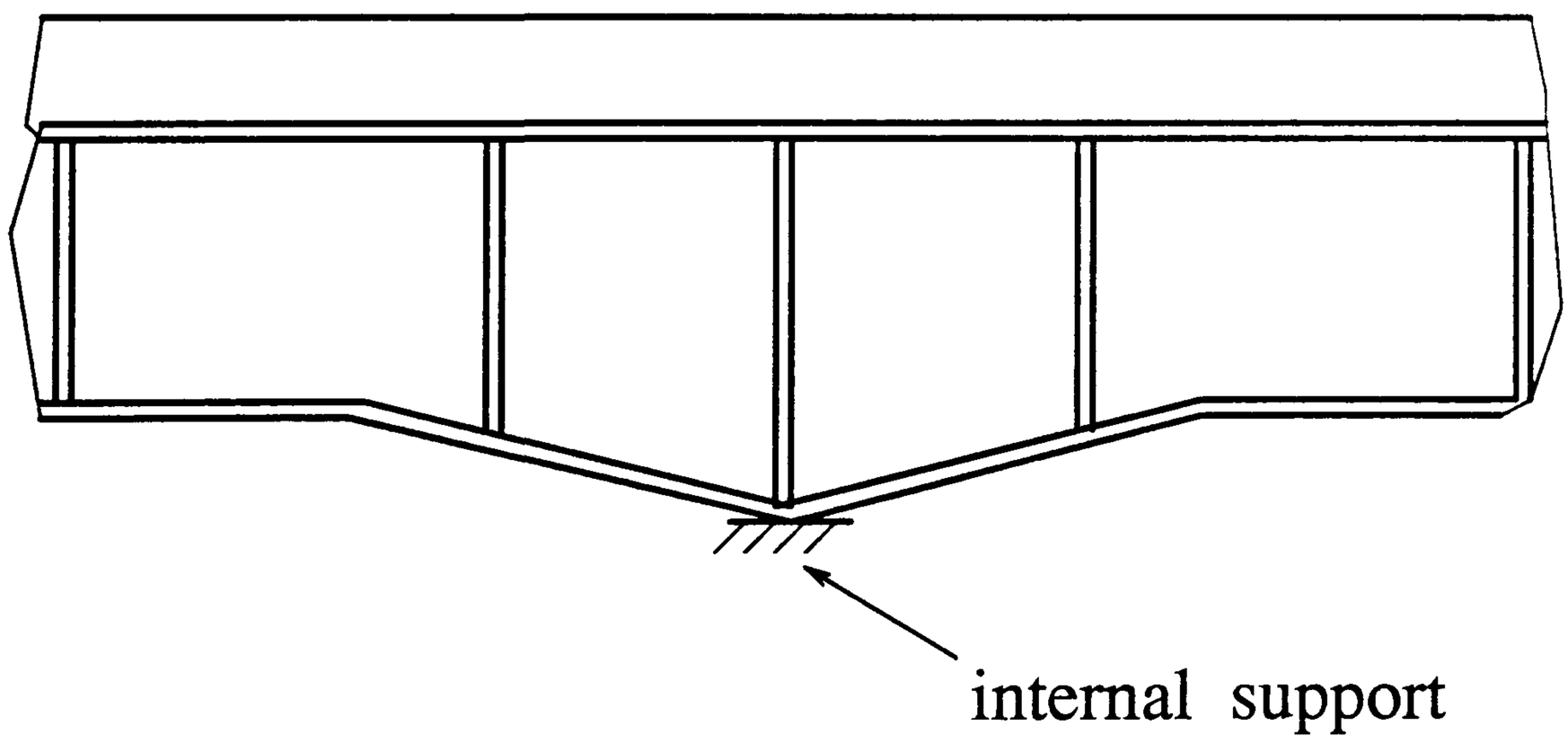

Figure 10.2: Variable depth of a steel girder

Publication and research reports

1. Johnson R. P. and Chen S., "Local buckling and moment redistribution in Class 2 composite beams", Structural Engineering International, 1991, **1**, Sept. 27-34.

2. Chen S. and Johnson R. P., "Experimental study of distortional lateral buckling of inverted U-frame composite girders," (I,II,III,IV), Progress Report on Contract 7012ESJ to SCI.

3. Chen S. and Johnson R. P., "Experimental study of distortional lateral buckling of inverted U-frame composite girders", Final Research Report on on Contract 7012ESJ to SCI, 1992, April.

Appendix A

Manual for programs SCC and MRTSCB

Introduction

Two programs have been written by the present author for non-linear numerical analyses of composite beams. Program SCC (simulation of composite cantilevers) is used to simulate the behaviour of composite cantilevers, regarding local buckling. Program MRTSCB (moment redistribution in two-span continuous composite beams) is used to assess the moment redistribution in two-span continuous composite beams. They were all based on program BAULS (described in Ph.D. thesis by Fan [15] and in a paper by Johnson and Fan [33]. Both programs are written in Fortran, and can be executed in any Fortran support computer system.

Both Programs use subroutine EMPHI (moment-curvature curves), which is described in the note on Program MRFEB [87]. The algorithm used in the two programs is described in chapters 3 and 4. Comments are now given with each program as follows.

Units and conventions of sign

All input and output in N, mm, radian units. All strengths of materials input as positive. Hogging moments and curvatures are positive, and so are tensile stress and strain.

- x – coordinates run from the internal support towards midspan(MRTSCB), or from the support to the free end(SCC),
- y – coordinates downwards from the top surface of the concrete slab,

Subroutines and functions

- EMPHI – moment-curvature curves (hogging/sagging), (SCC,MRTSCB),
- CONF – obtain force at internal support (MRTSCB),
- ROTOP1 – calculating rotation, pre-plastic (SCC,MRTSCB),
- ROTOP2 – calculating rotation, post-plastic (SCC,MRTSCB),
- SECTION – calculating properties of sections (MRTSCB),
- BMX – function to calculate moment distributions (SCC,MRTSCB).

Input files

- Program SCC
  - NB,ES,ER,HS,SS
  - CREF,NCFL,NW,NHF,BMHS,BMMS
  - BC,HC,BH,HH,ART,YRT,ARB,YRB,NRS,NPL
  - B(J),H(J),J=1,NPL
  - SYF,SRT,FCU,FRFC,EL
  - RPHI,RBMH
  - DL1,PLOD,UNCRI,CRI,NEH,FINCR
  - DB,STARTF
  - STARTM,SMLTR,SMDROP
  - H1,H2
  - BMHP
- Program MRTSCB
  - NB,ES,ER,AE,HS,SS
  - CREF,NCFL,NW,NHF,BMHS,BMMS
  - BC,HC,BH,HH,ART,YRT,ARB,YRB,NRS,NPL

- B(J),H(J),J=1,NPL
- SYF,SRT,FCYL,FRFC
- RPHI,RBMH
- DSPANL,DSPANR,WRA,NEH,NES,FINCR
- RLIMIT,STARTF,FMULT
- STARTM,SMLTR,SMDROP
- H1,H2

Output files

- Program SCC – BAOUT (data output file) and x.m, y.m (plot files),
- Program MRTSCB – BAOUT1 (data output file) and plot.m (plot file).

Notations for variables

- The following variables are the same as these used in Program MRFEB [87]:
  - NB,ES,ER,HS,SS,CREF,NCFL,NW,NHF,BMHS,BMMS,BC,
  - HC,BH,HH,ART,YRT,ARB,YRB,NRS,NPL,B(J),H(J),SYF,
  - SRT,FCU,FRFC,EL,RPHI,RBMH.
- The others are given as follows:
  - DL1 – L, beam length (SCC),
  - DSPANL,DSPANR – L_1 and L_2, span length (MRTSCB),
  - PLOD – point load(SCC),
  - WRA – w_2/w_1 (MRTSCB),
  - UNCRI,CRI – I_{cr}, I_{un} (SCC),
  - NEH – number of elements(hogging region),
  - NES – number of elements(sagging region)(MRFEB),
  - FINCR – increment of load factor,

- DB – depth of steel section (SCC),
- RLIMIT – the maximum discrepancy in rotations at the internal support (MRFEB),
- STARTF – initial λ for analysis,
- FMULT – multipler for FINCR(MRFEB),
- STARTM – factor applied to the initial support moment in analysis,
- SMLTR – fraction of M_p at which the programs stop,
- SMDROP –fraction of M_p by which the support moment drops,
- H1,H2 – K_1 and K_2,
- BMHP – M_p (hogging),
- S1,S2 – factors for UNCRI and CRI, in calculating the equivalent.

Programs control

The real and elastic curvatures at the moment BMHP give the value of ratio K_3 (for comparison with K_1). If $K_3 > K_1$, the falling branch is entered before BMHP is reached, and "maximum hinge moment" is out put.

The programs stop when

- a bending moment exceeds either BHL or BSL (the maximum values on M/ϕ curves);
- the hinge moment falls below 0.8*BMHP (M_p);
- an iteration fails to converge.

Appendix B

A device for measuring lateral displacement of the bottom flanges

A device capable of measuring the lateral displacement of the bottom flanges is designed (Fig.5.14). The measured values by the LVDT transducer are slightly different from those of ture relative lateral displcement in the bottom flanges, because rotation also occurs in the bottom flanges.

Assume the web distortion is negligible, so that the rotation of the bottom flange equals to the rotation of the web. Fig.A.1 shows the geometry of the device.

Let δ be the true relative movement of the bottom flange, $\delta\prime$ be the measured movement by the LVDT, and $\Delta\delta$ be an error correction. $\Delta\delta$ is derived as follows.

In Fig.A.1, δ_A, and δ_B are the absolute displacement of the bottom flange in each beam (at the intersection of the web and the bottom flange). They are different from the measured values of $\delta_A{}'$ and $\delta_B{}'$, because the positions where measurement is taken are different.

The relation between them can be derived as following;

for beam A,

$$\delta_A = \delta_A{}' - h_A\theta_A \tag{B.1}$$

and for beam B,

$$\delta_B = \delta_B{}' - acos\theta_B - gsin\theta_B \tag{B.2}$$

and also

$$g + e = asin\theta_B + h_Bcos\theta_B \tag{B.3}$$

so that it leads to

$$\delta_B = \delta_B{}' - acos\theta_B - sin\theta_B(asin\theta_B + h_Bcos\theta_B - e) \tag{B.4}$$

The relative lateral displacement δ is

$$\delta = \delta_A - \delta_B \tag{B.5}$$

and also

$$\delta' = \delta_A{}' - \delta_B{}' \tag{B.6}$$

Therefore, when $B \gg \delta$ and δl, and $sin\theta \sim \theta$,

$$\begin{aligned} \Delta\delta &= \delta' - \delta \\ &= h_A\theta_A + \theta_B(e - h_B - 0.5a\theta_B) \end{aligned} \tag{B.7}$$

This error correction factor $\Delta\delta$ was used in the test data processing. For particular, $e \sim h_B$, $\Delta\delta$ is then

$$\Delta\delta = h_A\theta_A - 0.5a\theta_B^2 \tag{B.8}$$

The accuracy of the device is influenced by accuracy in measuring rotation, and displacement, as well as dimensions of h_A and a. The accuracy of the LVDTs is better than 0.01 mm, and that of the inclinometer is better than 0.03 mrad, so that the error of the device can be minimized within 0.01 mm (b and $h_A << 1$ m).

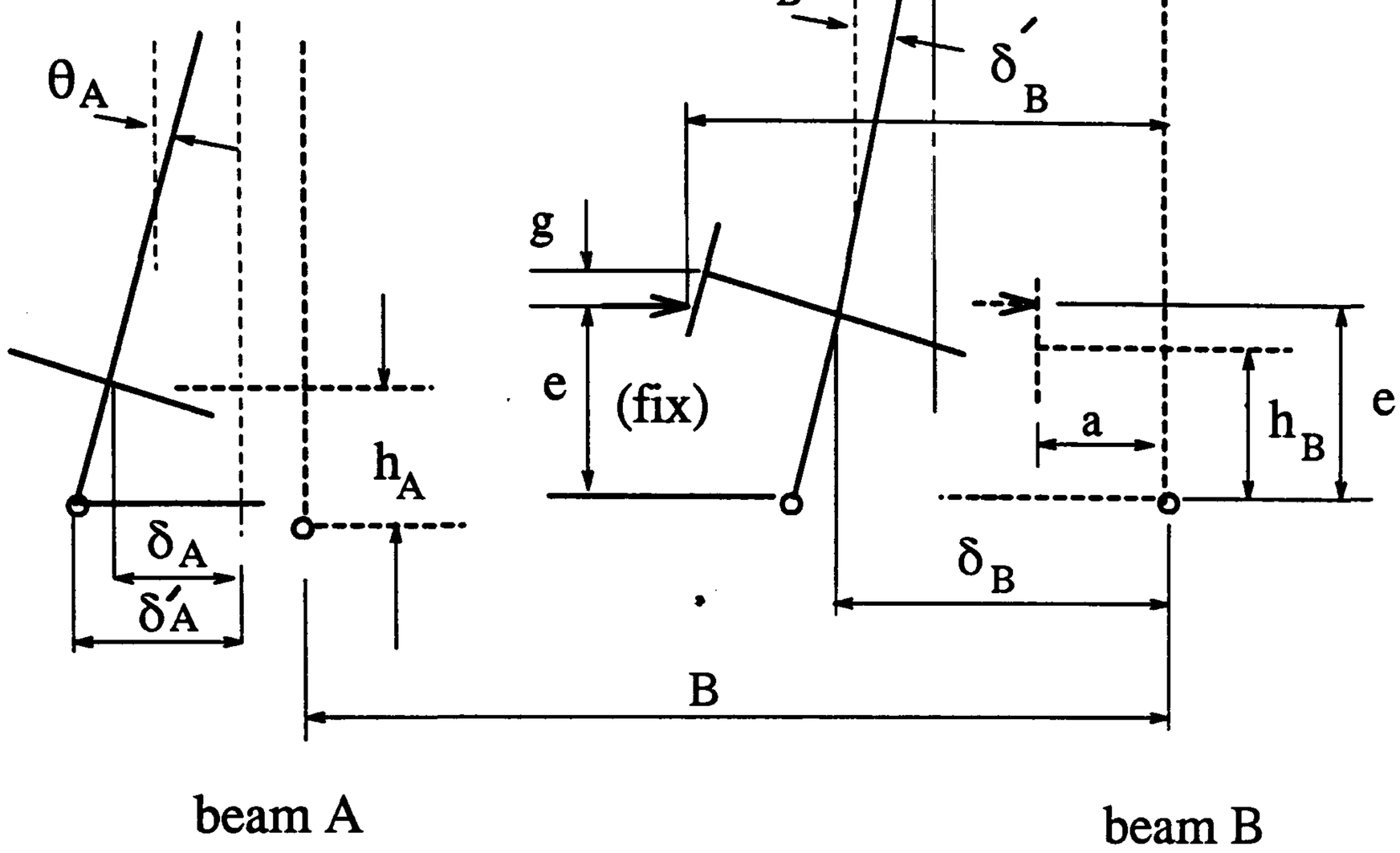

Figure B.1: Geometry of the device for measuring relative lateral movement

References

[1] Editorial Panel For Eurocode 4. *Design of composite steel and concrete structures: general rules and rules for buildings*. Eurocode 4: Part 1, revised draft, issue 2, 1991, Jan.

[2] British Standards Institution. *Steel, concrete and composite briges. Code of practice for design of steel bridges*. BSI, London, 1982, BS5400, Part 3.

[3] Bleich F. *Buckling strength of metal structures*. Engineering Socities Monographs, McGraw Hill, London, 1952.

[4] Bulson P.S. *Local stability and strength of thin-walled structures*. ed. by Chilver A. H., Part II, Chatto and Windus Ltd., 1967.

[5] Allen H.G. and Bulson P.S. *Background to buckling*. McGraw Hill, London, 1980.

[6] Stowell E.Z. *Compressive strength of flanges*. Technical Note No. 2020, National Advisory Committee for Aeronautics, 1950.

[7] Lay M.G. and Galambos T.V. Inelastic beams under uniform moment. *J. Struct. Div. Am. Soc. Civ. Engrs*, 1965, **91** No. ST6, Dec., 67-93.

[8] Southward R.E. *Local buckling in universal sections*. Internal Report, University of Cambridge, Engineering Department, 1969.

[9] British Standards Institution. *Structural use of steelwork in building. Code of practice for design of composite beams*. BSI, London, 1988, BS5950: Part 3.1.

[10] Editorial Panel For Eurocode 3. *Design of steel structures: general rules and rules for buildings*. Eurocode 3: Part 1 (2nd draft), 1989.

[11] Johnson R. P. *Continuous composite beams for buildings*. Steel in Building, IABSE-ECCS Symposium Report, Luxembourg, 1985, 195-202.

[12] Brett P. R. et al. Continuous construction in steel for roofs and composite floors. *Struct. Engr*, 1987, **65A**, No.10, Oct., 355-368.

[13] Discussion on the paper "Continuous construction in steel for roofs and composite floors" by Brett P.R. et al. *Struct. Engr*, 1987, **66**. No.14, July, 216-227.

[14] Kemp A.R. Available rotation capacity in steel and composite beams. *Struct. Engr*, 1991, **69**, No.3 Mar., 88-97.

[15] Fan C.K.R. *Buckling in continuous composite beams.* University of Warwick, 1990, PhD thesis.

[16] Kato B. Rotation capacity of H-section members as determined by local buckling. *J. Constr Steel Research*, 1989, bf 13, 95-109.

[17] Polyzois D. Web-flange interaction in slender plate girders. *Proc. of Structural Stability Research Council*, 1990, April, 291-303.

[18] Barnard P.R. and Johnson R.P. Plastic behaviour of continuous composite beams. *Proc. Instn. Civ. Engrs*, 1965, **32**, Oct. 180-197.

[19] Barnard P. R. *On the collapse of composite beams.* University of Cambridge. 1963, PhD thesis.

[20] Barnard P.R. and Johnson R.P. Ultimate strength of composite beams. *Proc. Instn. Civ. Engrs*, 1965, **32** Oct. 161-179.

[21] Van Dalen K. *Composite action at the supports of continuous beams.* University of Cambridge, 1970, PhD thesis.

[22] Johnson R. P. Research on steel-concrete composite beams. *J. Struct. Div. Am. Soc. Civ. Engrs*, 1970, **96**, No. ST3, March, 445-459.

[23] Climenhaga J.J. *Local buckling in composite beams.* University of Cambridge, 1970, PhD thesis.

[24] Hamada S. and Longworth J. Buckling of composite beams in negative bending. *J. Struct. Div. Am. Soc. Civ. Engrs*, 1974, **100** No.ST11, Nov. 2205-2222.

[25] Hope-Gill M. C. *The ultimate strength of continuous composite beams.* University of Cambridge, 1974, PhD thesis.

[26] Hope-Gill M.C. and Johnson R.P. Tests on three span continuous composite beams. *Proc. Instn. Civ. Engrs*, Part 2, 1976 **61**, 367-381.

[27] Hope-Gill M. C. Redistribution in composite beams, *Struct. Engr*, 1979, **57B**, March, 7-10.

[28] Ansourian P. Plastic rotation of composite beams. *J. Struct. Div. Am. Soc. Civ. Engrs*, 1982, **108**, ST3, 643-659.

[29] Bradford M.A. Local buckling analysis of composite beams. *Trans. Instn. Engrs Australia*, 1986, 4, CE28, 312-317.

[30] Schiling C.G. *Moment-rotation tests of steel bridge girders.* Report on Project 188, Autostress Design, American Iron and Steel Institute, 1985.

[31] Schiling C.G. and Morcos S.S. *Moment-rotation tests of steel girders with ultracompact flanges.* Report on Project 188, Autostress Design of Highway Bridges, American Iron and Steel Institute, 1988.

[32] Schiling C.G. *A unified Autostress method", project 51, Development of Design Specifications for Continuous Composite Plate-Girder Bridges.* American Iron and Steel Institute, 1989.

[33] Johnson R.P. and Fan C.K.R. Strength of continuous composite beams designed to Eurocode 4. *Proc. IABSE*, P-125/88,P-125/88, 1988, May, 33-44.

[34] Climenhaga J.J. and Johnson R.P. Local buckling in continuous composite beams. *Struct. Engr*, 1972, **50**, No.9, Sept., 367-374.

[35] Goodier J.N. and Barton M.V. Effects of web deformation on the torsion of I-beams. *Trans., Am. Soc. Mech. Engrs* 1944, **66A**, 35-40.

[36] Suzuki Y. and Okumura T. *Final report.* Eighth Congress, International Association for Bridge and Structural Engineering 1968, 321-31.

[37] Kollbrunner C. F. and Hadjin N. *Die Verschnungsmethode in der Theorie der dunnwandigen Stabe und ein neues Berechnungs modell des Stabes mit*

in seinen Ebenen defomierbaren Querschnitten. Publications, International Association for Bridge and Structural Engineering, 1968, 28-II, 87-100.

[38] Hancock G.T. Local distortional and lateral buckling of I-beams. *J. Struct. Div. Am. Soc. Civ. Engrs*, 1981, **107**, No. ST2, 355-370.

[39] Bradford M.A. and Trahair N.S. Distortional buckling of thin-web beam-columns. *Engrg Structs*, 1982, **4**(1), 2-10.

[40] Bradford M.A. Inelastic distortional buckling of I-beams. *J. Computers and Structures*, 1986, **24**, No.6, 923-933.

[41] Dowling P.J. *et al* stability of tapered frames. *Structural Stability Research Council*, Proc. Annual Technical Session, 1985, 379-395.

[42] Johnson R.P. and Bradford M.A. Distortional lateral buckling of unstiffened composite bridge girders. *Proc. Conf. Instability and Plastic Collapse of Steel Structures*, Granada, 1983, 569-580.

[43] Bradford M.A. and Johnson R.P. Inelastic buckling of composite bridge girders near internal supports. *Proc. Instn. Civ. Engrs*, Part2, 1987, **83**, March, 143-159.

[44] Weston G. and Nethercot D.A. Lateral buckling in continuous composite bridge. *Struct. Engr*, 1991, **69**, March 79-87.

[45] Crisfied M.A. *Large deflection elastoplastic buckling analysis of plates using finite elements*, 1973 Report LR 593, TRRL.

[46] Svensson S.E. Lateral buckling of beams analysed as elastically supported columns subject to a varying axial force. *J. Constr Steel Research*, 1985, **5**, 179-193.

[47] Willians F.W. and Jemah A.K. Buckling curves for elastically supported columns with varying axial force to predict lateral buckling of beams. *J. Constr Steel Research*, 1987, **7**, 133-148.

[48] Goltermann P. and Svensson S.E. Lateral distortional buckling: predicting elastic critical stress *J. Struct. Div. Am. Soc. Civ. Engrs*, 1988, **114**, ST7, July, 1606-1625.

[49] Lawson R.M. and Rackham J.W. *Design of haunched composite beams in buildings*. Steel Construction Institute, Ascot, 1989, Publication 060.

[50] British Standards Institution. *Structural use of steelwork in building. Code of practice for design in simple and continuous construction: hot-rolled sections.* BSI, London, BS5950: Part 1.

[51] Roik K. *et al.* Nachweisgegen Biegedrillknicken bei Verbundtragern. *Der Stahlbau*, 1990.

[52] Roik K. et al. *Background to Eurocode 4 clause 4.6.2 and Annex B.* Minister fur Raumordnung, Bauwesen and Stadtebau, Report RSII 2-674102-88.17, University of Bochum, 1990.

[53] Wakabayashi M. and Nakamura T. Buckling of laterally braced beams. *Engng Structs*, 1983, **5**, No.2, Apr., 108-118.

[54] Johnson R.P. and Fan C.K.R. Distortional lateral buckling of continuous composite beams. *Proc. Instr. Civ. Engrs*, Part 2, 1991, **91**, March, 131-161.

[55] Schaumann P. and Schleich J.B. Stability of composite bridge girders near internal support. *Proc. of Colloq., R&D within the field of Steel Construction*, Odense, Denmark, Sept. 1991.

[56] Trahair N.S. and Nethercot D.A. Bracing requirement in thin-walled structures. *Developments in thin-walled structures-2*, Rhodes J. and Walker A.C.(eds), Elsevier Applied Science Publishers Ltd, London, 1984, 93-130.

[57] Taylor A.C. and Ojalvo M. Torsional restraint of lateral buckling. *J. Struct. Div. Am. Soc. Civ. Engrs*, 1966, **92** ST2, April, 115-29.

[58] Nethercot D.A. Buckling of laterally or torsionally restrained beams. *J. Engng Mech. Div. Am. Soc. Civ. Engrs*, 1973, **99**, EM4, August, 773-91.

[59] Mutton B.R. and Trahair N.S. Stiffness requirements for lateral bracing. *J. Struct. Div. Am. Soc. Civ. Engrs*, 1973, **99**, ST10, Oct., 2167-2182.

[60] Medland I.C. A basis for the design of column bracing. *Struct. Engr*, 1977, **55**, No.7, July, 301-307.

[61] Wong-Chung A.D. and Kitipornchai S. Partially braced inelastic beam buckling. *Engng Structs*, 1983, **5**, No.2, April, 108-118.

[62] Wang Y.C. and Nethercot D.A. Ultimate strength analysis of three-dimensional braced I-beams. *Proc, Instn Civ. Engrs*, Part 2, 1987, **87**, March, 87-112.

[63] Stanway G.S. et al. A simply supported imperfect column with a transverse elastic restraint at any position. Part 2: behaviour. *Proc. Instn Civ. Engrs, Structs & Bldgs*, 1992, **94**, May, 205-216.

[64] Stanway G.S. et al. A simply supported imperfect column with a transverse elastic restraint at any position. Part 2: design models. *Proc. Instn Civ. Engrs, Structs & Bldgs*, 1992, **94**, May, 217-228.

[65] British Standards Institution. *Specification for steel girder bridges.* BSI. London, 1958, BS153.

[66] Johnson R.P. and Buckby R.J. *Composite structures of steel and concrete. Vol.2: Bridges*, Collins, London, 2nd edition, 1986.

[67] Chwalla E. *Hifstafeln zur Berechnung von Spannungsproblemen der Theorie zweiter Ordnung und von Knickproblemen.* Stahlbau-Verlag, Koln, 1959.

[68] Van de Pitte D. *Berekeningen van Constructies: deel II.* uitg. Story, Gent, 1980, 709 pp.

[69] Fukumoto Y. and Kubo M. Buckling in steel U-shaped beams. *J. Struct. Div. Am. Soc. Civ. Engrs*, 1982, **108**, ST5, 1174-1190.

[70] Albert C. and Dawe J.L. Buckling of continuous steel girders with flange restraint. *Canadian Journal of Civil Engineering*, 1990, **17**(2), 121-126.

[71] Johnson R. P. and Molenstra N. J. Strength and stiffness of shear connections for discrete U-frame action in composite plate girders. *Struct. Engr*, 1990, **68**, No.19, Oct., 386-392.

[72] Jeffers E. U-frame restraint against instability of steel beams in bridges. *Struct. Engr*, 1990, **68**, No.18, Sept., 359-366.

[73] Travers Morgan *An investigation into bracing systems and the use of the U-frames on steel bridges.* Contract Report, March, 1991(unpublished).

[74] Lukey A. F. and Adams P.F. Rotation capacity of beams under moment gradient. J. Struct. Div. Am. Soc. Civ. Engrs, 1969, **95** ST6, June, 1173-1188.

[75] Kuhlmann U. Definition of flange slenderness limits on the basis of rotation capacity values. *J. Constr. Steel Research*, 1989, **14**, 21-40.

[76] Kemp, A. R. Interaction of plastic local and lateral buckling. *J. Struct. Div. Am. Soc. Civ. Engrs*, 1985, III, ST10, October, 2181-2197.

[77] Eurocode 3. *Design of steel structures.* Commission of the EC, Brussels, 1988.

[78] Molenstra N. J. *Ultimate strength of composite beams.* University of Warwick, 1991, PhD thesis.

[79] Johnson R. P. and Chen S Local buckling and moment redistribution in Class 2 composite beams. *Structural Engineering International*, 1991, **1**, Nov., 27-34.

[80] British Standards Institution. *Design of composite bridges.* BSI, London, 1979, BS5400: Part 5.

[81] British standards Institution. *Tensile testing of metals.* BSI, London, 1983, BS18.

[82] British standard Institution. *Method for determination of compressive strength of concrete cubes.* BSI, London, 1983, BS1881: Part 116.

[83] Lindner J. Stabilisierung von Biegetragern durch Drehbettung eine Klarstellung. *Der Stahlbau*, 1987 Heft **56**, 12, 365-373.

[84] Timoshenko S.P. *Theory of elastic stability*. McGraw-Hill, London, 1961.

[85] Engesser F. Die Sicherung offener Brucken gegen Ausknicken. *Zentralblatt Bauverwaltung*, 1884, 415 and 1885, 93.

[86] Winter G. Lateral bracing of columns and beams. *J. Struct. Div. Am. Soc. Civ. Engrs*, 1958, **84**, ST2, Mar., 1-22.

[87] Johnson R.P. *Note for Program MRFEB*. Warwick University, 1985, July.